JAERI-M
83-182

ANNUAL REPORT OF THE FUSION RESEARCH CENTER FOR THE PERIOD OF APRIL 1, 1982 TO MARCH 31, 1983

November 1983

Fusion Research Center

日本原子力研究所
Japan Atomic Energy Research Institute

JAERI-Mレポートは，日本原子力研究所が不定期に公刊している研究報告書です。
入手の問合わせは，日本原子力研究所技術情報部情報資料課（〒319-11茨城県那珂郡東海村）あて，お申しこしください。なお，このほかに財団法人原子力弘済会資料センター（〒319-11 茨城県那珂郡東海村日本原子力研究所内）で複写による実費頒布をおこなっております。

JAERI-M reports are issued irregularly.
Inquiries about availability of the reports should be addressed to Information Section, Division of Technical Information, Japan Atomic Energy Research Institute, Tokai-mura, Naka-gun, Ibaraki-ken 319-11, Japan.

編集兼発行　日本原子力研究所
印　　刷　いばらき印刷㈱

JAERI-M 83-182

Annual Report of the Fusion Research Center for the period of April 1, 1982 to March 31, 1983

Fusion Research Center, Tokai Research Establishment, JAERI

(Received October 6, 1983)

Research and development activities of the Fusion Research Center (Department of Thermonuclear Fusion Research and Department of Large Tokamak Development) from April 1982 to March 1983 are described.

The JFT-2 tokamak was shutdown after 10 years operation. Operation test of a new device JFT-2M was near completion. In the joint JAERI-USDOE experiment on Doublet-III a record value of beta, 4.6 %, was achieved. Major efforts in theory and computation was on high beta tokamak stability, second stability regions being found for low m internal modes.

The JT-60 program progressed as scheduled, installation of the tokamak machine being initiated in February 1983. A 100 kV test was completed of prototype unit for JT-60 NBI. In the development of a high power klystron for JT-60 LH heating, a test fabricated tube generated 1 MW, 10 s RF pulses. Development of TiC coatings for JT-60 first wall was successfully concluded.

In the superconducting magnet technology, the Japanese coil for IEA Large Coil Task was installed in a test facility at ORNL after successful performance test at Naka site. A 10 T experiment of a Nb_3Sn coil with 60 cm inner bore was made. Construction of the Tritium Process Laboratory was started in February 1983.

Design studies of the Fusion Experimental Reactor and INTOR were continued.

Keywords: Annual Report, Plasma Confinement, Heating, Tokamak, JFT-2, JFT-2M, Doublet-III, JT-60, NBI Heating, RF Heating, Plasma-wall Interaction, Superconducting Magnet, Tritium Technology, Reactor Design, Fusion Experimental Reactor, INTOR

JAERI－M 83－182

核融合研究センター年報（昭和５７年度）

日本原子力研究所東海研究所核融合研究センター

（１９８３年１０月６日受理）

昭和57年度における核融合研究センターの研究開発状況をまとめた。

10年余におよぶＪＦＴ－２による実験を終結した。新装置ＪＦＴ－２Ｍの試験運転はほぼ完了した。ダブレット－Ⅲによる米国との共同実験においてベータ値4.6％を達成した。理論・計算の重点は高ベータトカマクの安定性におかれ，低モード数の不安定性に対する第２安定領域が見出された。

ＪＴ－60計画は順調に進められ，58年２月にはトカマク装置の組立作業が開始された。ＪＴ－60中性粒子入射装置原型ユニットの100 kV試験を完了した。ＪＴ－60高周波加熱用の大電力クライストロンの開発試験では，出力１ＭＷ，パルス巾10秒を達成した。またＪＴ－60 第一壁用のTiC被覆材の開発を終了した。

超電導磁石技術では，国際エネルギー機関による大型コイル事業のための日本のコイルが完成し，国内試験ののち，米国オークリッジ研究所の試験装置に据付けられた。また内径60 cmの大型Nb_3Snコイルの10Ｔ試験を行った。トリチウムプロセス研究棟が58年２月着工された。

核融合実験炉およびＩＮＴＯＲの設計研究を引続き進めた。

Contents

目　　次

I. PLASMA THEORY AND COMPUTATION

1. Introduction

Theoretical program at JAERI aims at developing methods for comprehensive theoretical analyses of a tokamak plasma under realistic conditions and analyzing the plasma to attain the basic understanding of the tokamak and contribute to the experimental programs of the JT-60 and JFT-2M tokamaks, and future fusion reactors. These objectives are pursued by developing the computer code system TRITON and solving physics problems on the plasma confinement, heating, and transport on the basis of the combined use of the fluid, kinetic, and particle models.

The most notable studies of this fiscal year are the comprehensive analyses of the MHD and kinetic stabilities with low toroidal mode number and introduction of a new model for resistive MHD instabilities which concern with disruption processes in a tokamak. Studies of heating processes by the kinetic and MHD models, development of high-performance equilibrium codes, and studies of various ideal MHD modes are carried out extensively. Studies concerning new numerical methods, development of various supporting codes and construction of the TRITON-I code system have been also continued.

2. Kinetic Studies

2.1 Introduction

In a high temperature plasma, kinetic effects often play important roles in stability properties and heating processes.

Previously developed techniques for a stability study of high-n ballooning mode (n: toroidal mode number) are extended to be applicable to longer wave length problems, i.e. analyses of low-n stability and heating processes of ICRF and shear Alfvén waves. It is found that the n=1 tearing mode is stabilized by the kinetic and toroidal effects.

2.2 Stability

2.2.1 Stability of ∇T_e-driven microscopic drift-tearing mode[1)]

Stability of the kinetic drift-tearing mode with a short wave length

is investigated by employing an energy-dependent electron-ion collision model. The electron temperature gradient can destabilize the mode in the range of the collisionality $1 < \nu/\omega_* < 20$ (ν: collision frequency, ω_*: drift frequency). The instability appears in a parameter range of intermediate β values, and the mode is stabilized by the magnetic shear when β value becomes O(1%) (β: plasma pressure/magnetic pressure).

2.2.2 Kinetic theory of global n=1 instabilities in toroidal plasmas[2)]

The kinetic theory of the global n=1 instabilities of finite-β tokamak plasma with circular cross sections is investigated in the collisionless limit. The wave-particle interactions and the finite gyro-radius effect are included as kinetic corrections. The toroidal effect is incorporated up to first order of $\epsilon \equiv a/R$, the inverse aspect ratio. The radial-poloidal eigenmode equations are directly solved numerically in the parameter range $q(0) \sim 1$ (q: safety factor). Analytical studies of the modes are made by use of the energy integrals and compared to the numerical results. Special attentions are paid for studying the transition between the MHD-type mode and the kinetic instabilities.

The m=1 internal/tearing mode, n=1 ballooning mode and m=2 tearing mode with a fixed boundary condition are identified in connection with the MHD mode. When the q=1 mode-rational surface exists in the plasma, the m=1 internal mode has large growth rate in a finite-β toroidal plasma; this mode turns out to be the m=1 collisionless tearing mode in the low β regime. The transition occurs around the parameters where the condition $\beta^2 \sim \epsilon^2 \rho_i/a$ is satisfied (ρ_i/a: ion gyro-radius divided by the plasma radius). The pressure driven ballooning mode, which becomes unstable when q-value becomes large and $\beta > a/2q^2R$ in the MHD limit, is connected to the electrostatic-like ballooning mode which is unstable with the growth rate of the order of drift frequency. The m=2 tearing mode is destabilized by the parallel current and is stabilized due to the coupling with the drift branch when β value increases. The toroidal coupling further stabilizes the m=2 tearing mode (Fig. I.2-1).

2.3 Heating

2.3.1 Kinetic Alfvén wave propagation in cylindrical tokamak[3)]

Propagation and absorption of kinetic shear Alfvén wave, which is launched by a helical oscillating current sheet, are examined in a

collisionless, current-carrying cylindrical plasma in a sheared magnetic field. Kinetic effects, such as effects of the finite gyro-radius, Landau resonance and collisionless resistivity, as well as finite-β effects, density, temperature and current inhomogeneity effects are included.

We find that the propagating shear Alfvén wave excites drift wave around the resonance layer, and the wave is absorbed through Landau resonance. The propagation is strongly affected by the magnetic shear, and the spatial distribution of the absorbed power is determined by the kinetic effect near the resonance layer. The calculated coupling coefficient to the antenna and heating efficiency are found to have strong dependence on locations of the antenna and shell.

2.3.2 Energy deposition profile of efficient heating by shear Alfvén wave[4)]

The energy deposition profile of the shear Alfvén wave in a cylindrical tokamak is obtained. The radial propagation and absorption are solved by use of the kinetic equations for collisionless inhomogeneous plasmas. The absorption is mainly by electron Landau damping, and occurs not only at the resonance surface, $k_{//}(r)V_A(r) = \omega$, but also in the propagation region, $|k_{//}(r)|V_A(r) < \omega < |k_{//}(r)|v_e(r)$ (V_A: Alfvén velocity, v_e: electron thermal velocity, $k_{//}$: parallel wave number and ω: frequency). The parameter dependence is studied and the magnetic shear and plasma profiles have important roles for the deposition profile. The efficient heating is possible if the condition $k_{//}V_A \sim \omega$ is widely satisfied in the propagation region. The bulk heating does not always correspond to the good antenna coupling, which often causes an unfavorable edge heating. For some typical parameters the energy input $\dot{W} \sim 1$ watt/cm^3 is expected when the wave amplitude $\tilde{B}_r$ is several gauss.

2.3.3 Kinetic theory of RF wave in a plasma in an inhomogeneous magnetic field[5)]

Kinetic effects on propagation and absorption of radio frequency (RF) wave in inhomogeneous and dispersive plasmas are studied, where effects of finite gyro-radius and wave-particle interactions are included. The generalized linear propagator in the presence of the inhomogeneity of magnetic field strength along the field line is calculated for obtaining the nonlocal conductivity tensor. Instead of a plasma dispersion function a new function is introduced. The influence of the inhomogeneity to

the RF wave-energy deposition scheme is found to be appreciable in high temperature plasmas. Parameter dependence of this new function is studied. We derive a kinetic wave equation taking the corrections due to the plasma inhomogeneity and dispersion. Nonlocal effects on the wave energy flux and on the power deposition to each plasma species are examined. This approach is applied to toroidal plasmas.

2.3.4 Kinetic analysis of propagation and absorption structure of ICRF wave[6)]

Propagation and absorption of waves in the ion cyclotron range of frequencies (ICRF) are investigated using the kinetic theory in a high temperature plasma. The wave equation which includes kinetic effects (such as finite gyro-radius effect and wave-particle interactions) is solved as a boundary value problem for a two-ion-component plasma (majority deuterium and minority hydrogen) with one dimensional inhomogeneities. The global structure of the wave field and the absorption mechanism is clarified; the power deposition profile for each plasma species and the coupling to the antenna are obtained. Mode conversion of the fast wave occurs associated with the two-ion hybrid resonance and the latter is absorbed by electrons and deuterium via Landau and collisional damping, respectively. Hydrogens absorb the wave which tunnels through the cutoff layer (or for low-field-side excitations) by cyclotron damping. Existence of cavity resonances is also confirmed, which makes considerable influence on the energy absorption.

2.3.5 Three dimensional structure of ICRF waves in a tokamak plasma[7)]

The three-dimensional structure of the ICRF waves in a tokamak plasma is studied. The toroidal field gradient, radial density inhomogeneity and the poloidal-toroidal localizations of antenna current are incorporated. The ICRF wave propagation and absorption in the two-ion species plasma (majority deuterium and minority hydrogen) are obtained by numerically solving the propagation equations in collisional cold plasmas. Two cases of the heating mechanisms, the ion-ion hybrid resonance and the cavity resonance (i.e., the forced excitation of damped eigenmode) are found in a three-dimensional configuration. Owing to the lack of homogeneity in the up-down direction, the global wave form, energy deposition profile and total energy absorption are affected, and considerable differences

from the two-dimensional calculations are found. In the case of the ion-ion hybrid resonance, the energy deposition profile is localized near the hybrid resonance surface; the energy absorption integrated over the plasma column is independent of the damping rate. On the contrary, the cavity resonance realizes a strong heating over the whole plasma column by a coherent wave, which satisfies the cavity resonance condition. This heating occurs in the absence of the cyclotron and the hybrid resonances. When we calculate the loading impedance by the poloidal current antenna with Faraday shield, we find that the cavity resonance can contribute to the wave absorption as much as (or more than) the ion-ion hybrid resonance for wide range of plasma parameters.

References

1) Itoh, K., Itoh, S-I., J. Phys. Soc. Japan 51 (1982) 1639
2) Itoh, K., Itoh, S-I., Tuda, T., Tokuda, S., "Kinetic theory of global n=1 instabilities in toroidal plasmas", IFSR-75
3) Itoh, S-I., Itoh, K., Nishikawa, K., Plasma Physics 24 (1982) 1027
4) Itoh, K., Itoh, S-I., "Energy deposition profile of efficient heating by shear Alfvén wave", HIFT-64
5) Itoh, S-I., Itoh, K., Fukuyama, A., "Kinetic theory of RF wave in a plasma in an inhomogeneous magnetic field", IFSR-74
6) Fukuyama, A., Nishiyama, S., Itoh, K., Itoh, S-I., Nucl. Fusion 23 (1983) 1005
7) Itoh, K., Itoh, S-I., Fukuyama, A., "Three dimensional structure of ICRF waves in tokamak plasmas", IFSR-88

3. MHD Studies

3.1 Introduction

The two main objectives of the computational analyses in the project TRITON are, presently, the clarification of the stability limit scaling and the mechanism of distruptive instabilities, especially, in a high beta tokamak plasma. As for these problems we have carried out various kinds of analyses and obtained new results concerning the internal kink mode, the second stability region of finite-n ballooning modes, parameter dependence of the positional instability, and effects of toroidicity and finite beta on the resistive MHD phenomena. In this section we describe

the results of MHD equilibrium studies, ideal MHD instabilities, and resistive MHD instabilities.

3.2 MHD equilibrium analysis

3.2.1 SELENE-ERATO interface module

Several equilibrium codes (SELENE codes) have been developed by the two different algorithms, the ordinary algorithm which solves the Grad-Shafranov equation in the (R,Z) plane (SELENE-40) and the inverse algorithm which solves the equation in the flux coordinates (SELENE-10, SELENE-50, SELENE-1F). An interface module which computes the metric quantities is necessary to analyze MHD stability of the equilibria obtained by the SELENE codes.

The interface module of the SELENE-40 code and the ERATO code (ERATO1) was proviously developed and used to analyze the stability of the internal kink and ballooning modes. A new interface module of the SELENE-10 code and the ERATO code was developed. This module computes the metric quantities by using the 3rd order spline interpolation in the flux coordinates; $R = R(\psi,\chi)$, $Z = Z(\psi,\chi)$. The metric quantities obtained from the new interface module are shown to be as accurate as those obtained from ERATO1 for the Solv'ev equilibria. The eigenvalue, γ^2 $(= -\omega^2)$, computed by the ERATO code with the new interface module has the same convergence curve as that computed by using the ERATO1 interface mocule (Fig. I.3-1) and the extrapolated values of the eigenvalue agree in high accuracy (< 0.05%).

3.2.2 MHD equilibrium with anisotropic pressure distribution

The code for the equilibrium with anisotropic pressure has been developed to study the equilibrium of the intensely heated tokamak plasmas. The pressure $p_{//}$ and $p_{\perp}$ are given as the functions of the poloidal flux ψ and the magnetic field strength B. The interface with the stability code, TERA, has also been developed.

3.2.3 MHD equilibrium without axisymmetry

The code for the equilibrium without axisymmetry to the toroidal direction has been developed. The finite beta effect on this class of equilibria has been studied and the self-stabilization effect due to the increase of the well near the magnetic axis has been simulated.

3.3 Ideal MHD instabilities

3.3.1 Internal kink mode in high β_p tokamak plasma[1)]

By using the ERATO code, the linear stability of internal kink mode (poloidal mode number m = 1 and toroidal mode number n = 1) is studied in wide range of poloidal beta value. The effects of the shear and ellipiticity on the stability of the mode are investigated. The internal kink mode becomes stable in high β_p region. However, the mode has wider unstable region for the high shear and/or elliptic tokamak plasma than the low shear and circular tokamak plasma (Fig. I.3-2).

3.3.2 Second stability region of finite-n ballooning mode[2)]

By using the ERATO code with the quasi-mode representation[2)], the dependence of the squared growth rate, γ^2, on the poloidal beta value, β_p, was studied for n = 3,10,50, and ∞. The stability diagrams in the (q_0,β_p) plane (Fig. I.3-3(a) and (b)) were obtained for different pressure profiles. For the equilibrium with the flat profile, the second stability region was found for lower n modes. In higher n modes (n = 50 and ∞), the localized modes remain unstable.

3.3.3 Positional instability[3)]

The stability of axisymmetric modes of a tokamak plasma (positional instabilities) is analyzed for the Solv'ev equilibrium by using the linear ideal MHD code ERATO-J. The dependence of the stability on various parameters, i.e. the ellipticity and triangularity of the plasma cross section, the aspect ratio, the safety factor at the magnetic axis, and the distance between the plasma and a conducting shell is investigated. Comparison of the results with those by the rigid model shows that the stability condition derived from the rigid model in terms of the decay index (n-index) of the external equilibrating field is a good approximation for the plasma with small triangular deformation (Fig. I.3-4). Also the results are compared with those of the rigid displacement model and applicability of the various models on the positional instability analysis is discussed.

3.4 Resistive MHD instabilities[4)]

3.4.1 Development of linear resistive MHD code

The accurate and efficient code for studying the linear stability of resistive mode in a tokamak has been developed. The basic equation is the reduced set of the resistive MHD equations, and the combination of the determinant method and the inverse iteration method is employed to solve the eigenvalue and eigenfunction. By using the mesh accumulation, growth rates of the resistive and the resistive internal modes in a cylindrical tokamak show good agreement with theoretical values in the wide range of resistivity. The combination of this code with the nonlinear MHD code AEOLUS saves the CPU time of the nonlinear simulation of the resistive mode.

3.4.2 Effects of toroidicity and ellipticity on major disruption process in a tokamak

The effects of toroidicity and ellipticity on the major distuption in a tokamak has been studied by using the linear stability code NOTUS and the nonlinear evolution code AEOLUS. The modification of the surface averaged current density due to the toroidicity and ellipticity has the stabilizing effect for tearing modes with m=2/n=1 and m=3/n=2, while the mode coupling has the destabilizing effect. Although both the toroidicity and ellipticity broaden the mode spectra and enhance the stochastic region of magnetic field lines, the essential behavior of the major disruption in a low β tokamak is the same as in a cylindrical plasma.

3.4.3 Finite-beta effect on tearing mode

The beta effect on the destabilization of the m=2/n=1 and m=3/n=2 tearing modes was studied by using the full set (the linear compressible code: NOTUS-C1) and the reduced set in helical symmetry (the linear code: NOTUS-I1 / the nonlinear code: AEOLUS-I1) of the resistive MHD equations. The compressibility increased the growth rate but the dependence on β_p and the resistivity η, was the same for both the compressible and incompressible cases. When the ideal mode was near the marginal point, the scaling of the growth rate with η was given by $\gamma \propto \eta^{3/5-c\varepsilon\beta_p/s}$, where ε and s were the inverse aspect ratio and $s = rq'/q$. The effect of β_p on the nonlinear evolution of the m=3/n=2 magnetic

island is shown in Fig. I.3-5. The saturated island width increased as β_p and decreased as the mode became close to the ideal one in high β_p region.

3.4.4 New reduced set of resistive MHD equations in a tokamak with finite poloidal beta

In order to study MHD activities in a tokamak with finite β_p, the new reduced set of resistive MHD equations has been derived under the assumption of the toroidal incompressibility, $\vec{\nabla}(\vec{v}/R^2) = 0$. Because no tokamak ordering is employed in this derivation, the resultant equations can express both resistive and internal modes in a tokamak with finite aspect ratio and finite β_p. Based upon the new set of MHD equations, the linear stability analysis code has been developed and the stability of the m=1 resistive internal mode has been studied in detail. Figure I.3-6 shows the dependence of the growth rate on the poloidal beta value for the analytic equilibrium correct up to second order of the inverse aspect ratio.

References

1) Takeda, T., et al., "Physics of intensely heated tokamak plasma", 9th international conference on plasma physics and controlled nuclear fusion research (Baltimore, U.S.A., 1982), IAEA-CN-41/P-1-3
2) Gruber, R., Troyon, F., Tsunematsu, T., Plasma Physics 25 (1983) 207
3) Kumagai, M., Tsunematsu, T. Tokuda, S., Takeda, T., "Positional instability analysis of tokamak plasmas by ERATO", JAERI-M 83-085 (1983)
4) Takeda, T., Azumi, M., Tsunematsu, T., "MHD computation at JAERI", in Proceedings of the US-Japan Workshop on 3-D MHD Simulation, March 7-11, 1983, Nagoya, Japan, IPPJ-632 1983 p.1

4. TRITON System and Computational Methods

4.1 Introduction

Before the completion of the first phase of the project TRITON (TRITON-I) in the next fiscal year various codes in the TRITON-I code system have been developed and some new physics results have been obtained through the analyses by using these code.

As for the code development the emphasis was put on the equilibrium codes and interface modules with high accuracy, resistive MHD codes based on the newly derived incompressible resistive MHD equations as described in the previous subsections, and various supporting codes for code development and maintenance. A matrix method for the analyses of a kinetic ballooning mode is developed and applied successfully to the analyses. A new difference method for advection-diffusion equation was devised and studied minutely.

4.2 TRITON system

In the project TRITON various kinds of numerical codes are being developed. These codes are classified into several code groups, i.e. the physics code group ASTRAEA[1], the numerical analysis code group PARIS, the graphic I/O code group ARGUS, and the supervisor and other supporting code group PEGASUS. In order to facilitate maintenance and use of the codes the TRITON-I code system is now being constructed by registering these codes to the index file supervised by the HARMONIA code.

In this fiscal year the MHD stability problems are studied extensively by putting emphasis on the relation with the disruption and the TRITON codes are used to analyze these problems as described in the previous subsection (see also Table I.4-1).

4.3 Supporting codes

Several supporting codes which facilitate development of codes in the TRITON system and supervise the system, are developed or being developed in this fiscal year. These codes are HARMONIA-200 (the supervisor code of the TRITON system), PLUTO-77 and PLUTO-R (codes for program analysis and documentation), GAEA-V1 and CLIO-V1 (data base management codes for results of numerical simulations), and ARGUS-V4 (a graphic I/O subsystem). As for the numerical analysis program package PARIS, vector processing algorithm is studied extensively in order to improve the performance of the linear and nonlinear MHD stability codes in a supercomputer[2]. In the following some of the above codes are described briefly.

<HARMONIA-200>

The TRITON codes are registered in the index file of the HARMONIA code by recording information and storing the codes themselves in a magnetic tape. The main part of the code was almost completed in the last fiscal year and in this fiscal year an additional module for automatic generation of documentation has been developed.

<PLUTO-77 and PLUTO-R>

PLUTO-77 is the code for the analysis and documentation of the programs written in FORTRAN77. The analysis of the statements characteristic in FORTRAN77 is added to the previously developed PLUTO-F (the analysis code for the standard FORTRAN program). The INCLUDE statement is replaced by the corresponding statements registered in the SYSINC file as is done in FORTRAN77. The documentaiton of a given source program is automatically produced by using the results of the analysis and the user's comments can be included in the document.

PLUTO-R is the code to make the list of the references of a computer code. The references are selected and sorted by key words.

<GAEA-V1 and CLIO-V1>

The GAEA-V1 and CLIO-V1 codes are supervisors of a data base on computational results, which facilitate to store, sort, and retrieve numerical results of large-scale simulations. The former code is developed to deal with comparatively small amount of numerical data which can be stored in a magnetic disk and the latter is developed to deal with a large amount of data which can be stored only in a magnetic tape. The features of these codes are; (1) necessary information for subsequent utilization of the data is automatically recorded and (2) the stored data are easily retrieved and, especially by the GAEA-V1 code, graphs or tables are easily displayed on a graphic display terminal by using a set of special TSS commands.

4.4 Computational methods

4.4.1 A new difference scheme for advection-diffusion equation

The advection-diffusion equation of the following form appears in the MHD equations, tokamak-transport equations, and Fokker-Planck

equation.

$$\frac{\partial f}{\partial t} + u \frac{\partial f}{\partial x} - D \frac{\partial^2 f}{\partial x^2} = 0.$$

This equation is usually solved numerically by using the finite-difference scheme. When the cell Reynolds number $R_c = u\Delta x/D$ is much greater than unity, the numerical static-instability $f \sim \exp(\kappa x)\cos(\pi x/\Delta x)$ can occur. This instability has been avoided by introducing an artificial diffusion. Therefore, the effects of real diffusion are screened.

A new difference scheme is proposed;

$$\frac{\delta f}{\delta t} + \frac{\delta \bar{f}}{\delta x} - D \frac{\delta^2 \bar{f}}{\delta x^2} = A \frac{\Delta x}{2} \left(\frac{\delta^2 f}{\delta t \delta x} + u \frac{\delta^2 \bar{f}}{\delta x^2}\right),$$

where, $\frac{\delta f}{\delta t} = \frac{f(t + \Delta t) - f(t)}{\Delta t}$, $\frac{\delta f}{\delta x} = \frac{f(x + \Delta x) - f(x - \Delta x)}{2\Delta x}$

$$\frac{\delta^2 f}{\delta x^2} = \frac{f(x + \Delta x) - 2f(x) + f(x - \Delta x)}{\Delta x^2}, \quad \bar{f} = \frac{f(t + \Delta t) + f(t)}{2}$$

and $A = \frac{\exp(R_c) + 1}{\exp(R_c) - 1} - \frac{2}{R_c}$.

This scheme assures the numerical stability (both dynamic and static stabilities) for all values of Courant number ($c = u\Delta t/\Delta x$) and R_c. The numerical diffusion is as small as that of the Lax-Wendroff method.

4.4.2 Matrix method for kinetic ballooning mode[3)]

A matrix method is developed to solve numerically the kinetic high-n ballooning mode. The method approximates directly the difference-differential equation by a finite difference method. Toroidal mode coupling effects and full electron and ion responses are described in the correct forms. Performance, convergence property and accuracy of the method are investigated.

References

1) Takeda, T., Azumi, M., Tsunematsu, T., "MHD computations at JAERI", in Proceedings of the US-Japan Workshop on 3-D MHD Simulation, March 7-11, 1983, Nagoya, Japan, IPPJ-632, 1983, p.1
2) Matsuura, T., et al., Comput. Phys. Commun. 26 (1982) 377
3) Tokuda, S., Itoh, K., Tuda, T., Itoh, S-I., "Matrix method for kinetic ballooning mode", JAERI-M 82-080 (1980)

Table I.4-1

	Linear analyses		Nonlinear analyses	
	Cylindrical plasma	Toroidal plasma	Cylindrical plasma	Toroidal plasma
Full set of ideal MHD equations	THALIA ■ m=2,3 growth rate of ideal modes	ERATO-J, TERA * internal kink mode ▲ ballooning modes △ positional instability	(AEOLUS-P) positional instability	
Full set of resistive MHD equations	NOTUS-C1 ■ effects of compressibility on m=2,3 modes	(NOTUS-CT) ▲ resistive ballooning modes		
New reduced set of resistive MHD equations	NOTUS-I1 * m=1 resistive internal mode ■ transition of m=2,3 ideal/resistive modes	NOTUS-IT * m=1 mode in whole beta-p regime (sawtooth to continuous oscillations) ▲ resistive ballooning modes	AEOLUS-I1 * m=1 resistive internal mode (continuous oscillations due to B_z) ■ finite beta effect on major disruption	(AEOLUS-IT) * m=1 mode in whole beta-p regime (sawtooth to continous oscillations) ▲ resistive ballooning modes
Reduced set of resistive MHD equations	NOTUS-R1 ■ transition of m=2,3 ideal/resistive modes	NOTUS-RT * finite beta effect m=1 resistive internal mode $O(\varepsilon)$ and numerical equilibrium □ shape effects on m=2,3 modes	AEOLUS-R1 * sawtooth oscillation ■ effects of aspect ratio and beta on major disruption	AEOLUS-RT * finite beta effect on m=1 resistive internal modes $O(\varepsilon)$ and numerical equilibrium □ shape effects on m-2,3 modes

* internal disruption and m=1 mode behavior in low and high poloidal beta regimes
■ major disruption analyses (aspect ratio, poloidal beta)
□ major disruption analyses (shape effects)
▲ ballooning mode analyses
△ positional instability

JAERI-M 83-182

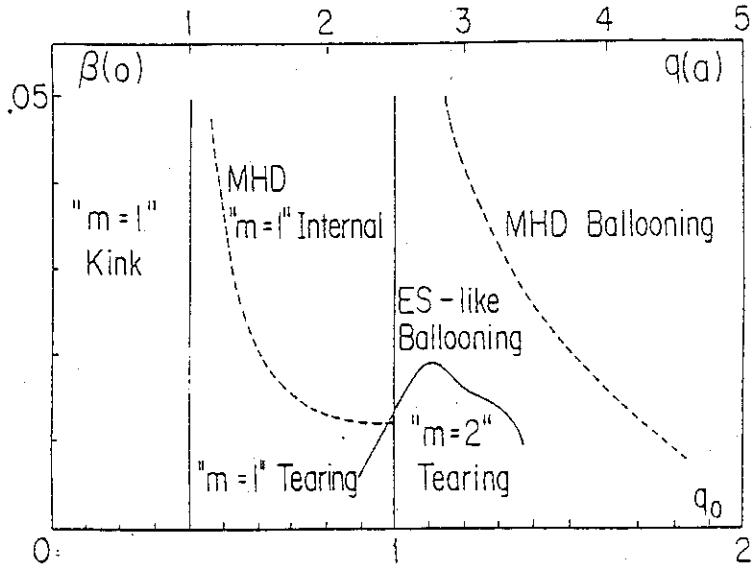

Fig. I.2-1 Stability and mode transition diagram on q_0-β(0) plane. Solid line shows the boundary for the unstable mode and dashed line denotes the transition from MHD to kinetic mode. m=1 internal/tearing mode exists for q(0)<1<q(a) and m=2 tearing mode is stabilized if β(0)>0.02. Other parameters are: R/a=3, s=2.25, q(a)/q(0)= 2.52, $\rho_i/a=1/200$, $\langle\beta\rangle\sim 0.4\beta(0)$, $T_e=T_i$, $M_i=1836M_e$. n is always chosen to be unity.

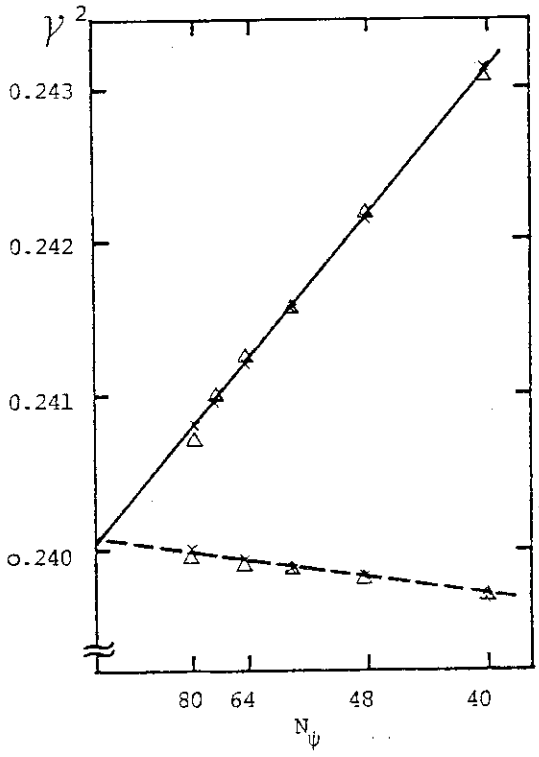

Fig. I.3-1 The convergence curve of the eigenvalue, γ^2, of the n=2 internal mode for the Solove'v equilibria. The flux coordinates used in the computation are the natural (solid line) and equi-arc length (dotted line) coordinates, respectively. The symbol × and Δ denote the results by the ERATO1 and the new interface module, respectively.

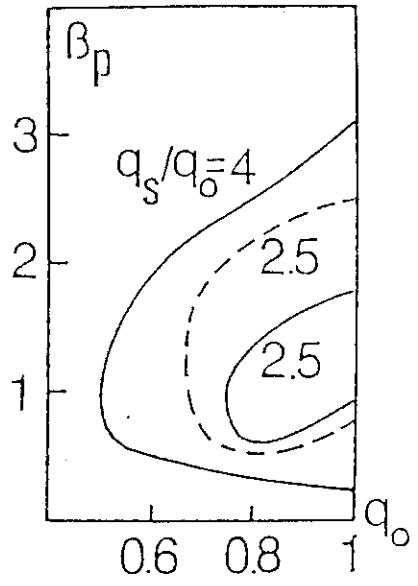

Fig. I.3-2 The stability diagram of the internal kink mode. Solid and dashed lines are for the circular and elliptic equilibria, respectively.

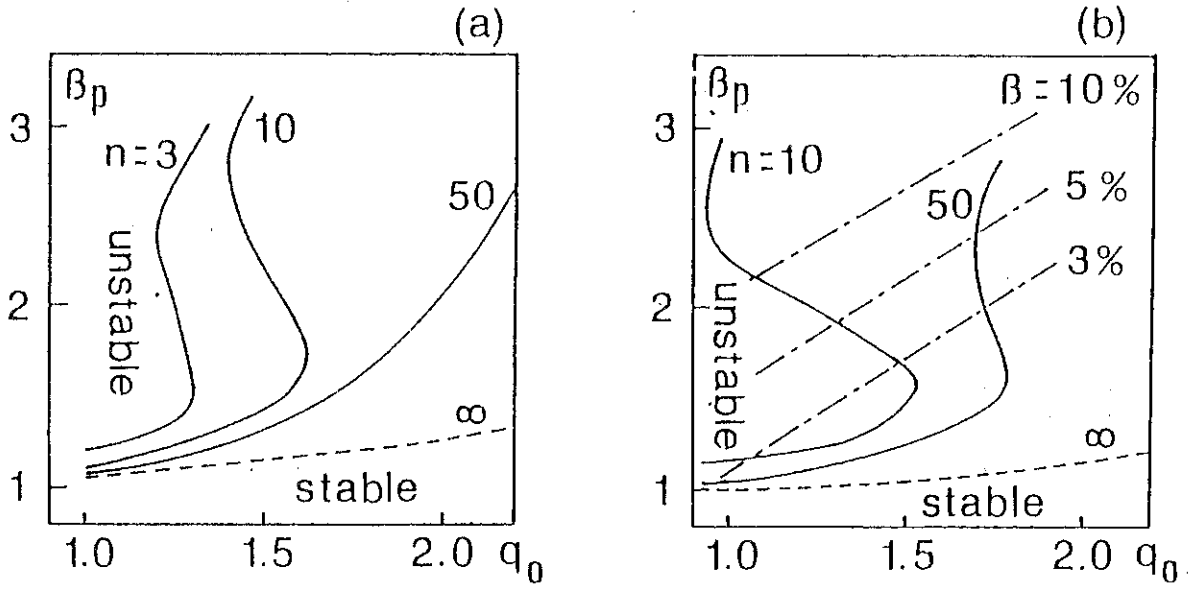

Fig. I.3-3 Finite-n ballooning modes: stability diagrams for peaked (a) and flat (b) pressure profiles.

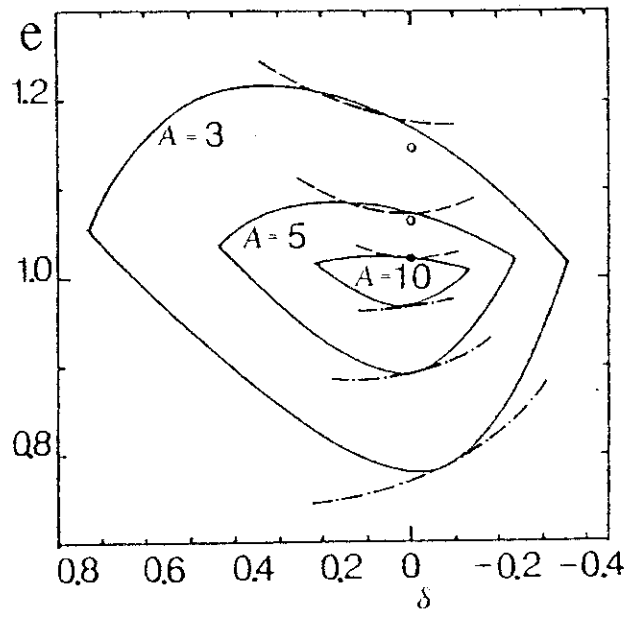

Fig. I.3-4
Stability diagram of the positional instability for the Solov'ev equilibrium (ellipticity e vs. triangularity δ, $R_{ext}=\infty$, $q_0=1$). Broken and dotted broken lines denote the stability limits determined by the magnetic field decay index n_i=0.0 and 1.5, respectively.

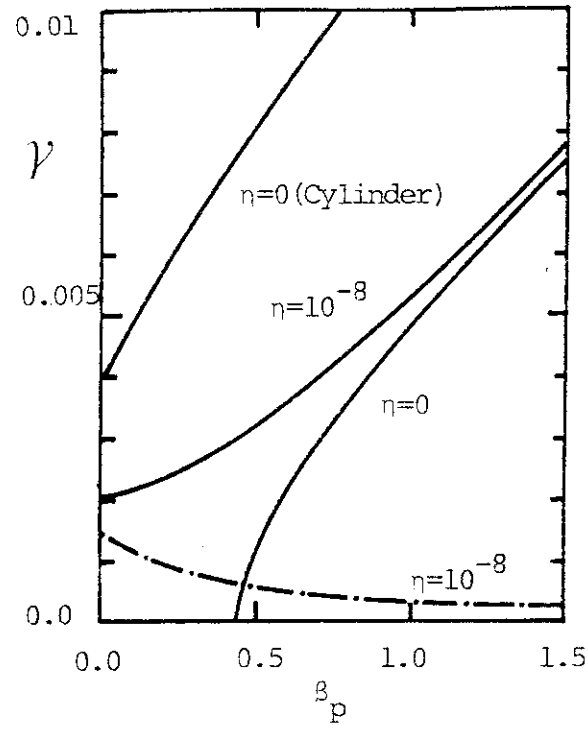

Fig. I.3-6 Dependence of growth rate of the m=1 resistive internal kink mode on β_p. Dotted broken line shows the result by the conventional reduced set of equations. Parameters are: A=10, $q(r)=\{0.91+(r/0.718)^4\}^{1/2}$, $p(r)\propto(1-r^2)$.

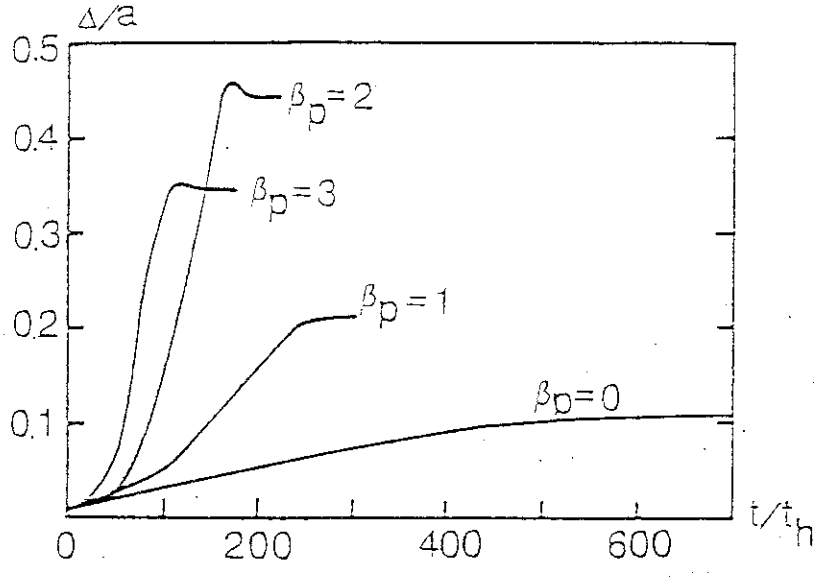

Fig. I.3-5 Time evolution of the m=3/n=2 magnetic island width for different β_p.

II. TOROIDAL CONFINEMENT EXPERIMENT

1. Introduction

After 11 years operation, the JFT-2 tokamak had been shut down on June, 1982. The last experiment of JFT-2 in this period were, transport study with intense additional heating, thereby, extended ICRF heating study, especially on electron heating by Bernstein wave mode conversion, was examined. Current drive study with lower hybrid wave was also made. Main concern in this study is shift down of wave phase velocity in the plasma column and its effect on driven current profile. The results of theses studies are described in subsections 2, 3 and 4.

On the other hand, manufacturing of the JFT-2M tokamak has been initiated from April, 1981. Installation of JFT-2M instead of JFT-2 is almost completed in March, 1983. In other words, this means 1 month is dedicated to removing the JFT-2 tokamak, 3 months to spadeworks on tokamak itself and poloidal field power supply, 5 months to assembling and preoperational test of all components including 2 MW NBI.

Initial start up of JET-2M is to be commence on April, 1983. In addition ICRF upgrading to 4.5 MW, fabrication of ECRH system of 60 GHz 200 KW and some diagnostics are on going in 1983. The experimental study with these is supposed to be commence on the early spring, 1984, when beta study with ICRF heating, and current startup and drive with LHRH and ECRH are main objectives.

Construction of poloidal field power supply for non-circular plasma shape are now on schedule. So that, we will achieve full modernization from JFT-2 to JFT-2M in about the early spring, 1985, when 500 kA D shape plasma with optimized additional heating will be in our hand. Another interest in the JFT-2M study is to cast some lights on behavior of edge plasma. Open type magnetic limiter configuration of JFT-2M is useful for this study. Furthermore, pellet injection and pump limiter system are also planned and prepared in 1983 for studing some versions of edge plasma control. Construction and commissioning of the JFT-2M tokamak is described in subsection 5.

2. Transport Study with Intense Additional Heating

2.1 Plasma properties of intense additional heating[1)]

The effects of intense heating with neutral-beam injection (NBI) and the ion-cyclotron range of frequency (ICRF) on transport processes have been studied in the JFT-2 tokamak, and the following results are obtained: (1) Typical global energy confinement time τ_E is about 10 ms in beam-heated discharges of 0.3 to 1.7 MW, and about 20 ms in only Ohmically heated discharges under optimum conditions. The global energy confinement time in beam-heated plasma depends weakly on plasma density ($\propto n_e^{1/2}$, as shown in Fig. II.2-1), and the toroidal magnetic field, but increases with plasma current ($\propto I_p^{5/4}$). Up to an additional net power level of 2.2 MW (1.7 MW NBI and 0.5 MW ICRF), the increase in poloidal beta is roughly proportional to the additional input power. (2) The global particle confinement time in beam-heated discharges is 20-30 % lower than for Ohmic heating. (3) The density clamp observed during beam heating is due to decreased recycling rate of neutrals from the plasma boundary. (4) The toroidal plasma rotation induced by the momentum input associated with NBI is unimportant in global confinement of high-β plasma. (5) Slow impurity accumulation occurs during counter-injection[4)]. (6) Sawtooth oscillations change into the continuous mode when β_p exceeds a critical values. (7) Significant plasma heating is observed with simultaneous NBI and ICRF heating. With a net additional power of 2.2 MW (1.7 MW NBI and 0.5 MW ICRF) into D^+ plasma at a plasma density of 6×10^{13} cm^{-3}, the central ion temperature increases from 0.4 to 1.4 keV.

2.2 Role of scrape-off and/or boundary layer on plasma confinement[1,2)]

The experimental results obtained in JFT-2 show that intense neutral beam heating does not significantly affect the hydrogen ion conduction near the plasma centre. However, even with the low beam injection of 0.3 MW comparable to Ohmic input power, apparent deterioration in τ_E was observed.

In this section, we discuss the role of scrape-off and/or boundary layer on the global plasma confinement in the beam-heated discharges.

In both cases of beam-heated and Ohmically heated discharges, substantial increases in a plasma density $\bar{n}_e$ are achieved via gas

puffing. Neutral injection into discharges with linearly rising $\bar{n}_e$ (fed by a constant gas puff) results in a "clamp" of $\bar{n}_e$ shortly after the beam turned on. Intense constant gas puffing can restore the slope of $\bar{n}_e(t)$ to its original value before the neutral beam injection, and this puffing has been used for the high density operation.

The density clamp phenomenon is explained by the following mechanism. A relatively large amount of injected power is deposited around the plasma boundary and increases the plasma boundary temperature, compared with the Ohmically heated discharge. The increase in sheath potential decreases the reflection coefficient of the incident ion flux onto the wall (or limiter). In addition, the low temperature neutral gas via the gas puffing is ionized near the plasma boundary, including the scrape-off, because the ionization rate of hydrogen increases with the temperature in the range ($T_e \lesssim 100$ eV). Thus, the density clamp occurs. To overcome the density clamp, the intense gas puffing is necessary as mentioned above. The cooling effect due to low temperature neutrals is much less than for Ohmically heated discharges and the boundary temperature is still high enough to ionize the low temperature neutrals, because the birth profile of fast ions depends on plasma profile and the large amount of the injected power is deposited around the boundary, including the scrape-off. Thus, broader density profiles are inevitably obtained in high density regions. At the same time, the scrape-off density in beam-heated discharge becomes much larger than for the Ohmically heated discharge, as shown in Fig. II.2-2. The higher plasma density at the plasma boundary region increases the deposition power near the boundary and decreases the deposition power of the plasma centre, as shown in Fig. II.2-3.

Thus, the density profile control may be one of the key factors in improving τ_E in beam-heated discharges.

2.3 Thermal load test of a TiC coated Mo limiter with beam-heated discharge[3)]

A TiC coated Mo material has been tested as a limiter in the JFT-2 tokamak. The surface temperature of the limiter is measured with an infrared scanning camera. The maximum surface temperature rise during a steady state discharge with a neutral beam power of 0.7 MW is around 230°C in 25 ms and the heat flux density to the limiter is 1-4 kW/cm^2. The maximum temperature rise during a current disruption with the beam

power of 1 MW is about 100°C in 100-600 μs and the density is the order of 50 kW/cm^2. The TiC coated Mo material can be proof against such a high load.

References

1) Yamamoto, S., Maeno, M. Sengoku, S., et al., in plasma Physics and Controlled Nuclear Fusion Research (Proc. 9th Int. Conf. Baltimore, 1982) Vol.1, IAEA, Vienna (1983) 73
2) Yamamoto, S., "JFT-2 Experiments with Additional Heating", in Proc. of US-Japan Workshop on "Anomalous Transport and Critical Beta Value", March 1983
3) Maeno, M., Sengoku, S., Nakamura, H., et al., Jpn. J. Appl. Phys. 21 (1982) 773
4) Kasai, S., Hirayama, T., Yamauchi, T., Sugie, T., Yamamoto, S., Maeno, M., Sengoku, S., Suzuki, N., Miura, Y., Kawashima, H., Ogawa, H., "Time- and Spatial-behaviors of Metal Impurity During Neutral-Beam Injection on the JFT-2 Tokamak", JAERI-M 82-164 (November 1982)

3. Study of the Current Drive by the Lower Hybrid Wave in the JFT-2 Tokamak

In this section, we decribe the calculation model indicating the coupling between the lower hybrid wave and electrons in a tokamak and then compare with the experimental results which were obtained in the JFT-2 tokamak. In particular, we investigated numerically the rf power deposition and the generated current by using a Fokker-Planck equation.

3.1 Calculation model

The rf interaction with electrons in tokamaks depends on a substantial amount of the rf power density and application of a large amplitude LH waves can strongly modify the electron velocity distribution function in the region of resonant electrons. However, binary collisions and/or losses of the resonant electrons tend to restore thermal equilibrium, thus is establishing startionary distribution function and wave absorption. The evolution of the distribution function in a tokamak is described by a coupled quasilinear Fokker-Planck equation with the loss term resulting from magnetic fluctuations[2,3]. Solving

the Fokker-Planck equation and wave damping in the WKB approximation at a local position under the steady state condition, we calculated the rf power density absorbed by the resonant electrons $P_{ab}(r)$ and the generated current density $J_{rf}(r)$ with τ being the distance from the minor axis in cylindrical co-ordinates. The n_z-spectrum of the rf power flux at a boundary of the plasma column is calculated from the Brambilla Grill theory.

The value of n_z varies in space for propagation. The propagation of the LH waves in a tokamak plasma is described in a geometric optics limit by means of ray tracing technique. For simplicity, we take account of only spatial variation of $\hat{n}_{z0}$. Then the n_z-spectrum at the minor radius of r is approximated by $P_{rf}(r, n_z(r)) \simeq P_{rf}(r, n_{z0} + \Delta\hat{n}_{z0}(r)$ where n_{z0} is the initial n_z and $\Delta\hat{n}_{z0}(r)$ is the increment of $\hat{n}_{z0}$ for the propagation. The n_z of the slow wave must satisfy certain accessibility conditions ($n_z > n_{Lc}$ with being critical value), otherwise, it will be converted to the outward propagating fast wave[4].

We also use a cylindrical model of tokamak density and temperature profiles given by $n_e(r) = n_{e0}\{1-(r/a)^2\}^{\alpha n}$ and $T_e(r) = T_{e0}\{1-(4/a)^2\}^{\alpha T}$, respectively and spatial variation of toroidal magnetic field $B_t(r) = B_{t0}\, R_0/(R_0 + r)$. The total power absorbed and current generated in the torus are $P_{ab} = \int_o^a P_{ab}(r) 4\pi^2\, R_0 dr$ and $I_{rf} = \int_o^a j_{rf}(r)\, 2\pi r dr$, respectively. The total power balance on the rf power is represented as $P_{rf}(a) = P_{ab} + P_f + P_t$ where P_f is the rf power converted into the fast waves and P_t is the slow wave power undamped until the center.

It should be noted that power absorbed by the resonant electrons goes into increasing the thermal energy $P_d(r,n_z)$ and enhancing the diffusion losses by the magnetic fluctuations. The ratio of two powers is given approximately by their respective time scales,

$$\frac{P_{ab}(r,n_z) - P_d(r,n_z)}{P_d(r,n_z)} = \frac{(v/\tau_E^* V_{Te})}{\nu_0 (v/v_{Te})^{-3}}$$

where v and v_{Te} are the velocities of resonant and thermal electrons, respectively. ν_0 is the collision frequency and τ_E^* is the energy confinement time. This effect reduces the efficiency of the bulk electron heating if the confinement of electron energy is poor compared with the collision time.

3.2 Calculated results and comparison with the experimental results

To compare with the experimental results obtained in the JFT-2 tokamak[5] the calculation was made under the following conditions; B_{t0} = 1.0 T, $n_{e0} = 0.9 \times 10^{19}$ m^{-3}, $\alpha_n = 2.0$, $T_{e0} = 550$ eV, $\alpha_t = 1.5$, $P_{rf}(a)$ = 130 kW and $\hat{n}_{z0} = 5.5$ (corresponding to $f_0/f_{lh} = 2.3$ and $c/(\hat{n}_{z0} \cdot V_{Te}(0)) \simeq 5.8$ with c and $V_{Te}(0)$ being the velocities of light and the central thermal electrons, respectively).

Figure II.3-1 shows the poloidal projection of the LH wave ray trajectories and the radial variation of the n_z. It is found that the waves penetrate to the center of the plasma column and then propagate outward. It should be noted that the radial variations of n_z with the initial n_{z0} = 3, 5.5, 8 are nearly in parallel shift each other. This indicates the reasonable approximation on the radial variation of the n_z-spectrum mentioned above. Calculated spatial development of the rf power spectrum and the relevant electron distribution function are shown in Figs. II.3-2(a) and (b), respectively. It is noted that the waves having low n_z (high phase velocity) interact effectively with electrons in the periphery plasma and most of the rf power with low n_z components is absorbed outside of the plasma. The quasilinear plateau on the distribution function is formed responding to the n_z-spectrum of the rf field. Figure II.3-2(c) shows the radial profile of the rf power, deposited power on the bulk electrons and the rf driven current. Considerable rf power is seen to be absorbed outside of the plasma. Resultingly, the main rf driven current flows near the boundary of the plasma. The total driven current, which is integrated over the minor radius, is 39 kA which is in rough agreement with that estimated from $(\Delta V_\ell/V_\ell) \cdot I_p$. While the total deposited power on the bulk electrons is comparable to amount of the decrease in the Ohmic heating power due to the drop in the loop voltage. This result seems to be reasonable because a little change in the electron temperature during the rf pulse provided that the energy confinement time of the electron does not change.

The soft x-ray energy spectrum estimated from the calculated distribution function shown in Fig. II.3-2(b) is illustrated in Fig. II.3-3. In the calculation, the cross section for Bremsstrahlung was taken from rf. The intensity of the soft-x-ray was integrated along horizontal chord through the center of the plasma[6]. The calculated spectrum is in good agreement with the observed one. For reference, the spectrum

without the loss term is also shown in Fig. II.3-3. The present calculation model shows that the effective and central CD and/or EH can be expected if the confinement time of the electrons coupled to the LH waves is sufficiently large compared to the collision time of the coupled electrons.

References

1) Yamamoto, T., IAEA Technical comittee Meeting on Non-Inductive Current Drive in Tokamaks, Culham 18-21 April 1983
2) Chan, V.S., Chiu, S.L., and Ohkawa, T., Nucl. Fusion 20, 1165 (1980)
3) Mynick, H.E., and Strachan, J.D., Phys. Fluids 24, 695 (1981)
4) Glagolev, V.M., Plasma Phys. 14, 301 (1972)
5) Annual report of the Fusion Research and Development Center for the period of April 1, 1980 March 31, 1981. JAERI-M 82-027 56 (1982)
6) Gluckstern, R.L., and Hull, H.H. Jr., Phys. Rev. 90, 1030 (1953)

4. Ion Cyclotron Range of Frequency (ICRF) Heating

ICRF heating experiment in JFT-2 was finished at June, 1982. In JFT-2, pure high field side excitation was investigated in deuterium majority with hydrogen minority plasma, at frequency 18 MHz which is near fundamental cyclotron frequency for hydrogen. In the following, the results of ICRF heating in JFT-2 are briefly described.

4.1 Antenna and the loading impedance[1)]

Loop antenna in JFT-2 is a pair of quarter turn coils located at the inner side of the torus. The antenna is made of all metals and the center conductor plate is separated from the plasma by a double layer Faraday shield.

The loading resistance is critically dependent on the plasma position and weakly dependent on the plasma density. Inward shift of the plasma decreases the radius of the plasma, but the distance between the antenna and the plasma does not change. On the other hand, outward shift increases that distance. The loading resistance decreases from 1 Ω to 0.3 Ω by the outward plasma shift of 5 cm. The measured values well agree with the calculated values.

4.2 Heating mechanism[3∿5)]

The mode conversion theory predict that hydrogen concentration in a deuterium plasma n_H/n_D is a key parameter to determine absorption mechanism. The n_H/n_D scan, where the toroidal magnetic field is optimized so as to place the mode conversion layer near the center of plasma, indicates that the heating efficiency defined $(\Delta T_{e0} + \Delta T_{i0})\ \bar{n}_e/P_{net}$ is irrespective of n_H/n_D[1)]. The results are consistent with a mode conversion theory, which predict that almost all of the wave energy is converted to the ion Bernstein wave in the case of high field side excitation[2)]. However, absorption mechanism changes by the hydrogen concentration, as follows.

4.2.1 Ion heating regime ($n_H/n_D \lesssim 10\%$)[3)]

The most prominent feature in this regime is change of the power partitioning among deuterium and hydrogen as a function of n_H/n_D. From the relatively low density and low power experiment ($\bar{n}_e \simeq 3 \times 10^{13}$ cm^{-3}, $P_{net} \simeq 100$ kW), we obtained the following results.

a) In the very dilute minority region (n_H/n_D = 2∿4%), second harmonic deuterium heating is dominant. Significant proton high energy tail also appears, but the rf power coupled to protons is much smaller than the one to deuterons according to the power balance analysis with the Fokker-Planck calculation.

b) The rf power to protons increases with increasing n_H/n_D and has the maximum value at $n_H/n_D \sim 10\%$. At last, half of the absorbed power goes to the proton component at $n_H/n_D \sim 10\%$.

In fact, in the case of n_H/n_D = 2∿4%, a deuterium high energy tail is detectable. Figure II.4-1 shows the deuterium and hydrogen energy spectra before and after the rf heating. The charge exchange analyzer is oriented slightly off perpendicular with respect to the toroidal magnetic field. A high energy tail is observed in the deuterium spectrum. The population of the high energy tail of deuterium increases as decreasing the plasma density, and as increasing the ICRF power.

The calculated distribution functions for the deuterium and hydrogen by two dimensional Fokker-Planck code are also shown in Fig. II.4-1. By comparing the experimental results with the calculation, rf power sus-

taining the high energy tails of deuterium and hydrogen are estimated, and the power of collisional transfer from electron to deuterium and the ion loss power due to conduction and convection are also estimated by 1-D tokamak code. The results of ion power balance study are summarized in table II.3-1. The input power and loss power are almost equal within permissible error. Thus, it is shown that in the dilute minority case, the second harmonic cyclotron damping is the dominant mechanism of ion heating[4].

The neutron measurement also reveals the high energy tail of deuterium. The correlation between the neutron count rate and the deuterium temperature is shown in Fig. II.4-2. The neutron emission is roughly proportional to T_{iD}^{4}[4] for maxwellian distribution. But in the case of Fig. II.3-1, the neutron counts are enhanced compared to other cases. This shows that the deuterium high energy tail enhances the neutron emission. The enhancement factor is consistent with the population of high energy tail in the deuterium energy spectrum[4].

Figure II.4-3 shows temperature profiles of the ion and electron in the case of $n_H/n_D = 2\sim4\%$, $n_e \simeq 5\times10^{13}$ cm^{-3} and $P_{net} \simeq 500$ kW. 1-D tokamak code is employed to analyze experimental electron and ion temperature profiles by assuming the ion and electron heat conduction coefficient to be neoclassical and $2\times10^{19}/n_e(m^{-1}s^{-1})$, respectively. From this analysis, it can be said that at least 60 % of rf power is absorbed by ion within 7 cm radius and electron does not absorb the rf power. Thus, the centrally peaking deposition profile is confirmed from the temperature profile analysis[5].

4.2.2 Mode conversion regime ($n_H/n_D \simeq 30\%$)[3,5]

In this region, the mode conversion is a dominant heating process. In order to obtain information about the power deposition profile, B_T was scanned from $12\sim15.5$ kG with fixed $n_H/n_D \simeq 30\%$, which corresponds to $0 \leq (R_{CR}-R_0)/a \leq 1.13$, where R_{CR} is major radius position of the cyclotron resonance layer.

Figure II.4-4 shows the increase of the central electron and ion temperature normalized by P_{net} as a function of B_T. It is found that both electron and ion temperatures have the maximum at $B_T = 15$ kG, where the mode conversion layer is 7 cm out from the plasma center. In contrast to the ion heating regime, the maximum increase of the temperature is obtained when the mode conversion layer is shifted by a certain length

out from the vessel axis.

The reason of this shift can be explained by the propagation characteristics of ion Bernstein waves. The fast wave excited from the high field side propagates to the mode conversion layer, and is converted to the ion Bernstein wave. The ion Bernstein wave propagates and returns back to the high field side. During wave propagation, the wave is absorbed by electron Landau damping. Therefore, the electron absorption region shifts slightly toward higher field side of the mode conversion layer. This explanation is confirmed by a ICRF ray tracing code and full wave kinetic code.

As is shown in Fig. II.4-4, significant increase of ion temperature at $B_T = 15$ kG cannot be explained by power transfer from electron to ion. Some mechanisms of the ion heating must exist in this regime. It becomes evident that the ion heating is sensitive to the amount of impurity ions such as Fe and Ti.

4.2.3 Origin of impurity during ICRF heating[3)]

Origin of impurity production was examined in the mode conversion regime ($n_H/n_D = 30\%$), where no energetic tail of minority species are observed in the plasma core. Figure II.4-5(a) shows B_T dependence on increment of Ti XII line intensity. Other impurity lines such as OVI, CIV, FeXV and MoXIII and total radiation loss showed similar behavior.

At the same time, we observed a fast ion flux(I_f) in the scrape off layer as shown in Fig. II.4-5(b), using an ion sensitive probe which can extract ions with energy higher than 1 keV. The probe was located at $R = 95$ cm and was scanned vertically. It is worth while noting that there is strong correlation between I_f and I_{TiXII}.

It seems that I_f begin to increase when the cyclotron layer across the antenna, that is, $B_T = 12$ kG. The probe signal I_f had a peak value at $Z = 27 \simeq 29$ cm by scanning the probe in the z direction. This indicates that the fast ions are localized in the scrape-off layer.

It can be concluded that the significant increase of impurity in lowering B_T has a strong correlation with fast ions localized in the plasma periphery. Taking into account the B_T-dependence and the electron density in the production region of the fast ions ($n_e = 5 \sim 20 \times 10^{10}$ cm^{-3}), coupling to the slow wave may be a possible explanation of these observation.

References

1) JFT-2 Group, in Proc. 3rd Joint Varenna-grenoble Int. Symposium, Vol.I 225, Vol.III 1099, 1191, Grenoble, Mar. (1982).
Kimura, H., Matsumoto, H., et al., JAERI-M 82-046 (1982).
2) Iizuka, S., et al., Phys. Rev. Lett. 45 (1980) 1256.
3) Kimura, H., et al., 9th Int. Conf. on Plasma Phys. and Cont. Nucl. Fusion Research, Baltimore, Sep. 1982 paper CN-41/J-3.
4) Miura, Y., Matsumoto, H., et al., "Analysis of Charge Exchange Spectra during ICRF Heating in JFT-2 Tokamak", submitted to Nucl. Fusion.
5) Matsumoto, H., Kimura, H., et al., "Power Balance Analysis of ICRF Heating Experiments in JFT-2 Tokamak", to be published in Nucl. Fusion.

5. Construction and Commissioning of the JFT-2M Tokamak

5.1 Tokamak machine

The photo of the completed JFT-2M tokamak is shown in Fig. II.5-1, including diagnostics. The vertical cross section is shown in Fig. II.5-2. The D shape vacuum vessel (415×595 mm) is made of stainless steel of 25 mm thickness, with two Tefron breaks which are shunted by SiC nonlinear resistors. The skin time of the vacuum vessel is nearly 7 ms and the baking temperature is 120 °C. The vacuum condition in the preoperational test without plasma is 5.5×10^{-8} torr of base pressure and $3\text{-}5\times10^{-9}$ torr l/sec of He leakage in each gaskets. Plasma radius is limited by back-up limiter (350×530 mm fixed) and by three movable limiters (outer, upper and lower side, graphite). Maximum toroidal field is 14.5 kG on geometrical center of the vacuum vessel and this toroidal field is produced by 16 coils. Poloidal coil system is composed by sub coils inside the toroidal coil (V_1, V_2, Q_1 and Q_2 in Fig. II.5-2) and main coils outside the toroidal coils (S_1, S_2, S_3 and OH). Power supply system for this poloidal coil is shown in Fig. II.5-3. The S coil power supply feeds the current to S_1, S_2 and S_3. The OH power supply to OH coil and the V_{up} to the upper coils of V_1 and V_2. The V_{low} to the lower coils of V_1 and V_2. Power supplies for Q series coils are supposed to be constructed in 1985. Each poloidal coil has several taps so as to optimize the relation among the plasma current, vertical field, the plasma position and shape. The S and OH coils power supplies are composed with capacitor bank for current start-up and thyrister rectifier

unit for constant current phase. A circular plasma of 300 kA plasma current will be achieved by this scheme of poloidal coil power system.

5.2 Plasma position control

The thyrister power supplies have minor current and voltage feed back loop themselves. Preprogrammed reference command for these power supplies are produced by mini digital computor and combined with the signal from plasma position sensers, such as flux probe (ψ) magnetic probes (B_θ,B_ρ), etc. This combined signal drives the PID controllers. All systems are composed with analog type operational amplifyers. A schematic example of this position control system is shown in Fig. II.5-4, where the hybrid control of vertical and horizontal position scheme is also described. That is, the difference of the vertical field of the two power supplies V_{up} and V_{low} generates the horizontal field. This method does not need a particular control system for horizontal position control. In this method, it is not required for a thyrister power supply to generate both positive and negative currents. Therefore, we can symplify the coil arrangement near tokamak.

5.3 Test of poloidal coils and power supplies

Poloidal magnetic fields produced by each coil were measured with hall detectors to estimate the fields by image current of the iron core. Experimental data showed a good agreement with values calculated by both analytic and computational methods. Coupling characteristics between different series of poloidal coils are also examined with measurement of the induced voltages of open circuit coils. On this basic data, we can estimate the magnetic configuration of flux swing, position, shape and so on.

Power supplies for OH and S coils are composed of a capacitor bank and thyrister unit as is shown in Fig. II.5-3. In this case thyrister unit should be protected from the high voltage from the capacitor bank. Meanwhile, capacitor bank should be fired under the condition of strong coupling between OH and S coils. Therefore, protective diode stacks are inserted between capacitor bank and thrister unit, and appropriate inductance between each capacitor bank and coil. Final check of system operation without plasma was carried out with simulating Q_2 coil as a plasma ring. All of system worked satisfactory and preoperational test was finished in March.

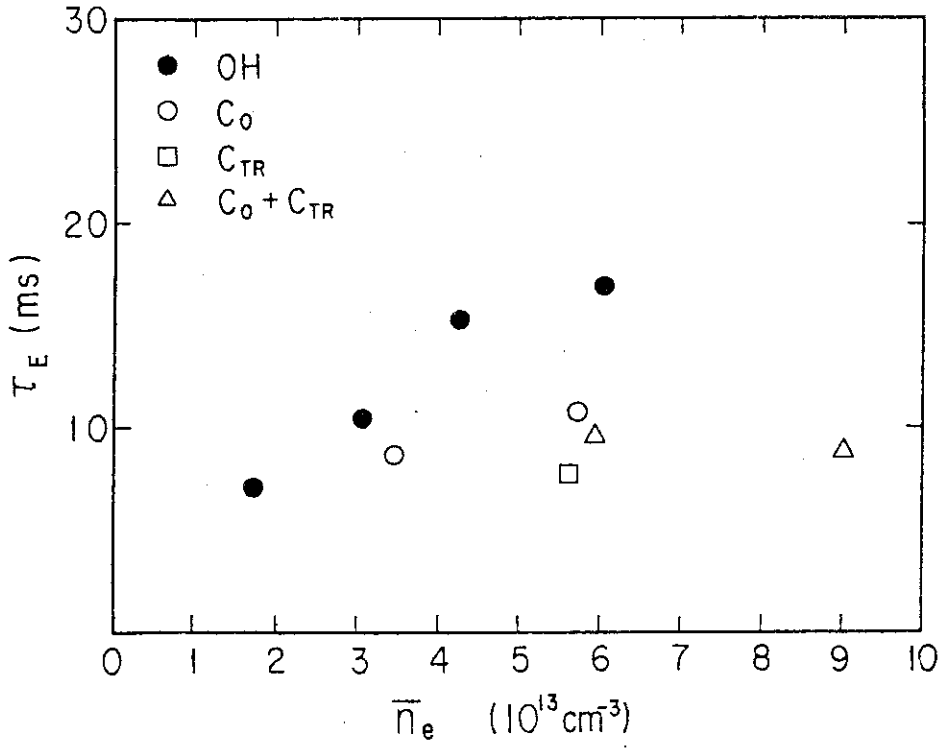

Fig. II.2-1 Global energy confinement time τ_E vs. line averaged plasma density. (●): Ohmically heated discharge, (○): 1 MW Co, (□): 1 MW Ctr, (△): 1 MW Co + 1 MW Ctr. B_T=(1.2-1.4)T, I_p=(120-140)kA, a_p=(22-25)cm.

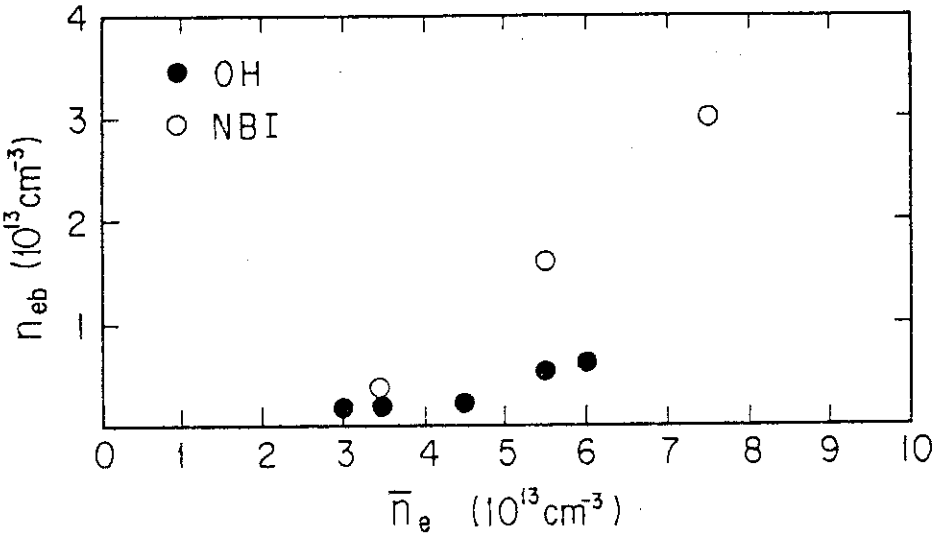

Fig. II.2-2 Scrape-off density n_{eb} vs. line averaged plasma density $\bar{n}_e$. (●): Ohmically heated discharge, (○): 1 MW Co, B_T=(1.2-1.4)T, I_p=(120-140)kA, a_p=(22-25)cm.

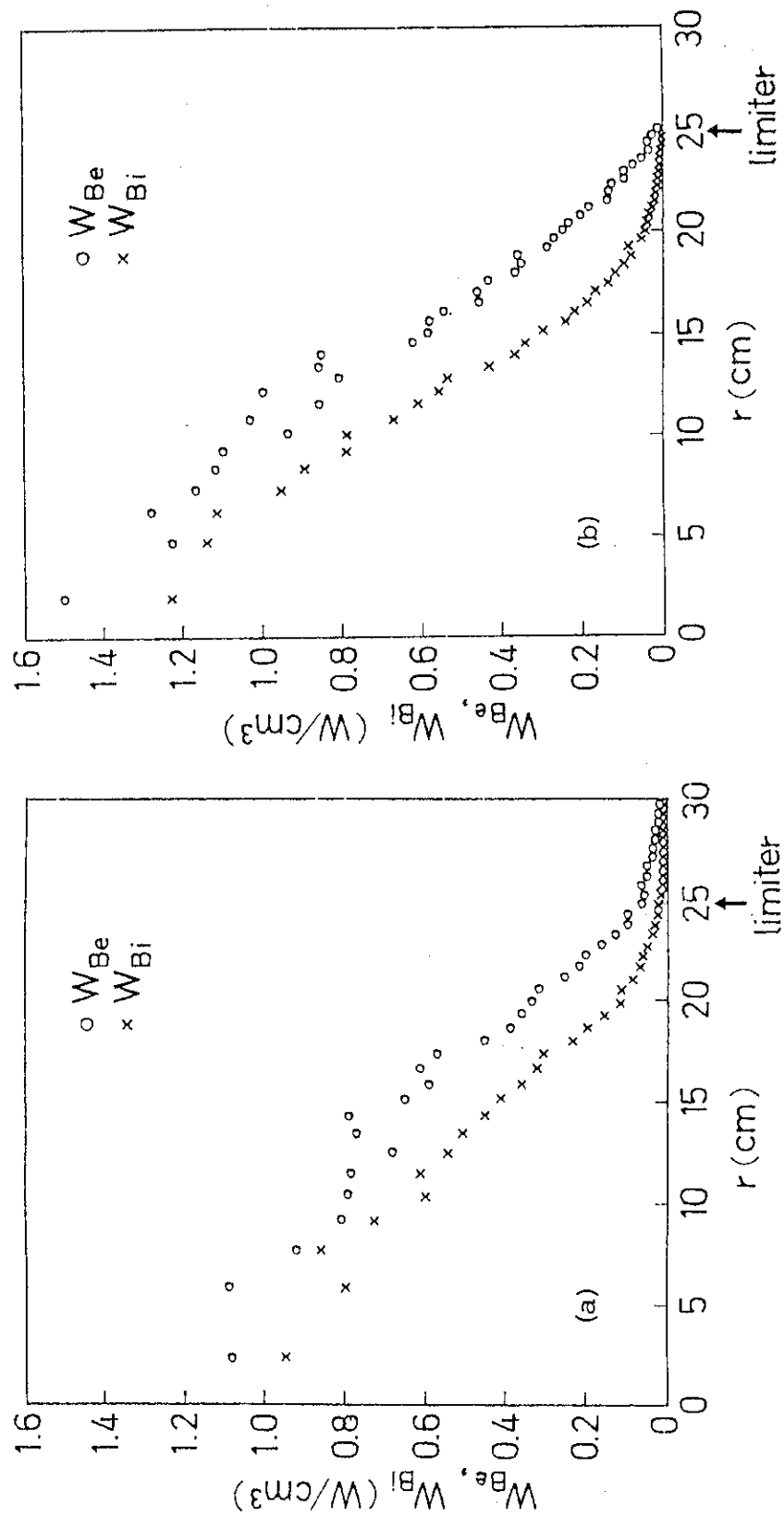

Fig. II.2-3 Power deposition profiles for experimentally observed plasma density: (a) including scrape-off density, (b) without including scrape-off density. W_{Be}: power deposition to electron, W_{Bi}: power deposition to ion.

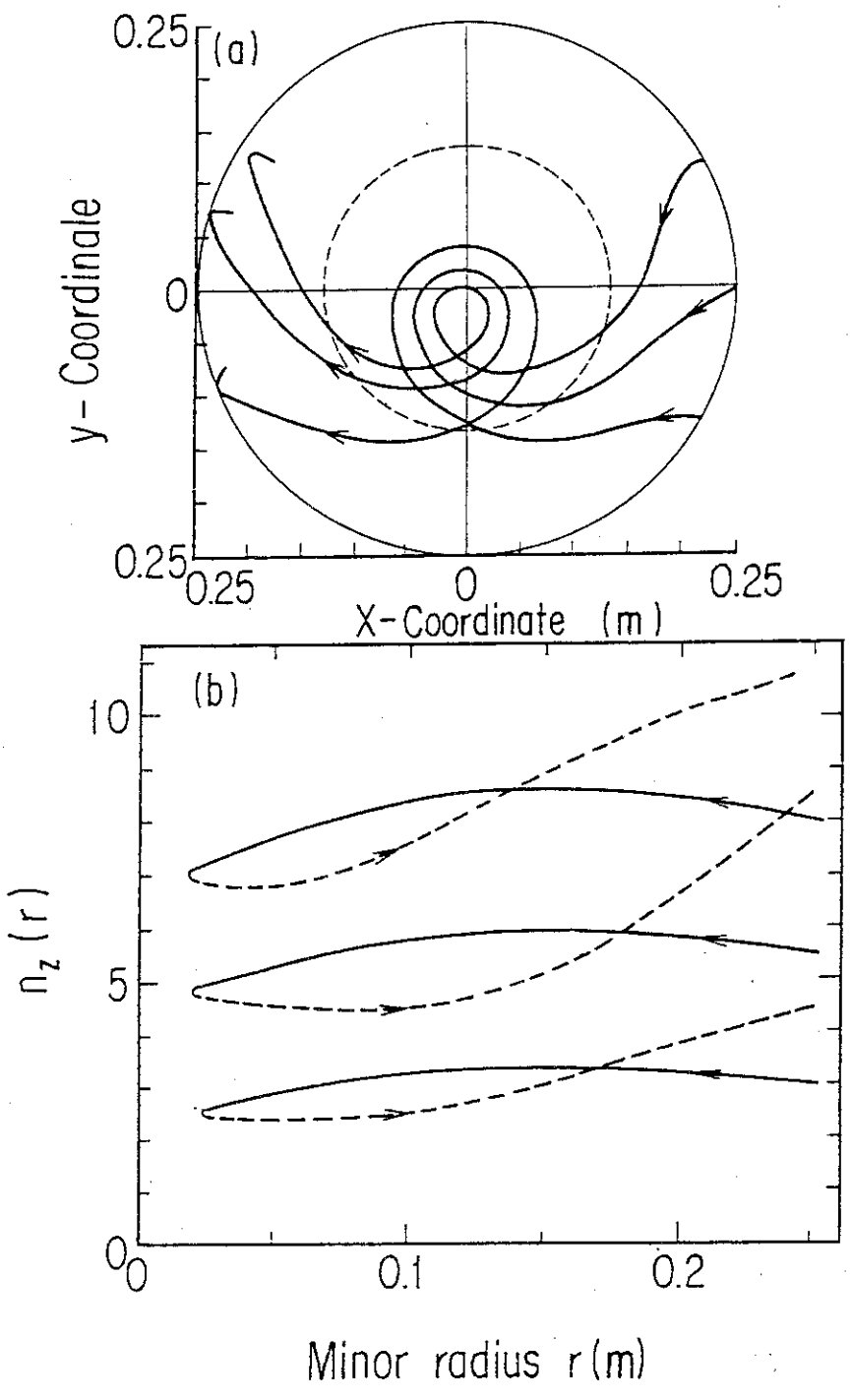

Fig. II.3-1 (a); wave trajectories in poloidal section at n_{z0}=5.5. (b); the spatial evolution of n_z as function of the ray for three initial values of n_{z0}=3, 5,5 and 8.

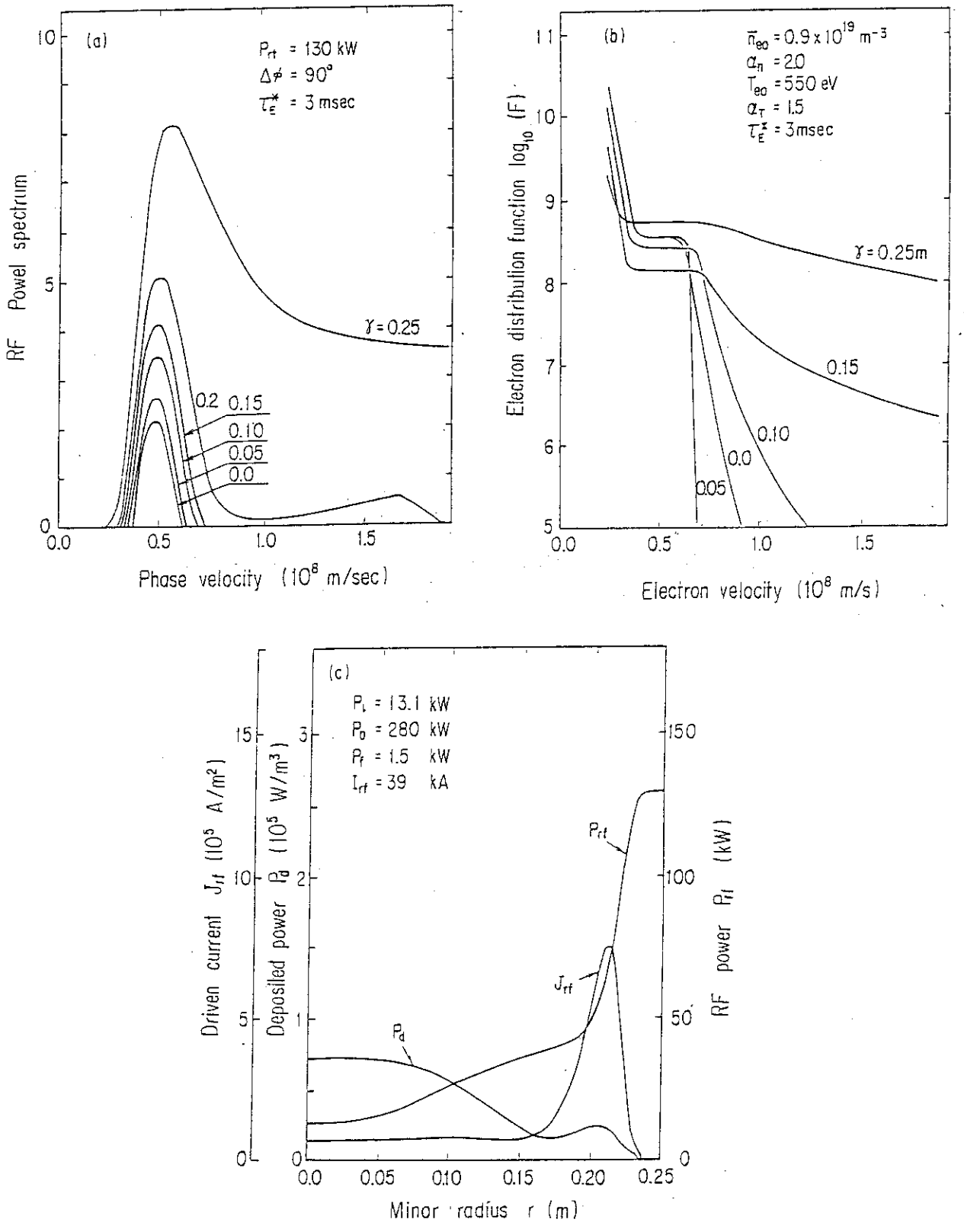

Fig. II.3-2 (a); the radial evolution of the rf power spectrum with respect to the phase velocity. (b); the radial evolution of the electron distribution function. (c); the radial profiles of the rf power P_{rf}, the deposited power P_d and the driven current J_{rf}. The calculation was made under the conditions described in the text.

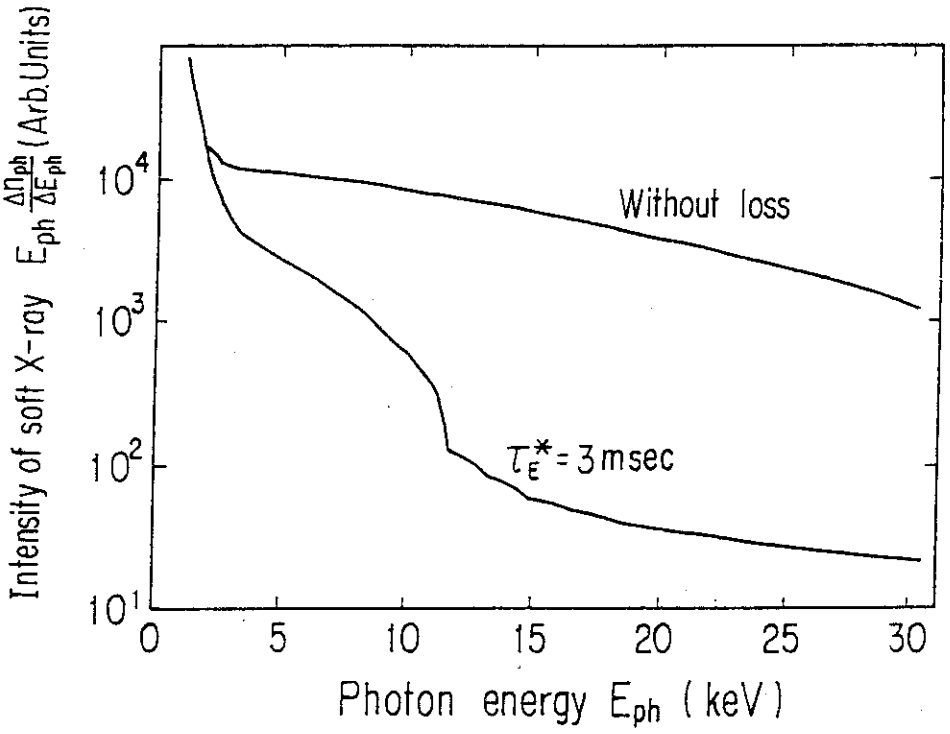

Fig. II.3-3 The calculated soft x-ray energy spectrum for the same conditions as in Fig. II.3-2. The spectrum was integrated along the horizontal chord through the center of the plasma assuming the uniform enhancement factor over the plasma core.

Table II.4-1 Ion Power Balance

Input power	=	0.35 ~ 0.56 W/cm^3
RF		0.21 ~ 0.41 W/cm^3
Hydrogen		0.08 ~ 0.09 W/cm^3
Electron		~ 0.06 W/cm^3
Loss power	=	~ 0.47 W/cm^3

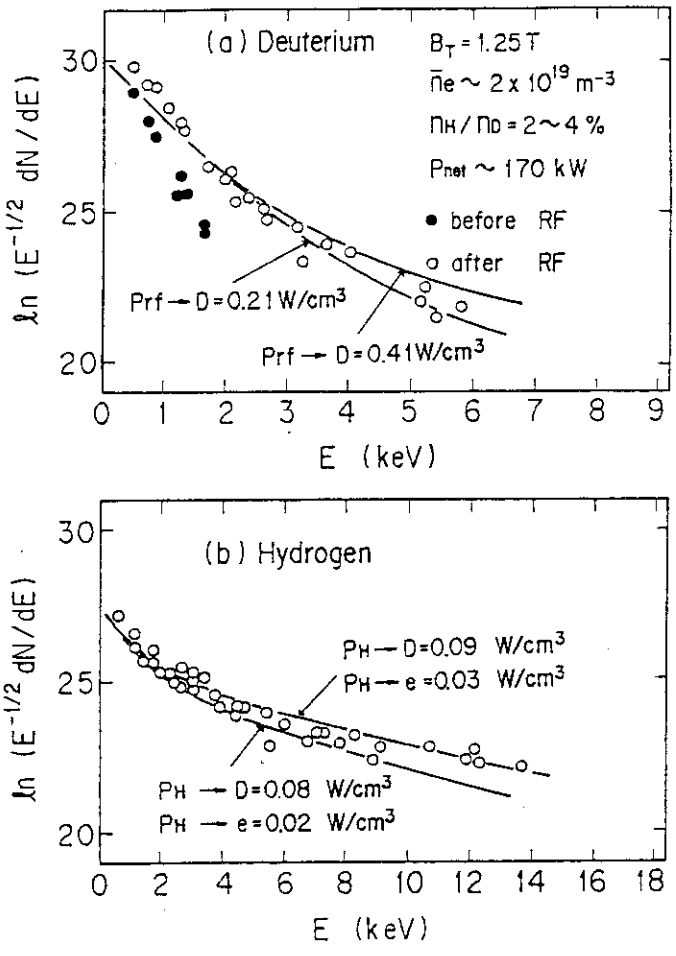

Fig. II.4-1 Charge exchange spectra of (a) deuterium and (b) hydrogen in the dilute minority case. Solid lines show the calculated distribution function which fits the experimental data.

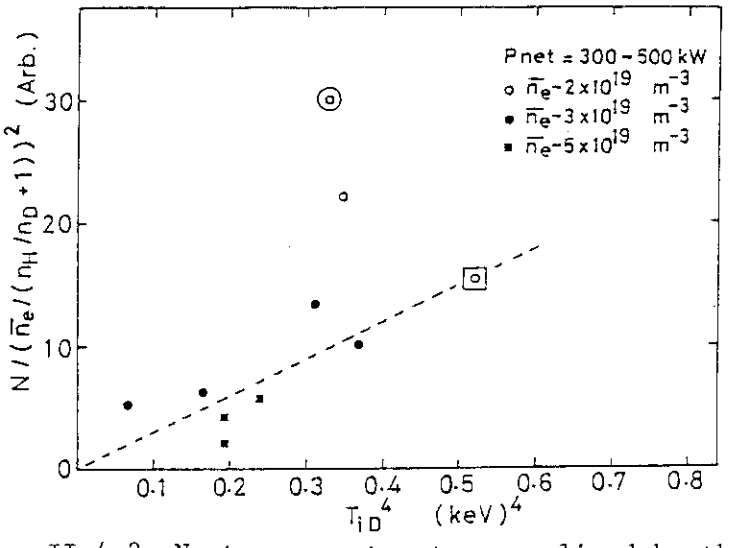

Fig. II.4-2 Neutron count rate normalized by the deuterium average density versus T_{iD}^4, where P_{net}=300-500 kw. shows ◎ the low density and the dilute minority case.

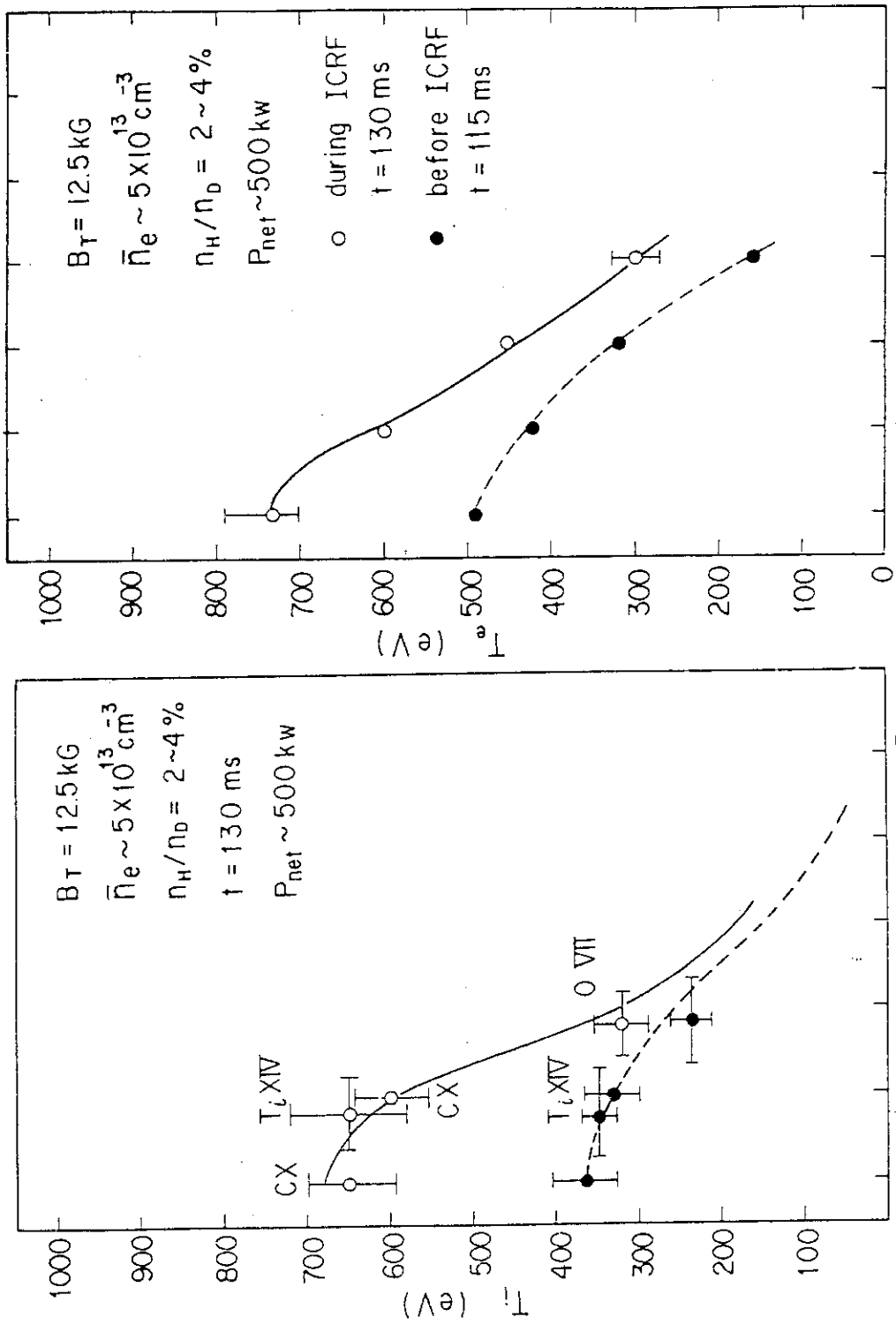

Fig. II.4-3 Temperature profiles of (a) ion and (b) electron during and before ICRF heating for the ion heating regime.

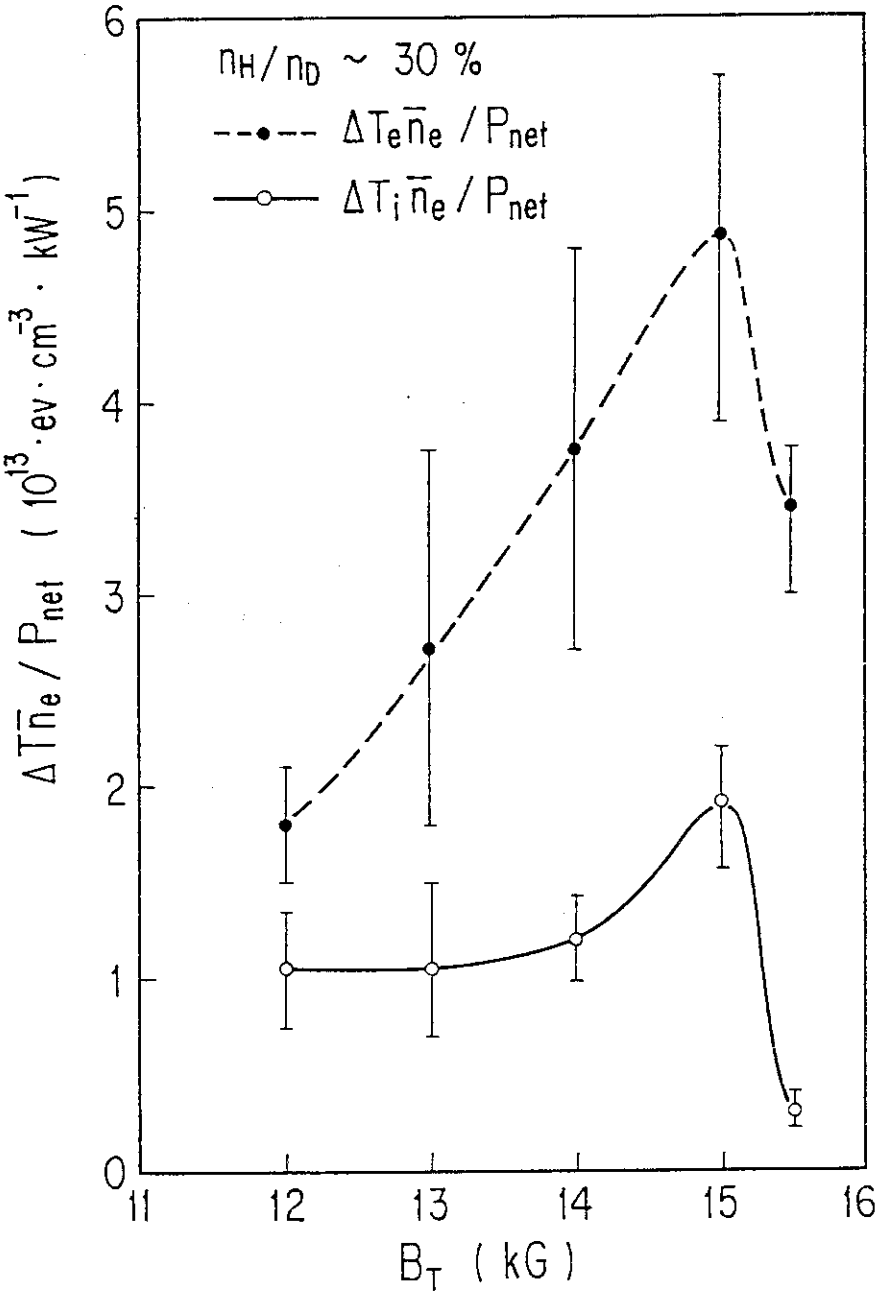

Fig. II.4-4 Increase of central electron and ion temperatures normalized by the net RF power and the electron density versus toroidal magnetic field B_T with n_H/n_D fixed at 30%.

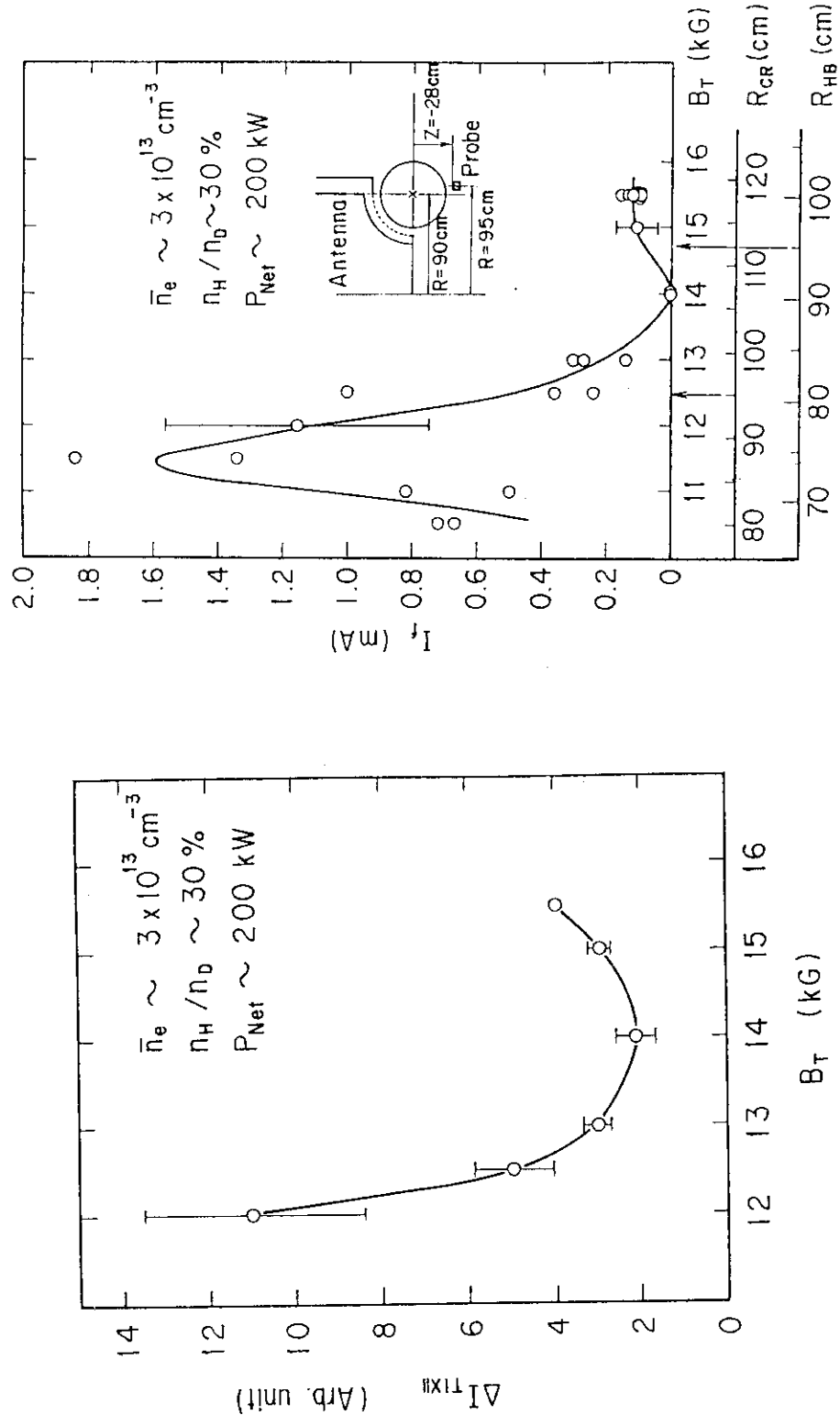

Fig. II.4-5 (a) Increment of spectral line intensity of Ti XII as a function of toroidal field in the mode conversion regime. (b) Corresponding data of fast ions measured by ion sensitive probe located in the scrape-off layer. The position of the probe, which is set on the ion toroidal drift side, is R=95 cm and Z=-28 cm. Horizontal axis indicates corresponding positions of cyclotron resonance layer R_{CR} and two-ion hybrid resonance layer R_{HB}.

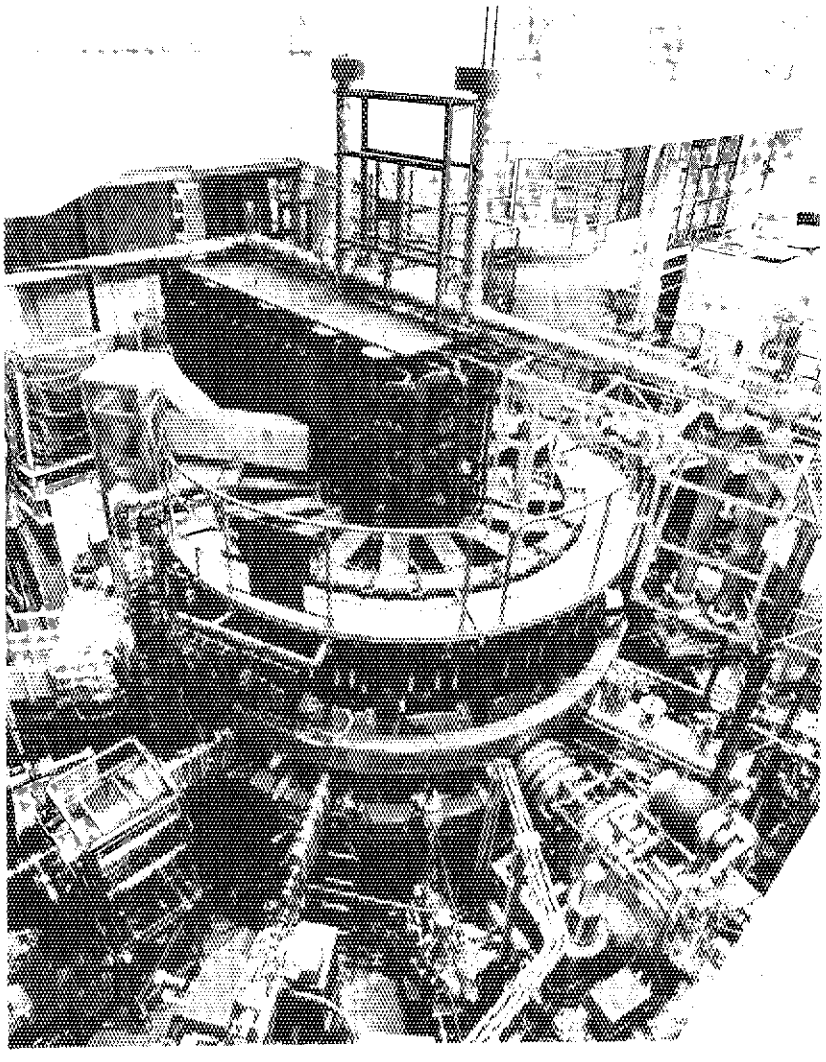

Fig. II.5-1 Photograph of the JET-2M tokamak.

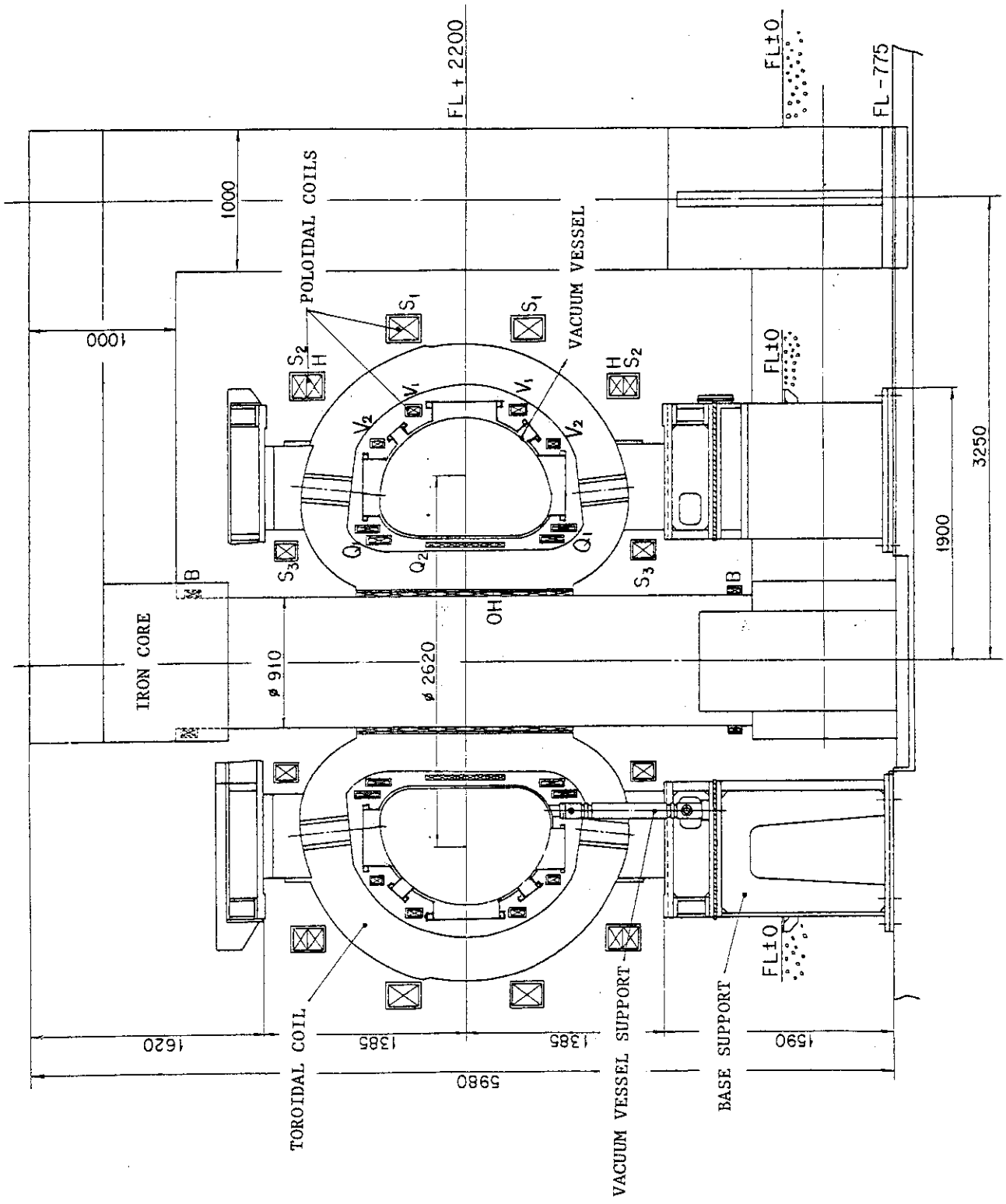

Fig. II.5-2 Vertical cross section of the JET-2M tokamak.

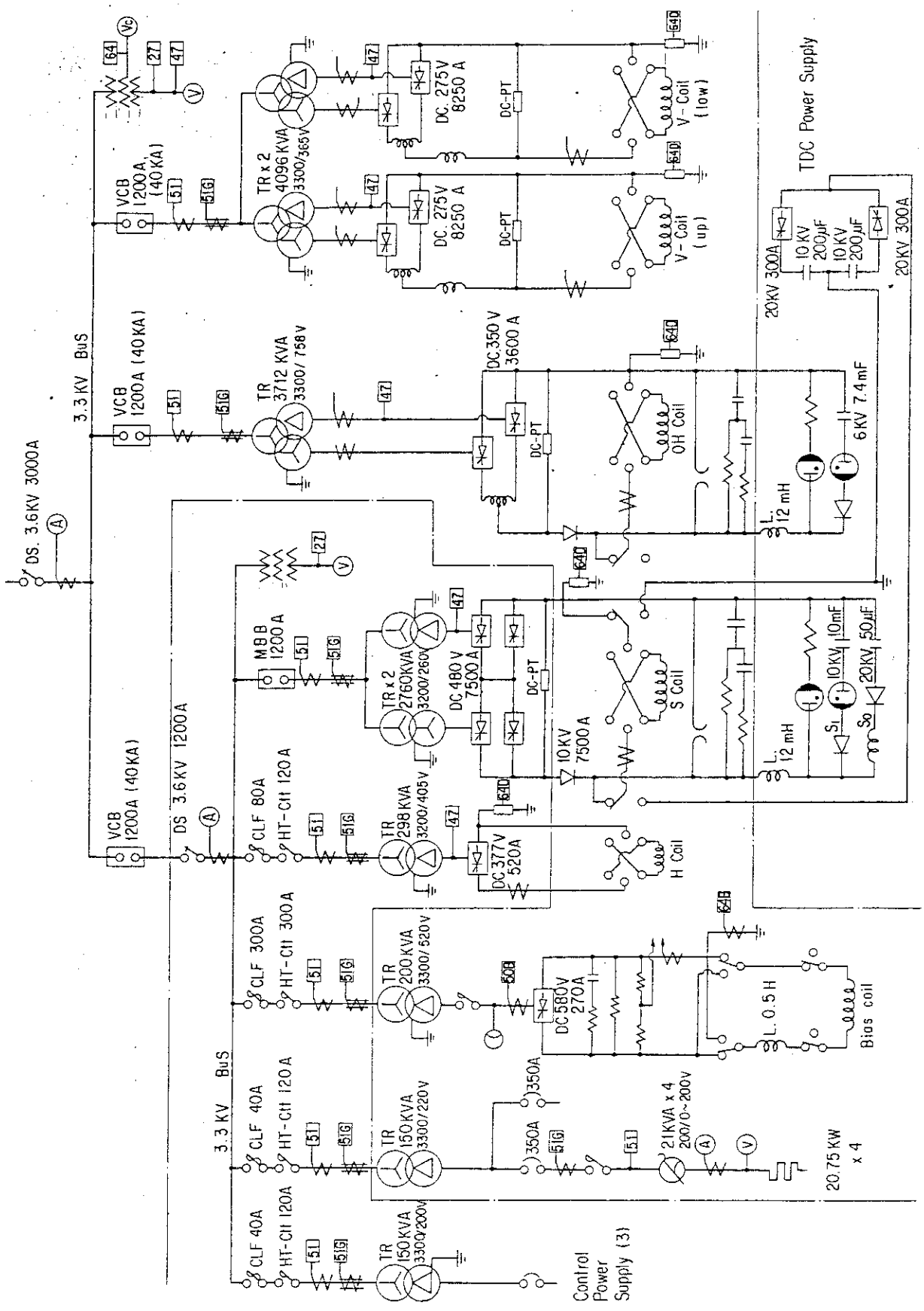

Fig. II.5-3 Schematic diagram of the poloidal coil power supplies.

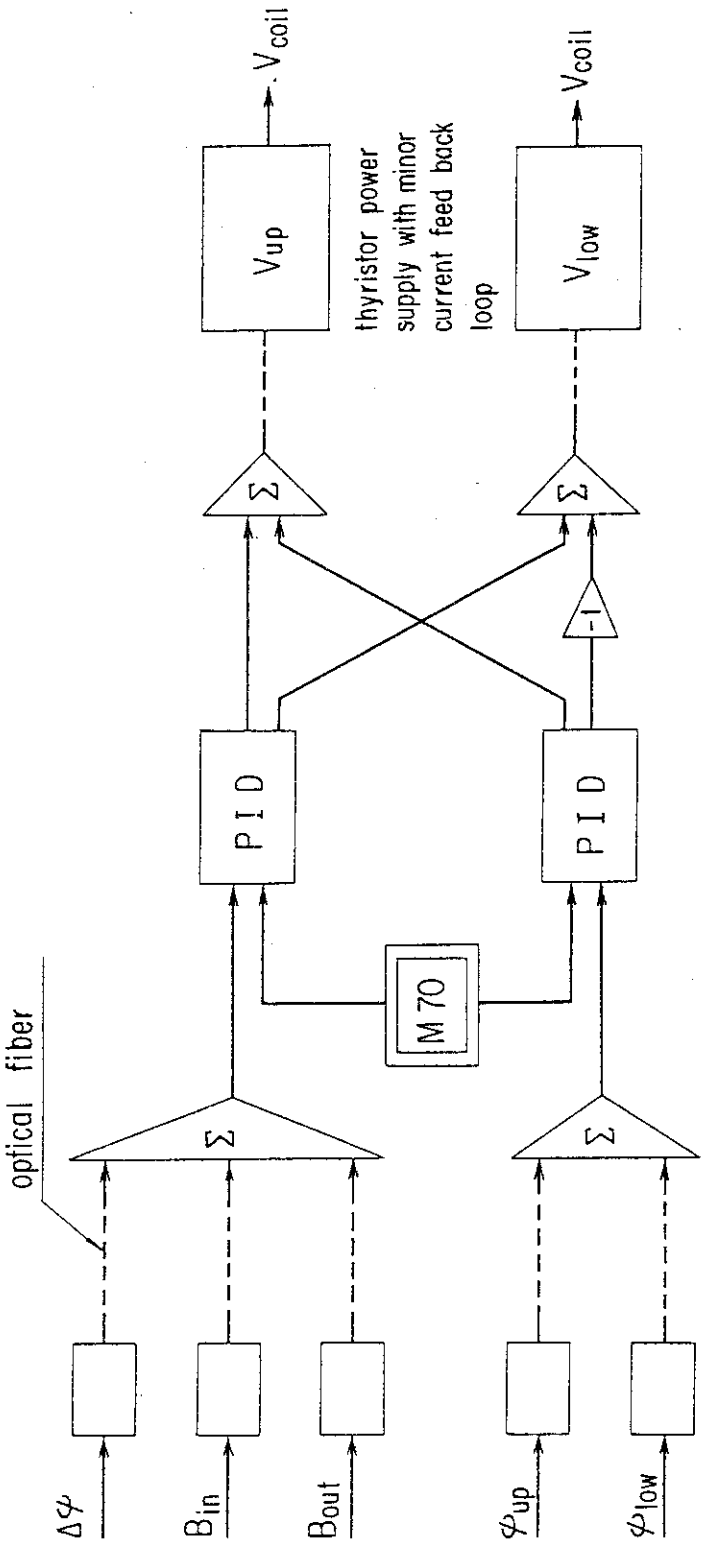

Fig. II.5-4 Schematic diagram of the feedback control circuit.

III. OPERATION AND MAINTENANCE

1. Introduction

Facility Operation and Engineering Section has been engaged in operation and maintenance of JFT-2 tokamak, Neutral Beam Injection (NBI) system, Lower Hybrid Heating (LHH) device and flywheel motor-generator (MG), and development of auxiliary equipments and instruments. On June the 18th, 1982 the JFT-2 was shut down with 279,711 times of the discharge since the beginning of its operation on April, 1972. Meanwhile JFT-2 has been remodelled into JFT-2M with partially using power supply, cooling system, pumping device and gas inlet device. NBI, LHH and MG were also adapted to JFT-2M. JFT-2M is to operate from April, 1983.

2. Operation and Maintenance

In this fiscal year JFT-2 was operated only for three months, but a lot of experiments (NBI, ICRF and LHH heating experiments) were achieved without big troubles. After shutting down JFT-2, power supply equipments, cooling device, vacuum equipments and peripheral device were overhauled. NBI system and LHH device were operated smoothly in the three months, however there were some troubles which were that a regulation tube of B-line and also the vanes of turbo-molecular pump in NBI were broken and changed. After shutting down JFT-2, four ion sources were adjusted to JFT-2M and improved the ratio of proton species. The operation schedule of JFT-2, NBI, MG and LHH is shown in Table III.2-1.

3. Development of Equipments and Instruments

3.1 Remodelling of JFT-2 (JFT-2M)

JFT-2 tokamak has been remodelling into JFT-2M tokamak in cooperation with this Section and Experimental Plasma Physics Laboraotry. Here we describe the works which were charged the Section.

3.1.1 Removal of JFT-2

Toroidal and poloidal coils, vacuum chamber, iron core and base of JFT-2 were removed and parts of them have been exhibited in Naka site.

3.1.2 Remodelling of toroidal field power supply

Because of changing the toroidal coils, the controller of toroidal field power supply had to be remodelled. The points were that in building up the toroidal current the generating voltage of MG was forced at 1.7 kV ("forcing" effect) and new control board was made.

3.1.3 Reinforcement of vacuum pumping system

Because of enlarging the volume of the vacuum chamber ($\sim$6,000 ℓ) the speed of exhaust of vacuum system had to be reinforced to get $\sim 10^{-6}$ Pa. as ultimate pressure. New vacuum plant is shown in Fig. III.3-1. It consists of a port of vacuum chamber, a 660 mm dia ceramics isolation flange, a manifold, A-line TMP, B-line TMP, C-line TMP and D-line Cryo pump of which measured speed were 3,300 ℓ/s, 1,050 ℓ/s, 800 ℓ/s and 1,580 ℓ/s, respectively, and the total speed of four lines was 6,790 ℓ/s. And further the system consists of measuring manifold and pumps, sputter ion pump for maintenance and roughing pumps.

3.1.4 Remodelling of poloidal power supply

Poloidal power supply in JFT-2M consists of S, OH, V, H and B coil power supply as shown in Fig. II.5-3. Within the power supply S and H thyristor power supply had been remodelled through B_{VC} and B_H in JFT-2M, and S'OH capacitors were also adjusted to JFT-2M. The details are descibed in section II.

3.1.5 Adjusting NBI system to JFT-2M

Because major and minor radii of JFT-2M are larger than those of JFT-2, the beam lines of NBI system had to be adjusted. The point was that two beam lines were moved backward and new vacuum tank was made and settled.

3.1.6 Remodelling of peripheral equipments

In gas inlet system new piezo-electric valves (∿100 Torr･ℓ/sec) and pipe lines were settled. And further some utilities (broadcasting system, pneumatic pipe lines and power source) have been newly equipped.

3.2 Stop pulse generator

Plasma current disruption in tokamak often happens as neutral beam injection heating, and if neutral beam is injected to the vacuum chamber without plasma, the chamber will be possible to be injured. For protection against the accident we invented a stop pulse generator. It consists of mainly Input Amplifier, Schmitt Trigger circuit and power supply. As input signals we use a one-turn loop voltage of plasma and a plasma current. The Input Amplifier provides six isolated and amplified signals. The Schmitt Trigger circuit compares the input signal amplitude with the pre-setting level. When the input signal gets over/down the threshold level, a 30 V p-p and 30 μsec pulse generates. This pulse stops the neutral beam injection. As using the instruments, the stop pulse generates and beam injection stops after 0.4 msec when the loop voltage gets over the threshold level. The same usage applys to ICRF heating operation.

Table III.2-1 Operation of JET-2, NBI, LHH and MG.

(Month)	1982 4 5 6 7 8 9 10 11 12	1983 1 2 3
JFT-2	operation and maintenance	under remodelling
NBI	operation and maintenance	under remodelling
M-G	operation and maintenance	under remodelling
LHH	operation and maintenance	under remodelling

Detail of the operation (JFT2, NBI, M-G and LHH)

	(Fiscal year)	1981	1982 APR-JUN	1982 JUL-SEP	1982 OCT-DEC	1983 JAN-MAR	TOTAL
JFT-2	Total days of operation (days)	131	39				39
	Times of discahrge (shots)	15024	4611				4611
	Baking (times)	4	3				3
	Discharge Cleaning (hours)	260	47				47
	Vent. of vacuum chamber (times)	12	3				3
	Ti coating (hours)	109	60				60
NBI	Total days of operation (days)	43	14				14
	Flashing and Injection (shots)	A: 6034 B: 8138	A: 1498 B: 1137				A: 1498 B: 1137
	Conditioning (shots)	A: 7932 B: 7563	A: 2194 B: 1309				A: 2194 B: 1309
	Vent. of vacuum tank (times)	5	2				2
	Baking (times)	5	1				1
	Change of filament (times)	0	0				0
M-G	M-G (#1)(hours)	1158	115				115
	M-G (#2)(hours)	1173	115				115
LHH	Total days of operation (days)	0	22				22
	Times of power injection (times)	0	5780				5780

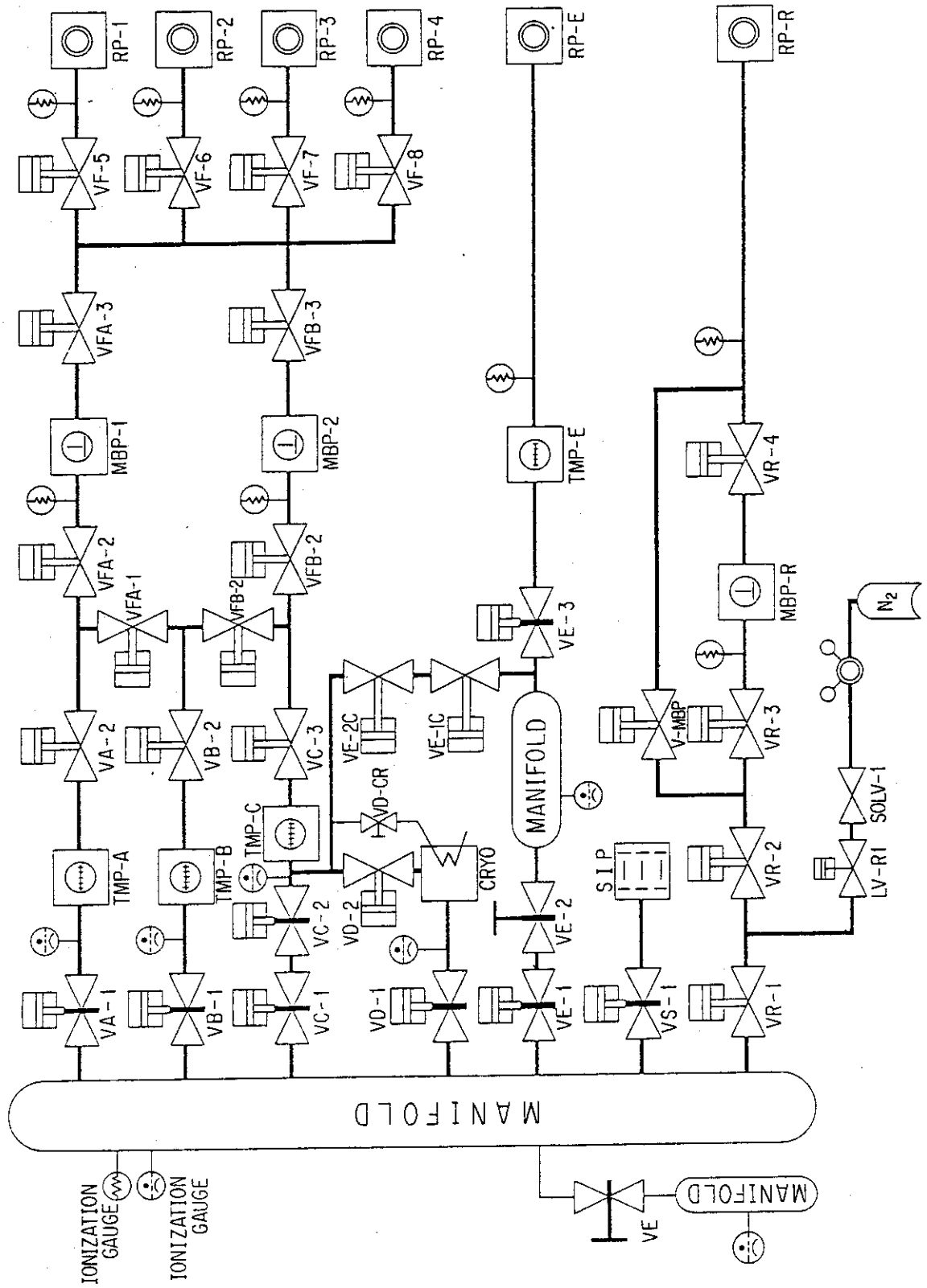

Fig. III.3-1 Diagram of new vacuum pumping system.

IV. JAPAN-US RESEARCH COOPERATION IN DOUBLET III

1. Japan - U.S. Joint Program

A cooperative program on thermonuclear fusion research between the United States and Japan was started in August 1979 using the Doublet III facility at the GA Technologies, Inc., California. A group of Japanese experimental scientists called the "JAERI team" is staying at GA and carrying out research as an independent group under their own leadership. They are sharing the Doublet III machine time with the American experimental team and the GA physics group.

The focus of activities on the part of the Japanese experimental team is to carry out experimental research on higher beta tokamak plasmas with a dee-shaped cross section.

Until March '81, Doublet III was operated for Joule-heating experiments. It was then shut down for six months in order to install two tanks of the neutral beam injection (NBI) heating with rating values of 80 keV, 7.2 MW and 0.5 sec pulse length. The NBI device started the operation in Sept. '81 and gradually increased the injection power. The 2 MW injection power was obtained in Dec. '81 and 5 MW in July '82. The NBI heating experiment with two NBI tanks was continued until mid-February 1983, and Doublet III was then shut down for five months to install NBI tank No.3. Fourteen months of experiments with three NBI (7-10 MW) are planned through the end of August 1984, the end of the present 5-year cooperation in Doublet III.

Several noteworthy results had already been obtained in the Joule-heated Dee-shape plasma experiments as was reported in the last issue.

A volume-averaged beta value of 4.6% was obtained in Aug. '82 and Nuclear Fusion Research at Baltimore where our results were one of the highlights. The JAERI team owes much of these successes to the outstanding cooperation and friendship of their GA colleagues.

2. Experimental Results

2.1 High β Dee-Shaped plasma experiments

During the ohmic heating experiment phase, plasma properties were

improved by Ti-gettering and TiC-coated carbon primary limiters; and high density, low-q discharges were stably obtained with dee shaped cross sections and a low toroidal magnetic field[1]. After the installation of the neutral beam injection system and during its power-up phase neutral beam heating experiments were carried out to investigate the dependence of β and τ_E on the discharge parameters as n_e, I_p, and elongation of plasma cross section K_a. The unique feature of Doublet III in this study was a very high plasma current up to 1 MA and a dee-shaped plasma cross section. A scaling of $<\beta_T>$ is

$$<\beta_T>[\%] = 3.3B_T[T]^{-2}\ I_p[MA]\ (0.5+0.4P_{abs}[MW])K_a^{-0.5}$$

which is shown in Fig. IV.2-1. This was obtained with up to 2.4 MW neutral beam injection. It was predicted from this scaling that $<\beta_T>$ of 5 % would be obtained when the machine status allowed plasma discharge with B_T = 0.6T, I_p = 350 kA, K_a = 1.4 (q^*=1.5), P_{abs} = 3.4 MW. As the beam power was increased, a record beta value of $<\beta_T>$ = 4.6 % was obtained with P_{inj} = 3.5 MW, B_T = 0.62T, I_p = 340 kA, K_a = 1.4 as was predicted, with one difference: a = 0.39 m. Typical data is shown in Fig. IV.2-2 where $q^{\psi} \sim 1.7$, $T_e(0) \simeq 550$ eV, and $\tau_E \sim 20$ ms. This result was reported at the Baltimore IAEA conference[2].

In the experiments between late 1982 and early 1983, a new discharge mode was found with an elongated single-null divertor configuration where the energy confinement time during neutral beam heating is proportional to $\bar{n}_e$ (on the INTOR scaling) and shows no deterioration with increasing ijection power. The result of analysis shows that a low particle recycling at the edge is the key to a good discharge. Figure IV.2-3 shows the electron temperature measured by Thomson scattering T_{eTS} and the central ion temperature $T_i(0)$ deduced from the neutron counter as a function of absorbed power P_{abs} for $\bar{n}_e \sim 5.5\times10^{13}$ cm^{-3} and B_T = 23-24 kG. In good low-recycling diverted discharges (open points), T_{eTS} and $T_i(0)$ are proportional to P_{abs}. The difference in T_{eTS} and $T_i(0)$ between the divertor and limiter discharges becomes larger at higher injection power. As shown in the figure, $T_i(0) \sim T_e(0) \sim 3$ keV are attained at $\bar{n}_e \sim 6\times10^{13}$ cm^{-3}. The highest stored energy of 280 kJ was also obtained with I_p = 750 kA, $P_{abs} \sim$ 4 MW and $\tau_E \sim 70$ ms[3].

2.2 Remote radiative cooling with neutral beam heating in diverted plasma

Impurity suppression and helium ash exhaust were demonstrated in the single null poloidal divertor experiments in Doublet III[4]. With the increase of the main plasma electron density, radiative cooling at the divertor region was also observed to increase which resulted in a reduction of the heat load to the divertor plate. All of these results, the impurity reduction with open divertor geometry, the helium ash exhaust, and the remote radiative cooling give a bright forecast to the solution of the crucial points of a future reactor design.

A high power hydrogen neutral beam up to ∿2.8 MW (P_{abs} < 3.1 MW) was injected into a diverted deuterium plasma to investigate the divertor characteristics in closer proximity to the reactor plasma. Experiments are done with B_T = 2.4T, I_p = 500 kA, and an average electron density in the main plasma $\bar{n}_e$ = 1 - 6 × 10^{13} cm^{-3}. The radiation power distribution measured by a 21-channel bolometer array shows a clear peak at the divertor region and the radiated power from the divertor region reaches as much as 0.9 MW, or ∿30 % of the total absorbed power of 3.1 MW.

Figure IV.2-4 shows the spatial profile of the electron density and temperature along the vertical divertor plates measured with a Langmuir probe array for three different main plasma densities[5]. Two peaks of each profile correspond to the upper (electron drift side) and lower (ion drift side) separatrix. The profiles of n_{ed} become broader as $\bar{n}_e$ is increased. In the high density case, electron density of as high as ∿3×10^{14} cm^{-3} is actually observed and the electron temperature at the same location is cooled to 3.5 eV which is ∿30 eV for the low density case. These results indicate the radiative cooling is very effective and the dense and cold plasma obtained in a single-null poloidal divertor provides the solution for the wall erosion problem.

2.3 Vertical stability of dee-shaped plasma[6]

Stability of the vertical position of the plasma in an elongated, dee-shaped plasma is an important consideration for the design of a future reactor system. Plasma stability theory predicts that beyond a certain critical elongation the plasma column will become vertically unstable, resulting in an uncontrollable motion of the plasma toward the top or bottom of the vacuum chamber. In Doublet III, the parallel-

connected field shaping coils surrounding the plasma acts as a stabilizing shell. In normal Doublet III operation, the vertical position of the plasma is stabilized by active feedback control of the field shaping coils. For the stability experiment, the feedback control signal was turned off after stable elongated plasmas were established. A series of experiments were done to investigate the stability limit of the elongation as a function of the plasma minor radius, or the distance between the plasma surface and the stabilizing parallel-connected coils. The result is shown in Fig. IV.2-5. "Vertically stable region" indicates that a plasma in this region is completely stabilized by means of active feedback control. In an "unactievable region", it is impossible to produce an elongated plasma. The stable region of an elongation is greatly decreased from 1.8 to ∿1.25 as the minor radius is reduced from ∿41 cm to ∿33 cm. A fat plasma (low aspect ratio) is superior in increase of elongation and decrease of vertical instability.

References

1) M. Nagami, et al., Nuclear Fusion 22 (1982) 409.
H. Yokomizo, et al., Nuclear Fusion 22 (1982) 797.
2) M. Nagami, et al., and D. Overskei, et al., paper IAEA-CN-41/A2 at the Ninth International Conference on Plasma Physics and Controlled Nuclear Fusion Research, Baltimore, Sept. 1982.
K. Burrell, et al., Nuclear Fusion 23 (1983) 536.
3) M. Nagami, et al., "Energy Confinement of Beam Heated Divertor and Limiter Discharges in Doublet III", Submitted to Nuclear Fusion.
4) M. Shimada, et al., Nuclear Fusion 22 (1982) 643.
M. Shimada, et al., Phys. Rev. Letters 47 (1981) 796.
5) S. Sengoku, et al., "Observations of Very Dense and Cold Plasma in Beam Heated Doublet III Tokamak with Single-Null Poloidal Divertor", Submitted to Nuclear Fusion.
6) H. Yokomizo, et al., paper IAEA-CN-41/R-1 at the Ninth International Conference on Plasma Physics and Controlled Nuclear Fusion Research, Baltimore, Sept. 1982.

This work was performed under a cooperative agreement between the Japan Atomic Energy Research Institute and the United States Department of Energy under DOE Contract No. DE-AT03-80SF11512.

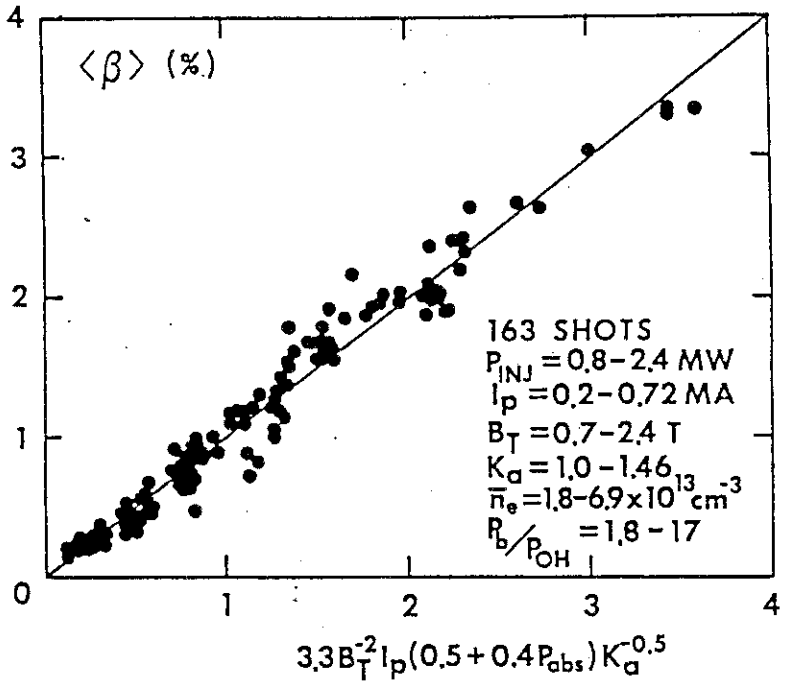

Fig. IV.2-1 β scaling of neutral beam heated discharges. This scaling predicts ⟨β⟩ ∿5% can be obtained with B_T=0.6T, I_p=350kA, K=1.4, P_{abs}=3.4MW.

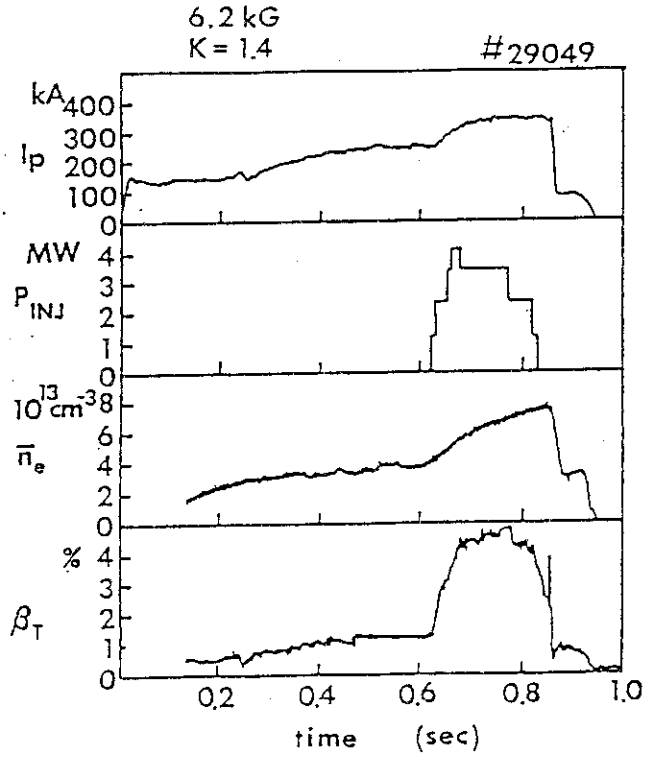

Fig. IV.2-2 Volume average beta ⟨β⟩ ∿4.6% was sustained for more than 0.1 sec with B_T=0.62T, K=1.4, P_{abs}=3.5MW. q^{ψ} ∿1.7, τ_E ∿20ms and $T_e(0)$=550eV.

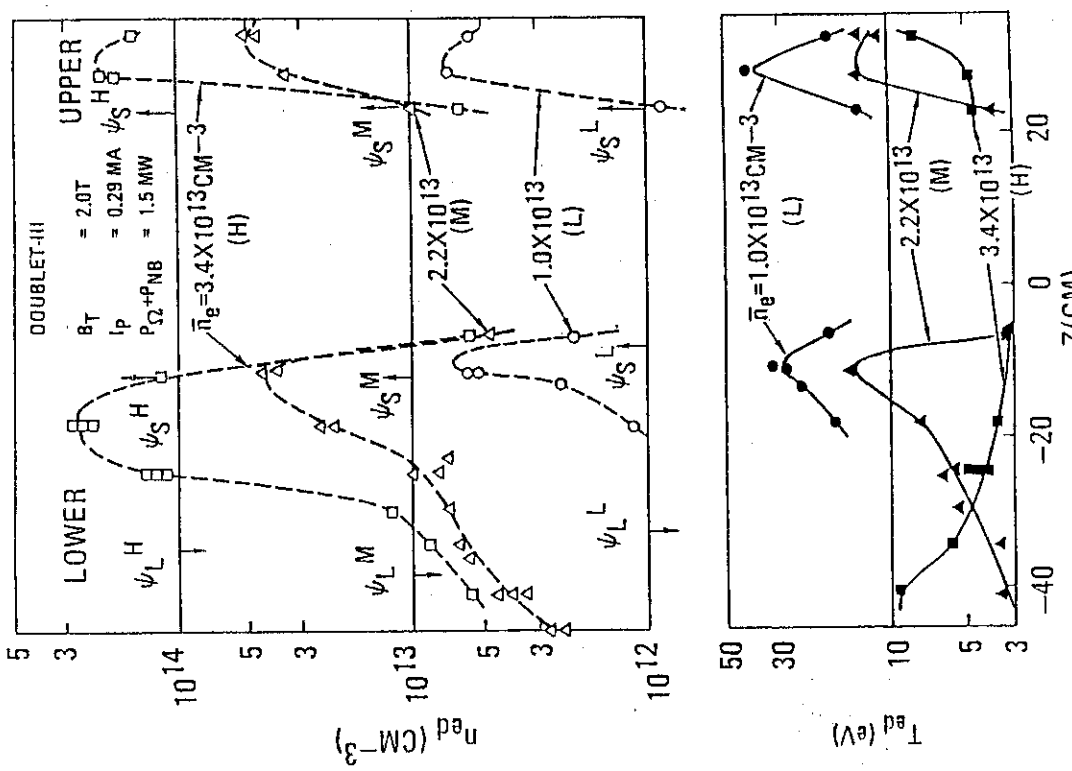

Fig. IV.2-4
Measured electron density n_{ed} and temperature T_{ed} profiles along the vertical divertor plates for three different values of the average electron density of the main plasma, $\bar{n}_e$=1.0×10^{13} cm^{-3}, 2.2×10^{13} cm^{-3} and 3.4×10^{13} cm^{-3}. "Upper" and "Lower" in this figure show the location of the upper and lower separatrix.

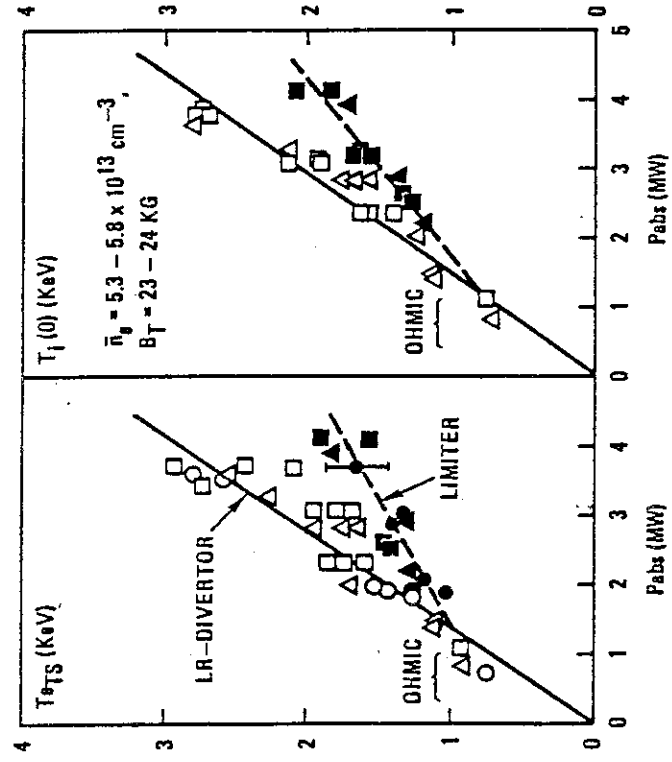

Fig. IV.2-3
T_{eTS} and T_i(o) measured with neutron counter vs. absorved power P_{abs} for low-recycling divertor and limiter discharges with $\bar{n}_e \sim 5\times10^{13}$ cm^{-3} and B_T= 23-24kG. Circle, triangle, square are I_p=480kA, 600kA, 750kA, respectively.

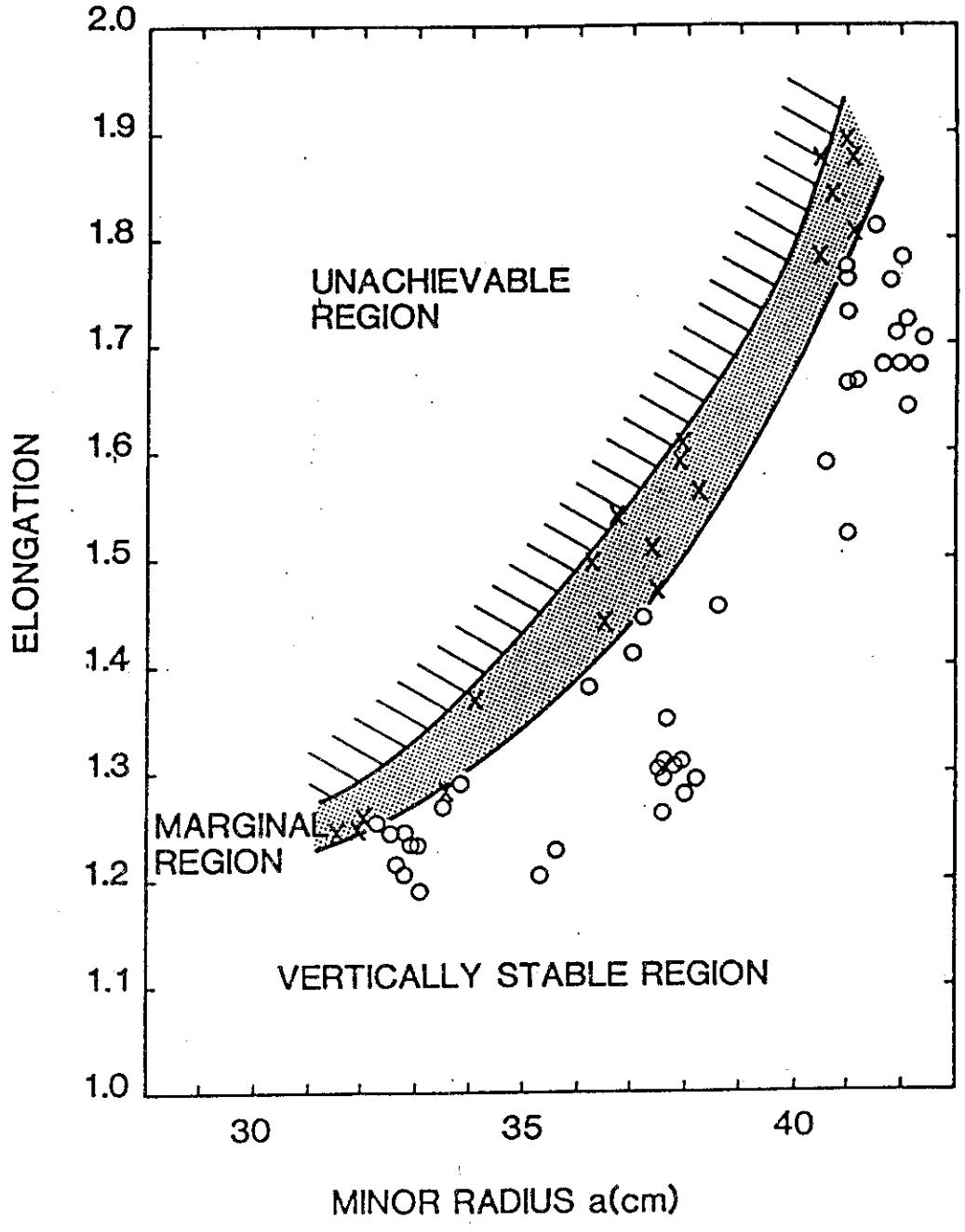

Fig. IV.2-5 Controllable elongation vs. minor radius with active feedback control. "Marginal region" means that a plasma is producible but vertically unstable and the discharge terminates before the programmed termination.

V. DEVELOPMENT OF PLASMA HEATING SYSTEM

1. Neutral Beam Injection System

1.1 Ion source development

The ion source for JT-60 NBI is designed to produced ion beams of 40 A at 100 keV for 10 sec. The maximum rated ion beam was obtained in March 1983. To raise the reliability of the ion source, improvements of the ion source are being continued.

1.1.1 Ion source for the prototype injector unit for JT-60

Operation of two ion sources installed on the prototype injector unit started in November 1981. The rated ion beam of 75 keV, 70 A, 10 sec was firstly extracted in February 1982. The system, however, had been designed to handle a 100 keV, 80 A, 10 sec ion beam for expanding the operation region. In March 1983, a 100 keV, 70 A, 10 sec ion beam was successfully extracted. Figure V.1-1 shows the various waveforms during the shot. The gas flow rate into each ion source and neutralizer are 0.88 Pa m^3/s and 1.1 Pa m^3/s, respectively, which gives about 90 % equilibrium neutralization line density for 100 keV proton.

The percentage power depositions on the beam line components are shown in Fig. V.1-2 as a function of pulse length. It should be noted that the power deposition to each component does not change during 10 sec pulse. This means that the beam divergence does not change during the pulse.

1.1.2 Improvements of the ion source for JT-60

The ion source used in the prototype unit satisfies our original design values for JT-60 NBI. Based on the test performed so far, we tried further improvements in the characteristics and the reliability of the ion source.

i) Improvements in proton ratio

An ion source with higher proton yield is desirable in order to reduce the surface heating and to deposit higher neutral power in the core of the plasma. The proton ratio can be improved with increasing

ion confinement time in the arc chamber. To realize this, the magnetic field strength at the inner surface of the arc chamber was increased from 1.4 kG to 2.7 kG and also the volume of the chamber was increased by 50 % compared with that of the prototype ion source. The proton yield measured both with the magnetic mass analyzer and doppler shift spectrometer indicated more than 90 %[1]. The comparison of species ratio with that of the prototype source is shown in Fig. V.1-3.

ii) Improvement of plasma grid

The plasma grid is exposed to the highest heat flux of the four acceleration grids due to the impingment of backstreaming electrons and the irradiation from the source plasma. In the ion sources for the prototype unit, some deterioration in beam optics during 10 sec pulse was observed. This may be due to thermal distortion of the plasma grid. In order to reduce such distortion, the thickness of the frame around the aperture region was increased from 1.5 mm to 5.0 mm, and large manifolds were attached to shield the frame from the irradiation. The cross sectional view of the improved plasma grid is shown in Fig. V.1-4 as well as that of the prototype grid. This grid was tested at the maximum heat loading in our operation region and occurred no significant deterioration in beam optics during the pulse.

iii) Tapered filament for long life cathode

Burn-out of a filament due to the concentration of arc discharge on the negative leg may be inevitable when the filament is heated directly by DC current. In order to overcome this problem, the tapered filament was developed.

A tungsten rod of 2.7 mm in dia. and 24.0 cm long is tapered such that the cross section of the filament increases gradually from the positive leg to the negative leg. The time dependent temperature distribution along the filament was calculated[2].

The result indicates that the overheat of the negative leg occurs during a long pulse discharge in the case of a conventional filament, while it does not occur in the case of the tapered filament. Thus, we can expect that the cathode life, depending on the evaporation at the negative leg, will be appreciably lengthened. This filament is now under test.

1.2 Performance test of the prototype injector unit for JT-60[3)]

Figure V.1-5 shows a detailed cross sectional view of the prototype injector unit and the target chamber. There is no major difference in the design concept and the structure between the prototype injector unit and the actual JT-60 neutral beam injector. (Details of the system have been reported elsewhere[4)].)

The rated ion beams of 75 keV, 70 A, 10 sec were extracted repeatedly with two ion sources in February 1982.

The injected neutral beam power to the target was over 1.4 MW, which satisfies the design value. In an attempt to expand the operating region up to an energy of 100 keV, the system was designed to handle a 100 keV, 80 A ion beam. In the operation performed in March 1983, we obtained a 100 keV, 70 A, 10 sec beam with two ion sources. Figure V.1-6 shows the power flow at 100 keV, 70 A, 10 sec operation.

The measured heat loads are within our design values. The inspection of each component after the operation showed no serious damage such as distortion, warp, or surface melting. During one and a half years test on the prototype injector unit, no serious troubles in the beam line have occurred.

The cryopumps have also been operated successfully.

References

1) Y. Okumura, et al., To be submitted for publication in Rev. Sci. Instrum.
2) S. Tanaka, et al., To be submitted for publication.
3) M. Akiba, et al., Rev. Sci. Instrum. 53 (12), 1864, 1982.
4) M. Kuriyama, et al., Proc. Symp. Eng. Problems of Fusion Research, Chicago 1981.

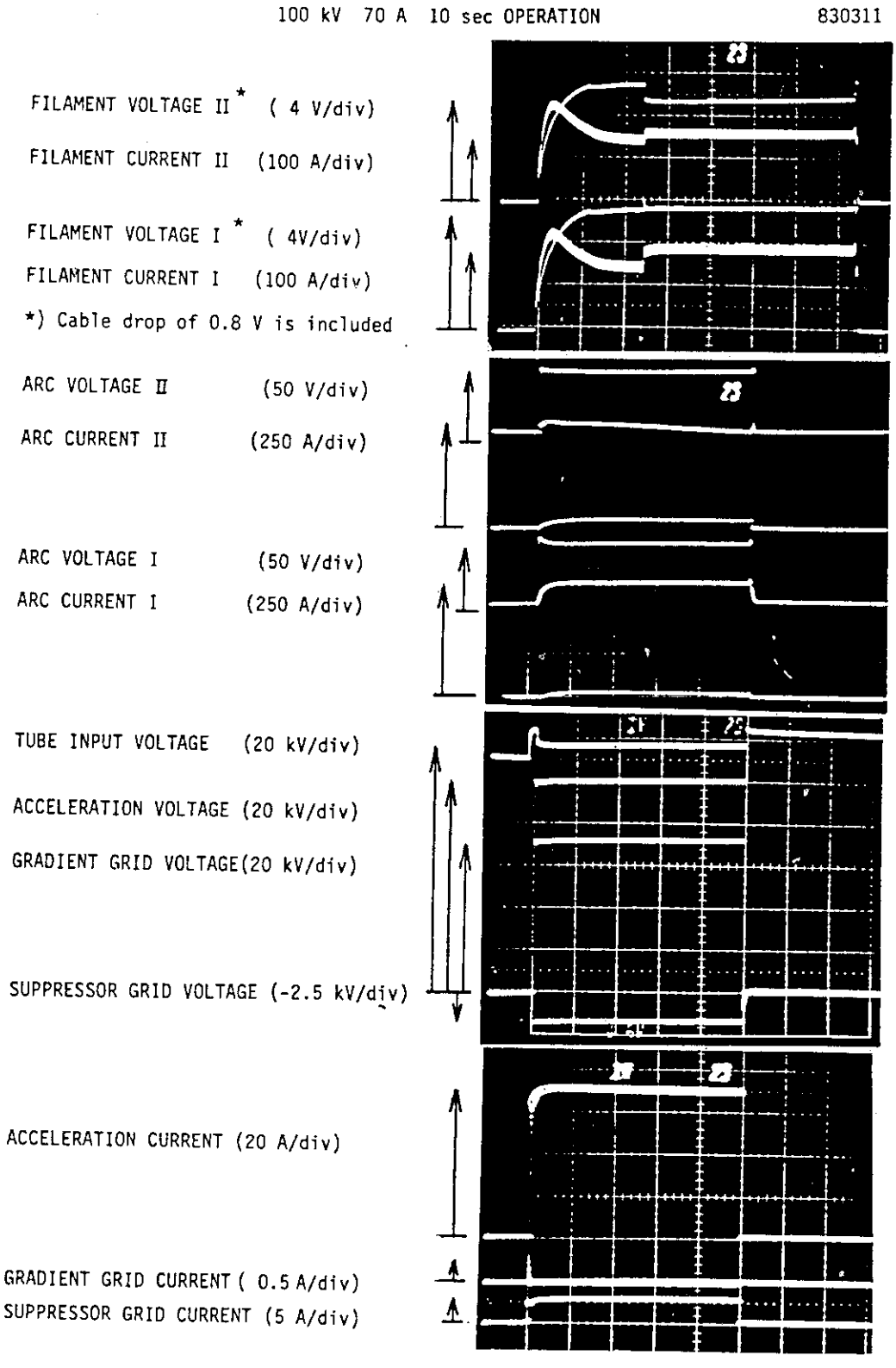

Fig. V.1-1 Typical waveforms of the 100keV, 70A, 10sec ion beam.

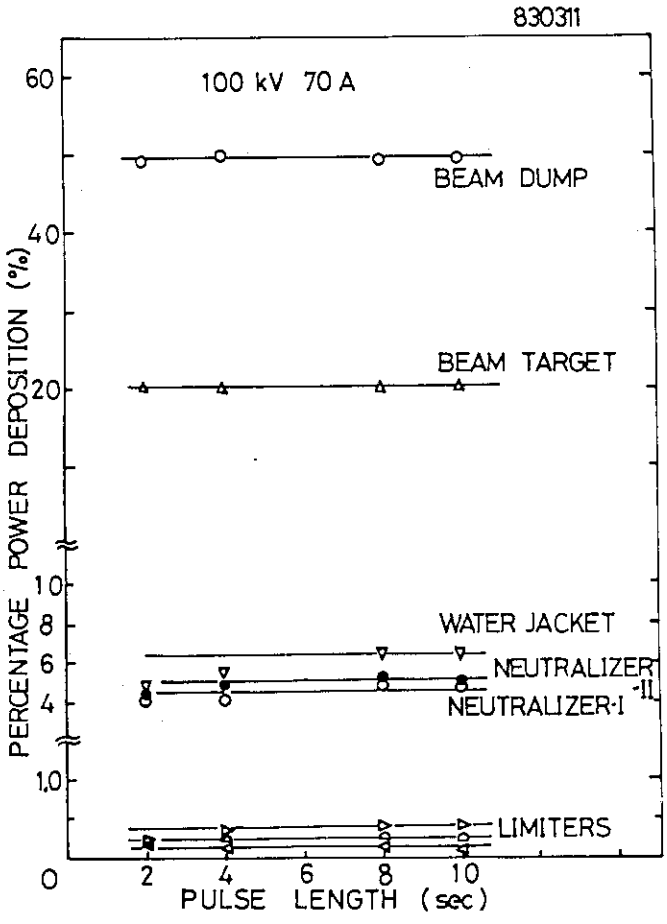

Fig. V.1-2 Percentage power depositions on the beam line component vs. beam pulse length.

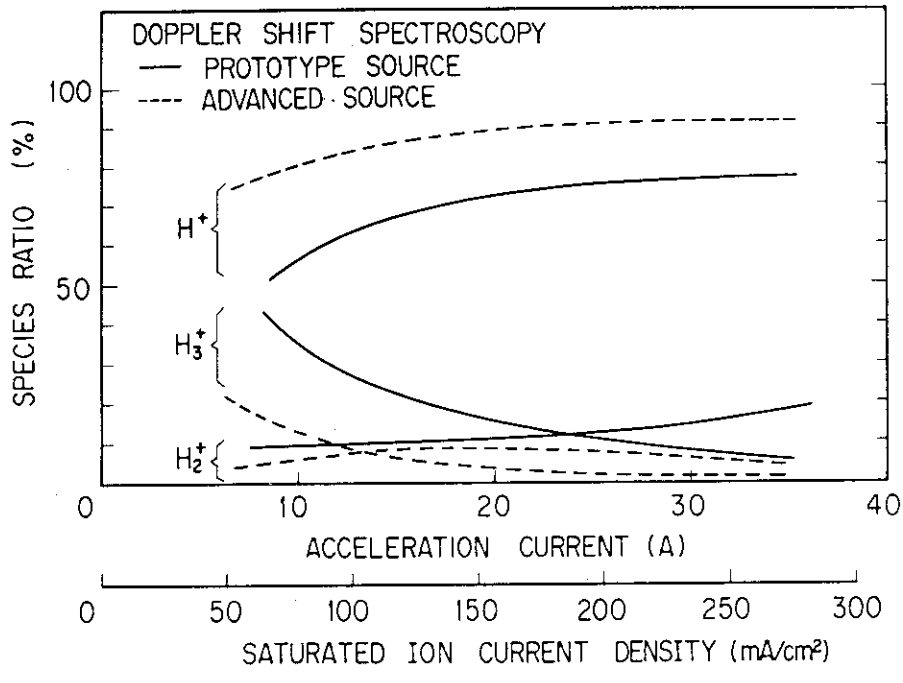

Fig. V.1-3 Comparison of the ion beam species ratio between the prototype ion source and the advanced ion source.

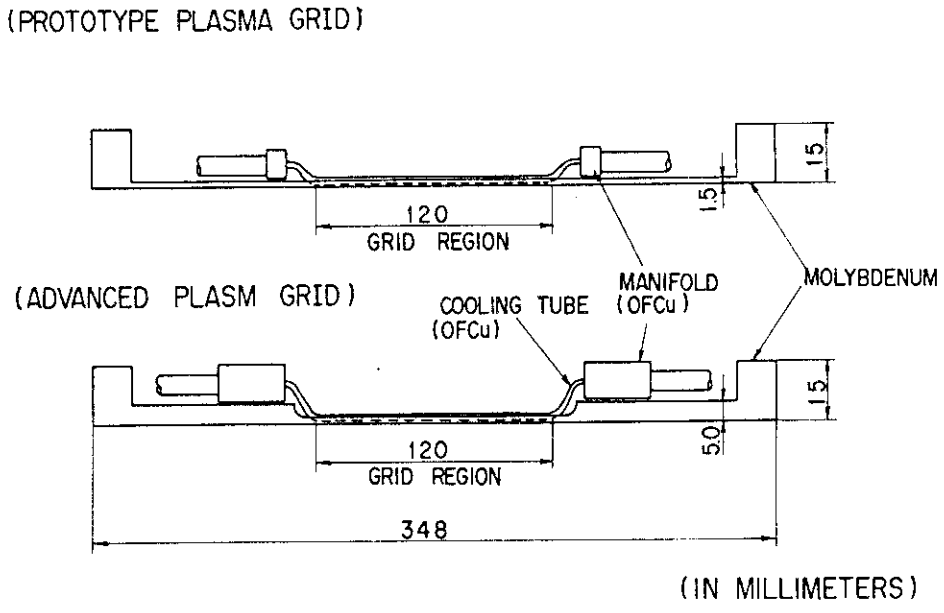

Fig. V.1-4 Cross section view of the advanced plasma grid.

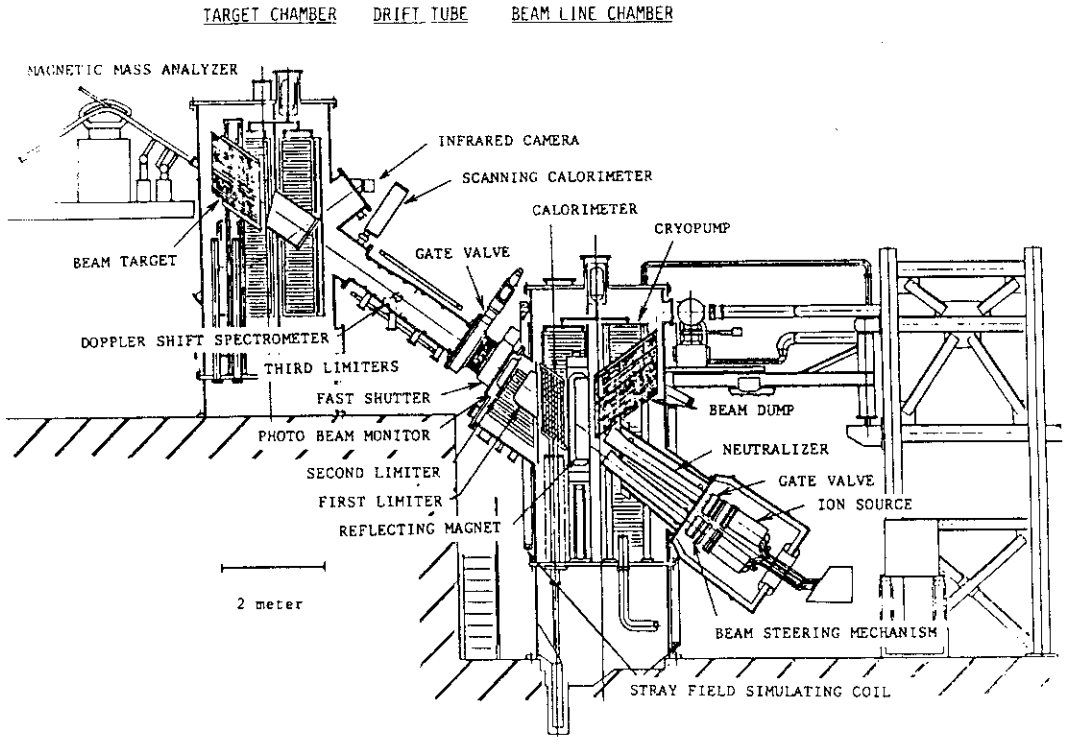

Fig. V.1-5 Cross section view of the prototype injector unit for JT-60.

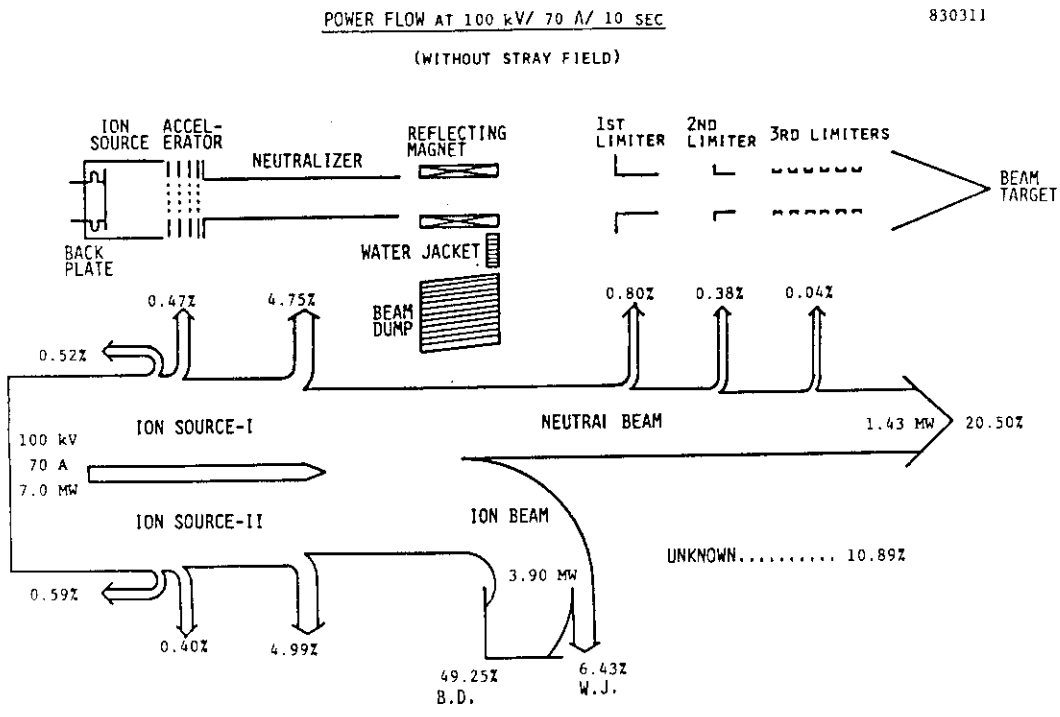

Fig. V.1-6 Power flow diagram at the 100keV, 70A, 10sec operation.

2. Radio Frequency Heating System

Recent experiments on RF heating are very promissing to realize the reactor level high temperature and high density plasma in tokamaks. In order to make the RF heating system in the large machine, we must further research and develop many renewed RF heating technologies. Among them the RF power source and the RF coupler system are the most important components in the RF heating facility.

In JT-60 project, we are planning the 10 MW - 10 sec power deposition into plasma core as an additional heating, which consist of LHRF and ICRF heating facilities. In the LHRF, a phased wave guide coupler was being developed on the basis of successful results in JFT-2[1,2] and the test stand experiments[3]. As for the ICRF, the design study of the ridged wave guide has been researched in cooperation with Tokyo Institute of Technology and Toshiba Electric Company (Toshiba). R & D work of high power klystron for LHRF of course continues under contact with Nippon Electric Company (NEC) and Toshiba in also this FY 1982.

Other R & D works are large gate valve of 750 mm diameter of double metal seal type (this work was performed in cooperation with Mitsubishi Heavy Industry Company), and high power and wide band (1.7 - 2.3 GHz) microwave circuits such as phase shifter, power divider and flexible waveguide. Results of these R & D are very successful and satisfied most of our final requirements.

2.1 R & D work of high power klystron

R & D work of the high power dlystron is the main item to complete the LHRF facility in JT-60. Key features of JT-60 klystron are (1) high power output (1.1 MW) (2) long pulse (10 sec) (3) wide range tuning (±5 MHz, instant; ±150 MHz, mechanical) (4) high speed response to the mechanical tuning (±150 MHz/500 ms) (5) strong endurance against the reflected power (3 of VSWR), which is equiped for the heating object of fusion plasmas not for the broadcasting and the accelerator.

The power supply (named JT-60 Klystron Test Facility) is constructed for the aging test and the output power test of this klystron having DC 100 kV, 35 A, 10.3 sec, 1/15 duty power activity. In this Test Facility, programmable operation of DC and RF aging is made using the control system with a micro computer.

RF power source klystron of 1.0 MW for 4.0 sec and 0.59 MW for 9.6 sec was now obtained at the beam of 66.7 kV, 17.7 A for 10 sec. The instant band width of ±6 MHz and the ±150 MHz mechanical tuning with 300 msec were already obtained successfully.

2.2 R & D work of coupling structure for RF heating

R & D work of the coupling structure is one of the most important items on the RF heating technology. From now, we have developed the satisfactorily coupling system in the JFT-2 lower hybrid heating experiment and RF test stand I experiment. Furthermore, RF test stand II experiments have started for the study of the JT-60 coupling structure.

2.2.1 The conditioning experiment of waveguide launcher on RF test stand I

We have already succeeded in the 2 kW/cm^2, 40 msec power density with real plasma loading in JFT-2. In RF test stand I, which is equiped by reconnecting the transmission line of JFT-2 lower hybrid system to the test stand and RF power source is JFT-2 klystrons. Following results are obtained in RF test stand I. (1) Input power density of 4 kW/cm^2, with 80 msec was achieved without breakdown in the H gas and in vacuum using SUS and Cu coated SUS launcher. (2) The multipactering breakdown was found in a certain power range. However it is shown that the multipactering effect can eliminate with increase of the RF power and the frequency. (3) It is shown that the sufficient aging about a thousand shots and high temperature baking about 200 °C with several days may lead the suppression of outgas going and the RF breakdown. (4) The inner wall of the used launcher was observed by Scanning Electron Microscope (SEM) to investigate the effect of the breakdown on the surface. Figures V.2-1(a) and (b) are the pictures of the inner wall of launchers. Figures V.2-2(a) and (b) are the SEM pictures of launchers. On the SUS launcher, the arc track (Fig. V.2-1(a)) and severe erosion (Fig. V.2-1(b)) are found with SEM (X 3000). On the other hand, the polished like discharge tracks are widespread (Fig. V.2-2(a)), and the local severe damage is not seen on the Cu coated SUS launcher (Fig. V.2-2(b)) with SEM (X 500).

2.2.2 RF test stand II experiment for JT-60 coupling system

The RF test stand II facility for JT-60 is bakable up to 500 °C to suppress the outgassing during RF pulse and is capable to test the power density up to 7.5 kW/cm^2 during 10 sec with four waveguide array, which is shown in Fig. V.2-3. Ceramic window to seal vacuum is the pill box type which is the same window as that of 1 MW klystron. Preliminary experiment of transmissible power density after the baking has been done, using a 1 MW klystron under development. Base pressure of launcher before and after the baking, power test is performed with dummy load termination. Power density of 2 kW/cm^2, 1 sec is so far achieved after half day RF conditioning.

References

1) K. Uehara and T. Nagashima; in Proceeding of the Joint Varanna-Grenoble International Symposium on Heating in Toroidal Plasma, Grenoble 1982, vol.II, p.485.
2) T. Fujii, T. Imai, K. Uehara, et al., Jpn. J. Appl. Phys. 22 (1983) 319.
3) T. Fujii, K. Sakamoto, K. Uehara, et al., in Proceeding of the Joint Varenna-Grenoble International Symposium on Heating in Toroidal Plasmas, Grenoble 1982, vol.III, p.1133.

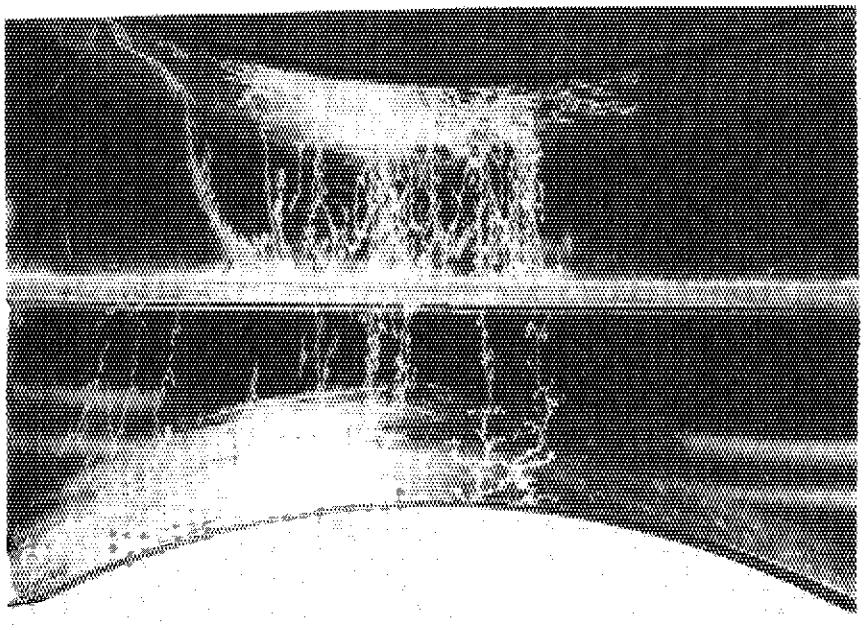

(a)

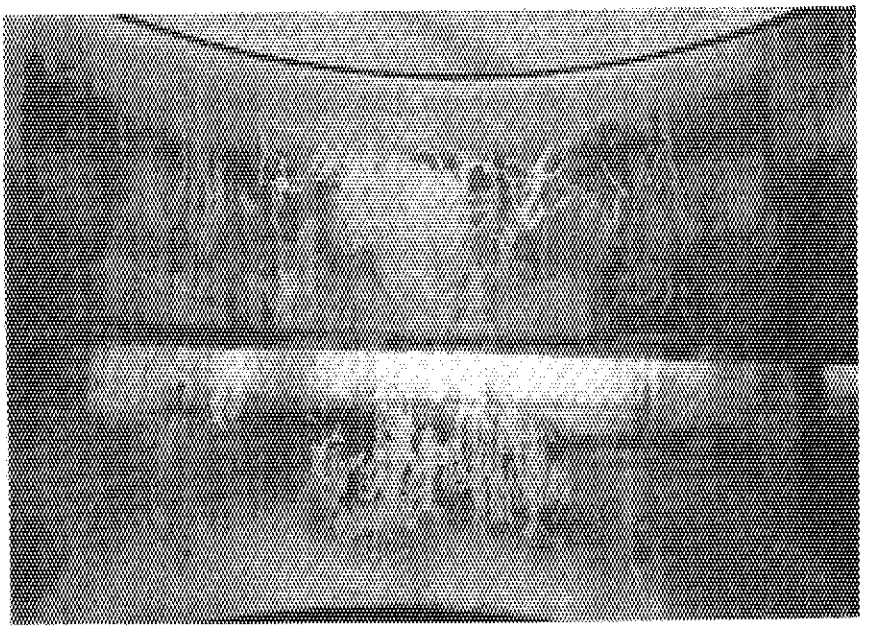

(b)

Fig. V.2-1 Pictures of inner wall of the launcher
(a) SUS launcher; The arc tracks are seen at the center
(b) Cu coated SUS launcher; The polished like arc tracks are seen in the center area.

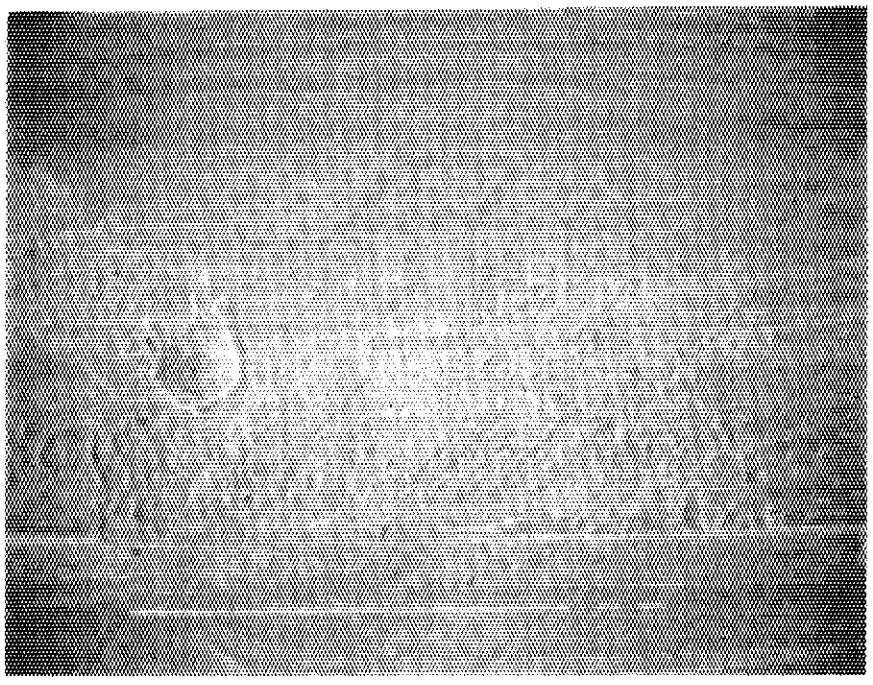

(a)

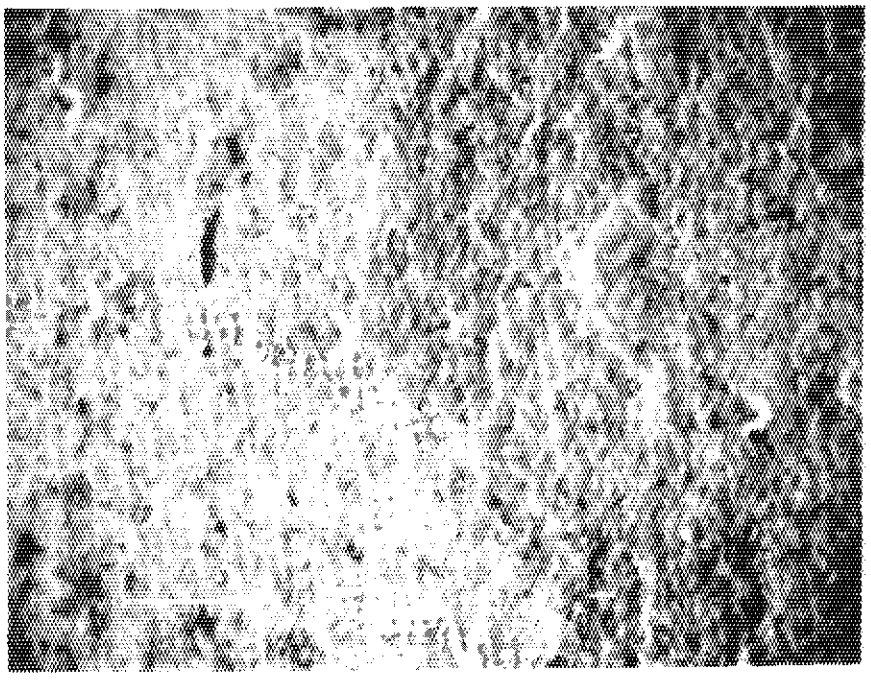

(b)

Fig. V.2-2 SEM pictures of the inner wall of the launcher
(a) SUS launcher; The melting surface corresponds to the arc track in Fig. V.3-1(a)
(b) Cu coated SUS launcher; The light area corresponds to the arc tracks in Fig. V.3-1(b).

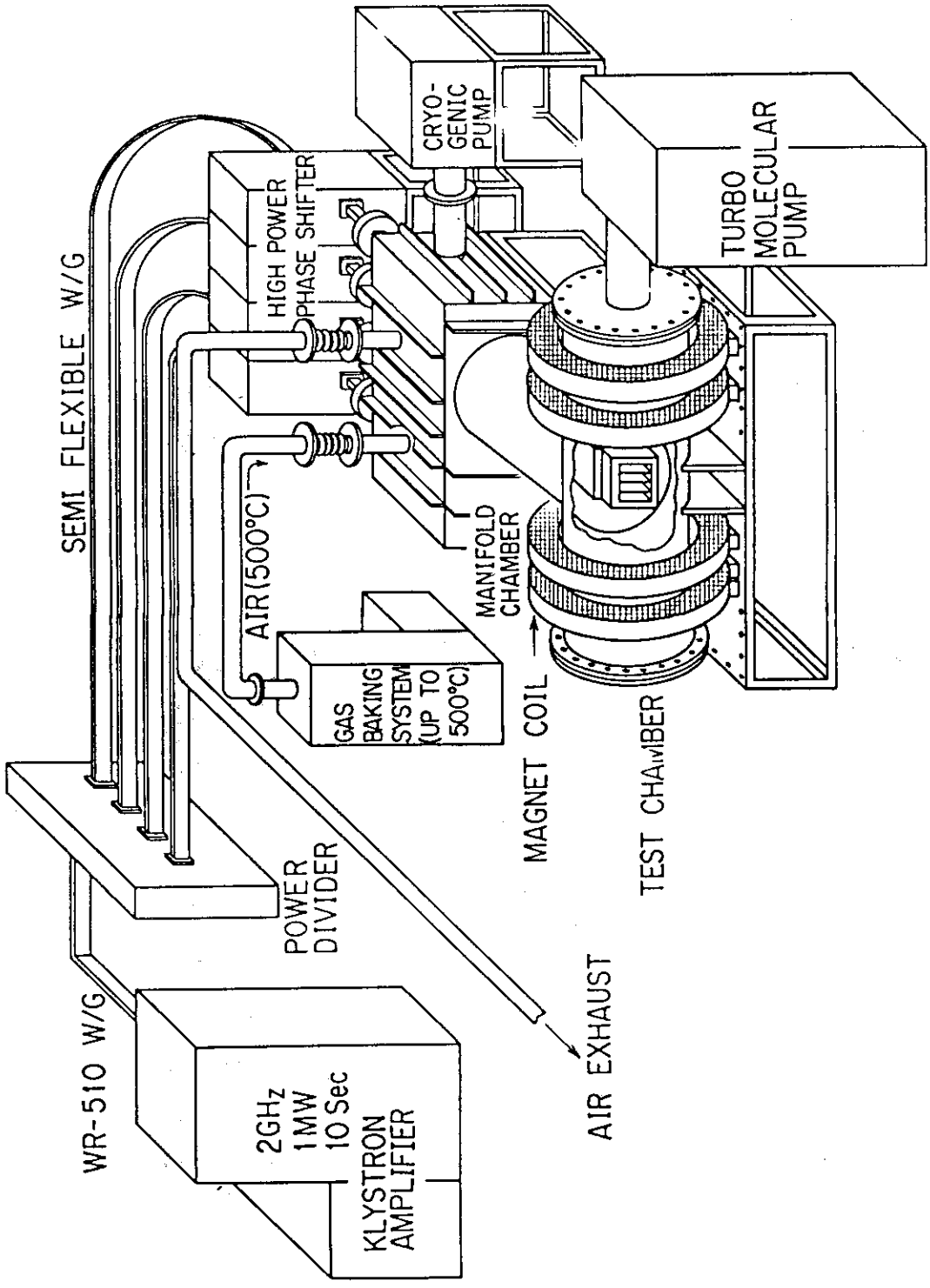

Fig. V.2-3 RF Test Stand II Facility for JT-60 Coupling System.

VI. SURFACE PHYSICS AND VACUUM TECHNOLOGY

1. Introduction

The plasma surface interaction studies for fusion materials have been continued in close connections with the JT-60 project and the design study of next step tokamaks. The primary objective of these studies is to investigate surface processes such as sputtering, hydrogen recycling and gas desorption by using ion accelerators and high vacuum apparatus.

In this fiscal year, significant progress was made with the improvement of a chemical sputtering model, the self-sputtering measurement and the study on hydrogen recycling in wall materials. Outgassing rates from TiC-coated materials were also measured.

As to vacuum and surface technological developments to be used in JT-60, see Chapter X.

2. Improvement of Chemical Sputtering Model in Carbon Materials

We previously obtained an experimental result that chemical sputtering (i.e. methane formation) by bombardment of various types of carbon materials with energetic protons (0.1-6 keV) has a maximum yield at approximately 1 keV incident energy[1]. It had not been explained so far by any conventional model. We succeeded in explaining the energy dependence by taking account of surface deposited energy and reflection of protons which are both dependent on the incident energy[2]. Our new model predicts the chemical sputtering yield S as follows:

$$S = A\left[\frac{J_o f_D}{\nu_o}\right]^{\ell} \frac{(1-B)\exp(-Q_1^{+}/RT)}{J_o\sigma + \tau_o^{-1}\exp(-Q_2/RT)}, \quad \frac{1}{2} \le \ell \le 1 \qquad (1)$$

where A is proportionality constant, J_o incident flux of ions, B backscattering coefficient, σ ion impact detrapping cross section, f_D surface deposited energy, Q_1^{+} effective activation energy of the chemical reaction rate for methane formation, $\nu_o = 10^{13}$ sec, and the term $\tau_o\exp(Q_1/RT)$ surface residence time of hydrogen atoms. In Fig. VI.2-1 is shown three comparisons between experimental and theoretical yields by giving the ℓ three different values. It is the best fit to give $\ell = 0.75$.

3. Selfsputtering of Molybdenum and Tungsten

It has been suggested that the selfsputtering yield is one of the important parameters to assess the erosion rate of the first wall, such as the divertor plate and the limiter, due to sputtering. In this fiscal year, the selfsputtering yield measurement was made on molybdenum and tungsten at normal incidence for the respective self ions in the energy ranges between 0.1 and 10 keV by means of the weight change measurement[3]. The selfsputtering yields are calculated from the formula

$$S = -\frac{N_0 \cdot \Delta m}{M_2 \cdot N} + 1 \qquad (2)$$

where N_0 is Avogadro's number, M_2 the target atomic mass, Δm the decrease of the weight change of the target and N the number of incoming projectile atoms. The selfsputtering yields obtained by using eq. (2) are shown in Figs. VI.3-1 and VI.3-2 for molybdenum and tungsten, respectively, as a function of the incident energy. Comparisons are made between the measured yields and the calculated ones from two different empirical formulae proposed by IPP Garching group (the IPP model[4]) and Nagoya group (the MYI model[5]) and it is found that agreement between the energy dependence of the measured yields and those of the calculated ones from two different formulae is reasonable within a factor of three for both molybdenum and tungsten.

4. Hydrogen Isotope Recycling in Wall Materials

4.1 Deuterium re-emission experiment

Re-emission measurements of deuterium were made in molybdenum, Inconel 625 and titanium carbide to support the development of low-Z coatings in JT-60. This experiment was made with close relations to the model calculations (see the next section 4.2) on particle recycling in JT-60. The result is shown in Fig. VI.4-1 for cyclic bombardments with 6 keV D^+ ions. In the first bombardment a , the initial deuterium re-emission rate in TiC increases more gradually than in Mo and Inconel 625, which suggests that incident deuterium atoms are trapped in the bulk.

During subsequent interruption of deuteron bombardment b , re-emission rate in TiC decreases very gradually (especially at 500 °C) compared to that in Mo and Inconel 625. In the second bombardment after 10 min interruption c , the initial increase of the re-emission rate in TiC is quicker than in Mo and Inconel 625 especially at 100 °C, which indicates that a considerable fraction of trapped deuterium atoms at the first bombardment still exists in the surface layers. From this experiment we estimated the diffusivity of deuterium atoms in TiC as

$$D(T)[cm^2/sec] = 9.2\times10^{-13}\exp(-3.05\times10^3[cal/mol]/RT), \qquad (3)$$

which was used in the following calculations of hydrogens in JT-60.

4.2 Modelling of hydrogen recycling at wall surfaces

A model calculation on hydrogen recycling at the wall in JT-60 was made for three different wall materials, molybdenum, Inconel 625 and titanium carbide[6]. Recycling coefficient should be suppressed below the following criterion value R with which keeping a constant particle density $\bar{n}$ has to be satisfied when high energy neutrals of flux Γ^{NBI} are injected.

$$R = 1 - \frac{1-\alpha}{b(1-\alpha)+\alpha} \cdot \frac{\tau_p \Gamma^{NBI}}{\bar{n}V} \quad , \qquad (4)$$

where α is the return fraction of charge exchange neutrals, b fraction of the total flux of impinging ions on the wall, τ_p particle confinement time, $\bar{n}$ average particle density in the plasma, and V plasma volume. When it is assumed that b = 0, α = 0.3, $\Gamma^{NBI} = 2.5\times10^{21}$ H/sec and V = 60 m^3, we obtain the values of R to be 0.75 and 0.92, for two different $\bar{n}/\tau_p$ values of 3.9×10^{20} and 1.17×10^{21} H/m^3 sec. By taking account of back-scattering from the surface, diffusion from the bulk and saturation overflow, the recycling coefficients for the three materials were calculated using the diffusion coefficient measured (see 4.1) as a function of time and wall temperature (for example, in TiC Fig. VI.4-2). From the calculations for 200 eV/400 eV Maxwellian energy distributions of charge exchange neutrals, we obtained the following results.

(1) In Inconel 625, the above criteria can not be satisfied at any

temperature except very low ones below room temperature.

(2) In molybdenum, we can find suitable temperatures below 110 °C which satisfies the above criteria for 10 sec discharge.

(3) In titanium carbide, we can find the suitable temperature between 150-500 °C for 10 sec discharge, except for low energies. Saturation overflow occurs at relatively low temperatures which abruptly increase the recycling coefficient.

5. Measurement of Outgassing Rate from TiC-coated Materials

To support the development of low-Z coatings for JT-60, we measured the outgassing rate from TiC-coated molybdenum and TiC-coated Inconel by a laboratory experiment. The TiC coatings on molybdenum were formed by chemical vapor deposition and those on Inconel were produced by activated reactive evaporation. Figure VI.5-1 shows the rates at a room temperature from these materials as a function of evacuation time. In this figure outgassing rates from non-coated molybdenum and Inconel are also indicated for reference. Compared with TiC-coated molybdenum, molybdenum or Inconel, the TiC-coated Inconel exhibits a slower decrease in outgassing rate with time. This may be due to the porous character of the coatings whose deposition procedure was consciously controlled to reduce internal stresses.

In spite of the different characteristics at room temperatures, the outgassing rates from all these materials after a 18-hr bakeout at 250 °C showed low values of less than 5×10^{-9} Pa·m^3/s·m^2 (3.7×10^{-12} Torr·l/s·cm^2) satisfying the specification of JT-60.

References

1) Yamada, R., Nakamura, K., Sone, K., and Saidoh, M., J. Nucl. Mater., 95 (1980) 278.
2) Yamada, R., and Sone, K., J. Nucl. Mater., 116 (1983) 200.
3) Saidoh, M., and Sone, K., Jpn. J. Appl. Phys., 22 (1983) 1361.
4) Bohdansky, J., J. Nucl. Mater., 93 & 94 (1980) 44.
5) Yamamura, Y., Matsunami, N., and Itoh, N., Radiat. Eff., 71 (1983) 65.
6) Sone, K., and Murakami, Y., submitted to the Symposium on Energy Removal and Particle Control in Toroidal Fusion Devices (July, 1983, Princeton).

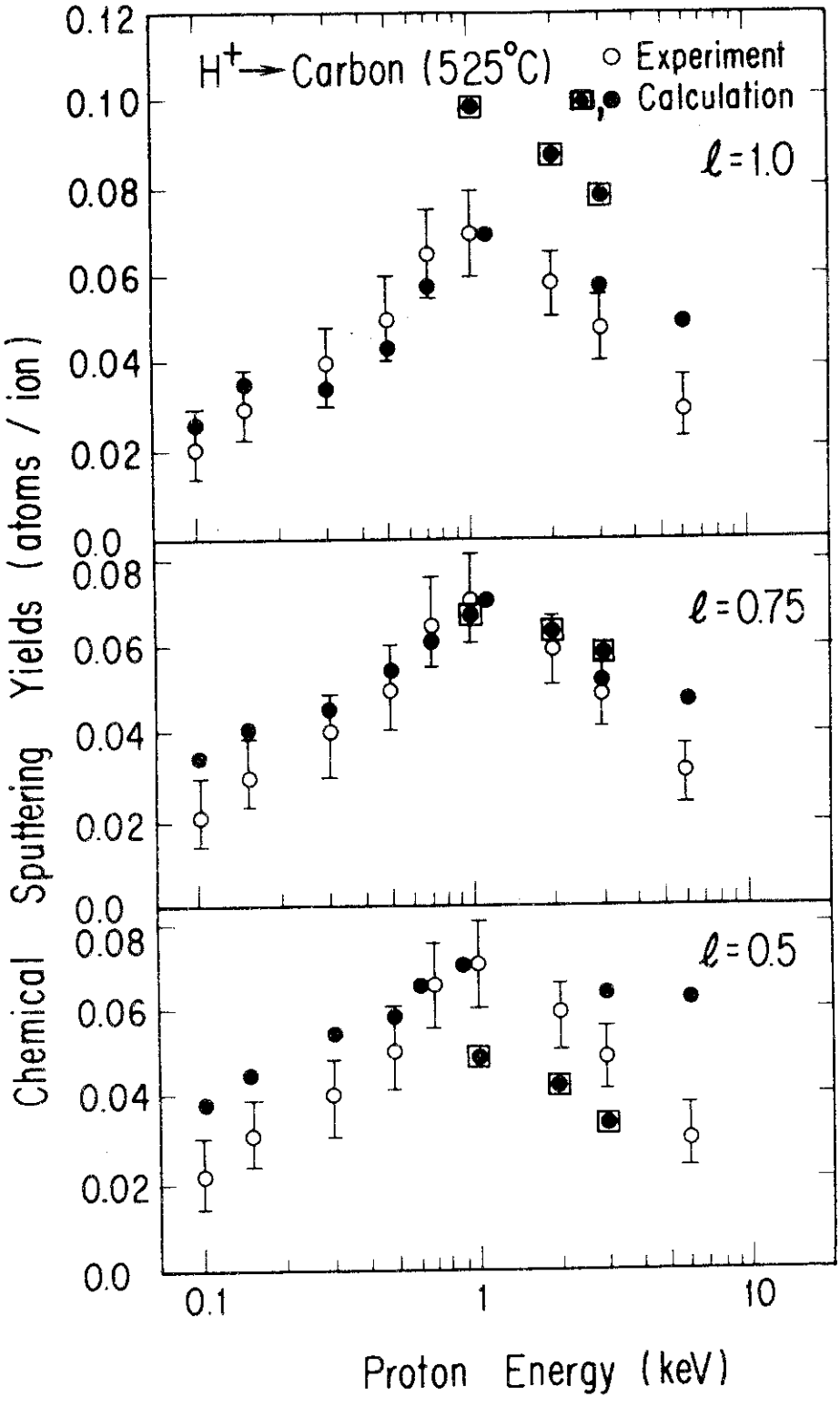

Fig. VI.2-1 Calculated energy dependence of chemical sputtering yield obtained using eq.(1) with changing the value of parameter ℓ. The symbol ◉ shows the calculated result for J_o ($\sim 10^{15}$/cm^2 sec) and the symbol ● for J_o ($\sim 10^{14}$/cm^2 sec).

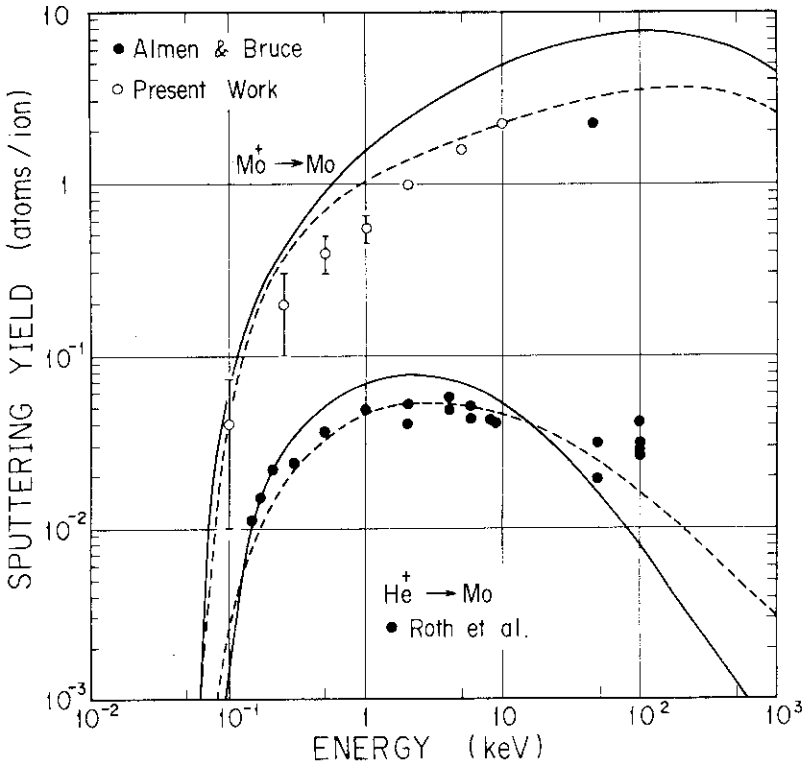

Fig. VI.3-1 Sputtering yield as a function of energy in molybdenum. Broken and solid lines show the IPP model and the MYI model, respectively.

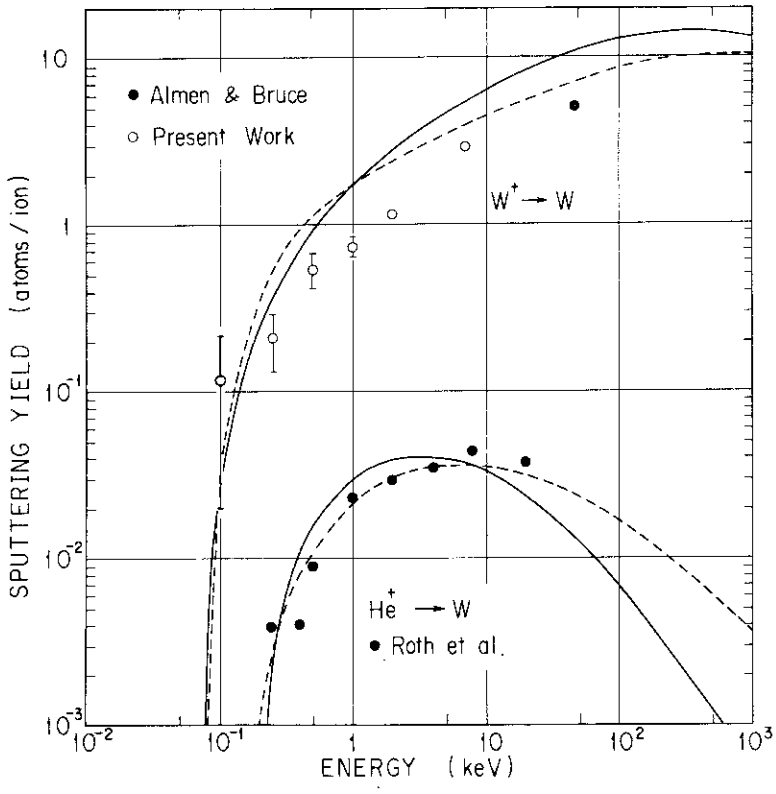

Fig. VI.3-2 Sputtering yield as a function of energy in tungsten. Broken and solid lines show the IPP model and the MYI model, respectively.

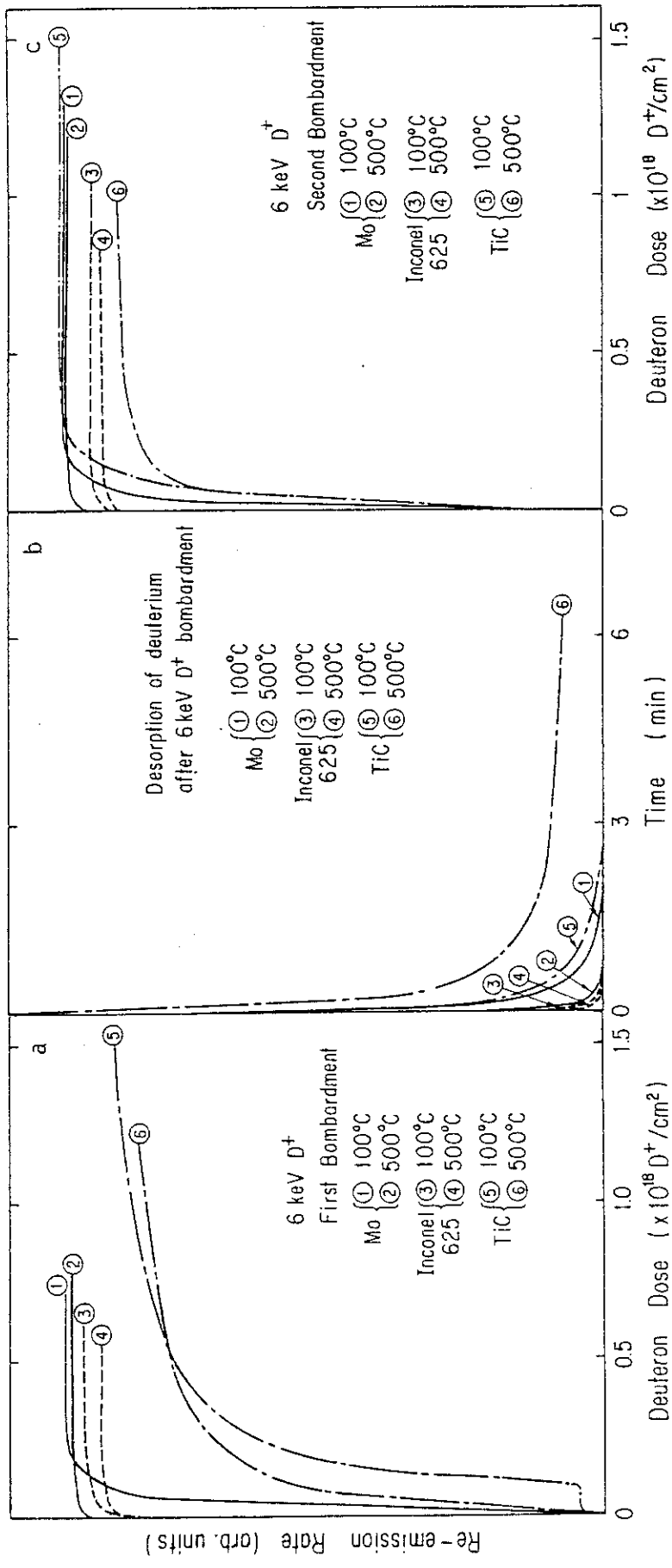

Fig. VI.4-1 Measured re-emission rates of deuterium in Mo, Inconel 625 and TiC for cyclic bombardments with 6 keV D^+ ions.

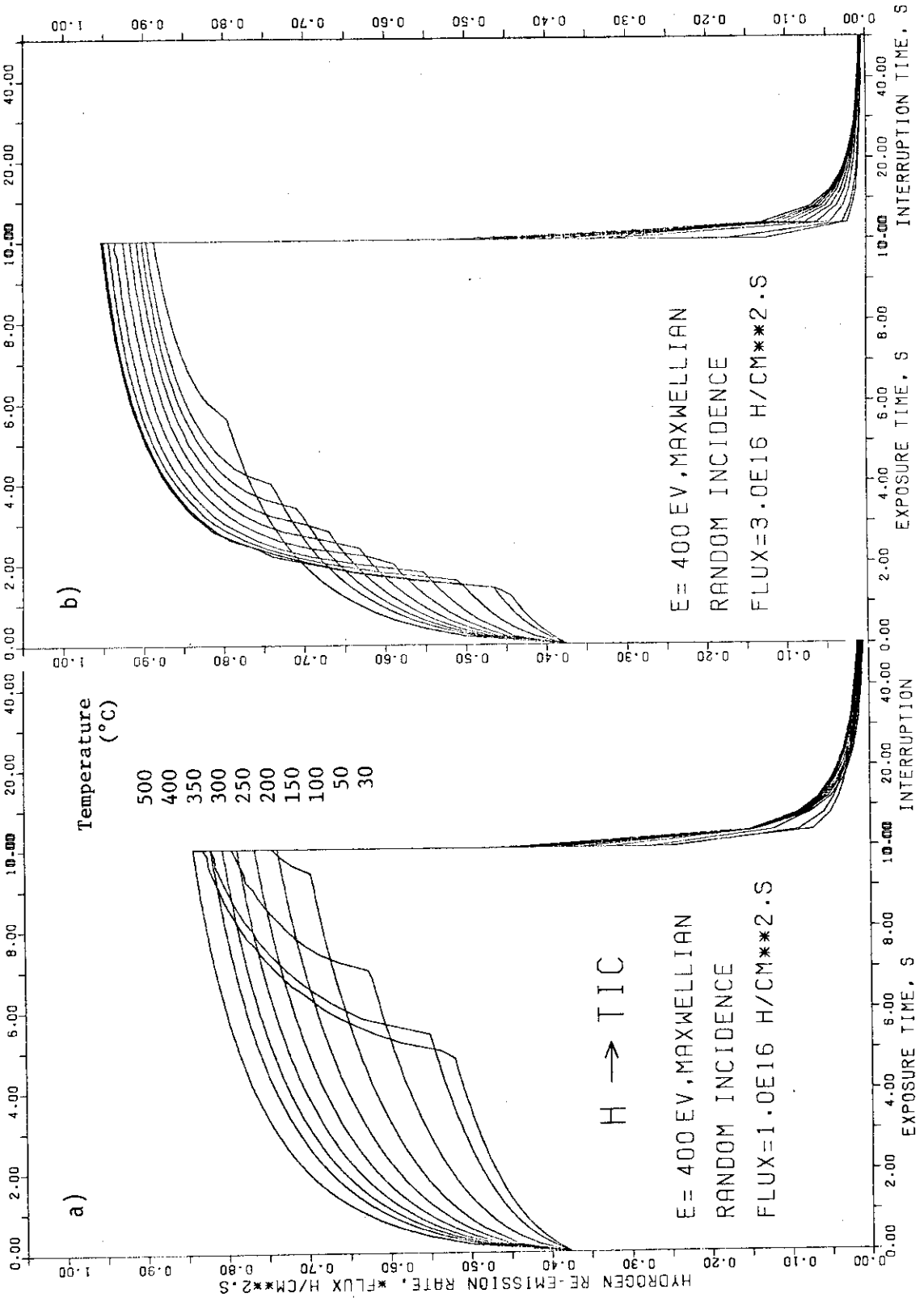

Fig. VI.4-2 Calculated recycling coefficients as a function of time and wall temperature in TiC. Assumed energy distribution of charge exchange neutrals: 400 eV Maxwellian.

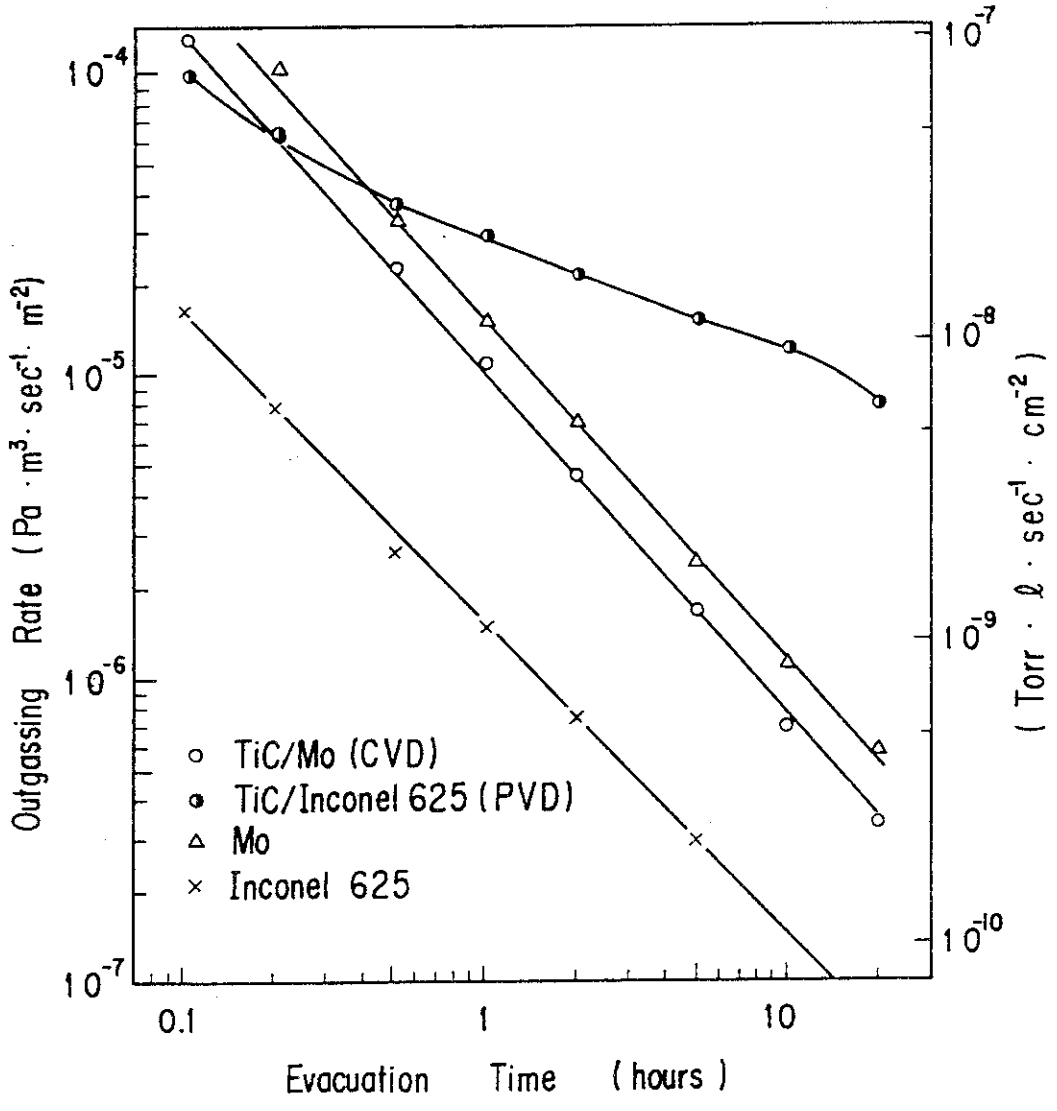

Fig. VI.5-1 Outgassing rates at a room temperature from TiC-coated molybdenum, TiC-coated Inconel, non-coated molybdenum and Inconel as a function of evacuation time.

VII. SUPERCONDUCTING MAGNET DEVELOPMENT

1. Introduction

The superconducting magnet development in JAERI is being carried out for Fusion Experimental Reactor after JT-60 machine.

Cluster Test Program for high field generation and Large Coil Task for scaling-up of coil are being evolved as toroidal coil development. Practice fabrication of high current pulsed conductor has been performed for poloidal coil development. Main achievements in FY 1982 in JAERI Superconducting Magnet Laboratory are as follows.

1) Success of the domestic test of the Japanese LCT coil and the delivery to ORNL
2) 10T generation with Nb_3Sn Test Module Coil in Cluster Test Program
3) Success of 10 kA pulsed conductor test for poloidal coil
4) Completion of conceptual design of Superconducting Tokamak Test Assembly

As a whole FY 1982 brought a number of achievements after elaborate work of previous several years.

2. Cluster Test Program

2.1 The first test on the test module coil (TMC-I)

The cluster Test Program (CTP) was started at 1977 as the development of toroidal coil in tokamak machine. A high magnetic field of toroidal coil is required, because the efficiency of fusion machine increases with higher magnetic field. For example, the Fusion Experimental Reactor (FER) designed as a self ignition machine, proposes a high field toroidal coil of 12 T. Therefore, the main objective of this program is to demonstrate high field generation in large bore.

The Test Module Coil I (TMC-I) is the first test coil in the CTP, the main purpose of TMC-I is to demonstrate that multifilamentary Nb_3Sn conductor is applicable to large-current and high field coil. A fabrication of the TMC-I was started in the beginning of 1980 and was

completed in July, 1982[1]. Table VII.2-1 and Fig. VII.2-1 show the parameters and overview of the TMC-I. And the first test of the TMC-I was carried out in September, 1982[2].

(1) Cool-down and warm-up

Three coils system is composed of three independent helium vessels which serve as coil case. The cool-down weight is 7.2 ton and 6.6 ton for the TMC-I and one CTC, respectively. The cool-down was carried out using a refrigerator which has a capacity of 220 W at 4.2 K. A helium gas flow rate of each coil was in 3-5 g/sec, automatically controlled by the computor based on the data measured from a low temperature flow meter, and the temperature difference between the TMC and the CTC was controlled within 30 degrees as shown in Fig. VII.2-2. The warm-up of three coils was also controlled by the computor on the same condition as the cool-down for a total times of 75 hours.

(2) Current charge test

After a magnetic field of 6.9 T was generated without a back-up field from the CTC, the TMC-I was achieved to be in a field of 10.2 T at 6,050 A with a back-up field of 3.3 T from the CTC without any trouble. The maximum strain due to electromagnetic force at 10 T on the Nb_3Sn conductor in the innermost turn was 0.13 %. Therefore, the total strain of Nb_3Sn was 0.67 % including a bending stress of 0.54 % during winding.

(3) Stability test

Stability test was carried out with use of 30 cm length heater which is located in the highest field zone in the innermost turn. Figure VII.2-3 shows a typical trace of tap voltage and the temperature rise of the conductor at 10 T and 6 kA. The input energy to the conductor was 3.7 J/cc. A normal zone appeared in 0.1 second after the heat input and disappeared in 2 second.

(4) Manual Dump test

A manual dump test of the TMC-I was carried out without charging the CTC. After dumping with 14 seconds of time constant, liquid helium losses were measured. Figure VII.2-4 shows the loss of energy by

calculation of latent heat on lost liquid helium (Q_{loss}), and ratio of the loss of energy to stored energy for all ranges of dumping current.

2.2 Research and development for the TMC-II

The research and development works for the Test Module Coil-II, the second test coil in the Cluster Test Program, were started in this period. The major parameters of the TMC-II are shown in Table VII.2-2. The key objectives of this work are high current density, high rigidity of winding and low losses against poloidal field. One of the method to achieve these objectives is use of a bundle type-forced cooling conductor with high purity aluminium stabilizer. According to this guide line, a 12 T-10 kA Nb_3Sn conductor was designed by JAERI as shown in Fig. VII.2-5. Two verification tests were carried out in this period. To check the usefulness of the Nb alloy thermal barrier in Fig. VII.2-5, the stability tests of two test solenoid, wound by the conductors with and without the barrier, were carried out by using the heater. From these experimental results, it is indicated that the thermal barrier is effective to the stability of the conductor. Secondly, it was found that the electric resistivity of a high purity aluminium was lower than that of a copper, even if applied in cyclic strain.

3. Large Coil Task of IEA

3.1 Domestic test of LCT coil

The domestic test of the Japanese test coil for the Large Coil Task was successfully carried out at JAERI in June, 1982[3]. In the Large Coil Task, six test coils, three of which are manufactured by the United States and others are by Euratom, Switzerland and Japan, are to be tested in toroidal array at Oak Ridge National Laboratory. The Japanese test coil is the first coil which was completed and was tested.

At the domestic test, the coil was set in the Superconducting Engineering Test Facility, and then, was cooled down, charged up, examined and warmed up. Figure VII.3-1 and Table VII.3-1 show the photograph and the major parameters of the Japanese LCT coil, respectively.

(1) Cool-down and warm-up

As shown in Fig. VII.3-2, the coil was cooled down automatically by the helium refrigerator which was controlled by the computer system. The cool-down rate was dominated by the limit of temperature difference in the coil of 96 K which was determined not to exceed the allowable thermal stress. It took 120 hours to cool down the coil and 100 hours to warm up.

(2) Charge up

During the domestic test, the coil was charged up to the nominal current of 10,220 A four times without quenching. The fastest charging rate was 10,220 A/hr. The measured maximum magnetic field was 6.4T. The stored energy of the coil calculated from the self-inductance and the transport current is 106 MJ.

(3) Stability test

The Japanese LCT coil is designed to be stable even if a half turn of the conductor is suddenly normalized. To investigate the stability of the coil, the normalcy was observed. Figure VII.3-3 is the voltage and temperature profiles achieved when a half turn of the conductor was normalized at fully charged state, and this shows that the coil is cryostable. The estimated stability limit of the coil is 12,700 A at 8 T which is in good agreement with the preliminally calculated value, whereas the normal operating condition at ORNL is 10,220 A at 8 T.

(4) Strain measurement

In order to observe the mechanical behavior of the coil, a number of strain gauges are attached on the conductor and on the coil case. Figure VII.3-4 shows the measured strain curve of the conductor which is in good agreement with the calculated one qualitatively, but is higher than the calculated one. This difference is considered to be mainly due to the complicated composite winding structure of the coil. About the strain of the coil case, the measured values agree with the calculated ones.

(5) Manual dump test

The manual dump test was performed in order to get the dump characteristics and to confirm the safety of the coil when there appears the state that the coil must be dumped. Figure VII.3-5 shows the typical temperature trace measured when the coil was dumped manually from the fully charged state, and this shows that the peak temperature was 24 K. The initial dump voltage appeared at this test was 1 kV which was just the rated value. The energy, extracted from the coil to the external resistor, was more than 98 % of the energy stored in the coil, and around 2 % of the stored energy was consumed in the coil and the liquid helium of about 800 l in the coil evaporated as a result. No damage was found on the coil after the dump test.

3.2 Status of the Japanese test coil in ORNL

After the domestic test in June 1982, the Japanese LCT coil was removed from the test facility, packaged and shipped from JAERI in September 22, for the delivery from JAERI to Oak Ridge National Laboratory (ORNL). The test coil was arrived at ORNL in November 12, and the acceptance tests at room temperature was carried out by ORNL. No damage was found in the test coil, installation work was started in the middle of December, 1982. Figure VII.3-6 shows the Japanese test coil installed in the vacuum tank in ORNL. The installation work of the guide duct and the sensor leads are under way. The initial coil test is expected to be performed in the end of 1983.

4. Pulsed Poloidal Coil Development

(1) Highlights

Research and development for superconducting poloidal coils of the Fusion Experimental Reactor (FER) has been progressing. In 1982, three pulsed coils, Pulser-C, Pulser-D, and Pulser-E were constructed and successfully tested at the Superconducting Engineering Test Facility (SETF) of JAERI. In addition, a 30 kA forced-cooled conductor, JF-30, and two 50 kA pool-cooled conductors, JA-50 and JB-50, were fabricated[4,5]. Figure VII.4-1 shows cross sections of these conductors.

(2) Pulsed coils

JAERI developed Pulser-C to generate pulsed background field for testing of large-current pulsed conductors and coils. Pulser-C is a 3 kA, 5.4 T pulsed coil which has sufficient reliability at the pulsed operation of 10 T/s. When JAERI started the development of Pulser-C, some pulsed coils in the U.S., which employed CuNi in addition to NbTi and Cu to reduce pulsed field loss, had showed very low stability. However, through research and development of Pulser-C, a stability problem of pulsed conductors, which employ CuNi, was revealed. Increase in the resistivity of Cu stabilizer near CuNi thin layer (a few micron thickness) was observed. This easily brings high joule generation at the moment of normalization, and thus less stability than designed. Therefore, in the design of Pulser-C conductor, major part of Cu stabilizer was arranged to be separated from CuNi layers and the decrease in the stability was avoided.

Pulser-D and Pulser-E were constructed for verification of 10 kA pulsed conductors, JA-10 and JB-10, developed by JAERI. Major features of these pulsed coils are the high stability by high cooling for Pulser-D and the high reliability by mechanical rigidity for Pulser-E. Testing arrangement and major parameters of these coils are shown in Fig. VII.4-2.

At first Pulser-C was successfully tested and it was charged to the rated current in 3 sec and discharged by the time constant of 0.7 sec, which corresponded to +1.8 T/sec and -7.7 T/sec. Even in the case of the latter fast discharge, measured pulsed field loss was about 3 kJ, which was about 0.2 % of the stored energy (1.3 MJ).

In the second and the third experiment at the SETF, Pulser-D and Pulser-E were tested under background field of Pulser-C. Test results of both experiments were successful and major results are shown in Table VII.4-1. Pulsed field losses of Pulser-D and Pulser-E were less than detection level of thermal measurement, proving the designed low pulsed field loss.

5. Cryogenic System Development

5.1 Development program

The construction of Fusion Engineering Reactor (FER) which is a superconducting tokamak after JT-60 at JAERI absolutely requires a

large, reliable and efficient helium cryogenic system[6]. Typical characteristics required are 10-20 kW refrigeration power at 4 K, reliable for more than 8,000 hours and high energy efficiency more than 1/500. The energy efficiency is defined as a ratio of the refrigeration power to the required input power at room temperature. Therefore, extremely larger cryogenic system than the present one is indispensable to construct the FER. For this purpose, JAERI has been developing cryogenic system in accordance with the development program as shown in Table VII.5-1. By using the Cluster Test Facility (CTF) and the Superconducting Engineering Test Facility (SETF)[7], JAERI has almost achieved the second step toward the cryogenic system for the FER.

5.2 Liquid helium transfer test

Development of liquid helium transfer technology is important requirement for the FER in which 100 m liquid helium transfer piping will be installed. In order to verify flow behavior of liquid helium in real size cryogenic piping, JAERI constructed Liquid Helium Transfer Test Facility which was around 50 m in length with 1/2 B pipe. The following items were measured in the facility.

(i) pressure drop of liquid, 2 phase and gas helium
(ii) heat transfer coefficiency of liquid and 2 phase helium
(iii) thermal performance of cryogenic piping
(iv) cool-down characteristics of cryogenic piping

Figure VII.5-1 shows measured heat leakage of the piping as a function of temperature of shield plate set between inner and outer piping. The Liquid Helium Transfer Test Facility brought an appreciable amount of technical information to construct the cryogenic system for the FER.

6. Development of the New Cryogenic Structural Material

We have been developing the new cryogenic material for the Fusion Experimental Reactor (FER) which has yield strength of more than 1,200 MPa, Charpy absorbed energy of more than 100 J, fracture toughness of more than 200 MPa$\sqrt{m}$ [8]. These are very high values compared with mechanical properties of austenitic stainless steel 304 LN and 316 LN[9].

Figure VII.6-1 shows the relation between Charpy absorved energy and yield strength at 4.2 K. There are twelve satisfactory materials

which have the above requested values. These materials are devided into austenitic stainless steel and high manganese austenitic stainless steel. The best balanced material is the austenitic stainless steel which has yield strength of 1,465 MPa and Charpy absorbed energy of 174 J. Fracture toughness test of the high manganese austenitic stainless steel which has yield strength of 1,200 MPa and Charpy absorbed energy of 126 J has been completed. This material has fracture toughness of 202 $MPa\sqrt{m}$ and satisfies all the above requirements.

Since several excellent materials are produced by industrial quantity such as 15, 70 ton melting, it will not take a long time before these new cryogenic materials have practical application and we will use one of these new cryogenic materials as the structural material of superconducting toroidal coils in the near future.

7. System Design of the Superconducting Tokamak Test Assembly

JAERI is developing the coil and cryogenic system for the Fusion Experimental Reactor (FER) which is the next tokamak to follow after JT-60. As a step to develop a large and reliable superconducting tokamak coil system such as FER, construction of a medium sized tokamak system is indispensable. On the basis of the tentative parameters chosen through the design work in JAERI, design works on the coil system and cryogenic system[6] for the medium sized machine, maximum field of 8 T, have been carried out.

The coil system is composed of 12 superconducting toroidal coils which have similar configuration to those of a test coil for the Large Coil Task (LCT), and 12 superconducting poloidal coils whose diameter is 1.6-10 m, and the other facilities for the power generation. The major radius and plasma current is to be specified 2.4 m and 2.7 MAT respectively. A cable-in-conduit type is selected for both toroidal coil and poloidal coil conductor. Plate type structure with spiral slot to accept the conductor, which is the same conception as a Westinghouse LCT coil, is employed for the toroidal coil. The major parameters of the coil system is listed in Table VII.7-1.

The capacity of the cryogenic system for the coil system is specified to be 3,000 liters of liquefaction per hours or 12 kW of refrigeration at 4.4 K, reliable for more than 6,000 hours and high

energy efficiency more than 1/500. This cryogenic system is expected as a unit of the cryogenic system for the FER.

References

1) Ando, T., et al, International Cryogenic Engineering Conference (ICEC9) proc., 1982.
2) Ando, T., et al., '82 Applied Superconductivity Conference (Knoxville Dec., 1982).
3) Shimamoto, S., et al., ibid.
4) Shimamoto, S., et al., International Cryogenic Engineering Conference (ICEC9) proc. 1982.
5) Takahashi, Y., et al., '82 Applied Superconductivity Conference (Knoxville Dec., 1982).
6) Shimamoto, S., et al., '82 Applied Superconductivity Conference (Knoxville Dec., 1982).
7) Tada, E., et al., International Cryogenic Material Conference (ICMC) Kobe May 1982.
8) Yoshida, K., et al., ibid.
9) Takahashi, Y., et al., Advanceds in Cryogenic Engineering, Vol.28, 1982.

Table VII.2-1 Parameters of the Test Module Coil I (TMC-I).

Coil Shape	Circular
Coil Size	
Winding Inner Diameter	600 mm
Winding Outer Diameter	1584 mm
Winding Width	300 mm
Winding Method	10 Double Pancakes
Cooling Method	Pool Cooling
Grading Method	Two Grades (10/6.2 T)
Maximum Magnetic Field	10.2 T
Operating Current	6,056 A
Average Current Density	30 A/mm^2 (in winding)
Magnetmotive Force	4.39 MAT
Self Inductance	0.46 H
Superconducting Materials	Nb_3Sn / Nb-Ti
Structure Materials	304L / 316L
Final Assembly	Electron Beam Welding
Liquid Helium Inventory	191 Liter
Coil Weight	7.17 Ton

Table VII.2-2 Major parameters of the TMC-II.

Coil shape	oval
Winding size	0.76 m x 0.92 m
Maximum field	12 T
Operating current	10 kA
Current density in winding	37 A/mm^2
Stored energy	20 MJ
Superconductig material	Nb_3Sn
Cooling method	Forced Cooling

Table VII.3-1 Major parameters of the Japanese LCT coil.

Superconductor	Nb-Ti	
Cooling	Pool cooling at 4.2 K	
Winding concept	Edge wise, 2 gradings	
	20 double pancakes	
Rated current for 8 T	10,220 A	
Current density	overall	26.6 A/mm^2
	8 T grading	24.2 A/mm^2
	5 T grading	30.3 A/mm^2
Self inductance	2.0 H	
Number of turns	658	
Structural material	304 LN stainless steel	
Assembly	Bolt and seal welding	
Conductor type	Soldered cable in a rectangular copper stabilizer with roughened surface	

Table VII.4-1 Test results of 10-KA pulsed coils.

	PULSER-D	PULSER-E
COOL DOWN SPEED	-10 K/h	-15 K/h
100-% CHARGING	10kA OK (6.7T)	10kA OK (5.8T)
PULSED CHARGING	10kA/6sec OK	10kA/6sec OK
FAST DUMP	-13 T/s OK	-16 T/s OK
Extended Charging	Not Yet	154% (6.9T) No Damage

Table VII.5-1 Helium cryogenic system development program.

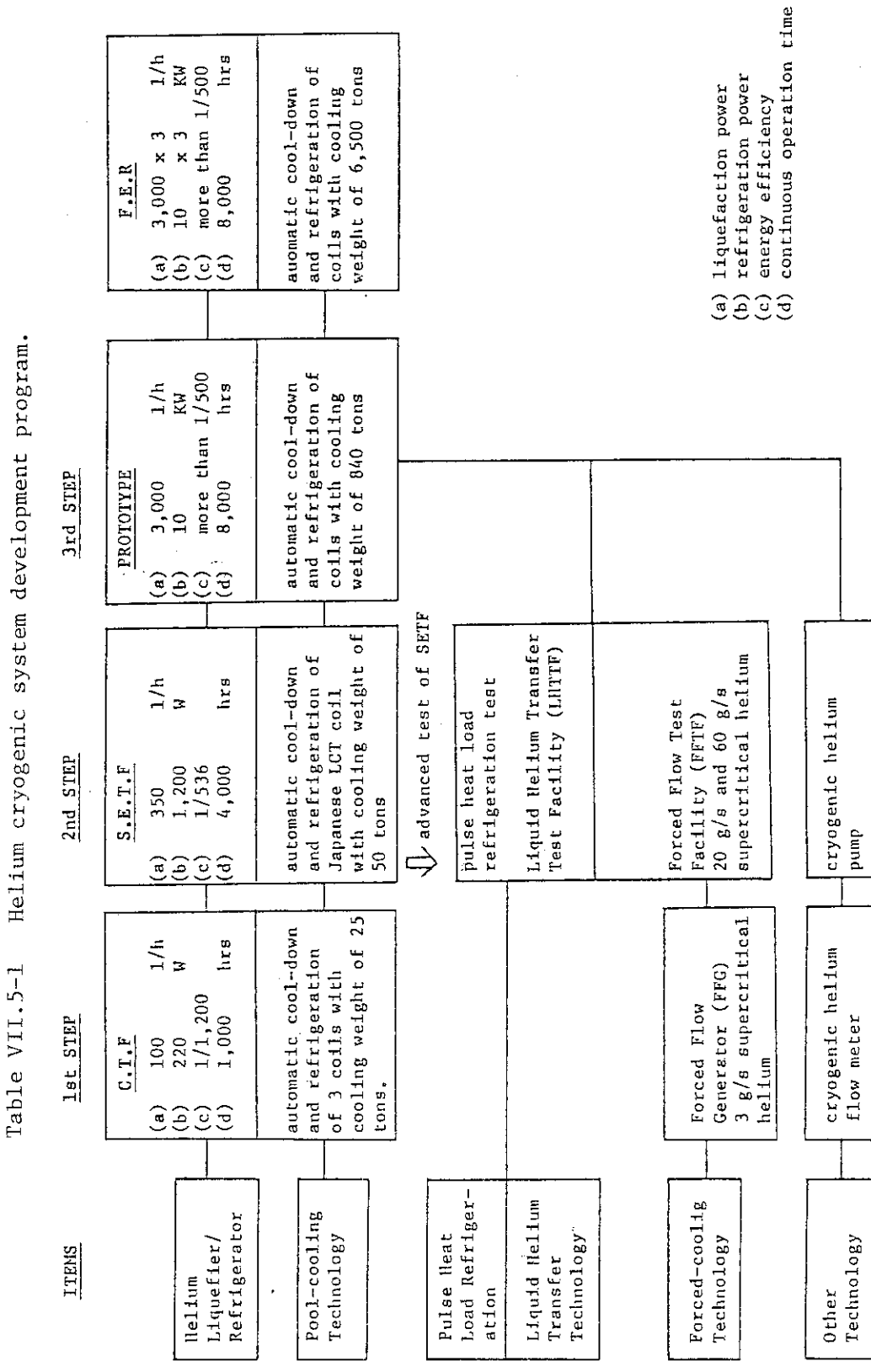

Table VII.7-1 Design parameter of STTA-LCT.

TF Coil	Given Condition	Major Radius of Plasma	2.39 m
		Clear Bore	2.5 m × 3.3 m
		Plasma Current	2.7 MA
		Number of Coils	12
		Toroidal Field	5 T or more
		Maximum Field	8 T
	Design Assumption	Average Current Density	19.2 A/mm^2
		Operational Current	16.4 KA
		Conductor Material	Nb_3Sn
		Cooling Method	Forced Flow
		Winding Concept	Spiral Pancake in Disk Plate
		Assembling	Through Bolt
PF Coil	Given Condition	Coil Diameter	0.8 m ~ 5.0 m
		Number of Coils	12
		Ampere Turns	2.7 ~ 8.6 MAT
	Design Assumption	Average Current Density	25.0 A/mm^2
		Operational Current	30 KA
		Conductor Material	NbTi
		Cooling Method	Forced Flow
		Winding Method	Double Pancake

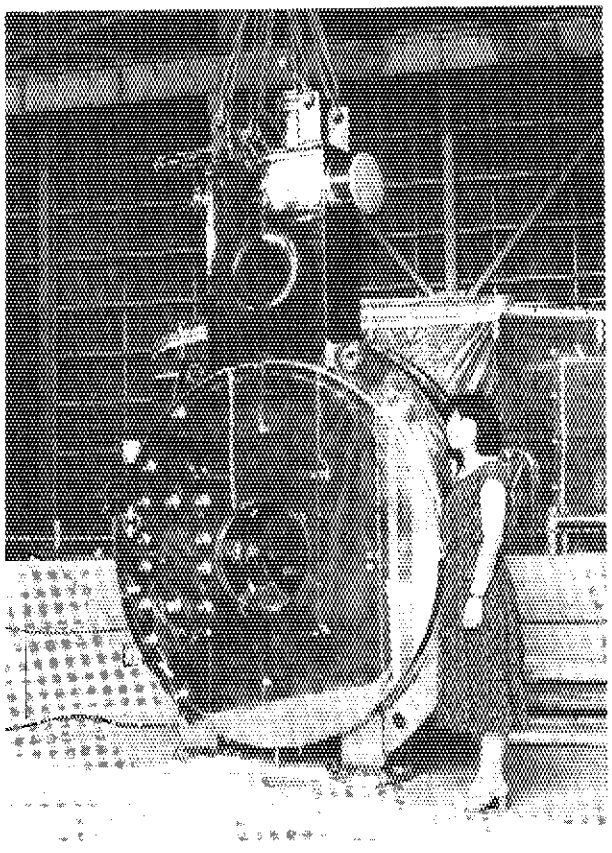

Fig. VII.2-1 Test Module Coil I (TMC-I).

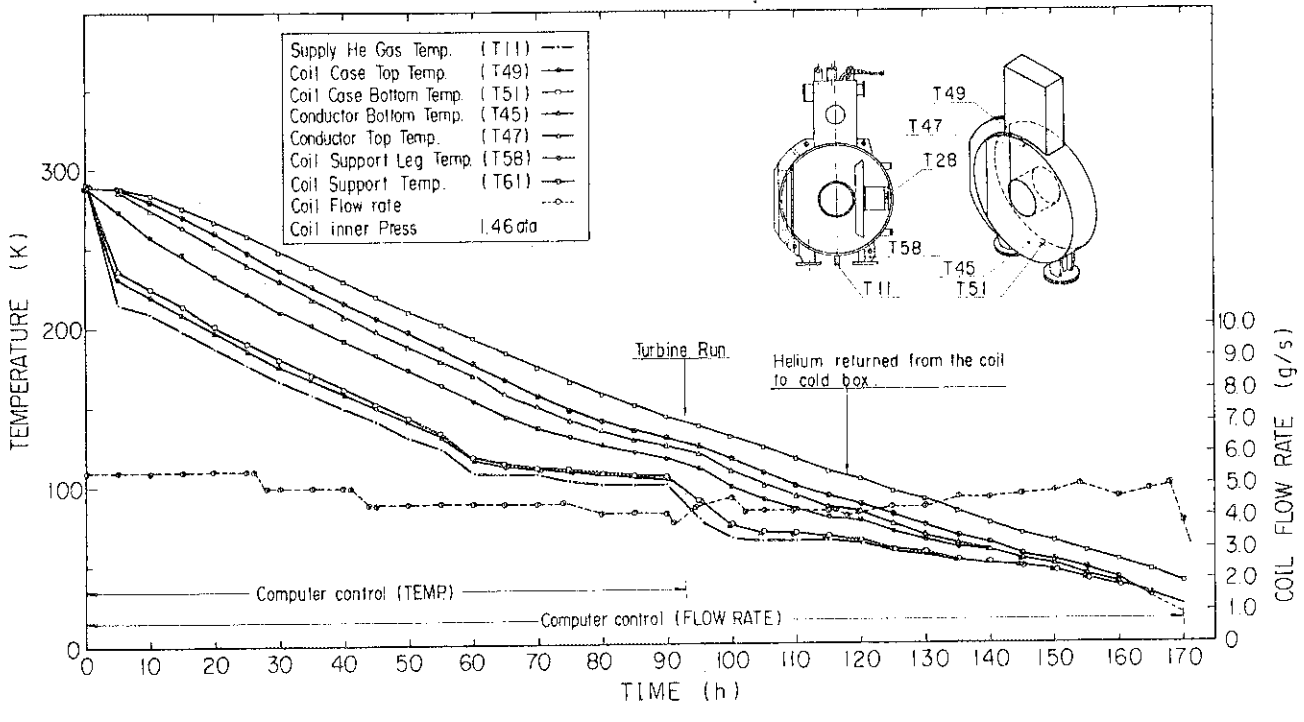

Fig. VII.2-2 Cool-down characteristics of the TMC-I.

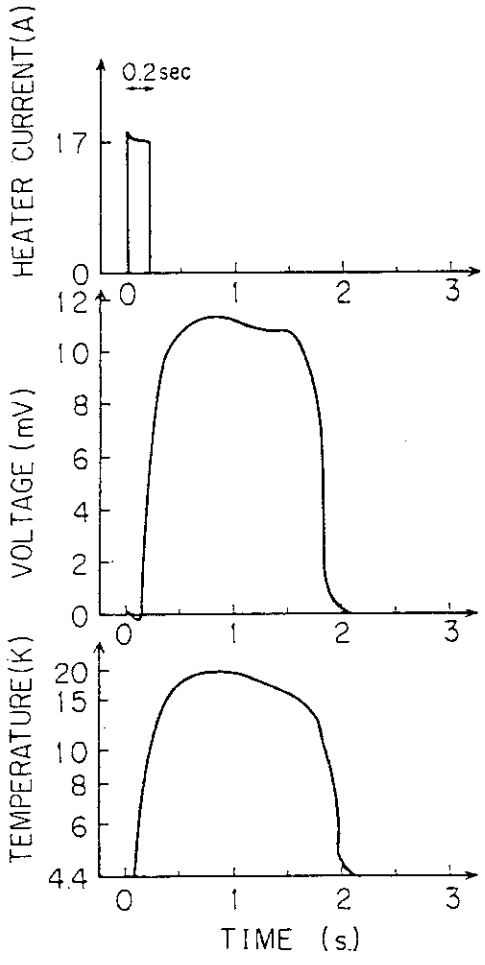

Fig. VII.2-3
Result of the heater test at 6 kA, 10 T.

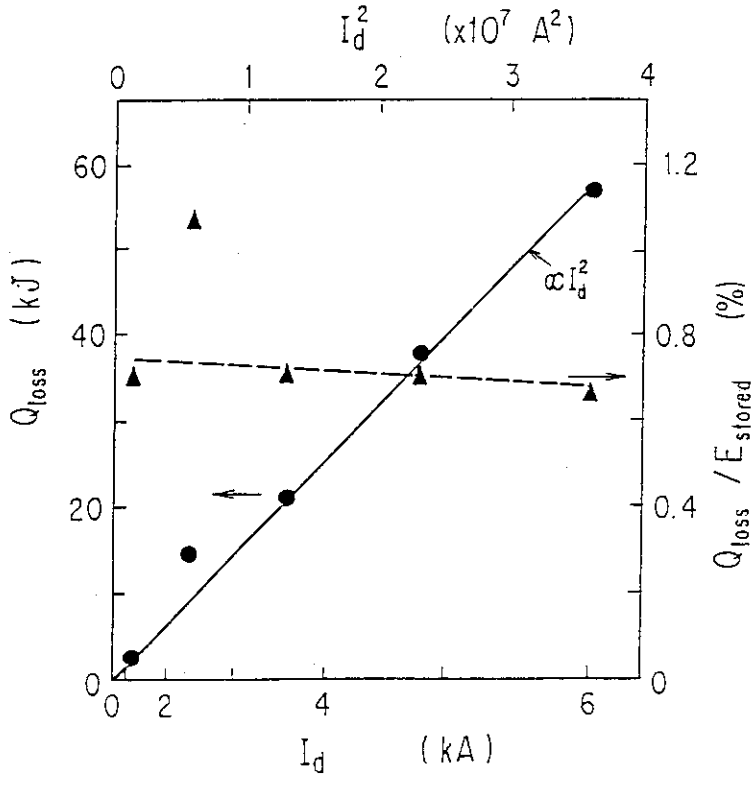

Fig. VII.2-4 Dump losses and ratio of dump losses to stored energy as a function of dump current.

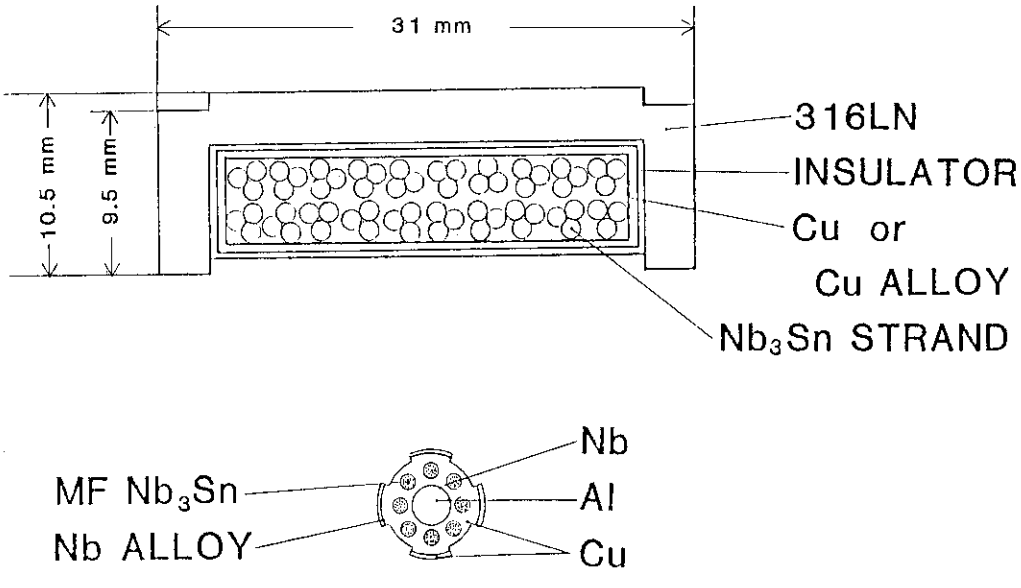

Fig. VII.2-5 Cross sectional view of the conductor for the TMC-II.

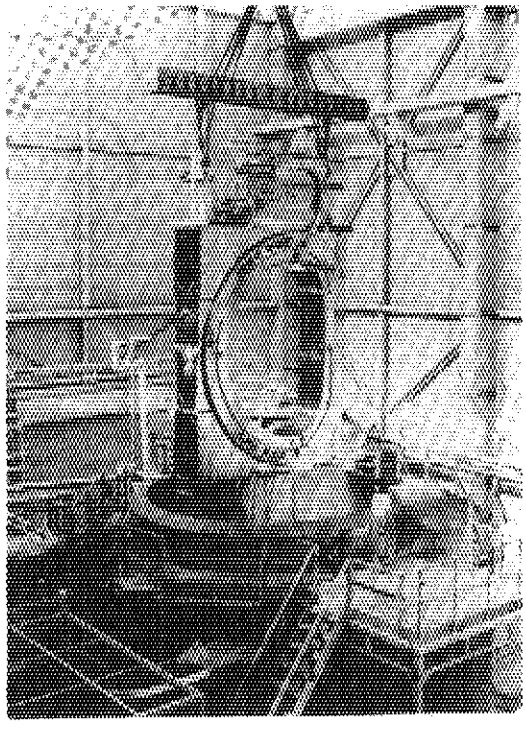

Fig. VII.3-1 The Japanese LCT coil being installed in the vacuum tank in Superconducting Engineering Test Facility (SETF) at JAERI.

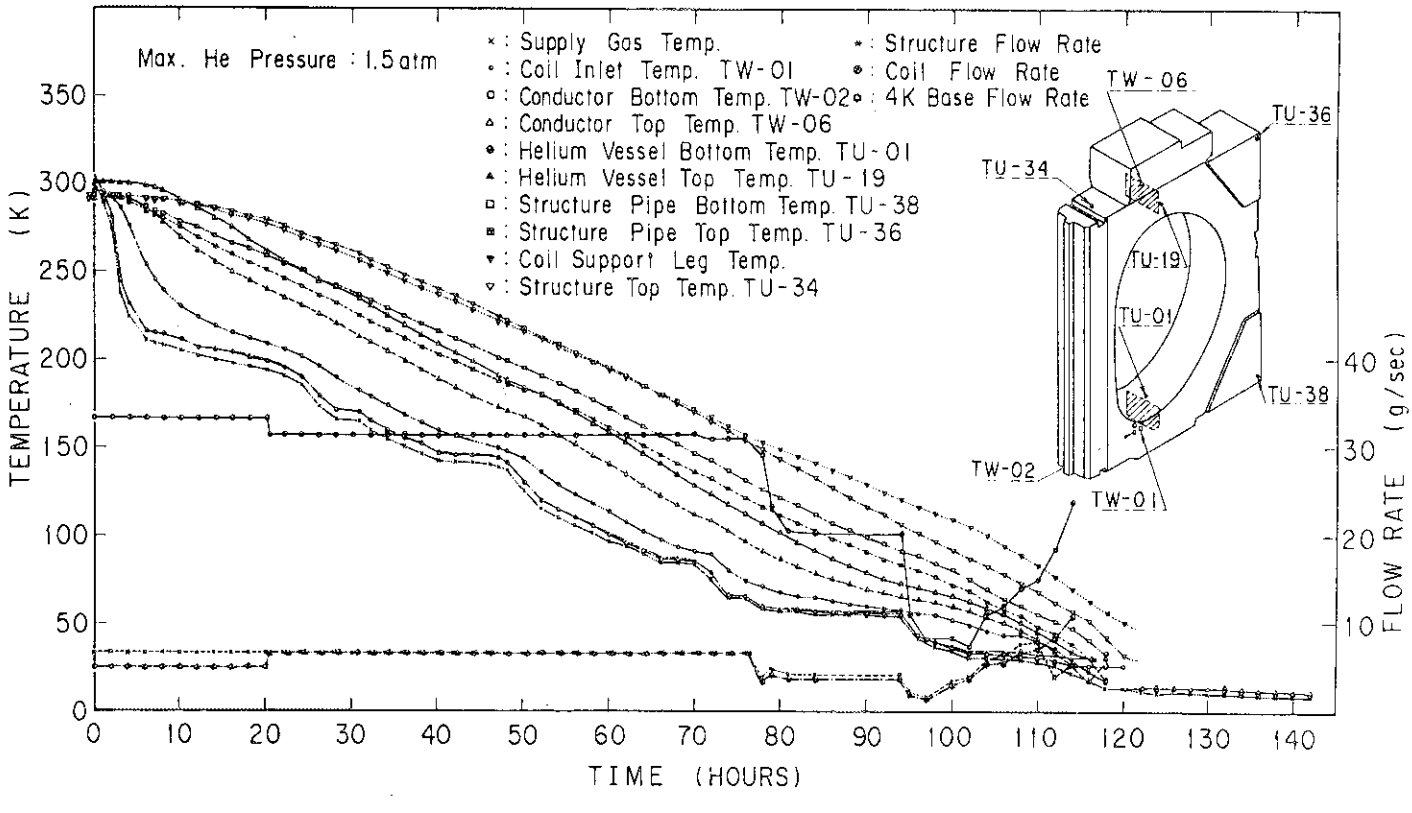

Fig. VII.3-2 Cool-down characteristics of the Japanese LCT coil.

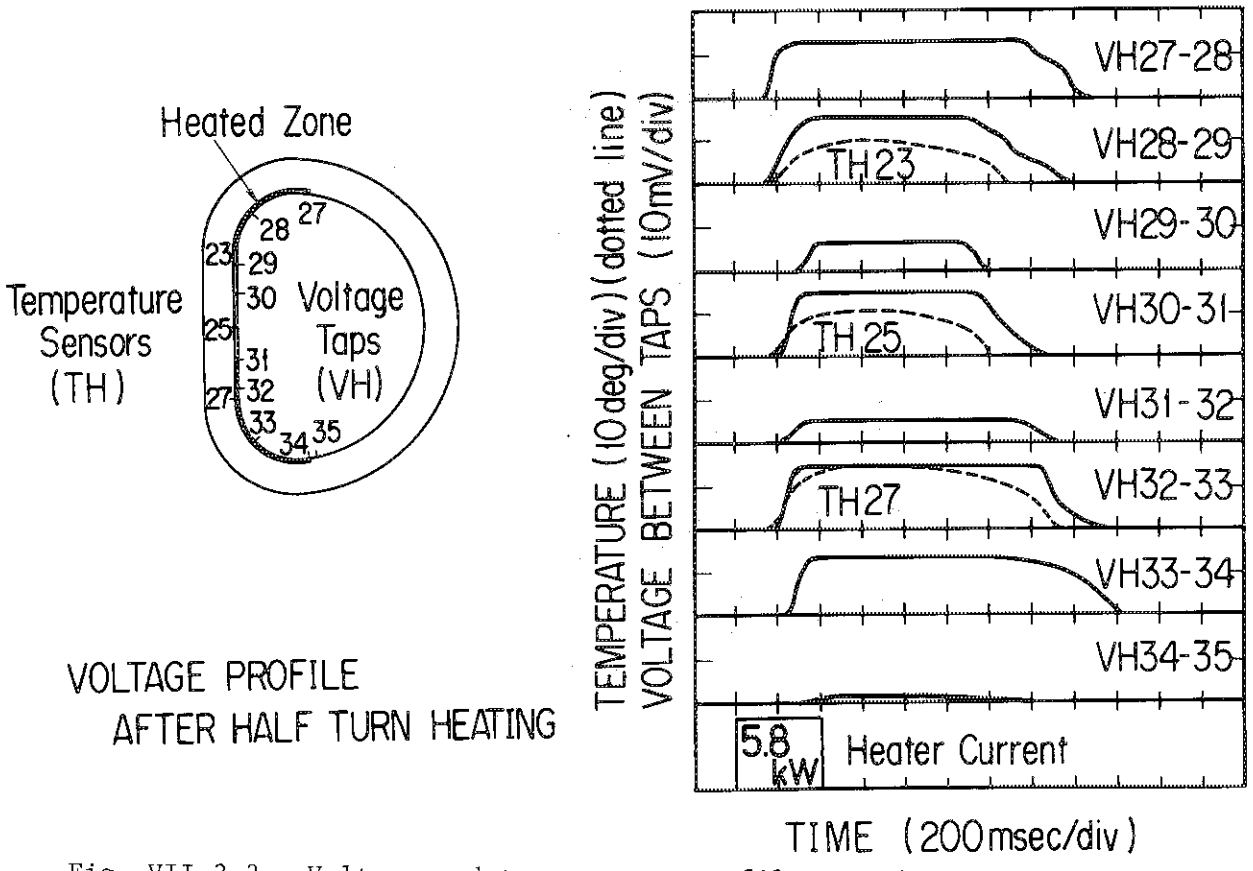

Fig. VII.3-3 Voltage and temperature profiles on the normalized harf turn in the innermost of the middle pancake at 10,220 A.

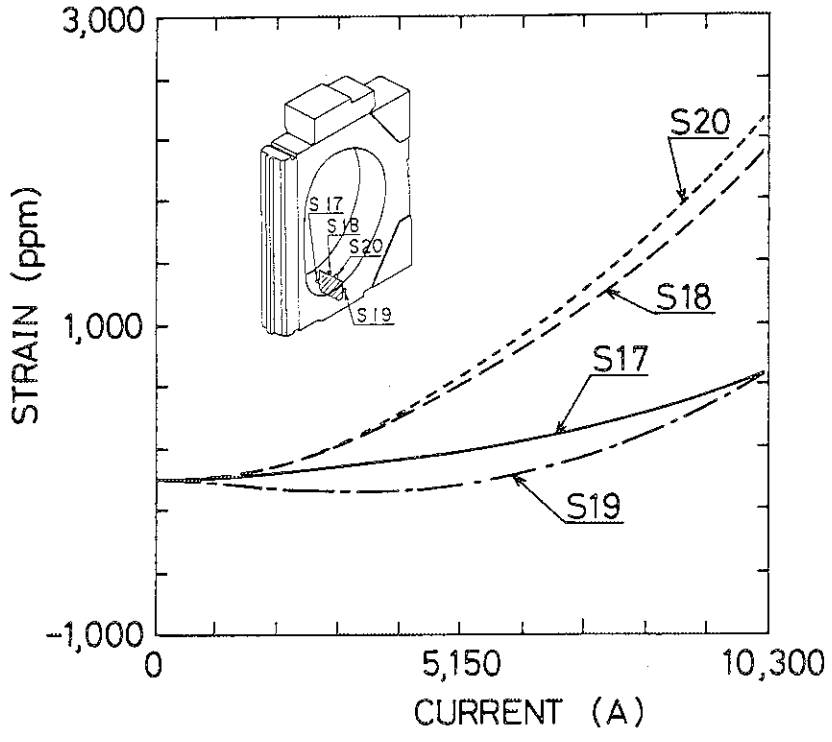

Fig. VII.3-4 Measured strain curves of the conductor in a function of the coil current.

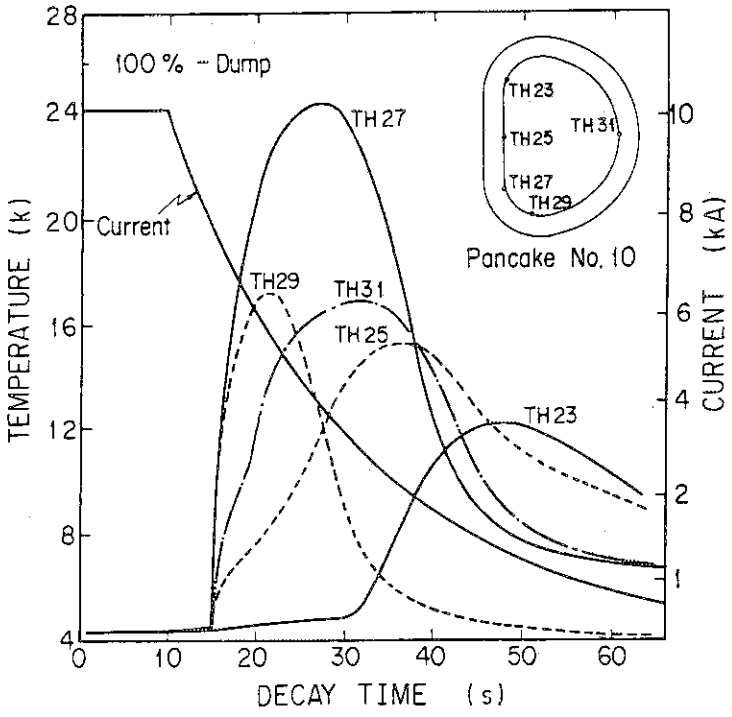

Fig. VII.3-5 Temperature increase due to manual dump from 100% current (innermost turn of the middle pancake).

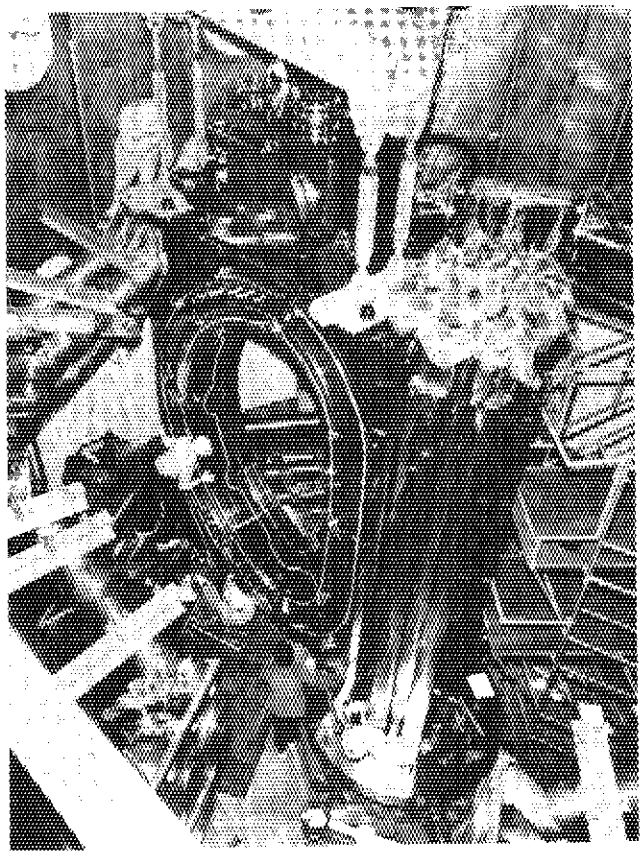

Fig. VII.3-6 The Japanese LCT coil being installed in the vacuum tank in the Large Coil Test Facility at ORNL.

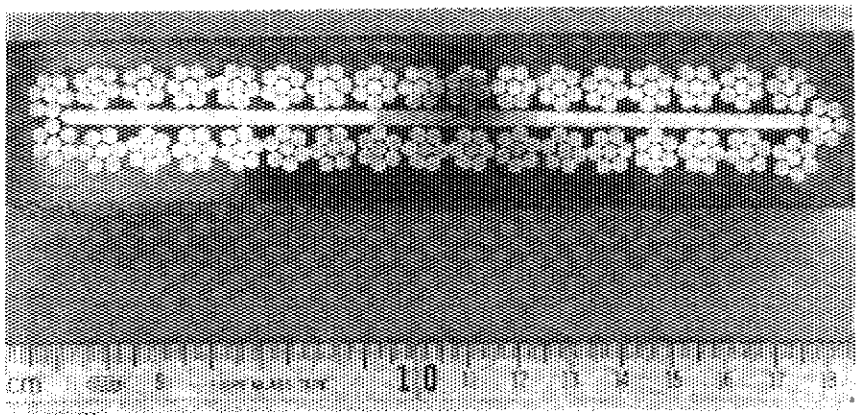

JA-50 (7T, 50kA, Pool Cooled)

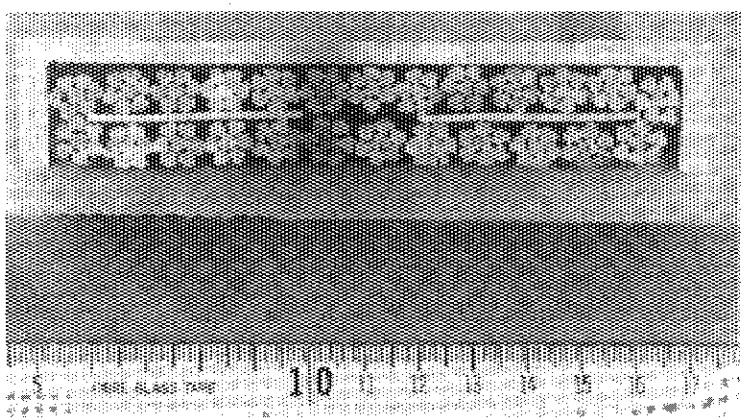

JB-50 (7T, 50kA, Pool Cooled)

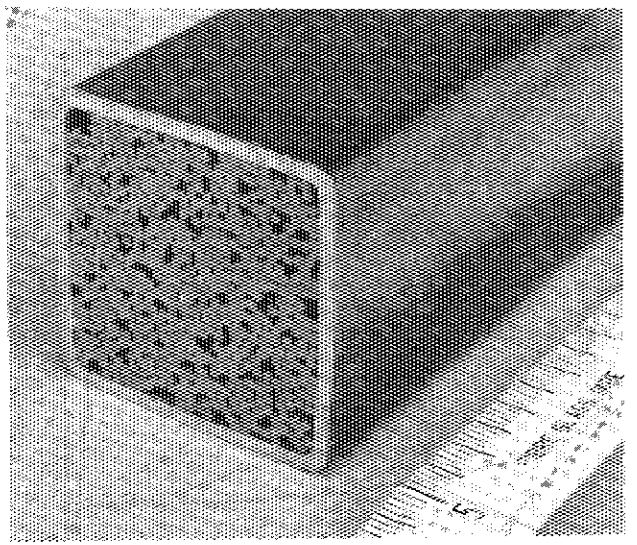

JF-30
(7T, 30kA, Forced Cooled)

Fig. VII.4-1 Cross sections of JA-50, JB-50 and JF-30.

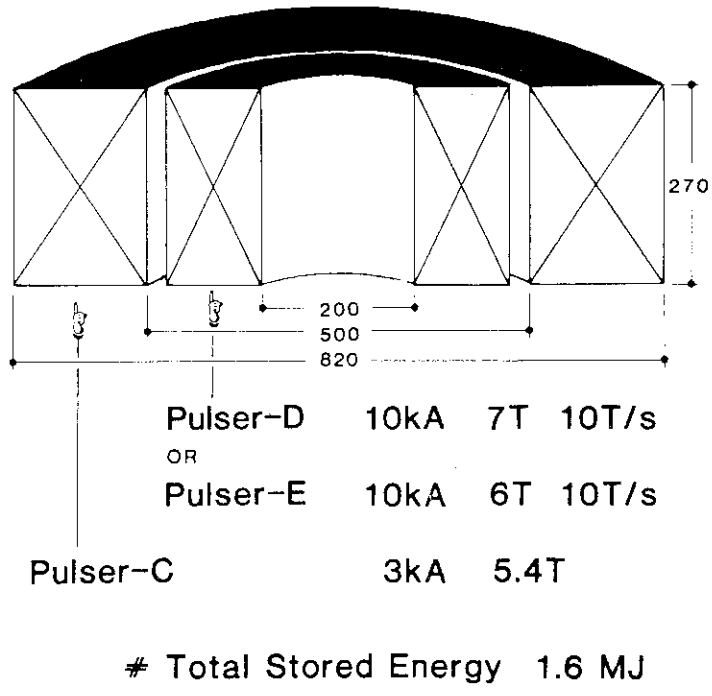

Fig. VII.4-2 Testing arrangement at 10-KA pulsed coils.

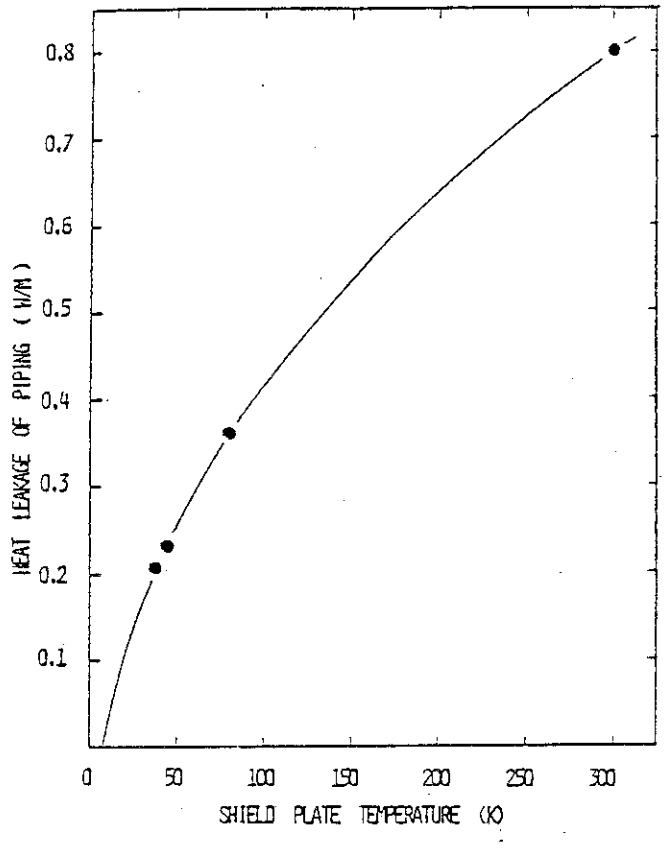

Fig. VII.5-1 Thermal performance test results.

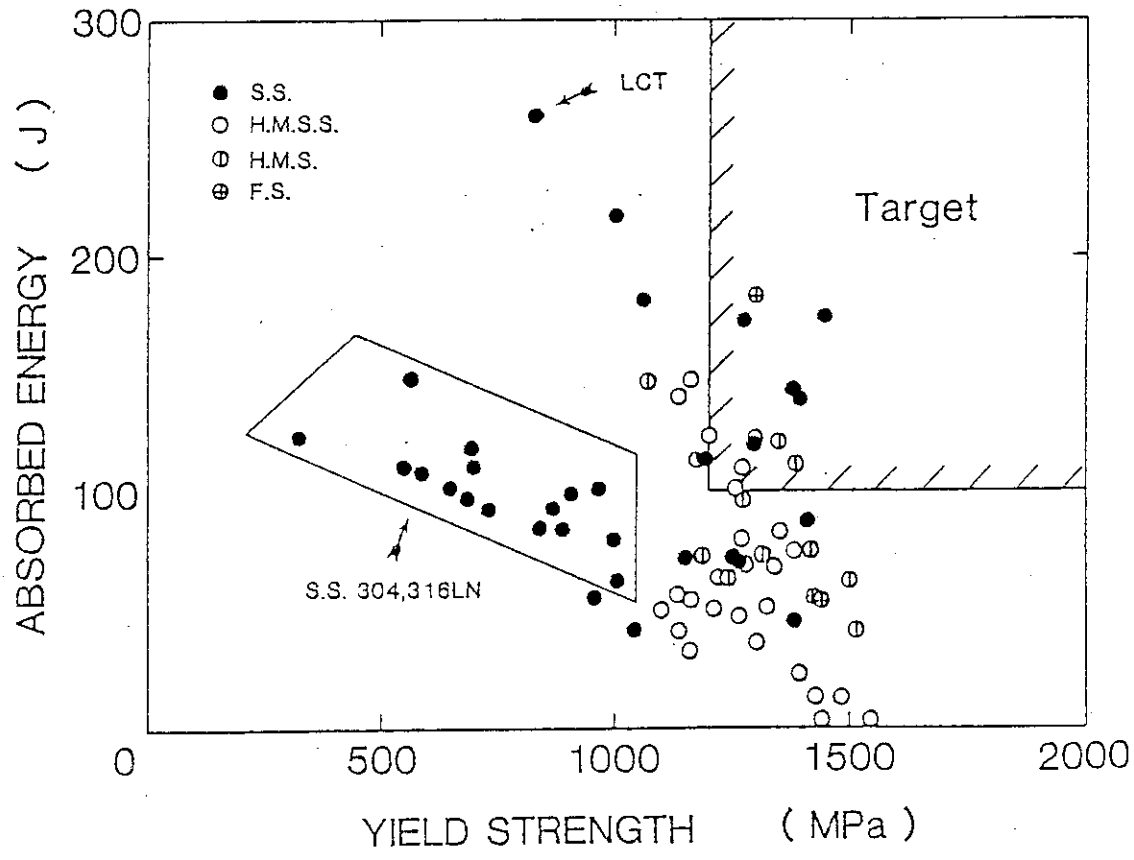

Fig. VII.6-1 Relation between charpy absorbed energy and yield strength at 4.2K.

VIII. TRITIUM TECHNOLOGY

1. Development of Tritium Processing Technology

1.1 Fuel purification

1.1.1 Water decomposition by ceramic electrolysis cell

The characteristics of the solid electrolysis cell using a stabilized zirconia have been studied for an application to the process of the tritium recovery from tritiated water which will be produced in a fusion fuel cycle.

Figure VIII.1-1 shows the schematic arrangement of experimental apparatus for water vapor electrolysis.

Figure VIII.1-2 shows the theoretical characteristics of the cell calculated by the Nernst's equation. Conversion ratio of water to hydrogen depends on the open-circuit voltage. The ratio close to unity is likely to independent on the operating temperature.

Based on the experimental and theoretical feasibility study of this method, several new concepts of tritium recovery system composed of the electrolizer were proposed for a fusion reactor fuel system. Figures VIII.1-3 and VIII.1-4 show the examples of the application.

1.1.2 Water decomposition by catalytic reduction bed

Experimental and theoretical feasibility studies of a catalytic reduction method were carried out for an application to the tritium recovery processes in fusion reactor systems. Experimental conditions of water decomposition were the following: temperature 350∿650 K; H_2O vapor concentration 10^3∿10^4 ppmv; mole ratio of CO to H_2O 1∿10; space velocity 2×10^2∿2×10^4 hr^{-1}. The catalyst was a mixture of CuO, ZnO and Cr_2O_3. Figure VIII.1-5 shows the theoretical conversion factor of water vapor against temperature at various CO gas mole ratios.

1.2 Hydrogen isotope separation

Hydrogen isotope separation is one of the key processes in a fuel circulation system for fusion reactors. Cryogenic distillation is best suited to the process because of its many advantages that is simple

cascade layout for multi-component hydrogen isotope separation, small size of separation columns, short equilibrium time, low tritium permeation, etc..

As the first stage of the study for this method, separation experiments of N_2 and Ar was initiated by using a cryogenic distillation column. Principal objects of the present study are to compare the experimental observation with the computer predictions and to examine the column performance. Another objective is to find operational problems. Useful information for the next stage of experimental work with hydrogen isotopes can be obtained through this preliminary experiment.

Figure VIII.1-6 shows a conceptual flow diagram of the experimental apparatus. The column dimensions are 1.94 $cm^{ID} \times 50$ cm^{H}, the type of packing is Dixon-ring, which is one of the most popular packing. The dynamic column performance is measured under the condition of total reflux operation mode.

Figure VIII.1-7 shows an example of comparison between the calculated values and experimental ones. The dynamic column behavior predicted by the computer simulation agrees well with the experimental results. The HETP value was measured under different vapor flow rates in the column. The typical value was approximately 5.5 cm, and it remained constant in the range from 20 mol/hr to 70 mol/hr.

1.3 Blanket technology

1.3.1 Tritium recovery from lithium-based materials

Tritium release behavior in neutron-irradiated lithium compounds has been studied with the purpose of accumulating the basic data for the selection of blanket materials. When the neutron-irradiated materials such as Li_2O, LiOH, $LiAlO_2$, Li_2SiO_3, Li_2TiO_3, Li_2ZrO_3, LiH, Li_2C_2, Li_3N, LiAl and Li_7Pb_2 were heated under vacuum, the tritium was released on the chemical forms of HT, HTO, CH_3T and $C_2H_{2n-1}T$ (n=1,2,3). Table VIII.1-1 presents the distribution of tritiated species. From the oxide materials the tritium was released mainly in the form of HTO, while HT was the major species released from the other materials which contained no oxygen.

Diffusion coefficients determined for the thermal release of tritium from Li_2O, Li_2C_2, LiAl and Li_7Pb_2 are shown in Fig. VIII.1-8.

The rate-determing step of the HTO release from Li_2O was found to be diffusion of tritium (T^+) in the solid, although HTO molecules would eventually be evolved through the thermal decomposition of LiOT at solid surface. In the sintered pellet, trapping of HTO molecules in grain boundaries would affect to reduce the HTO release rate.

Diffusion of tritium was found to control the HT release from Li_2C_2 and LiAl. The Arrhenius parameters of tritium diffusion in Li_2C_2 and LiAl were comparable with that reported for self-diffusion of hydrogen (H^-) in LiH crystals.

1.3.2 Water adsorption in Li_2O-H_2O-He sweep gas system

Adsorption characteristics of water vapor on Li_2O pellets in the helium gas stream were experimentally studied to give a technological information on the tritium inventory and operating conditions for sweep type fusion blanket design.

The amount of water vapor adsorbed on the pellets was represented by the following experimental equation;

$$I_A = 56.3 \times 10^{-2} \exp(13800/RT) \cdot P_{H_2O}^{0.64}$$

where I_A is the sorption amount (mol-H_2O/ton-Li_2O), R is the gas constant (1.986 cal/mol·K), T is the temperature (K), and P_{H_2O} is the partial pressure of water vapor (atm). The critical conditions of producing LiOH, which will increase tritium inventory in the Li_2O blanket, by the reaction $Li_2O(s) + H_2O(g) \rightleftarrows 2LiOH(s,l)$ were determined for the water vapor pressure and temperature.

2. System Analysis

2.1 Cryogenic distillation column for hydrogen isotope separation

A computer-aided simulation procedure is established for a single cryogenic distillation column with a feedback stream for separation of protium and tritium (Fig. VIII.2-1). It is shown that the error in estimation of mole fractions of HT in the two products can be significantly large unless special cares are taken in the simulation. This

problem posed by the presence of the feedback stream is overcome by solving a specific single-variable nonlinear equation introduced by using the Newton method. The simulation results indicate that the effect of the sidestream location on the column performance is markedly large.

2.2 Dynamic analysis of cryogenic distillation column

Details of the dynamic behavior of a hydrogen isotope distillation column is further investigated. Characteristics of proportional-integral control modes for the column are also studied, and a great deal of information are obtained. A simple parameter setting method for the two PI control parameters is proposed for designing a successful control system. The method has the following advantages: the nonlinearity of the column is taken into consideration; and the unstable region can be predicted in the design stage.

2.3 Falling liquid film condenser for removal of helium from hydrogen isotopes

Parametric surveys are made for a cryogenic falling liquid film helium separator considering the tritium concentration in the top gas as the most critical parameter. Higher operating pressure, larger flow rate of the protium stream added to the feed and longer packed section results in a lower tritium level in the top gas. The tritium concentration can be kept below an adequately low level, and the top gas can directly be transferred to the Tritium Waste Treatment.

2.4 Multistage-type water/hydrogen exchange

A new simulation procedure is developed for a multistage-type water/hydrogen exchange column (Fig. VIII.2-2). The procedure can be applied to a column processing all the isotopic species, H_2, HD, HT, D_2, DT, T_2, H_2O, HDO, HTO, D_2O, DTO and T_2O. A number of numerical experiments made indicate that converged solutions are quite rapidly presented by this procedure.

2.5 General simulation procedure for stage process

Developed is a new general simulation procedure which is applicable

to almost all types of stage processes essential in the fusion fuel cycle and usual chemical engineering systems. Even if the heat balances are essential or chemical reactions are promoted, the algorithms of the procedure remains unchanged. The application of the procedure is quite successful even in cases where the equilibrium ratios are strongly dependent on the composition and the liquid phase separation occurs. The independent variables are always the mole fractions in one of the phases considered.

3. Present Status of Tritium Processing Laboratory

The construction of the Tritium Processing Laboratory (TPL), which specifications had been determined through the design study performed for the last four years, started at December of 1982 and will be completed in April of 1984.

Final design studies for major equipments, that is gloveboxes, detritiation systems, tritium storage system, and tritium monitoring and control system, were also in the stage of contract for construction.

For experimental apparatus the design study are successively carried out.

Table VIII-1 Tritiated Species Released on Heating under Vacuum.

Material	Upper temp.[1] °C	% of total tritium				
		HT	HTO	CH_3T	C_2H_nT	Retention
LiH	750	99.5	0.3	0.3	0.03	0.1
Li_2C_2	700	95.9	1.2	0.4	2.6	0.01
Li_3N	950	98.6	1.1	0.2	-	0.1
Li_7Pb_2	600	89.8	5.4	1.2	0.1	3.5
LiAl	800	93.2	5.3	1.2	0.03	0.3
Li(1%)-Al	750	44.5	53.7	1.8	0.03	0.01
LiOH	600	0.3	99.4	0.1	0.2	0.01
Li_2O	600	0.9	98.0	0.9	0.1	0.1
Li_2O pellet (78.5%TD)	600	3.5	95.4	0.5	0.03	0.6
Li_2CO_3	600	1.7	96.9	0.3	1.0	0.1
$LiAlO_2$	750	8.1	87.1	1.2	3.6	0.03
Li_2SiO_3	750	2.5	97.1	0.4	-	0.01
Li_2TiO_3	900	0.9	97.9	0.7	0.2	0.4
Li_2ZrO_3	900	(0.7)	(99.0)	(0.2)	(0.1)	

[1] The temperature was raised stepwise from 200°C to the upper one.

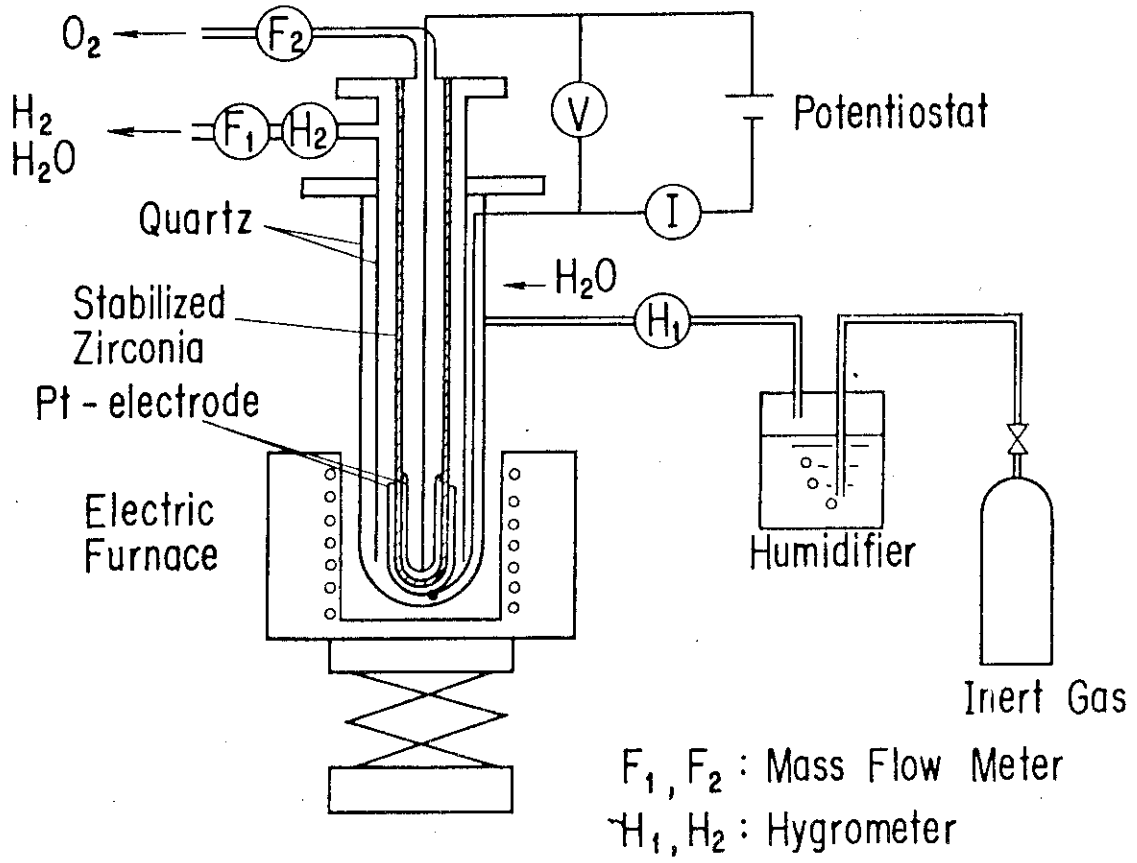

Fig. VIII-1 Arrangement of the experimental apparatus.

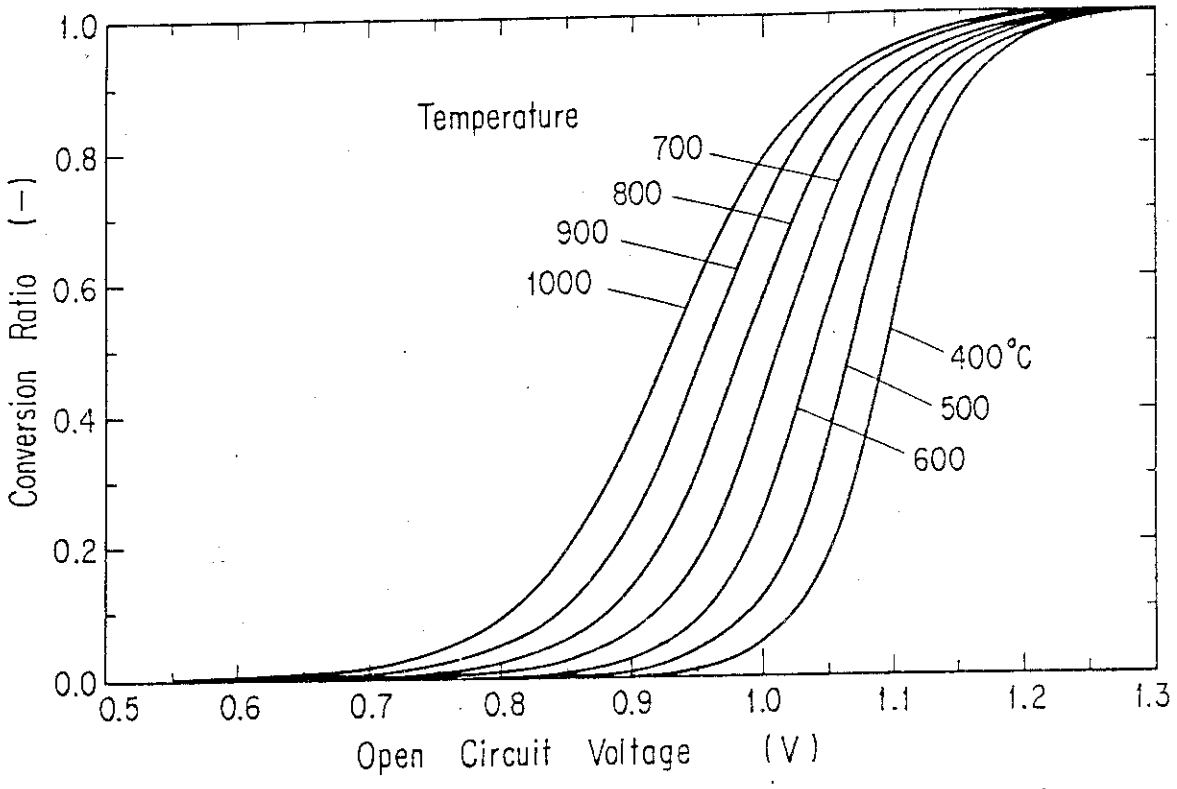

Fig. VIII-2 Relations between voltage and conversion ratio of H_2O vapor to hydrogen at various temperature (numerically calculated).

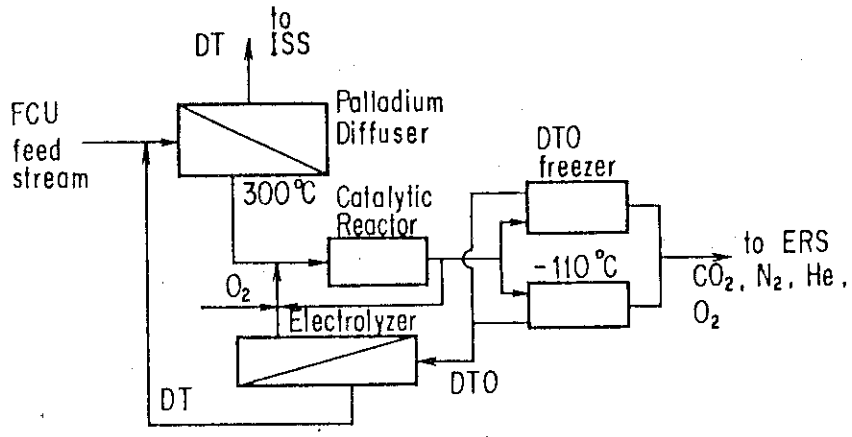

Fig. VIII-3 Fusion reactor fuel cleanup system(FCU) equipped with the ceramic electrolizer.

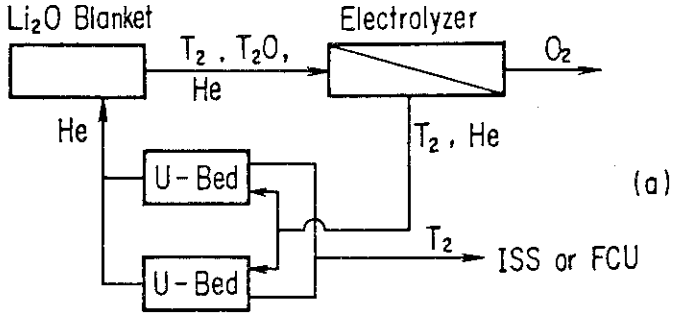

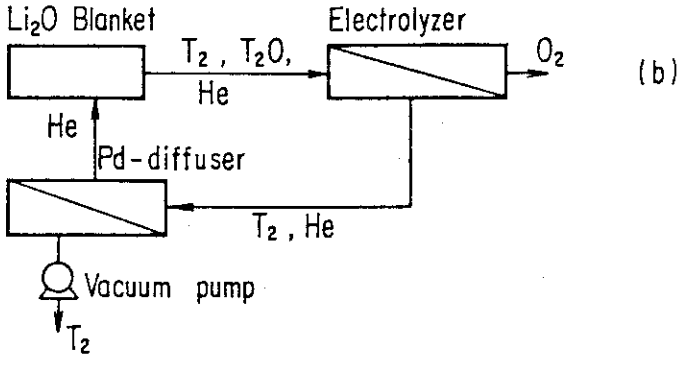

Fig. VIII-4 Blanket tritium recovery system with the ceramic electrolizer.

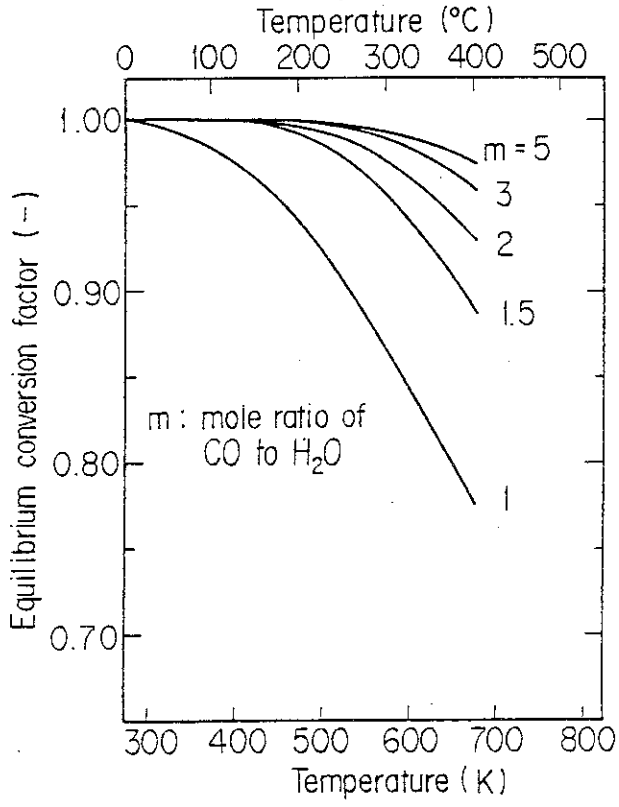

Fig. VIII-5 Equilibrium conversion factor of H_2O vapor in the catalytic reducing reaction $H_2O(g) + CO(g) \rightleftarrows H_2(g) + CO_2(g)$.

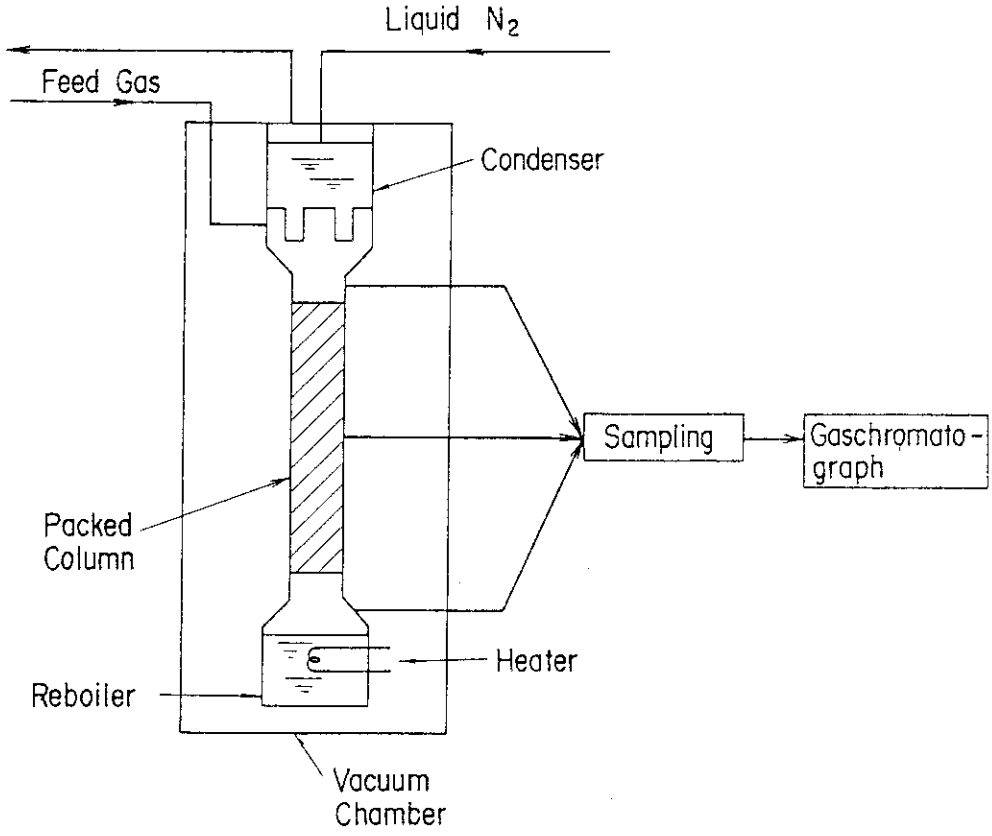

Fig. VIII-6 Conceptual flow diagram of the experimental apparatus.

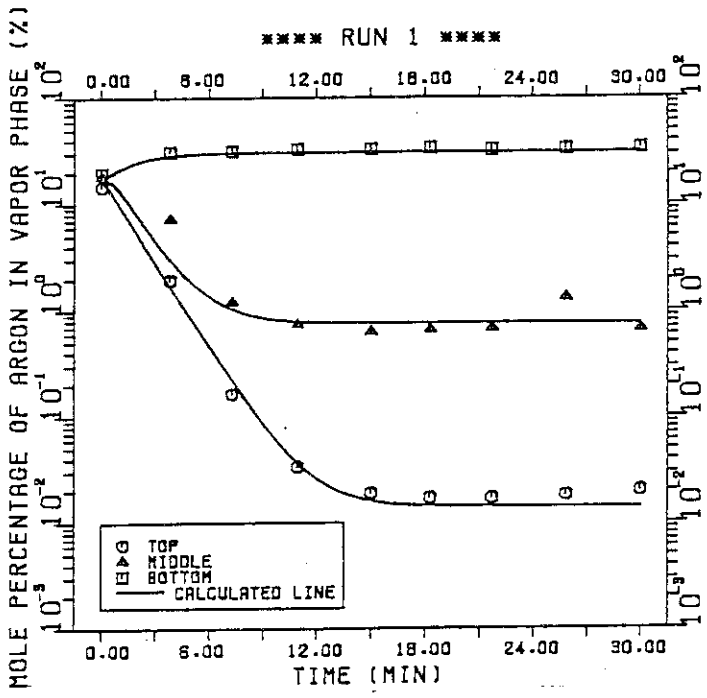

Fig. VIII-7 Typical result of Ar-N_2 separation under total reflux condition of cryogenic distillation column.

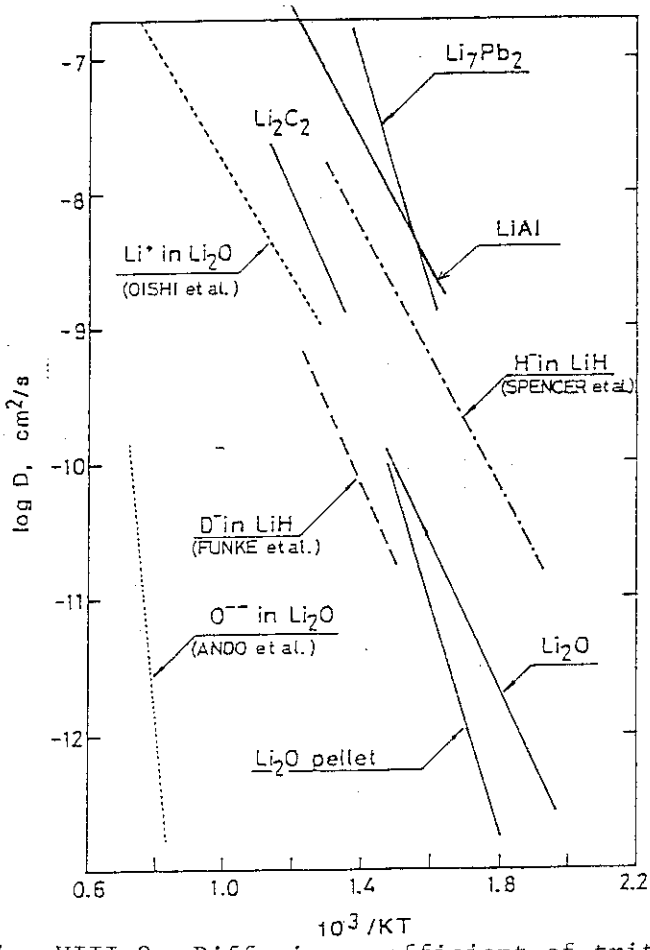

Fig. VIII-8 Diffusion coefficient of tritium in various lithium-based materrials.

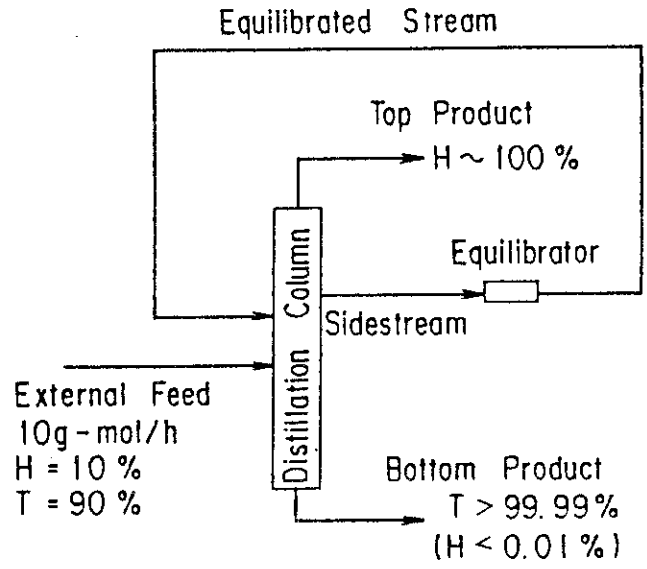

Fig. VIII-9 Simulated single cryogenic distillation column schematic with a feed back stream.

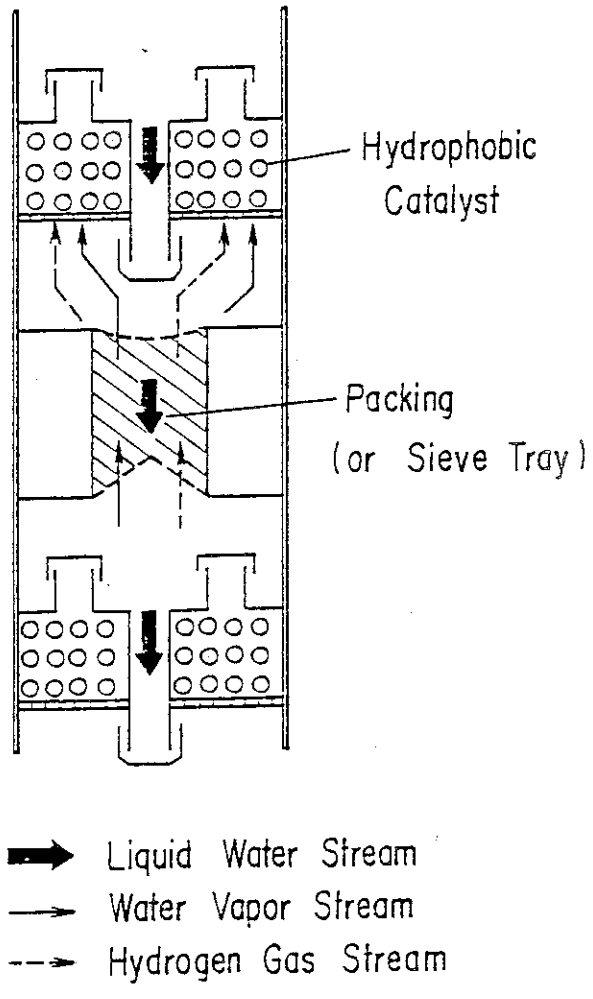

Fig. VIII-10 Simulated model of water/hydrogen exchange column.

IX. DESIGN STUDIES OF FUSION REACTOR SYSTEM

1. Design Study of Tokamak Power Reactor

A design study of tokamak power reactor utilizing the deuterium/tritium/lithium fuel cycle based on a swimming pool type reactor (SPTR) concept was completed[1]. The objective of the power reactor design (SPTR-P) is to develop an attractive reactor concept which is acceptable as a commercial power reactor.

The SPTR concept has been developed: to simplify technologies for repair and maintenance, to achieve a compact and light-weight reactor, to reduce radioactive waste disposal and to ease radiation streaming shielding. The major design features are: steady state operation, RF wave for plasma heating and current drive, solid tritium breeding material (Li_2O), modified austenitic stainless steel as first wall and blanket structural material, pumped limiter for ash exhaust, unified assembling of blanket and vacuum vessel and pressurized water cooling. The huge and heavy solid shield structure protecting superconducting magnets which brings about great difficulties in repair and maintenance is eliminated by submerging the reactor in a water pool. The water plays a role of shielding. The SPTR-P concept and the reactor building are shown in Fig. IX.1-1.

The key parameters are listed in Table IX.1-1. The plasma current of 16.0 MA is drived by an 80 MW RF-power launched into plasma and the electric power required for the RF-system is 160 MW. The scenario adopted for attaining stable equilibrium of the high β_t (7%) plasma is based on low q and low β_p, which meets the stability criterion of high-n ballooning mode.

References

1) Tone, T., et al.: "Design Study of a Tokamak Power Reactor", Proc. 3rd IAEA Technical Committee Meeting and Workshop on Fusion Reactor Design and Technology, Tokyo, Oct. 5 - 16, 1981, II-8 (in press); Tone, T., et al.: "A Study of the Reactor Structure Concept of the Tokamak Power Reactor SPTR-P", JAERI-M 83-031 (1983), (in Japanese). Fusion Reactor System Laboratory: "Conceptual Design of Swimming Pool Type Tokamak Power Reactor (SPTR-P)", JAERI-M 83-120 (1983), (in Japanese).

Fig. IX.1-1 Reactor Building of SPTR-P.

Operation mode	Steady state
Net electrical power (MW)	1000
Fusion power (MW)	3200
Thermal power (MW)	3700
Average neutron wall load (MW/m^2)	3.3
Major radius (m)	6.9
Minor radius (m)	2.0
First wall radius (m)	2.2
Plasma elongation	1.6
Average plasma temperature (keV)	20
Average plasma density n_e (m^{-3})	1.1×10^{20}
Plasma current (MA)	16.0
Safety factor q_a/q_s	1.3/2.3
Average toroidal beta	0.07
Poloidal beta	1.2
Toroidal field on axis (T)	5.2
Maximum toroidal field (T)	12.2
Plasma current drive method	Lower hybrid RF
RF power for current drive (MW)	80
Plasma heating method	Lower hybrid RF
Number of TF magnets	14
Toroidal field coil material	Nb_3Sn/NbTi
Poloidal field coil material	NbTi
Blanket structural material	PCA*
Tritium breeding material	Li_2O
First wall/blanket coolant	Pressurized water
Inlet/Outlet coolant temperature (°C)	290/330
Coolant pressure (MPa)	16
Ash exhaust	Pumped limiter
Power to pumped limiter (MW)	100
Average surface heat flux on first wall (W/cm^2)	80

* Prime candidate alloy (titanium modified austenitic stainless steel)

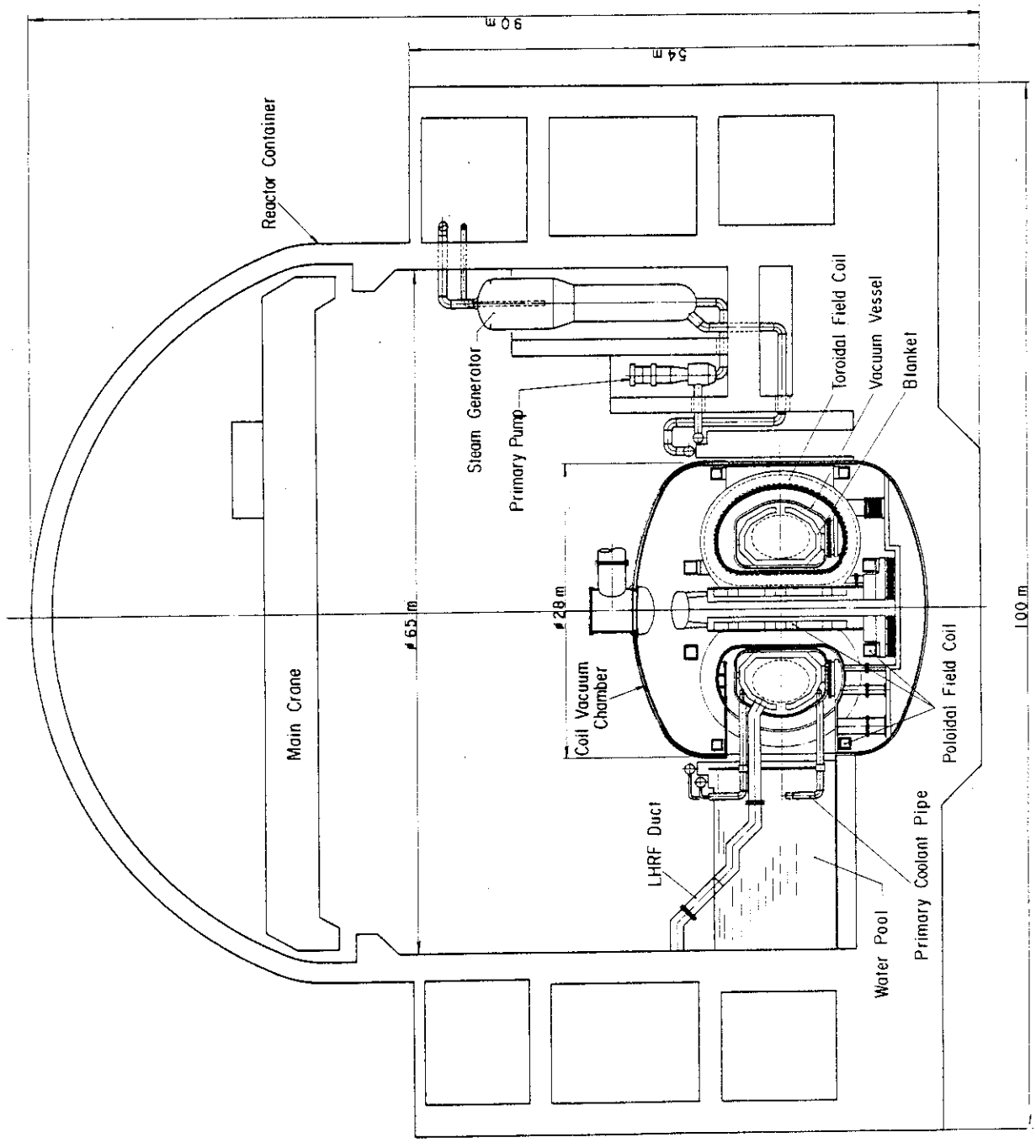

Fig. IX.1-1 Reactor Building of SPTR-P

2. Design Study of Fuel Producing Blanket

Design study of the fuel producing blanket installed in a Swimming Pool-Type Tokamak Reactor (SPTR), which began in 1980, has been completed. The nuclear, thermal and mechanical aspects of the blanket were revised to improve its fuel producing capability. Preliminary investigations of the fuel exchange scheme and safety of the blanket were also made. A tritium breeding ratio of about 0.9 was achieved solely by the inboard blanket loaded with Li_2O and Be at the mixing ratio of 1 to 9. The fuel producing blanket covering 42 % of the plasma surface was loaded with UO_2 and Li_2O, and was cooled with helium gas. This blanket yielded the supplemental tritium breeding of 0.1, energy multiplication of $\sim$2.4 and Pu production rate greater than 0.5. The productions of both energy and fuel are shown to increase by as much as 40 % with the burn up to 4.6 years.

3. Safety and Environment

Understanding of fusion reactor safety has increased considerably because the safety of the Fusion Experimental Reactor (FER) has been studied in detail for the first time and a Japan - U.S. Workshop on Fusion Safety has been held in JAERI on January 24-27, 1983.

As regards the tritium safety of FER, the fuel circulating system, blanket tritium recovery system, primary cooling water processing system and tritium containment system have been studied in detail. Tritium inventory and its leakage to the reactor room and to the environment have been estimated. However, the uncertainties in tritium data on permeation, adsorption, release and oxidation have been found to be large and need to be reduced.

X. DEVELOPMENT OF A LARGE TOKAMAK JT-60

1. Introduction

Efforts made by the JT-60 Project was rewarded by the progress achieved in this year. Assembling and installation work of its major components - tokamak machine, power supplies, and central control system - were started at the Naka site. Construction of JT-60 buildings and other facilities advanced as planned. The completion of JT-60 is expected in March 1985.

Efforts are also focussed on detailing experimental and operation programs to raise productivity of the JT-60 Project.

2. Outline of the Progress of JT-60

Development of the JT-60 project proceeded satisfactorily during the fiscal year 1982. Significant progress was made with the fabrication and installation of major equipments for the JT-60 device. Many heavy components were delivered to the Naka site. Assembling and installation of the central control system and the poloidal field power supply including its motor-generator were completed. The transformers for the toroidal field power supply were also installed. Assembling work of the tokamak machine started in February 1983. Fabrication of major components of the tokamak machine at factory reached the final stage. The power distribution system, the emergency power supply and the secondary cooling system were installed and put under test; they will be delivered to JAERI in October 1983.

Construction of the major buildings for JT-60 advanced as planned; the power supplies building and the control building were completed, and construction of the experimental building entered the final stage. Construction of the 275 kV power substation was advanced; it will be completed near the end of 1983.

Specifications of JT-60 plasma heating systems were completed and given to vendors for quotation. Fabrication of the diagnostic systems was advanced as planned.

The experimental program was reviewed based on the current progress in fusion research development. Concept of real time plasma control was introduced and improvements were made of the JT-60 performance.

The operation program was also examined in detail concerning the organization and personnel for operation.

The time table of the JT-60 program is shown in Fig. X.2-1.

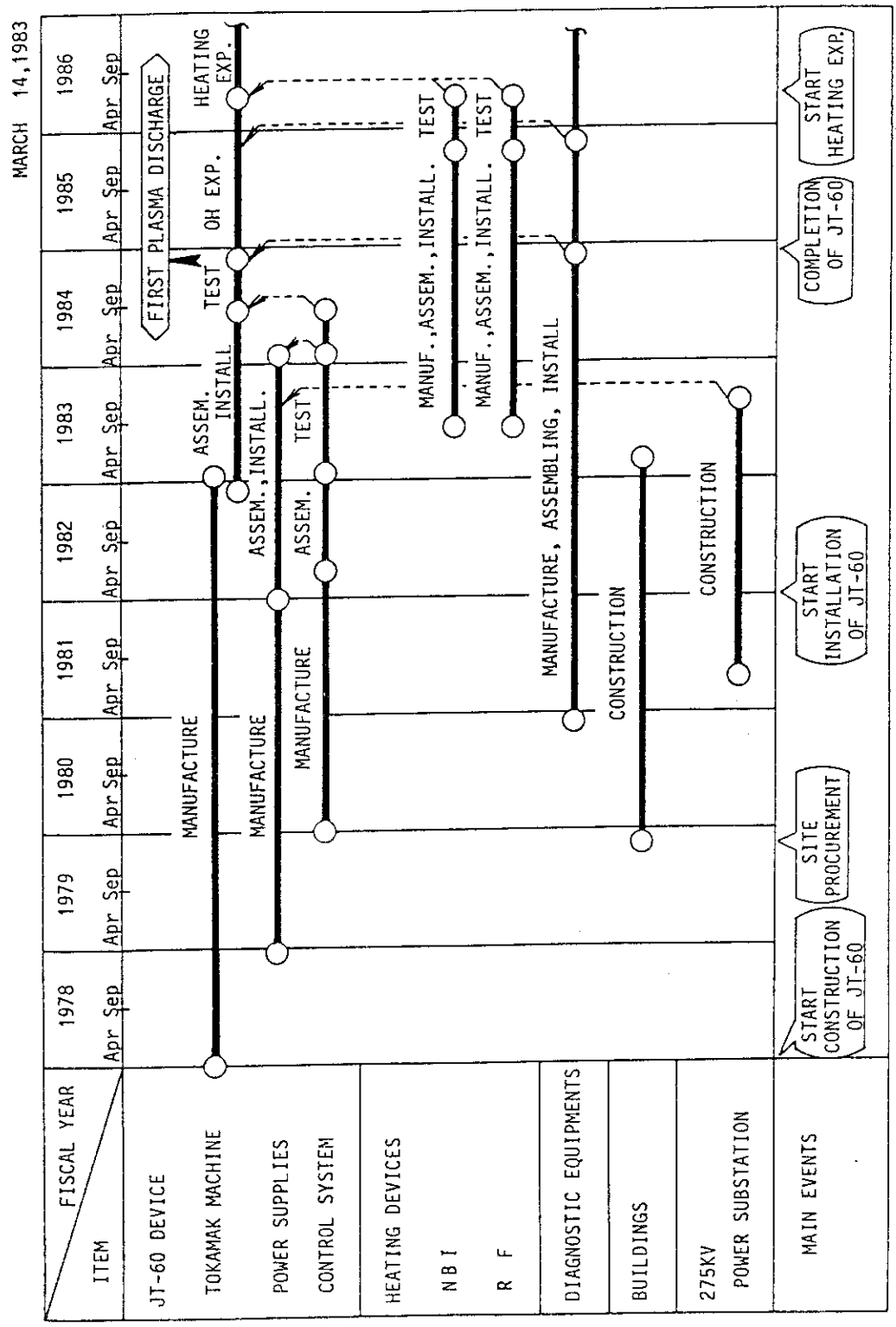

Fig. X.2-1 JT-60 Project Schedule.

3. Status of Tokamak Machine

3.1 Major activities

The tokamak machine of JT-60 is composed of a vacuum vessel, toroidal field coils, poloidal field coils, support structures, a primary cooling system, a vacuum pumping system, fast movable limiters, a preionization system, a gas-feed system, adjustable limiters and a control system.

Fabrication of these components has been continued progressibly. Assembling of two 180° sectorial vacuum vessels is nearly completed in the factory. Magnetic limiter coils, electric heaters, cooling channels, thermal insulators, and electromagnetic sensors were attached to the vacuum vessels. Many kinds of tests such as baking tests and helium leak tests are under way. All of the nineteen toroidal field coils have been stored in the factory from 1981. All inner poloidal field coils were assemblied to the coil support structures. The vacuum pumping system, fast movable limiters, adjustable limiters, and control system have finished fabrication in the factories. Fabrication of the gas-feed and preionization system is in progress.

Installation of the machine components at the Naka site started in February 1983. The support structures including the foundation bases and the bases for the support columns of the vacuum vessel were set up in the tokamak hall. Primary cooling system was also set up at the site.

Investigations concerning the machine performance were also made successfully. Computer codes for the eddy current analyses of a Tokamak machine have been developed. These codes provide the data necessary for the evaluation of machine performance. Measurements of thermal contact resistance, which is related to heat removal from the first wall components, have been made for actual size samples. Measurements of emissivity have also been performed for both molybdenum and Inconel 625 alloys at temperatures ranging from R.T. to 1500 K. Secondary electron emissivity has been measured in details.

3.2 Status of machine components

3.2.1 Vacuum vessel

The assembling of two 180° sectorial vacuum vessels was nearly

completed in the factory. Electric heaters, cooling channels and thermal insulators for the temperature control were mounted on the outer surface. Various tests were carried out and main results are the following. Helium leak was not detected within the sensitivity of about 10^{-10} Pa·m^3/s after baking. Temperature distribution of the vessel and the rising up and cooling down times for the baking up to 500 °C respectively satisfied the specification. After these tests, three magnetic limiter coils were assembled inside the vacuum vessel. Figure X.3-1 shows the inside view of the vacuum vessel. A half of ports were finished fabrication.

Thermal and mechanical stress analyses of first wall have been almost completed. The stress analysis shows that the maximum mechanical stress is 13 kg/mm^2 in armor plates for a 3 msec disruption even if a dynamic factor of 2.0 is assumed. A lifetime analysis which includes thermal stress and fatigue are in progress and will be completed in the middle of 1983. Fabrications of the Inconel 625 and molybdenum first wa-ls advanced in this FY and will be completed in early FY 1983. Figure X.3-2 shows molybdenum neutral beam armor plates. For the purpose of detailed evaluations of the maximum heat removal capability, thermal contact resistance and emissivity have been measured. Based on these measured values, detailed analyses on the maximum capability of JT-60 first wall will be performed in the coming fiscal year.

3.2.2 Toroidal field coil

Fabrication of the toroidal field coils was completed in July 1981. All of the coil units are being stored in the factory. Careful consideration has been given to the arrangement of the feeders and cooling pipes and a few changes have been made to avoid geometrical interferences with other components.

3.2.3 Poloidal field coil

The poloidal field (PF) coils consist of five coil groups; ohmic heating coils (OH coils), vertical field coils (V coils), quadrupole field coils (Q coils), horizontal field coils (H coils) and magnetic limiter coils (M coils).

In this fiscal year, the design of the PF coils has almost been completed and significant progress has been made in their fabrication

and assembling in the factory.

Bending tests of model coil stacks were carried out to determine both mechanical strain limit of the electric insulators and the allowable bending stress of the welded joints of conductors which are to be connected on site. It was found from these tests that the mechanical strength of the coil stacks was influenced considerably by the bonding effect of the epoxy-impregnated fillers inserted between each turn. Based on this result, the stress evaluation was performed.

All PF coils were fabricated and their dimension inspections and dielectric tests were completed. The PF coils to be placed near the torus axis are in the final stage of assembling in the factory as shown in Fig. X.3-3.

The fabrication of the bellows for the M coil jackets was completed in August 1982. The winding and insulating works of the M coil conductors were advanced and the assembling of the jackets, which were composed of a large number of bellows and rigid rings, was completed in February 1983. The M coils after completion were installed into the vacuum vessel.

The assembling and installation of the feeders for both PF coils and TF coils were completed.

3.2.4 Support structures

Fabrication of the support structures was completed in the beginning of this fiscal year. They were delivered to the Naka site for assembling one by one.

Assembling of the support structures started in February 1983 and the central base, the foundation base, the base for the vacuum vessel support column and the lower base were assembled with sufficient accuracy at the end of this fiscal year.

3.2.5 Vacuum pumping system

Fabrication of the vacuum pumping system (VPS) was completed in the factory except the vacuum diagnostic system.

After the VPS was assembled in the factory (See Fig. X.3-4), the following inspections were finished in December 1982.

(a) Pumping speed measurement (H_2, N_2, Ar)

(b) Ultimate pressure measurement

(c) Leak test
(d) Residual gas analysis
(e) Bake out test and cool down test
(f) Pressure proof test
(g) Withstand voltage test
(h) Operation test by control system

These results show that the VPS satisfies sufficiently the requested performance. The installation at the Naka site started in October 1982. The roughing pump system, forepump system and peripheral systems were installed in February 1983.

3.2.6 Primary cooling system

The major components of the primary cooling system including pumps, heat exchangers, filters and others have been installed in the primary cooling pump house. The motor control center has also been installed. Cabling and piping works are now in progress.

3.2.7 Fast movable limiters and adjustable limiters

The final inspection test of the fast movable limiters was completed in September 1982. Its performance was tested before the installation to the tokamak machine in the beginning of 1983. The adjustable limiter system was also completed at the factory in September 1982.

3.2.8 Gas feed and preionization system

The fabrication design of the gas feed and preionization system has been completed. Its subsequent fabrication is now in progress. The gas throughput for the piezoelectric valve (PEV) and fast magnetic valve (FMV) and the ionized current from the electron gun (EB) and JxB gun were checked and good results were obtained. The performance test of them under the CAMAC control system will be finished in September 1983.

3.2.9 Tokamak machine control system

The fabrication of the control panels including CAMAC system has been completed in FY 1982. Testing for the control panels and CAMAC softwares in the factory progressed well. Installation of the control panels and cabling work of the control system will be continued till August 1983.

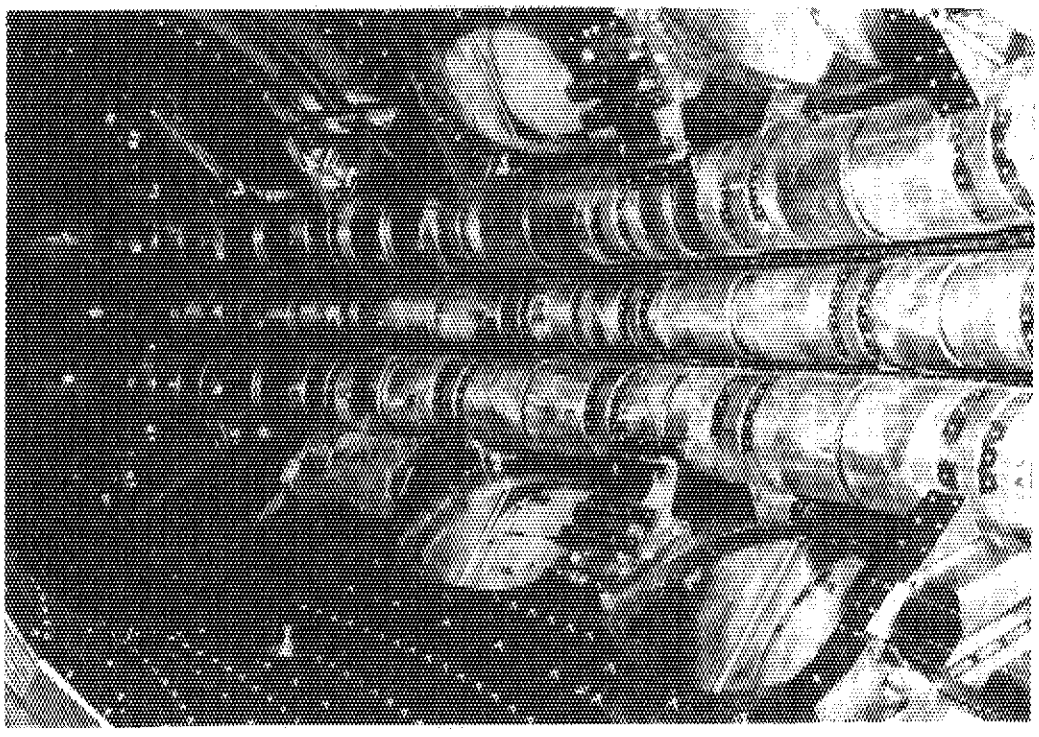

Fig. X.3-1 Inside view of vacuum vessel with magnetic limiter coils.

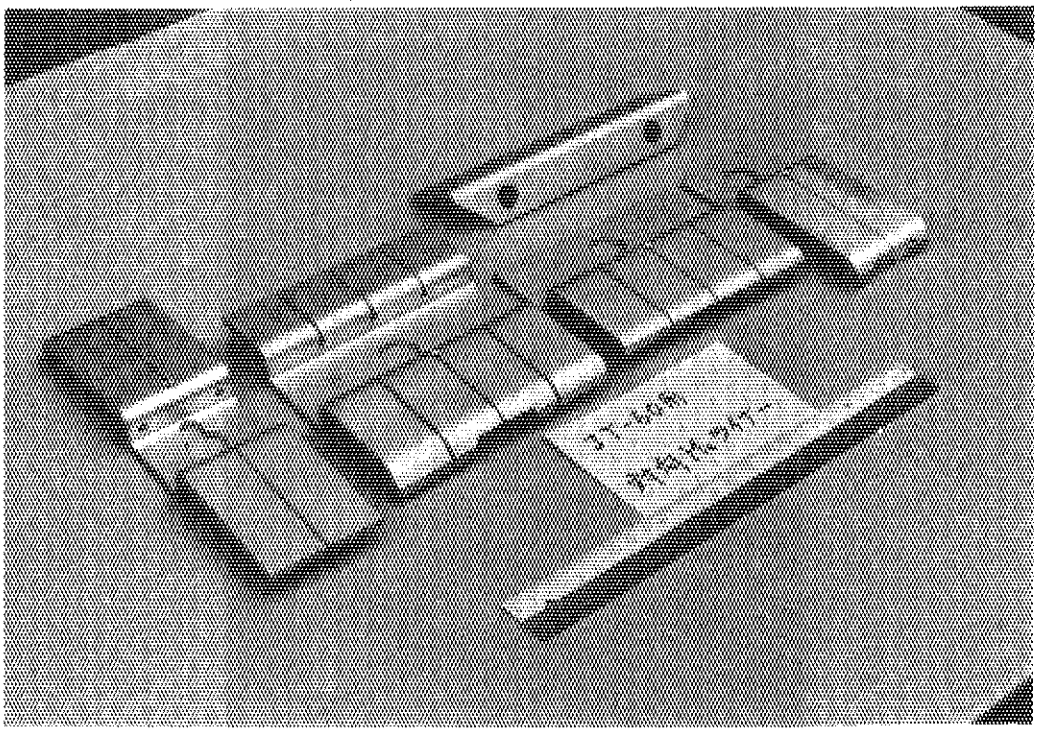

Fig. X.3-2 Several types of neutral beam armor plate, 5 mm thickness of molybdenum.

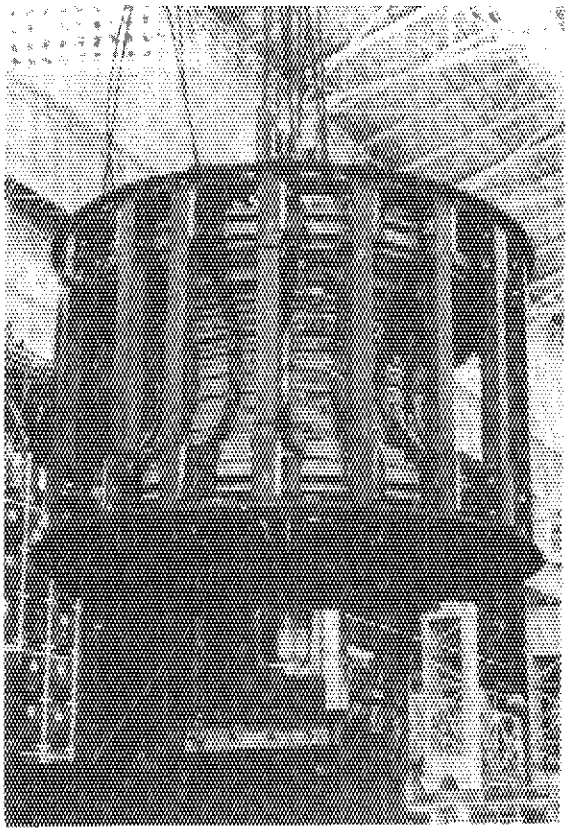

Fig. X.3-3 Assembly of inner poloidal field coil in factory.

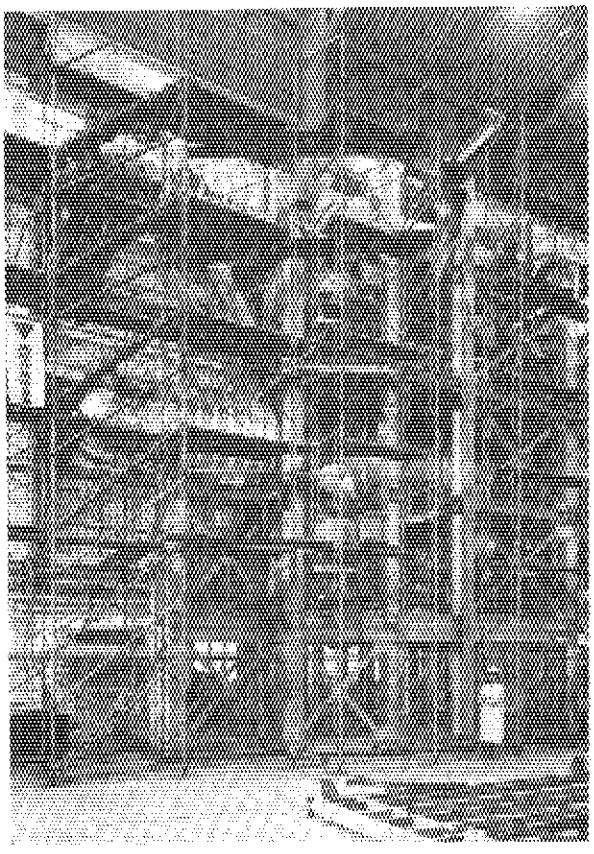

Fig. X.3-4 Assembly of VPS in factory.

3.3 Related studies

3.3.1 Eddy current analysis[1)]

Many kinds of numerical analyses were carried out using the newly developed computer program (EDDYMULT) for solving the eddy current problem in a multi-torus system. Because the developed numerical model includes most of the JT-60 main components such as a vacuum vessel, toroidal magnet system, a central support structure and the other support structures, reasonable results were obtained within the required accuracy. For the control analysis of JT-60 plasma, the magnetic structure of each eddy current mode was individually studied. Figure X.3-5 shows an example of the magnetic structure due to one of the obtained eigen modes of JT-60 eddy current.

Our expansion technique of distributed eddy current into eigen modes is useful for the study of plasma control analysis by the linear state-space approach. Efforts are now being centered on the development of the computer package for the analysis and synthesis of tokamak control system including an eddy current effect.

3.3.2 Thermal contact resistance measurement of first wall component

Continued from FY 1981, measurements of thermal contact resistance have been done in 10^{-4} Torr and at 200 $\sim$ 600 °C with using actual size samples.

Molybdenum samples are 50 mm in diameter and 5 mm (armor plate) and 20 mm (limiter, magnetic limiter plate and beam limiter) in thicknesses, respectively. The samples were fixed to an Inconel pedestal by a bolt, which simulated first wall component.

Results show that the thermal contact resistance varies from 4.5 to 9 $\times$ 10^{-3} m^2h °C/kcal at 86 kg/cm^2 for 20 mm^t samples and from 1 to 4 $\times$ 10^{-3} m^2h °C/kcal at 297 kg/cm^2 for 5 mm^t samples. It appears furthermore that the thermal contact resistance has a strong temperature dependence. For example it varies from 4 $\times$ 10^{-3} to 1 $\times$ 10^{-3} m^2h °C/kcal with decreasing the temperature from 600 °C to 200 °C in 20 mm^t samples. With these results, detailed evaluations of the maximum heat removal capability in JT-60 first wall will be done in FY 1983.

3.3.3 Emissivity measurement of first wall materials

Measurements of emissivity have been performed for molybdenum and Inconel 625 at R.T. ∿ 1500 °K.

The emissivity of Inconel 625 depends slightly on temperature and varies from 0.1 to 0.2. On the other hand, it depends strongly on temperature for molybdenum and vary from 0.03 to 0.2. These measurements have revealed relations of emissivity versus wave length and temperature. Emissivity spectrum of both materials strongly depends on wave length. Therefore, a heat conduction code which includes the wave length and temperature dependences is necessary for detailed evaluations of the maximum heat removal capability planned in FY 1983. The emissivity of TiC coated molybdenum will be measured in FY 1983.

3.3.4 Secondary electron emission rate under the electron bombardment

Plasma-wall interaction is one of the important problems for plasma fusion devices such as JT-60. This interaction includes several fundamental processes. We have studied the secondary electron emission, which is one of the fundamental processes. The secondary electron emission rate and the electron temperature of a plasma boundary determine the sheath potential which is one of the most important parameters of the edge plasma. In cases of SUS 304 and Mo we have confirmed the universal curve for the yield of secondary electron emission. In accordance with cleanliness of the surface, the secondary electron emission rate is decreased gradually to a constant value. In an energy range of 200 eV ∿ 1 keV, we have the secondary electron emission rate larger than 1 for the clean surfaces of both SUS 304 and Mo, as shown in Fig. X.3-6. The maximum secondary electron emission rate γ_m and the corresponding energy E_m are followings; γ_m = 1.12, E_m = 360 eV for SUS 304 and γ_m = 1.23, E_m = 410 eV for Mo, respectively.

References

1) Nakamura, Y. and Ozeki, T.: "Eddy Current Analysis in JT-60", 12-th SOFT, Jülich, 1982.

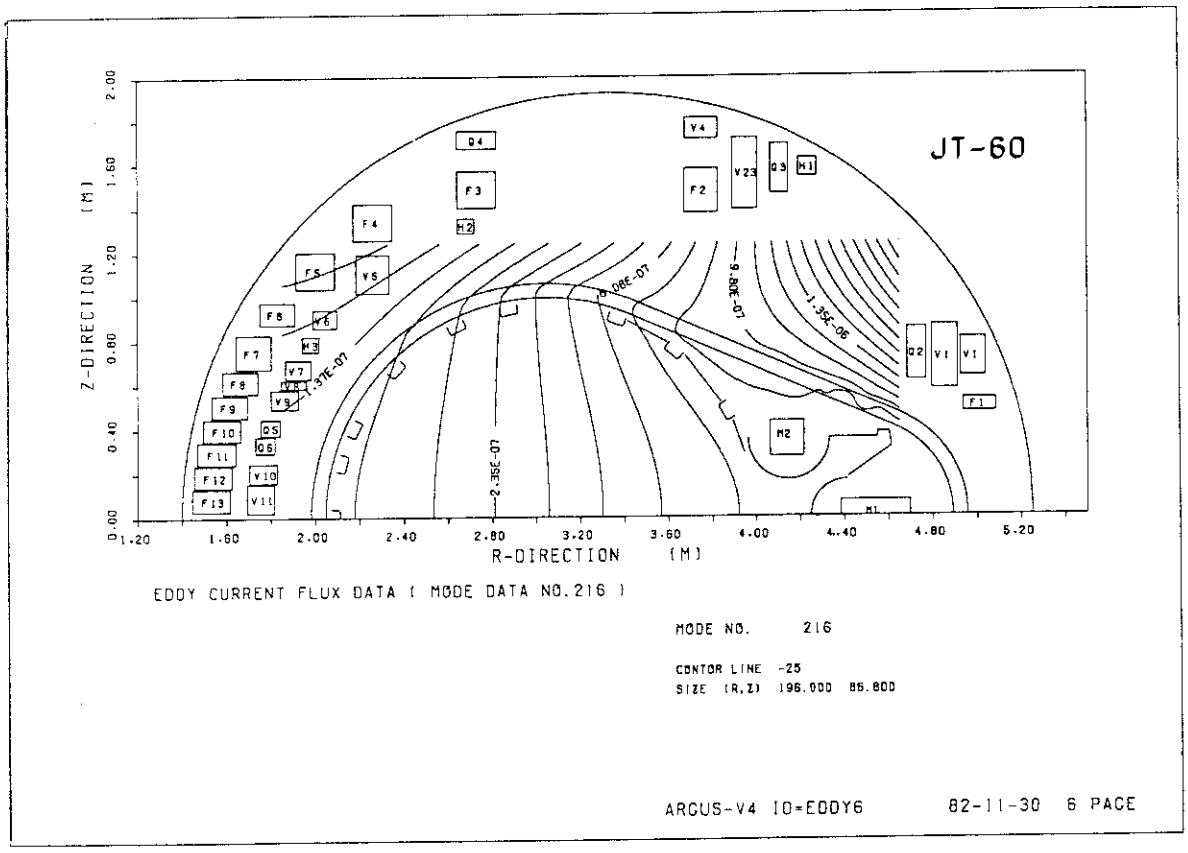

Fig. X.3-5 Typical magnetic structure of JT-60 eddy current.

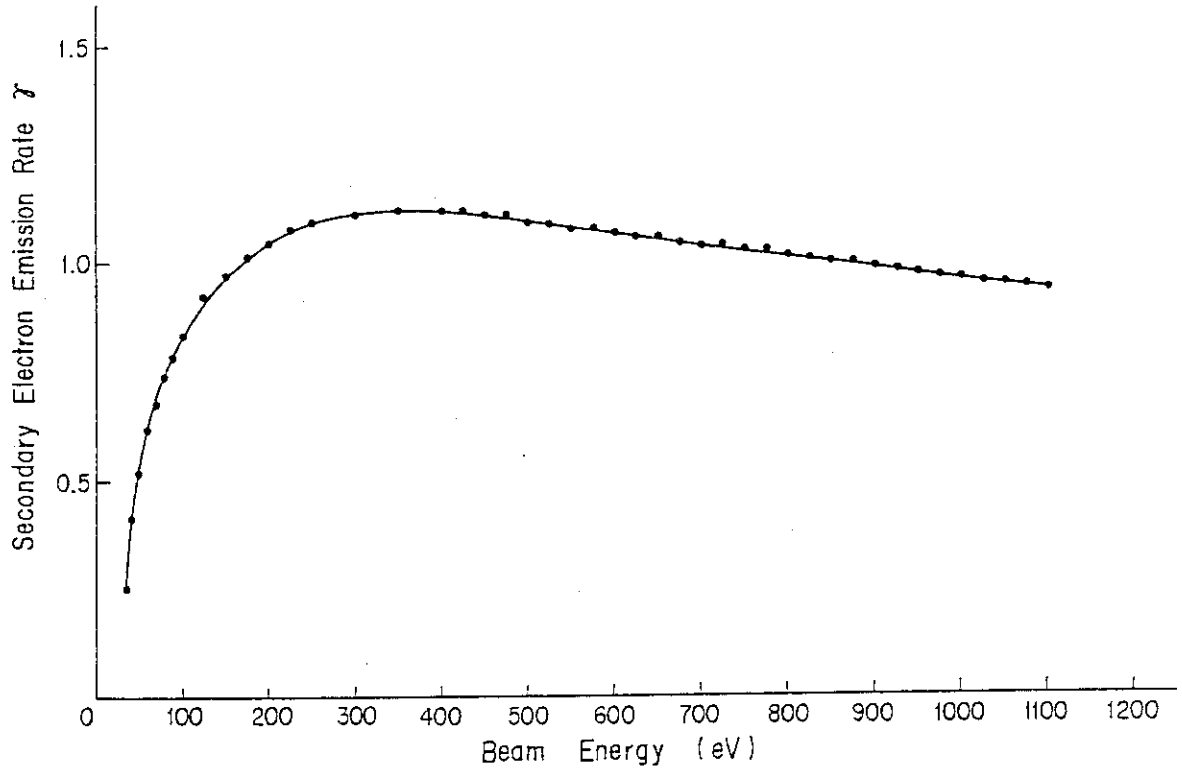

(a) SUS 304

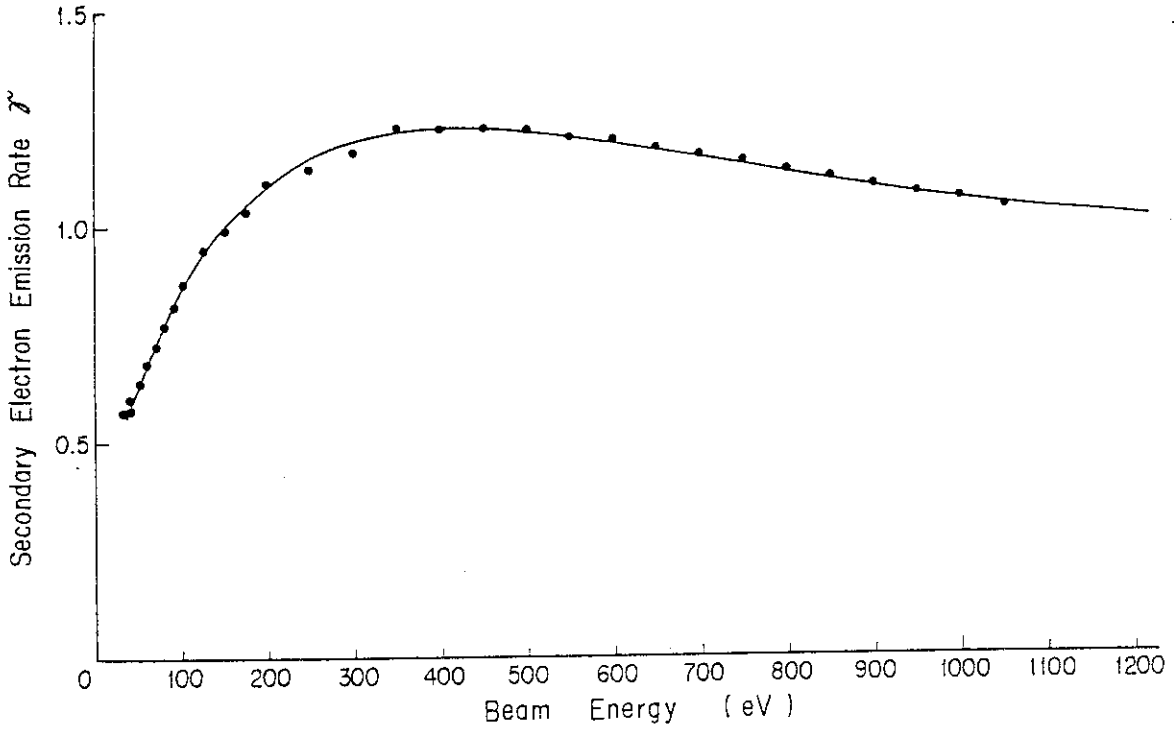

(b) Mo

Fig. X.3-6 Secondary electron emission rate versus electron energy for clean surfaces of (a) SUS304 and (b) Mo.

4. Status of Power Supplies

4.1 General status

The assembling and installation of the poloidal field power supply (PFPS) including a 500 MVA motor generator, thyristor convertors and transformers were started in April 1982, and now have been almost completed except a small part of its control subsystem. The component test of PFPS started recently and is expected to expand its scope rapidly in the next year. The control system of PFPS is now at the final stage of manufacturing.

A half of the electric power required for operation of the toroidal field coils is supplied by another 215 MVA-4000 MJ flywheel generator. The manufacturing of this generator has been finished in the factory. Its assembling and installation work in the JT-60 generator building will be started shortly. Among the major components of the toroidal field power supply (TFPS), the rectifier-transformers were already installed in the transformer yard. The power conversion diode system is now under testing in the factory. The systems design of the control system of TFPS has made progress and the manufacturing of hardwares was started partly.

The manufacturing of the third generator of 400 MVA-2600 MJ to be used for the neutral beam injection heating system and the radio-frequency wave heating system is underway.

The construction of the generator building, the rectifier building and the transformer yard were completed. The construction of the JT-60 grounding system will be finished in June 1983.

4.2 Poloidal field power supply

The poloidal field power supply of JT-60 is shown schematically in Fig. X.4-1, and the main characteristics of the main components are summerized in Table X.4-1. The inspection test of the motor generator (MG) of poloidal field power supply was carried out in February 1982 and after that it was delivered to the JT-60 Naka site. The assembly and installation of it in the generator building were started from April 1982. Figure X.4-2 shows the 500 ton rotor of 500 MVA MG of poloidal field power supply. This MG is expected to be in operation from September

1983. The other components of poloidal field power supply were completed in the factory day after day and delivered according to the schedule of the installation on site. Poloidal field power supply has many high power thyristor convertors. To carry out the inspection test in the factory, the limit of the electric power available to the no-load rated current test greatly affected to the schedule. Because these tests demand the electric reactive power of several MVA, actual test days were always ahead or behind of schedule. Figure X.4-3 shows the largest transformer of poloidal field power supply, which is a reactor for inductive energy storage (IES), 4 mH-92 kA 150 ton, being moved to the place in the transformer yard.

All essential components for the poloidal field power supply were delivered at the end of 1982 with one exception (control system), and successively the assembly work on DC buswork, AC cables and trays, AC distribution/switch gears and its control wires were started. The installation of all the poloidal field power supply were finished by carrying out the Hie-Pot test of total system at the beginning of April of 1983. This means the end of installation phase and the start of the preoperational testing of poloidal field power supply. Figure X.4-4 and X.4-5 show the installed DC interruptor for OH coil and the thyristor convertors in the JT-60 rectifier building.

Table X.4-1 Specifications of major components of the poloidal field power supply.

Generator	Vertical shaft salient pole type		1	set
	Pole		16	poles
	Capacity		500	MVA
	Voltage		18	KV
	Current		16	KA
	Frequency		78-54	Hz
	Flywheel effect		5,500	Ton-m^2
	Revolution		585-405	RPM
	Energy yield		1.3	GJ
D.C circuit breaker	Vacuum circuit breaker		2	set
	Voltage		25,15	KV
	Current		92	KA
	Commutation capacity		1.0/1.7	mF
Inductive energy storage coil	Reactor of iron core with air gap		2	set
	Inductance		1.12,2,32/4.56	mH
	Total inductance		8	mH
	Current		92	KA
	Resistance		7.5	mΩ
Thyristor,Diode convertor	OH coil and IES coil	PSF1	SCR 24 pulse 101KA - 2500V	
		PSF2	SCR 24 pulse 101KA - 2500V	
	Vertical field coil	PSV11,12	SCR 24 pulse 58KA - 5000V	
		PSV13	SR 24 pulse 58KA - 5000V	
		PSVR	SCR 24 pulse*8.6KA - 5000V	
	Quadru-pole field coil	PSQ	SCR 12 pulse*±25KA - 900V	
	Horizontal field coil	PSH	SCR 12 pulse*±22KA - 500V	
	Magnetic limiter coil	PSM	SCR 12 pulse 120KA - 1000V	
			*bi-polar	

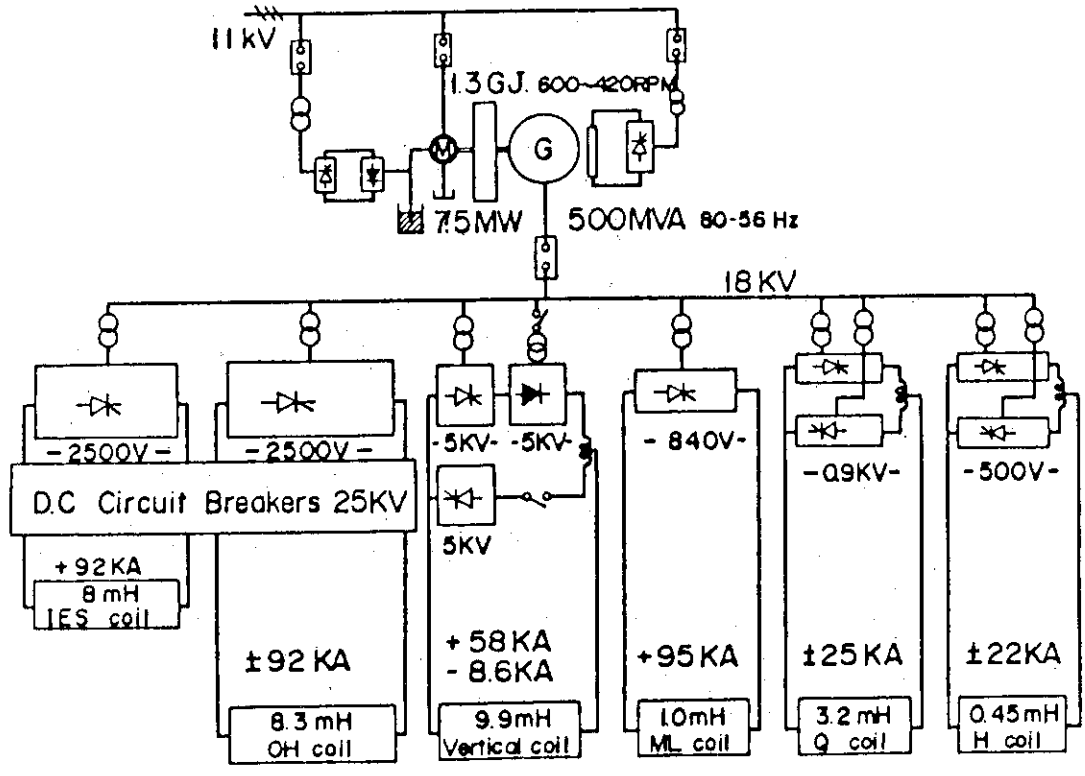

Fig. X.4-1 Schematic diagram of the poloidal field power supply.

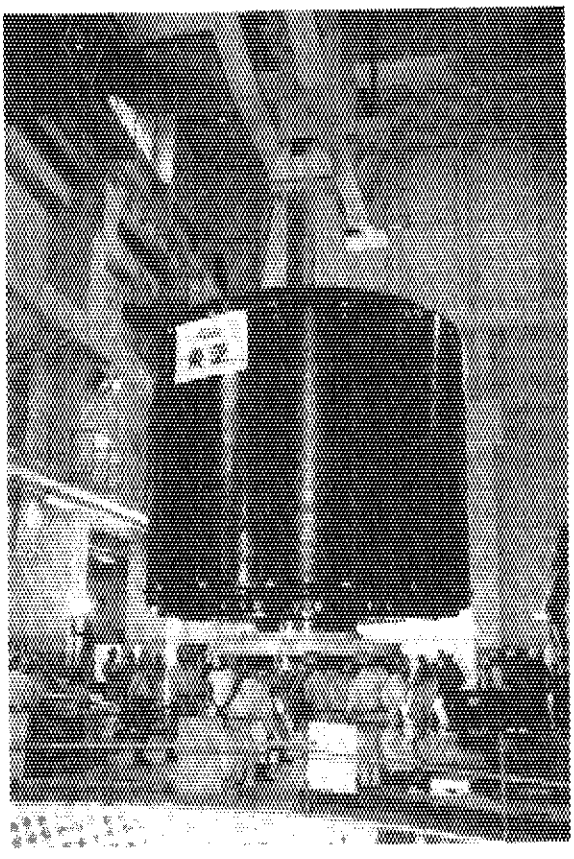

Fig. X.4-2 500 ton rotor of 500MVA PFPS generator being lowered into the pit.

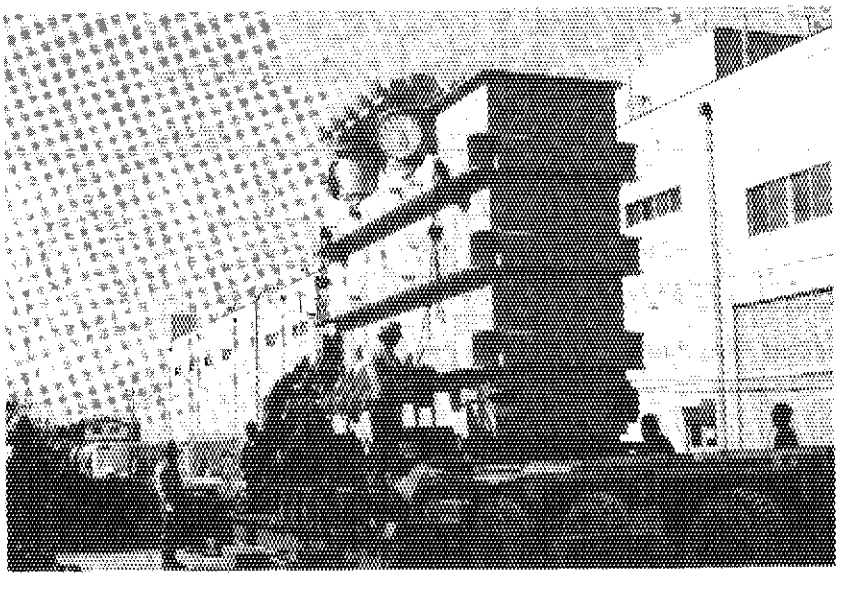

Fig. X.4-3 The largest transformer (150 ton) being moved to the place in transformer yard.

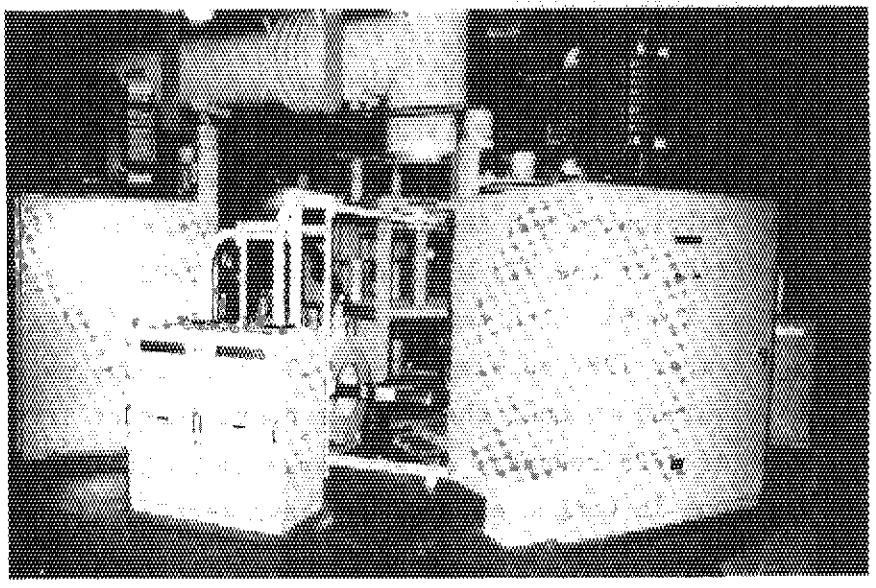

Fig. X.4-4 DC interruptor of OH coil.

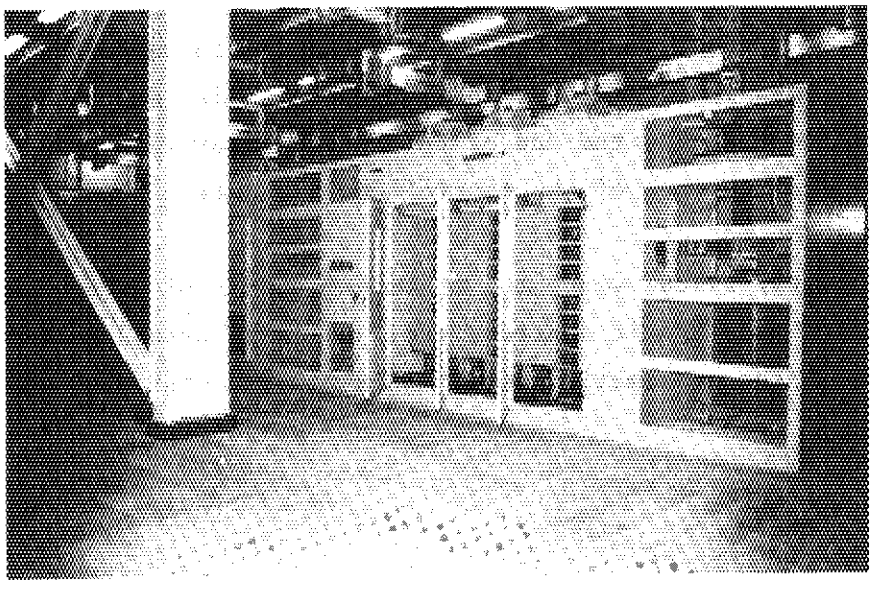

Fig. X.4-5 Thyristor convertor of poloidal field power supply.

4.3 Toroidal field power supply

After the contract in March 1980, the ratings of the components of the toroidal field power supply (TFPS) have been reexamined, and the manufacturing of them in the works has been going on. Several components of TFPS have been fabricated and installed at the new site already.

The manufacturing of the 215 MVA generator of TFPS was finished in November 1982 (Fig. X.4-6). Its test under inspection of JAERI was carried out in December 1982 to examine its electrical and mechanical characteristics required to meet the various operations of TFPS.

The flywheel of TFPS consists of six large disks having 6.6 m in diameter and 107 tons in weight each. They have been forged and machined. The inspection tests by the ultrasonic and magnetic particle methods were carried out to search small defects of the disk. Furthermore, in February 1983, the inspection tests of measuring the GD^2 value and checking the dynamic balance of the flywheel were carried out (Fig. X.4-7).

The installation of the generator with flywheel will be started at the new site in April 1983.

The transformers for the 24-pulse diode convertors and the auto-transformer for the discharge cleaning operation of TFPS were tested under inspection of JAERI in November and in December 1982 respectively. The AC and DC reactors for the thyristor static starter of TFPS and all the transformers mentioned above have been installed at the transformer yard of the new site by the end of this fiscal year (Fig. X.4-8).

The reexaminations of the control and protection scenarios of TFPS have been going on.

In the next fiscal year, the other components of TFPS (diode convertors, thyristor static starter, etc.) will be installed at the new site and then the systematic test of TFPS will be started.

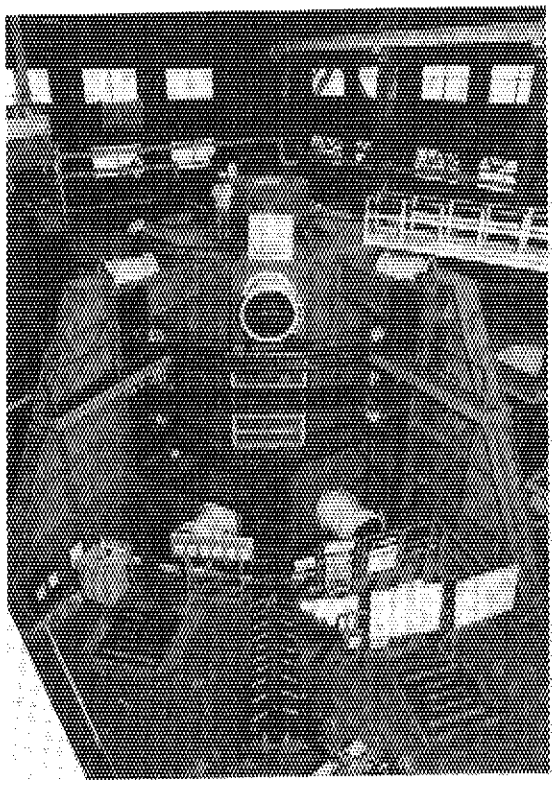

Fig. X.4-6
The generator of the toroidal field power supply.

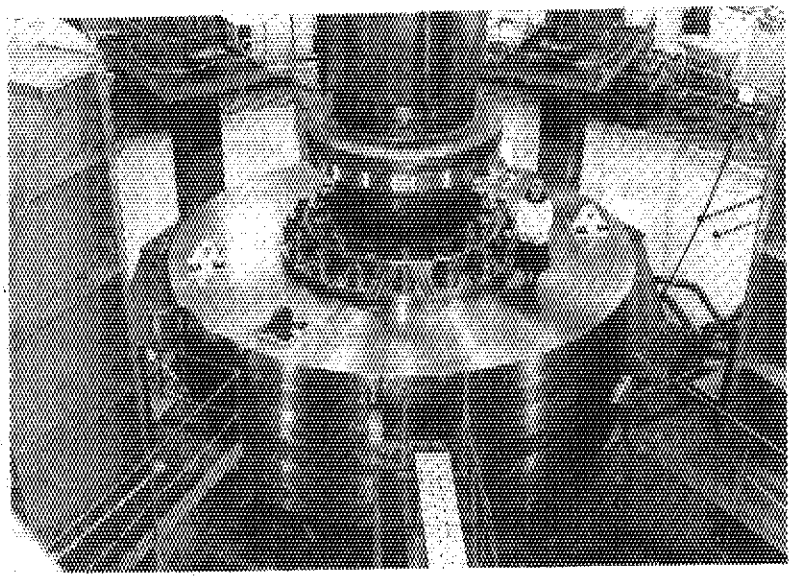

Fig. X.4-7
The flywheel of the toroidal field power supply.

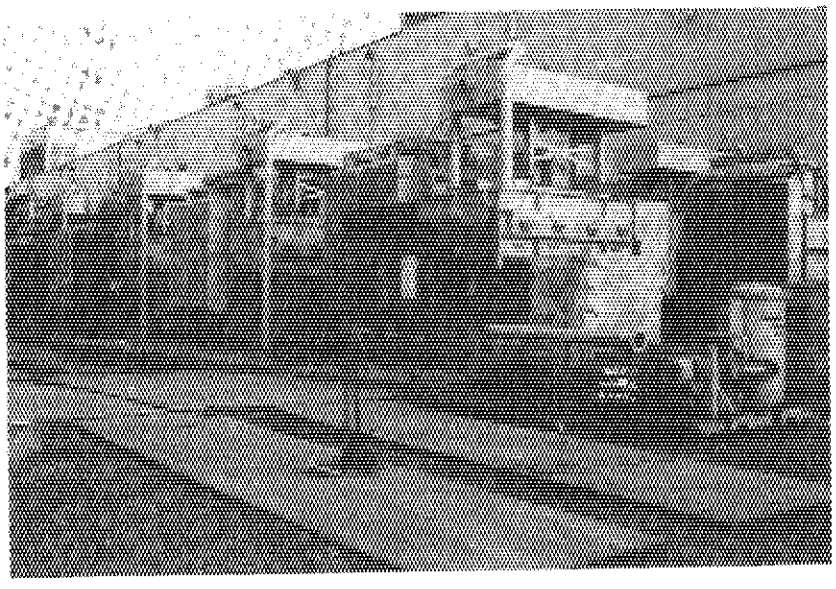

Fig. X.4-8 The transformers for the 24-pulse diode convertors of the toroidal field power supply.

4.4 Motor generator for plasma heating system

The motor generator for the plasma heating system of JT-60 is shown schematically in Fig. X.4-9. This motor generator with flywheel (MGF) supplies electric power for both the neutral beam injection heating system and the radio-frequency heating system. The peak power required by the loads is about 400 MVA with released energy of about 2600 MJ during a pulsed operation of 10 sec. The specifications of the MGF are summarized in Table X.4-2.

After the contract was made in March 1982, the final design examination has been continued. The mechanical design of the MGF has been determined. The cross section of the MGF is shown in Fig. X.4-10.

The manufacture of the MGF was started and the forging of three large flywheel disks having 6.1 m in diameter and 106 tons in weight each has been almost finished. At the new site the bases of the MGF were set in the MG pit in October 1982. The installation at the new site is expected to start at the end of 1983.

Table X.4-2 Specifications of 400 MVA motor generator with flywheel for plasma heating system.

Generator	Vertical shaft salient pole type	1	set
	Capacity	400	MVA
	Voltage	18	KV
	Current	12.8	KA
	Frequency	77.6 - 54.2	Hz
	Power factor	0.62	
	Flywheel effect (with Flywheel)	11600	ton-m^2
	Revolution	582 - 406.5	RPM
	Energy yield	2.65	GJ
Induction motor	Capacity	15	MW
	Control	Stationary scherbius system and Water rheostat	

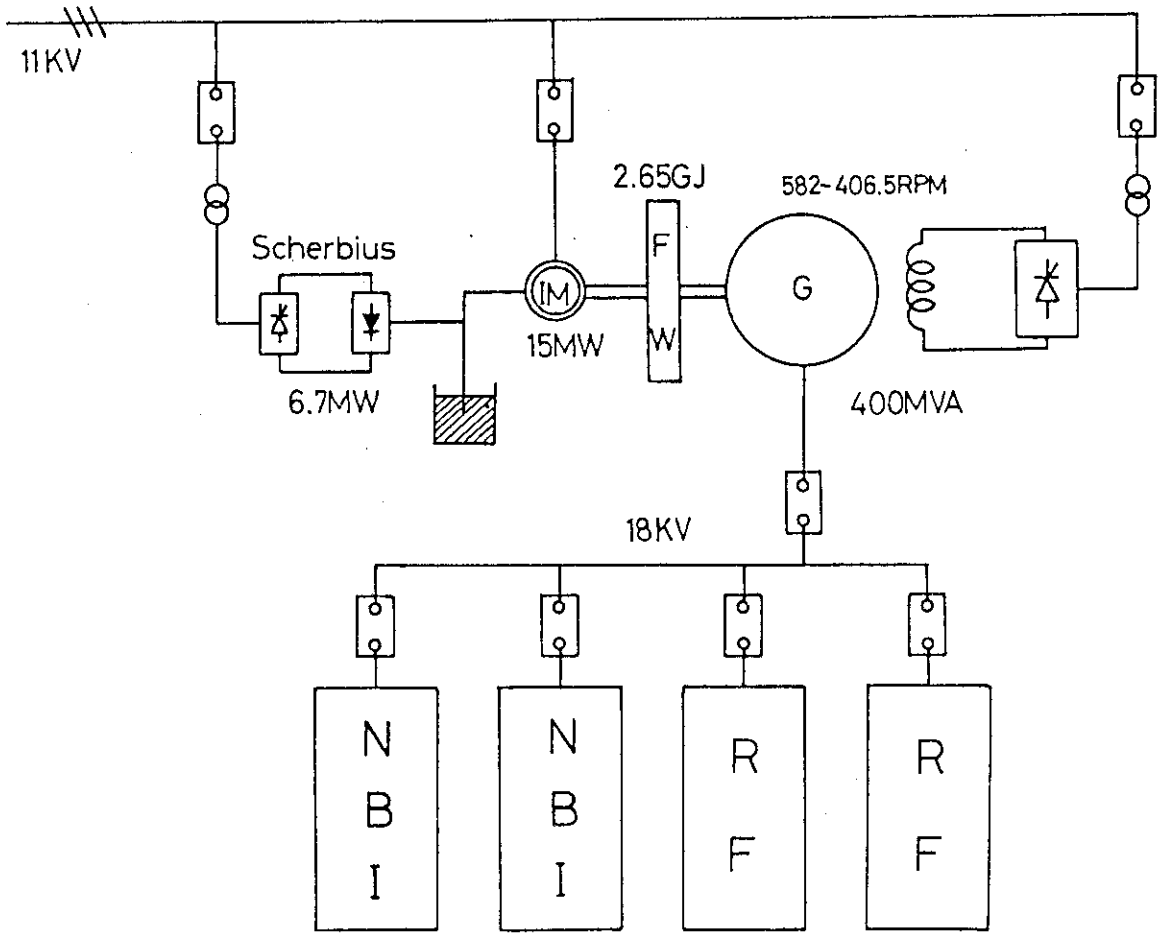

Fig. X.4-9 Schematic diagram of 400 MVA motor generator with flywheel for plasma heating system.

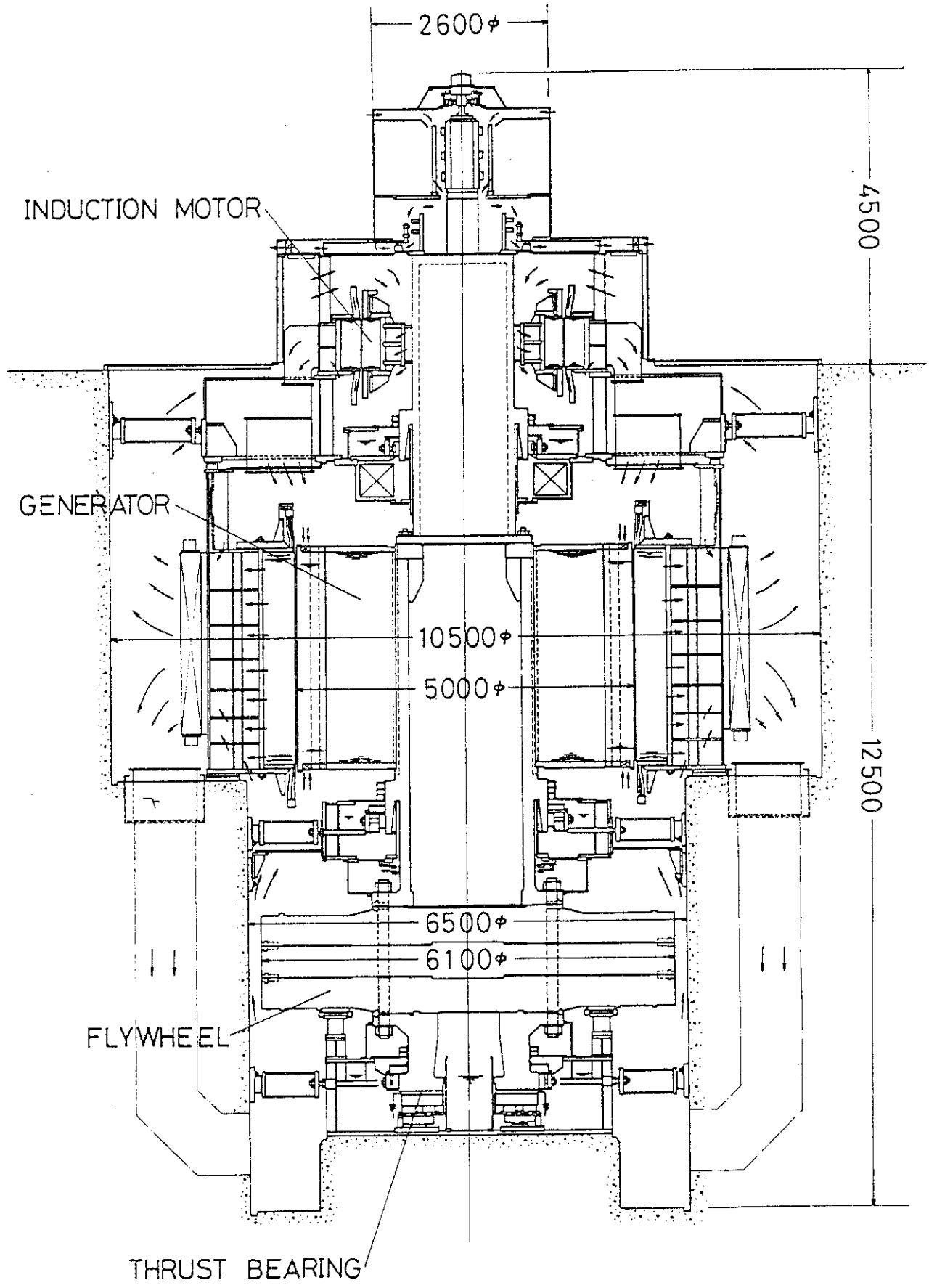

Fig. X.4-10 Cross section of the motor generator with flywheel.

5. Status of Control and Diagnostic Systems

5.1 Major activities of control and diagnostic systems

Since JT-60 central controller, ZENKEI, was contracted in March 1980, the manufacturing design and the fabrication has been actively carried out.

All the functions of ZENKEI, such as plant support, discharge, real time and feed back control, man-machine communication, data logging, inter communication and fault analysis were finally set and the whole devices, those are, computers, timing system, protective interlock, consoles and CAMAC interfaces were fabricated. The software for the computers was also designed and made.

Testing programs were also made and used for the pre-test of ZENKEI and the other control systems at both the factory and the site.

The control consoles and panels were installed in the central control room and the other components of ZENKEI were also assembled and tested.

As for the diagnostic system, according to the executive plan which was made in 1980, the whole diagnostic systems of A group were designed and represented in the ordering specific forms and some of them were ordered to manufacturers. The ordered systems are as follows; A-1 Electron Density Measuring System, A-2 FIR Spectrometer Subsystem, A-3 Ion Temperature Measuring System, A-4 Impurity Measuring system, A-5 High Counting Rate PHA Subsystem, A-6 Signal Processing Subsystem for Electro-Magnetic Probes, A-6 Visible TV Subsystem, A-7 Data Processing System and A-8 Diagnostic Support System.

5.2 Present status of control system

During this term, ZENKEI has made its progress in establishing the software covering the whole performance including plant support, discharge control, real-time control, man-machine, data filing etc., and the main hardware such as the computer system, CAMAC system, timing system, protection interlock system etc., through inspection tests in the factory, transportation to the site and positioning there.

This discharge control software has been established as a combination of the following performances. They are,

1. Handling of discharge condition and preprograms,
2. Discharge sequence control,
3. Checks before and after shot,
4. Handling of discharge data.

The discharge condition of JT-60, which is arranged for the operator to be able to set it up easily, is hierarchically constituted of three levels; the preparation condition (X), the executive condition (Yi) and the subsystem condition (Zij) as shown in Fig. X.5-1.

The preparation condition X determines the preparation state of devices necessary for executing the discharge. This condition is set up in the discharge preparation mode. The mode shift to discharge mode is permitted when the preparation of all devices are accomplished. The operator can, hence, grasp the operation state of subsystems easily in the discharge mode. This operation state is checked every 10 minutes by the plant support computer Ia.

The executive condition Yi determines the total discharge sequence, operation time sequence, repetition times of discharge, etc. There are eight discharge types in JT-60 (experimental discharge with/without inter-shot discharge cleaning, two types of long pulse discharge cleanings, short pulse discharge cleaning, TDC and two types of test discharge sequences), among which the discharge type permitted by the condition X can be chosen, and the condition Yi is set up to the discharge control computer (Ib).

The subsystem condition Zij is constituted of the detail conditions for the subsystems, the ZENKEI timing system, the real-time control and the feed-back control computers (Ibr and IIb). The operator makes the condition Zij in the form of physical parameter, which is converted to the machine the operator is converted to the condition of tap exchanger in the subsystem by using the conversion table of it. The operator can, hence, make the condition Zij without knowledge of the detail items of machine condition.

These conditions X, Yi and Zij are checked by the computer before being set up to the computer Ib. The upper/lower limit, the logical relations between their items, the consistency of the combination of X, Yi and Zij, etc., are checked. The table of permissibe operation range, in which the maximum coil current, the maximum input power of NBI and RF,

etc. are set up, is used to check the condition Zij. The items of this table are set up according to the adjustment state to the subsystems, the level of acquired control technique and the experimental planning.

The discharge control computer Ib supervises the total discharge control according to the time sequence predetermined by the condition Yi, and transmits the control commands to the subsystems, the ZENKEI timing system and the computer Ia. The set-up of the condition Zij ('discharge request sequence') and the collection of experimental data are also conducted by the computer Ib. The ZENKEI timing system, which starts 1 minute before shot according to the command of 'start discharge', conducts the detail time sequence before and during shot. Each subsystem conducts its own control sequence (NBI flashing, MG re-acceleration, etc.) according to the command from the computer Ib and the ZENKEI timing system, and answers the operation state to the computer Ib. The computer Ia, which collects the plant monitoring data from the subsystems at the constant period, collects parts of them necessary for the pre-shot checks I and II and the post-shot check mentioned in the following section.

Figure X.5-2 shows the safety control function of each computer and the safety interlock system corresponding to the discharge sequence.

The items of the pre-shot check I, II and the post-shot check are summarized in Table X.5-1.

Before starting the successive discharge sequence, the soundness of whole system is checked in the pre-shot check I. The operation state of the subsystems, which are determined by the condition X and the mode condition, is checked by the computer Ia every 10 minutes, and the last result is checked by the computer Ib in this process.

The pre-shot check II is conducted in the discharge request sequence (about 2 minutes before shot) where the devices of subsystems are preset according to the condition Zij. All the answer-backs from the substems, which check the preset state of their devices by themselves, are checked by the computer Ib. The temperature of the vacuum vessel, the water flow of primary cooling system, etc., necessary for machine safety, are checked by using the process data table located in the shared memory. The influence of discharge on the commercial power network (variation of frequency, induction of higher order harmonics, etc.) is calculated with the discharge condition. The prediction algorithm for an undesirable state is under consideration.

The post-shot check is conducted to confirm the soundness of whole system after the discharge operation and to see if the discharge was conducted as expected. Each subsystem checks the operation state after shot, the items of which are defined in each subsystem. If all the anwser-backs are normal and no alarm comes up, the computer resets the 'discharge alarm' status. The influence of discharge on the commercial power network is calculated with the experimental data. This result is to be reflected to the next discharge.

Table X.5-1 Check items at each stage of discharge sequence.

	Check items	Examples
Pre-shot check I	1. Check of alarm status 2. Check of operation mode 3. Check of rotation of MG	Exsistance of alarm level I, II Operation status of subsystems Rotation of MG $\geq$ 70 %
Pre-shot check II	1. Check of preset status of discharge conditions 2. Check of operation status of subsystems 3. Check of power supply conditions by calculation 4. Check of dangeous operation by calculation	Answer-back from subsystems 89 GP 1 → OFF, etc Baking heater → OFF Temperature of V,V $\leq$ ○○℃ Prediction of effective power, reactive power, frequency variation etc. Runaway operation etc
Post-shot check	1. Check of status of subsystems after shot ① Sequence check of subsystems ② Check of machine status of P and T-P/S ③ Check of alarm broken out during shot ④ Check of stop of clock for DDC and II_b 2. Judgenent of discharge status ① Rectangular converted current flow time of P-coil ② Check of electro-magnetic probes ③ Check of power supply conditions ④ Check of operation result of NBI and RF	Check of machine status after shot Cross-check by using monitoring data Exsistance of alarm level I, II Confirmation of stop of clock $T = \frac{1}{I_{MAX}^2}\int_0^t I^2(t)dt < T_{MAX}$ Cross-check of plasma positions measured by different series of magnetic probe Cross-check between operation result and experimental condition

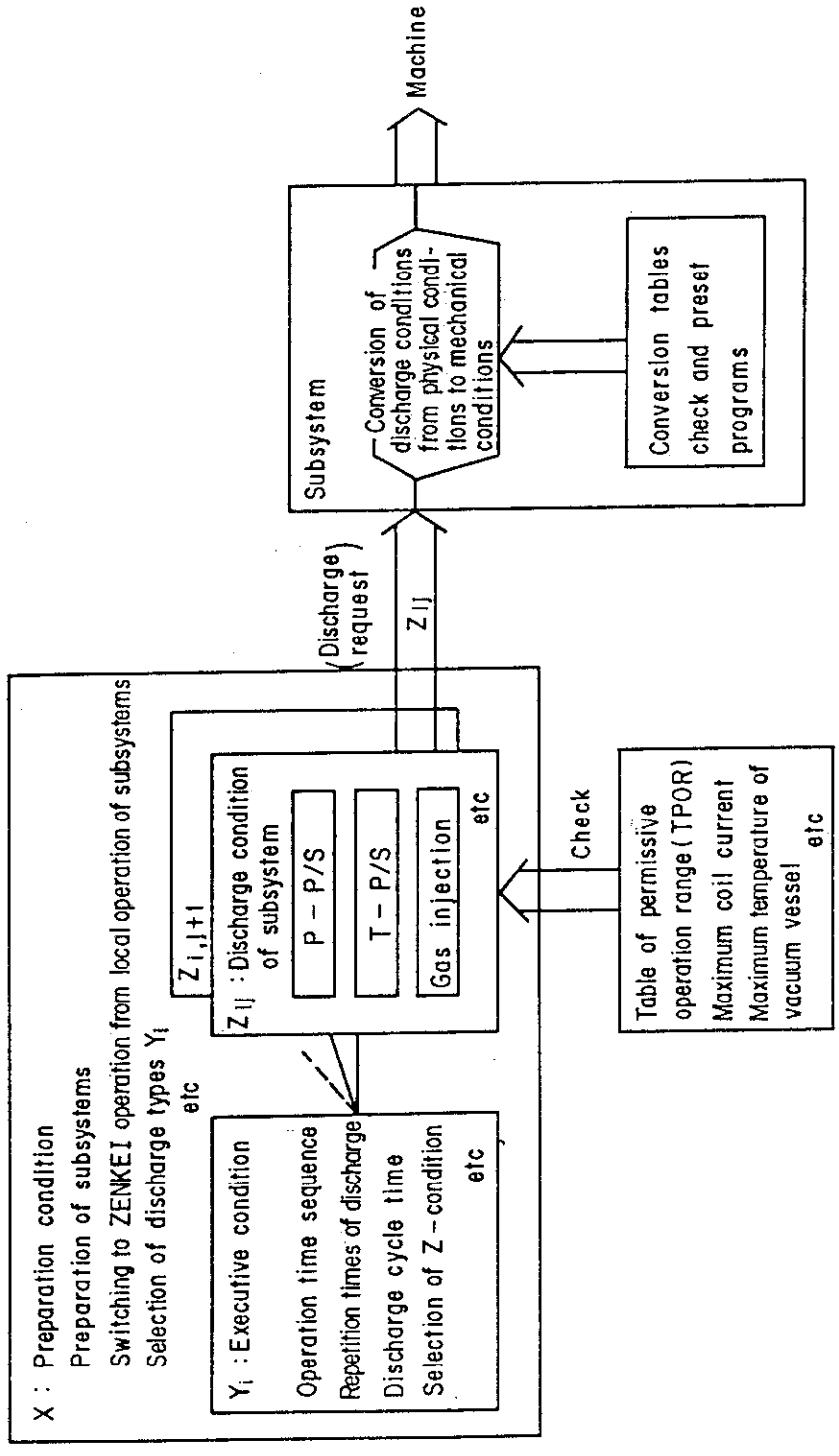

Fig. X.5-1 Structure and items of discharge condition.

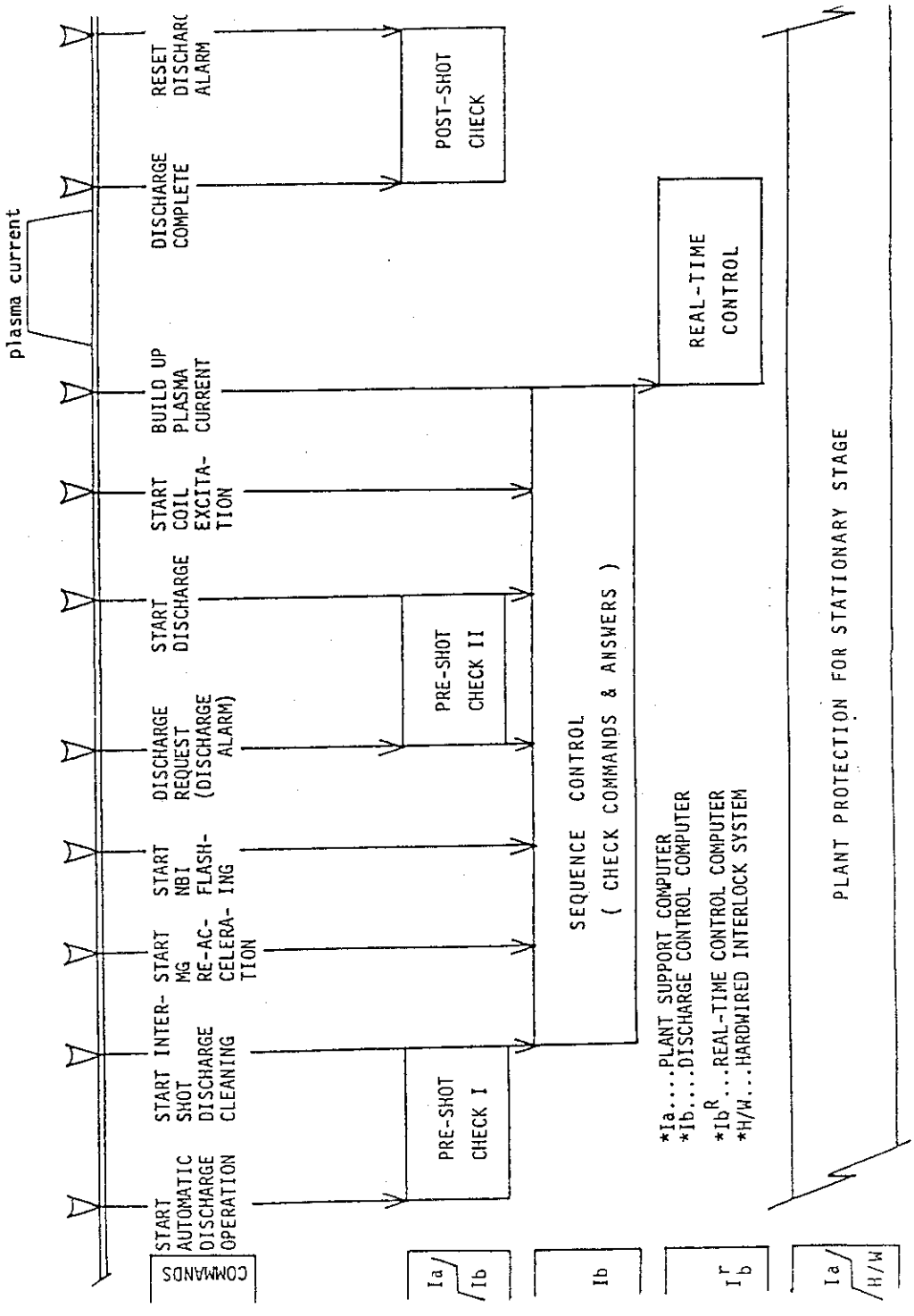

Fig. X.5-2 Safety control functions and their relation to discharge sequence.

5.3 Present status of diagnostic system

5.3.1 Introduction

Diagnostic instruments for JT-60 are divided into two groups, Group A and Group B, according to their characteristics. The greater part of efforts has been placed on the design and fabrication of Group A instruments (see Table X.5-2) for the last fiscal year. Group A instruments have been designed to meet the requirements of providing high accessibility to the tokamak torus. Particularly, spectroscopic, bolometric and soft X-ray measuring units were so designed as to meet the above requirements with sufficient compactness and standardization in size.

5.3.2 Electron density and temperature measuring systems (A-1 and A-2)

Construction of A-1 system and A-2-a subsystem were continued and completion will be within the fiscal year of 1984 and 1983, respectively. The CO_2 laser oscillator for sub-mm wave (119 μm) laser was constructed and the adjustment aiming at high operating power levels has started in the firm.

5.3.3 Ion temperature and impurity measuring systems (A-3 and A-4)

A-3-c subsystem will be completed in summer 1983 and the other subsystems of A-3 system will be completed within the fiscal year of 1984. The beam source test for A-3-c subsystem will be completed in FY 1983 in the firm and will be re-tested in FY 1984 at JAERI. A-4 system will be completed within the fiscal year of 1984.

5.3.4 Radiation flux and peripheral plasma measuring systems (A-5 and A-6)

A-5-a subsystem will be completed in FY 1983. A-6-b, A-6-c and A-6-d subsystems will be completed in FY 1983.

5.3.5 Data processing system and diagnostic support system (A-7 and A-8)

Data processing system for JT-60 except an inter-shot processor will be completed within the fiscal year of 1984. The specifications for the inter-shot processor including various softwares were fixed by the end of FY 1982, and the inter-shot processor will be concluded within FY 1983. Diagnostic support system will be completed within the fiscal year of 1984.

Table X.5-2(a) JT-60 diagnostics (A group)(part 1).

System	Symbol	Diagnostics	Specification	Feature
A-1 Electron Density Measuring System	A-1-a	Sub-mm Wave Interferometer	Main Plasma $\Delta n_e \geq 10^{12}cm^{-3}$, $\Delta t \sim \mu S$, X_i: 5 points, ΔX = 12 cm Divertor Chamber $\Delta n_e \geq 4 \times 10^{12}cm^{-3}$, $\Delta t \sim \mu S$	CH_3OH (200 mW) λ=118.8 μm Mechanical vibration free (with HeNe laser interferometer)
	A-1-b	MW Wave Interferometer	Main Plasma $\Delta n_e \geq 4 \times 10^{11}cm^{-3}$, $\Delta t \sim \mu S$ X_i: 2 points, ΔX = 6 cm	2 mm Wave (1W)
A-2 Electron Temperature Measuring System	A-2-a	FIR Spectrometer	$\Delta t \sim 10$ mS, X_i: 40 points ΔX= 15 ∿ 30 cm	Fourier Spectrometer real time FFT
	A-2-b	MM Wave Radiometer	$\Delta t \sim \mu S$, X_i: 10 points, ΔX= 15 ∿ 30 cm	126∿280 GHz
	A-2-c	Multipulse Laser Scattering Apparatus	$\Delta t \sim 20$/shot, X_i: 12 points ΔX= 12 cm	SHG(λ=0.526 μm) of Glass Laser(λ=1.053 μm)
A-3 Ion Temperature Measuring System	A-3-a	Neutral Particle Analyzer (E.S.)	E=0.1∿30 keV, $\Delta E/E$=0.05∿0.1 Δt=50∿500 mS, Z_i: 3 points	Electro-Static Analyzer
	A-3-b	Neutral Particle Analyzer (E.S. & M.A.)	E=0.1∿30 keV, $\Delta E/E$=0.1 Δt=50 mS, X_i: 1 point	Electro-Static with mass Analyzer E//B type (H & D)
	A-3-c	Active Beam Probing Apparatus	$\Delta T_i/T_i$=0.1, Δt=10∿100 mS Z_i: 1 point, ΔX=5cm, ΔZ=20cm	Beam: 3.5 A, 200 keV, He^+ Analyzer: E//B type, MCP
	A-3-d	Neutron Counter	E_n-E_{th}∿2.45 MeV, Δt=1∿100 mS X_i: 1 point	NE-213, PHA

Table X.5-2(b) JT-60 diagnostics (A group)(part 2).

System	Symbol	Diagnostics	Specification	Future
A-4 Impurity Measuring System	A-4-a	Light Impurity Spectrometer (Special Resolution)	λ=5∿500 A, Δt∿10 mS, Z_i: 15 points, ΔZ= 7 cm	Toroidal holographic grating, Flat field, Array detector
	A-4-b	Light Impurity Spectrometer (Doppler)	λ=1000∿2350 A (λ_i: 5 points) Δt∿1 mS, X_i: 1 point	Concave grating
	A-4-c	Heavy Impurity Spectrometer (Doppler)	λ=0.1∿10 A (λ_i: 3 points) Δt∿10 mS, X_i: 1 point	Crystal grating, Array detector
	A-4-d	Spectrometer for Divertor	λ=20∿1200 A, Δt∿10 mS, X_i: 1 point near x point	Same as "A-4-a"
	A-4-e	Visible Spectrometer for Absolute Calibration	λ=2000∿7000 A, X_i: 1 point	Photomul & Photograph
	A-4-f	Grazing Incidence Spectrometer for Absolute Calibration	λ=10∿1300 A, X_i: 1 point	Same as above
	A-4-g	A-4 System Calibration Devices		Light Source etc.
A-5 Radiation Flux Measuring System	A-5-a	High Speed Counting PHA	E=1∿200 keV, Δt∿10 mS X_i: 3 points	Si(Li) or Ge(I)
	A-5-b	High Speed Counting PHA Array (Spatial Resolution)	E=1∿200 keV, Δt∿1∿10 mS Z_i: 15 points	Same as above
	A-5-c	PIN Diode Arrays	Δt∿25 μS, Z_i: 15 points	PIN Diode or SSD, Computer Tomography
	A-5-d	Bolometer Arrays	Δt∿10 mS, Z_i: 15 points	Thermistor
	A-5-e	Runaway Monitor	Δt∿1 mS, X_i: 1 point	Hard X-ray Detector Array

Table X.5-2(c) JT-60 diagnostics (A group)(part 3).

System	Symbol	Diagnostics	Specification	Future
A-6 Peripheral Plasma and Wall Surface Measuring System	A-6-a	Infrared TV	t = 10 mS/Frame	Picture Elements; 100 × 100/frame
	A-6-b	Visible TV	t < 50 mS	Fields of view; overall > ±90°
	A-6-c	Electro-Magnetic Probe	Magnetic Probes Rogowski Coils One Turn Coils Saddle Coils Thermo-Couples	
	A-6-d	Spectrometer for periphery	λ=1000∿7000 A, Δt∿10 mS Z_j: 10 points at periphery	Real Time
	A-6-e	Hall detectors		
A-7 Data Processing System		(1) Inter Shot Data Processor (2) Real Time Data Processor (3) CAMAC Systems		General Purpose Computer
A-8 Diagnostic Support System		(1) Diagnostic Stages (2) Carriers (3) Cabling & Piping (4) Vacuum Connecting Instruments (5) Shielding Cases (Magnetic & Radiation Shield)		

6. Status of Auxiliary Systems

6.1 Secondary cooling system

The manufacturing of machinery of the secondary cooling system was finished in July 1982 as scheduled. After the inspection, it was transported from the factory to the Naka site and the installation work was started. The erection work of this system was finished as scheduled in March 1983.

(i) Cooling tower

The construction work of the cooling tower was started in December 1981. After furnishing blowers, eliminators, and other components, it was completed in November 1982.

(ii) Main pump of cooling system and water treatment system

The installation of pumps and water treatment system and the construction work of piping were started in July 1982 and were completed in February 1983.

(iii) Electric equipment and control system

Main electromotor (high voltage system) and cables were also installed and the testing of individual component was carried out. After the installation of the central control system (ZENKEI), the control subsystem of the secondary cooling system will be connected with ZENKEI and linkage test will be started from April 1983.

6.2 Power distribution system and emergency power supply

The system of power distribution and emergency power supply were completed in the factory in August 1982. After the inspection by JAERI, this system was transported to the Naka site, and the installation was finished in December 1982.

The power line diagram for the system is shown in Fig. X.6-1.

6.2.1 Power distribution system

The installation of high tension system (6.6 kV M/C) and low tension system (400 V, 200 V P/C) was begun in August 1982, and in December, the electric endurance test was done. Receiving of electric power from the central substation was started in December 1982.

6.2.2 Emergency power supply

High tension system (6.6 kV M/C), low tension system (400 V, 200 V P/C) and no break power supply system were installed in January 1983.

The battery system was also installed in the rectifier building.

6.2.3 Control system

Control devices including operation monitoring system and CAMAC system were already installed.

The component test of these systems were started in December 1982 and ended in March 1983. The static type invertor (CVCF) is now in the long term test. After the component tests, this system is connected with other subsystems of JT-60 and various items will be tested to verify its performance. This is scheduled to start in April 1983.

A schematic diagram of the power distribution system and the emergency power supply is shown in Fig. X.6-2.

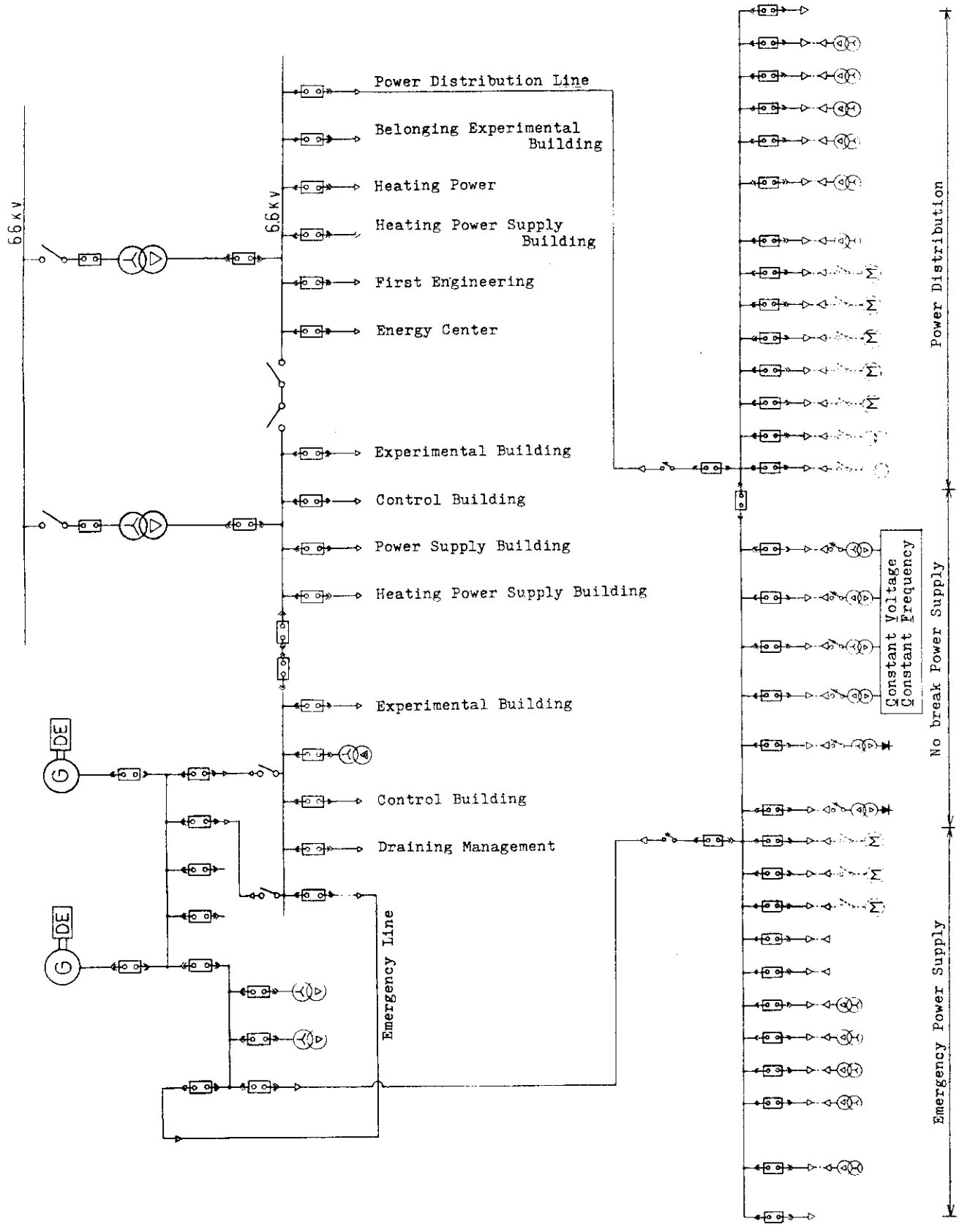

Fig. X.6-1 Schematic diagram of regular power line.

7. Status of Heating System

7.1 Construction of neutral beam injectors (NBI) for JT-60

For additional plasma heating, 20 MW neutral beam injection system is planned. The number of injector units is 14. Each unit is designed to inject a 1.43 MW neutral hydrogen beam into the plasma for 10 sec, using two ion sources rated at producing a 75 keV, 35 A ion beam.

The total system consists of 14 beam line units, 14 power supply units, a helium refrigeration system, a liquid nitrogen supply system, a cooling water circulation system, auxiliary evacuating system, and their control and diagnostics system. Figure X.7-1 shows a cross sectional view of the JT-60 neutral beam injector, where two injector units (a lower unit and an upper unit) are shown.

Each injector unit is composed of two ion sources, two neutralizers, a reflecting magnet, magnetic shields, a beam dump, a water jacket, a calorimeter, a fast shutter, and six plates of cryopump.

Refining the design is still continued. In 1982, a contract was signed for the construction of liquid nitrogen transferlines, water cooling lines, and the sole plates of the beam line chamber.

Construction of the lines were completed in March 1983. The sole plates are now under construction, and will be completed in August 1983.

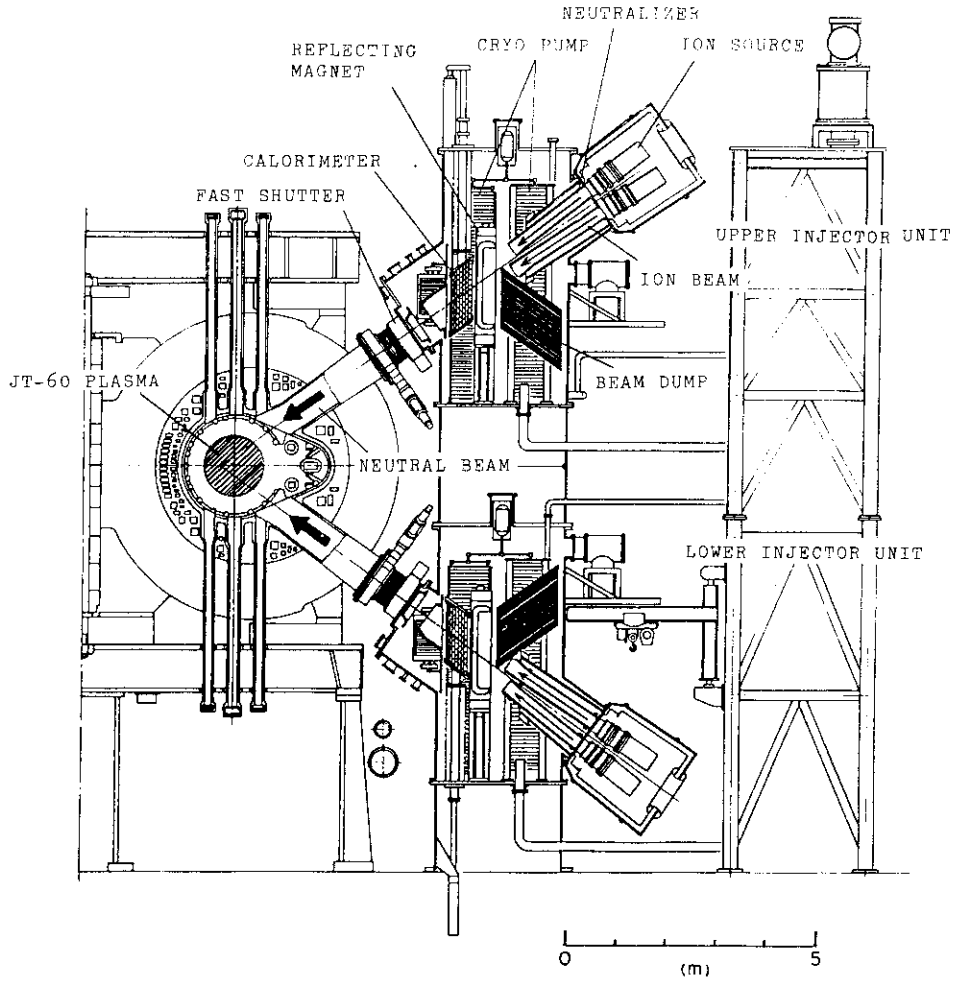

Fig. X.7-1 Cross section view of the JT-60 Tokamak and the two neutral beam injectors.

7.2 Radio frequency heating system in JT-60

The specification of the RF heating system was accomplished in FY 1982. Specifications of the system are described in Table X.7-1. The RF heating system consists of three LHRF units and one ICRF unit.

Recent success in the second hamonic ICRF heating experiment on the RLT[1)] device have raised up the power and the frequency of ICRF unit in JT-60. The latter item makes it possible to use the waveguide system in ICRF system. Eight tetrodes per one unit is planned to equip for the ICRF power source in JT-60. The frequencies are 110 MHz, 120 MHz and 130 MHz, which are for the second harmonic ion cyclotron frequency in JT-60 toroidal magnetic field strength. Figures X.7-2 (a) and (b) are the top views of the ICRF ridged type wave guide launcher in JT-60 with and without Faraday shield, respectively. The possibility to use this ridged waveguide structure in JT-60 depends on further theoretical considerations of the ridged waveguide system and also the results of the JFT-2M ICRF coupling experiments using the parallel plates similar to the ridged waveguide system in JT-60.

A part of the primary water cooling pipes and the coupler system for JT-60 RF heating facility were constructed by the end of March 1983, not to interfere other JT-60 instruments, since other torus instruments will be located prior to the additional heating facility itself. These are the primary water cooling pipes in JT-60 underground ducts, the high temperature nitrogen gas pipes and the vacuum pipes for the coupler system in the pumping room and in the PIG power supply room, sole plates for scaffolds of the coupler system in the torus hall and the cable trays in the heating ducts I and II.

Reference

1) D.Q. Hwang, et al., paper IAEA CN-41/I1, at the 9th International Conference on Plasma Physics and Controlled Nuclear Fusion Research, Baltimore, September 1982.

Table X.7-1 Specifications of the RF heating system for JT-60

	LHRF	LCRF
Number of unit	3	1
Frequency	1.7 - 2.3 GHz	110, 120, 130 MHz
Injection power	10 MW	
RF pulse length	10 sec	
Duty	1/60	
High power amplifier	Klystron (8 tubes/unit)	Tetrode (8 tubes/unit)
Launcher	Phased array of waveguide (4 rows × 8 columns)	T-Shaped ridged waveguide (2 rows)
Waveguide size	115 mm × 35 mm	496 mm × 320 mm
Baking temperature	400 - 500 °C	

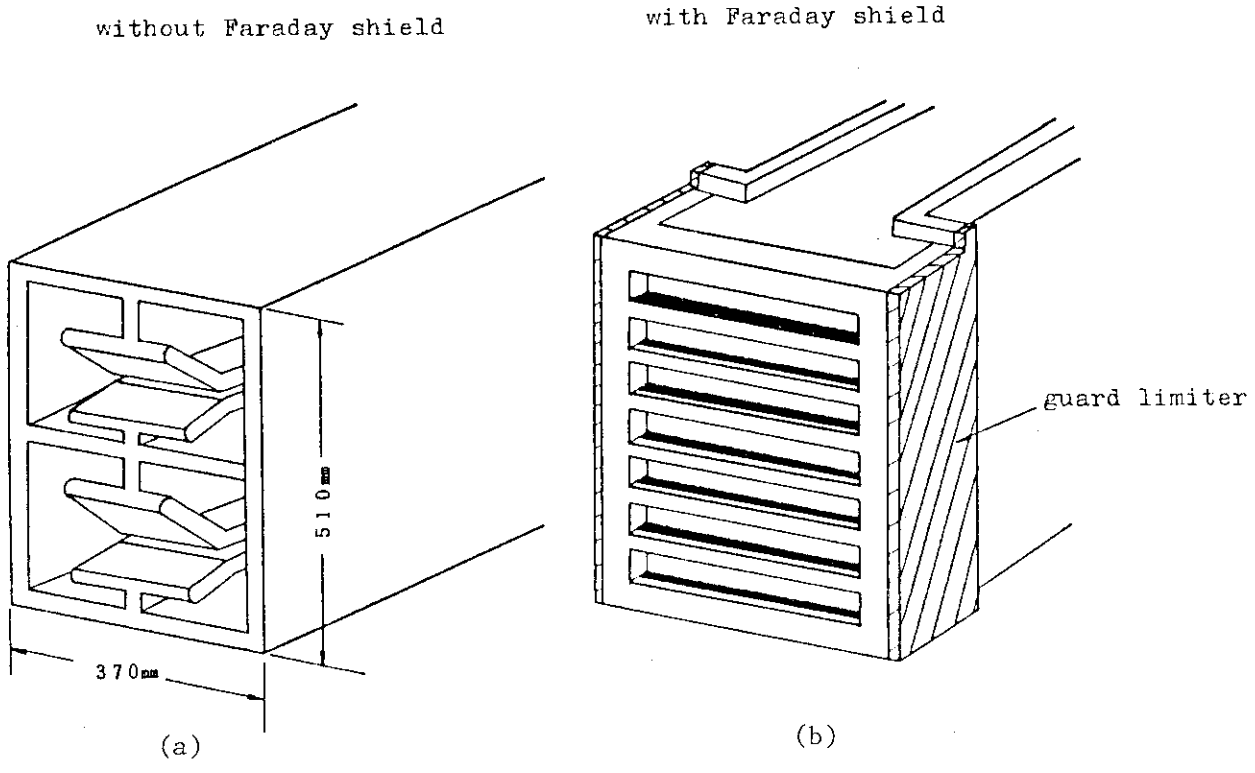

Fig. X.7-2 Top of the launcher in JT-60 ICRF.

8. Vacuum Technological Development for JT-60

8.1 Introduction

The JT-60 device created a necessity for solving new problems in the vacuum and surface technological area. They include elaborate surface preparation such as coating of low-Z materials and cleaning, and leak hunting techniques for the large vacuum vessel and components[1]. In this fiscal year, significant progress was made with the development and testing of full-sized TiC-coated walls, an in-situ coating device and a leak location device.

8.2 Development and testing of TiC-coated first walls[2]

From the small sample tests performed in FY 1981, titanium carbide was chosen as the coating material for the first stage use in JT-60 since CVD-TiC on molybdenum and PVD-TiC on Inconel produced a favorable result in both refractory character and coating - substrate adhesion. In FY 1982 the effort was mainly directed to the improvement of CVD method to find out how to reduce the deposition temperature and to the ascertainment of the industrial capability to massproduce coatings on full-sized first wall structures for JT-60. In this development, the temperature of TiC deposition could be successfully reduced to about 900 °C where recrystallization of molybdenum was found to be inconsiderable (see Fig. X.8-1). Figure X.8-2 shows TiC-coated first walls (a fixed limiter and an armor plate) prepared after the new CVD method.

8.3 Development of an in-situ coating device[3]

In-situ coating techniques are also being prepared for the repair of TiC-coated walls which will be eroded or damaged by plasma wall interactions. This project is intended to develop a new device which can work not only for the recoating of the first wall in its entirety but also for the repair of small areas of the wall according to the circumstances. The coating method must fulfill selfish conditions such as low deposition temperature ($\leq$400 °C) and low working gas pressure ($\leq 5\times10^{-5}$ Torr). In the JT-60 device, four vertical ports of 20 cm in diameter, about 90° toroidally apart each other, will be provided to to mount coating devices.

In FY 1981 a reactive evaporation method using Ti and C_2H_2 was found to fulfill the above conditions and to produce a favorable result in chemical composition and structure of the coatings. In order to apply this method to the JT-60 torus vessel, it is required to develop a large Ti-vapor source which can be inserted from the port through a vacuum lock and handled with ease in the vessel. Figure X.8-3 shows a conceptual design of the in-situ coating device now under development and testing for JT-60.

8.4 Development of a leak location device

If vacuum leaks occur during machine operation due to applied stresses or plasma wall interactions, it will take a lot of time to locate and fix the leaks and to recover a clean wall condition. After the preliminary experiment in FY 1981 by using JVX-II, it was planned to develop a small manipulator with built-in motors, improved unidirectional gauges and their control systems. Figure X.8-4 shows a prototype manipulator under testing in atmospheric pressure which was developed in FY 1982.

8.5 Performance tests of metal-sealed gate valves[4)]

Nearly 100 metal-sealed gate valves of 9 - 30 cm in gate diameter will be installed in diagnostic ports of JT-60. Performance tests of a prototype 20 cm valve were made from FY 1978 through 1982. The vibration test in closed position showed that the maximum acceleration to the valve is limited to about 3 G because the sealing materials suffer from fretting corrosion at higher accelerations. Table X.8-1 shows a relation between cleanliness in assembly rooms and a sealing characteristic after assembly. These results were reflected in the design and fabrication of the valves and will be considered for the JT-60 operation.

References

1) Y. Murakami, Proc. 9th Intern. Vacuum Congress (Madrid, 1983)
2) Y. Murakimi, T. Abe and H. Nakamura, J. Nucl. Materials 111 & 112 (1982) 861
3) T. Abe, K. Inagawa, K. Obara and Y. Murakami, Proc. 12th Symp. on Fusion Technology (Julich, 1982) p.221
4) K. Obara, T. Abe, Y. Murakami, M. Yamamoto, M. Shimizu, K. Chiba and K. Itoh, J. Vac. Soc. Japan 26 (1983) 435 (in Japanese)

Table X.8-1 Relation between cleanliness in assembly rooms and leak amount after assembly.

Cleanliness*	Leak amount ($Pa \cdot m^3/sec$, He)	
	at 1st closure	at 100th closure
2.2×10^3	$< 1.3 \times 10^{-11}$	$< 1.3 \times 10^{-11}$
1.8×10^5	5.7×10^{-8}	1.1×10^{-9}
7.5×10^5	1.2×10^{-6}	2.9×10^{-7}

* number of dusts (≥0.5 μm) in a volume of 1 ft^3.

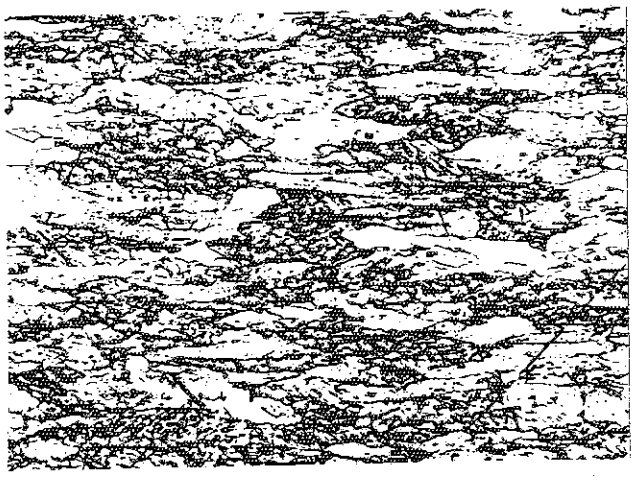

BEFORE COATING

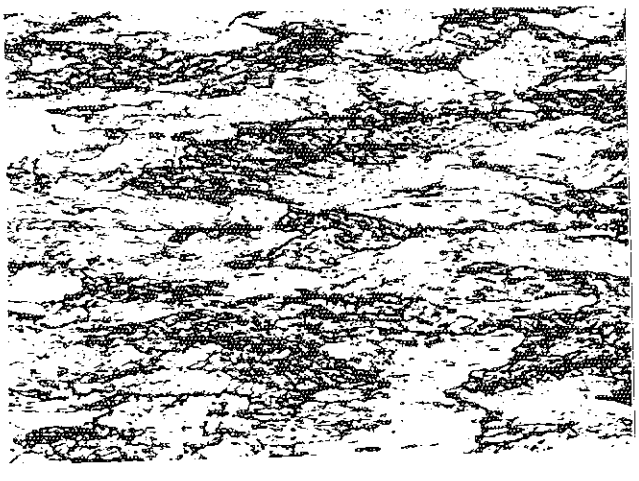

AFTER COATING

Fig. X.8-1 Photomicrographs of the structure of molybdenum plate before and after coating of TiC by a new CVD method.

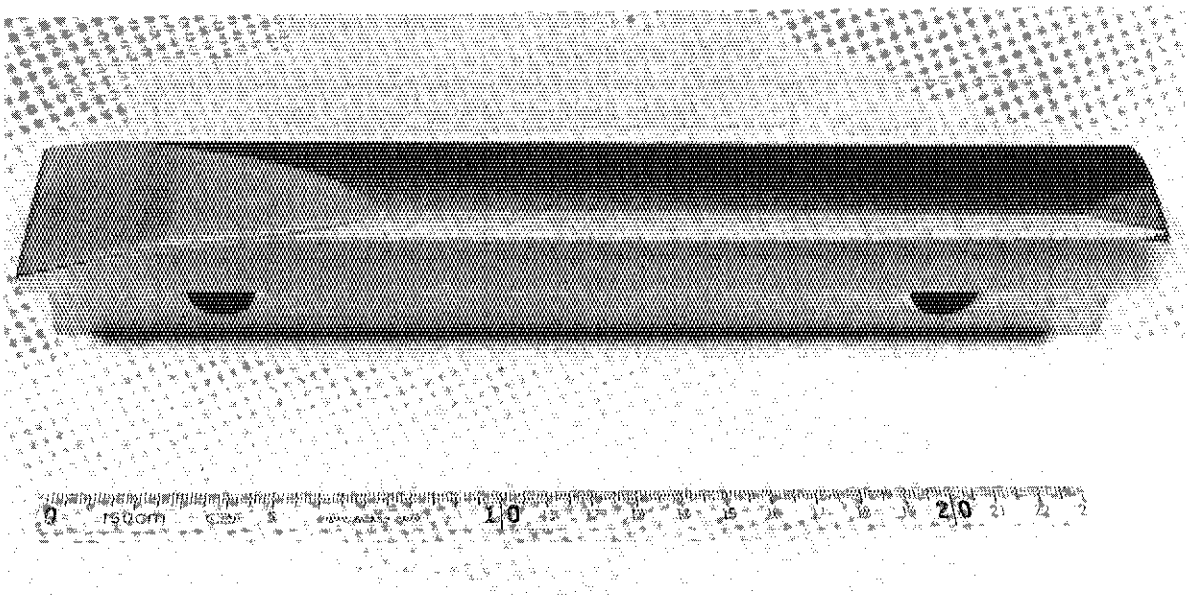

(a)

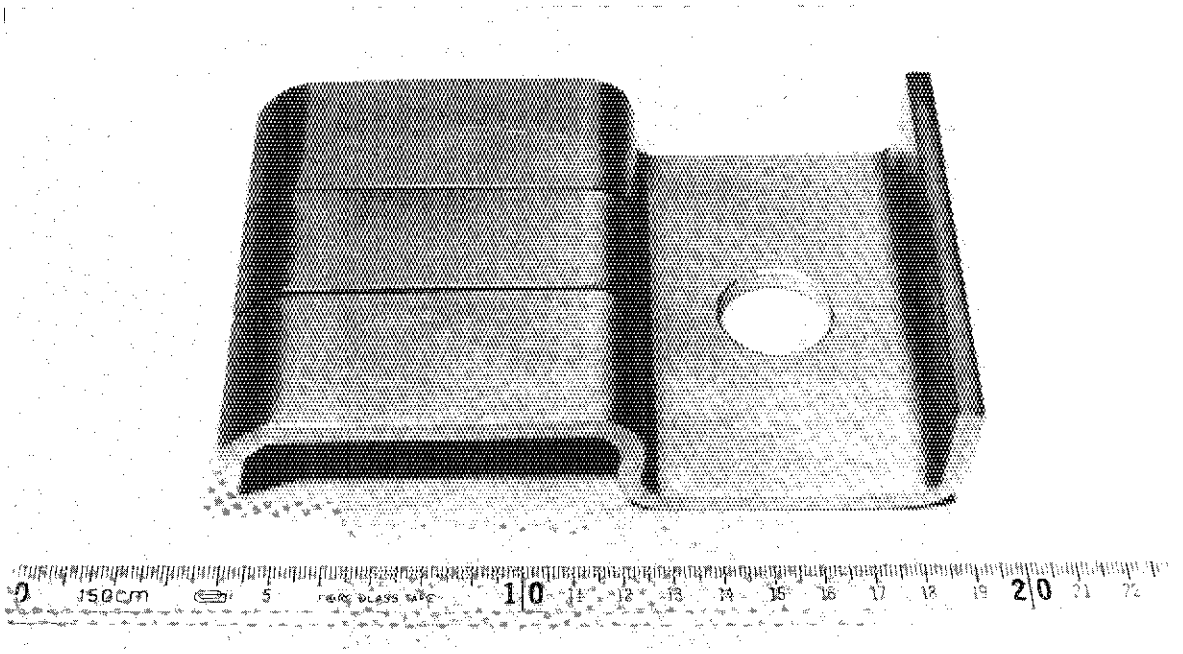

(b)

Fig. X.8-2 TiC-coated first walls prepared after a new CVD method ((a) a fixed limiter, (b) an armor plate).

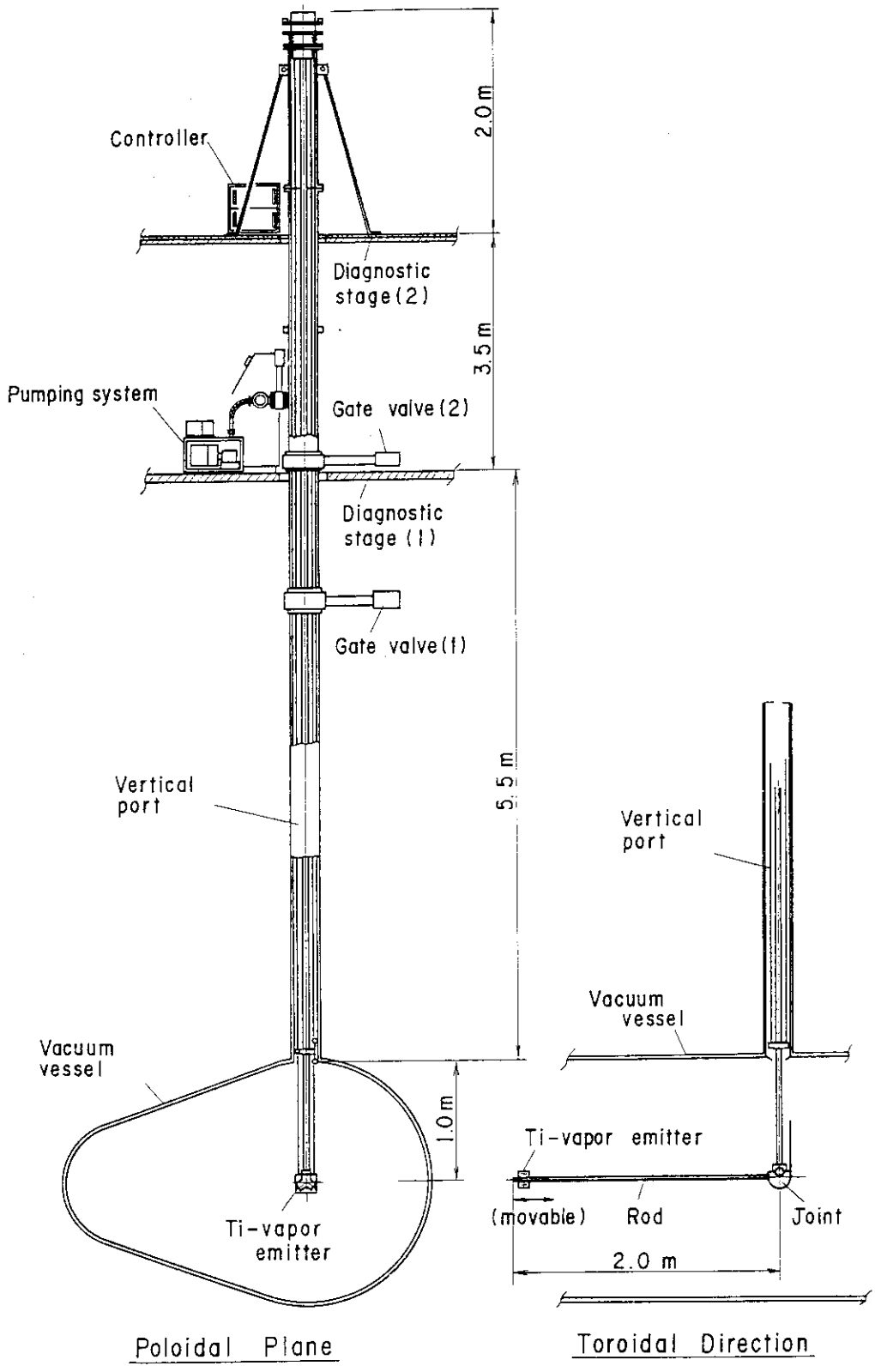

Fig. X.8-3 A conceptual design of an in-situ coating device.

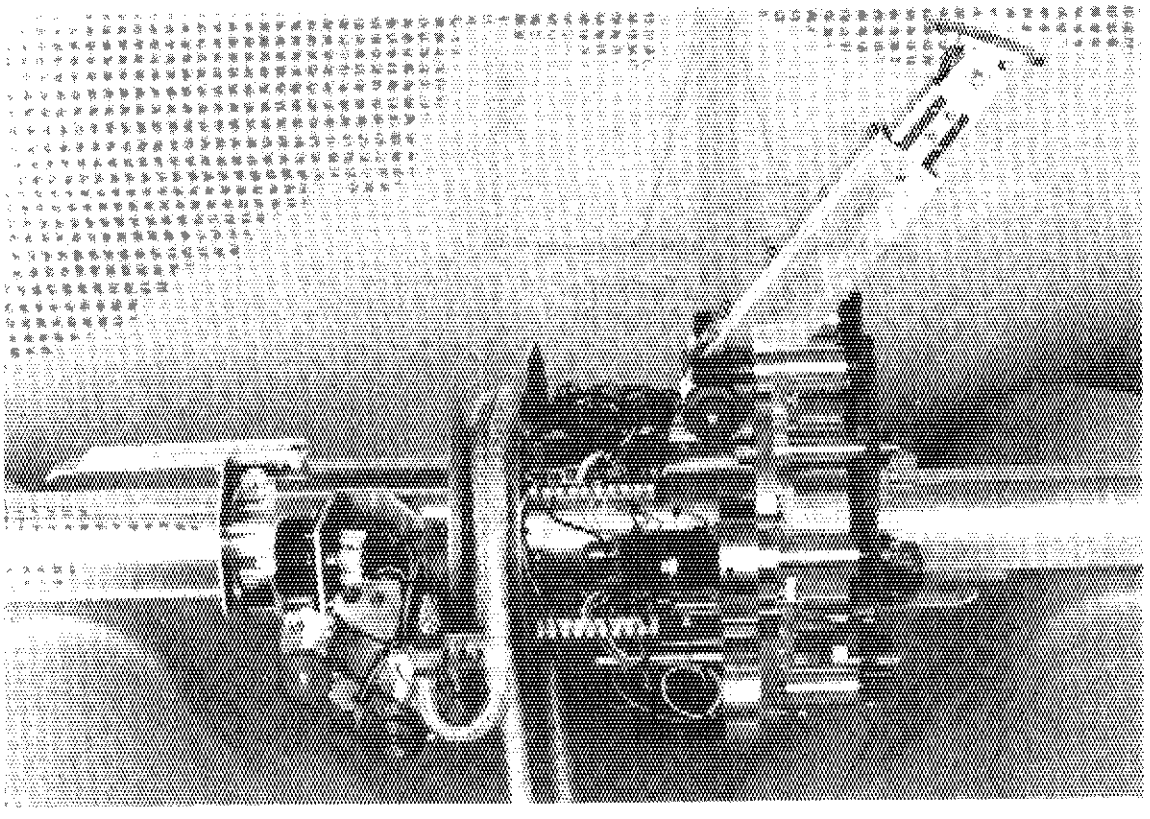

Fig. X.8-4 A prototype manipulator with built-in motors being tested in atmospheric pressure.

9. JT-60 Experimental Planning and Plasma Consideration

9.1 Experimental program and schedule

The experimental schedule was modified as shown in Fig. X.9-1, keeping original experimental programs.
The objective of JT-60 is the study of a reactor grade plasma including plasma-machine interface phenomena. In other words, technology to generate and maintain a reactor grade plasma has to be investigated and it is necessary to show how we can build up and control a reactor core with realistic methods. The experimental programs are summarized in Fig. X.9-1 and are briefly summarized as follows:

1. Preliminary Experiment

   2.7 MA discharge with and without divertor
   NBI, ICRF and LHF heatings
   RF current drive

2. Reactor Like Plasma Experiment

   $\bar{n}\tau_E = (2\text{-}6)\times10^{19}$ $m^{-3}s$
   $\bar{T}$ = 5 - 10 keV
   P_h = 30 MW
   t = 5 - 10 s
   V_p = 60 m^3

3. R & D for Reactor Core Plasma Experiment

   a) Impurity Control with a High Power & Long Pulse Heating
      Simple Poloidal Divertor
      Boundary Plasma Control
      First Wall Material

   b) Long Pulse & High Power Heating
      NBI (20 MW/75 - 100 keV/10 s)
      LHRF (7.5 MW/1.7 - 2.3 GHz/10 s) → Modification
      ICRF (2.5 MW/Wave Guide)

   c) Tokamak Plasma Improvement
      RF Current Drive

High β (4 % with B_t = 4.5T, profile control)
Disruption Control

4. Advanced Experiment

9.2 Plasma control

In a large tokamak, careful plasma control is essential not only for production of a high quality plasma but also for safety and machine protection. From this point of view, as well as for the position and shape control of a plasma, the real time control system is employed for other important features, e.g. controls of separatrix configuration, heating power, gas influx and disruption. All diagnostic instruments can be used as sensors for the real time control system to supply feedback informations to the major actuators; the poloidal coil system, divertor coils, hydrogen and impurity gas supply systems, 14 NBI injectors and 4 units of RF systems. Disruption control and soft plasma quenching will be intensively investigated as well as control of conventional plasma parameters.

A shallow poloidal divertor study is one of the most important experiments in JT-60. Then a dynamic simulation code for the divertor configuration control has been developed. The main flow of this code is shown in Fig. X.9-2.

A typical magnetic configuration with the divertor is shown in Fig. X.9-3. In this configuration, the separatrix magnetic surface has not to intersect any material except the divertor plate and following geometrical factors have to be controlled.

R_p*: plasma center position (Fig. X.9-3)
δ_{30}: the most serious clearance between the separatrix magnetic surface and the toroidal limiter (Fig. X.9-3)
δ_t : clearance between the separatrix and the surface of the main divertor coil (Fig. X.9-3)
x_p : position of the separatrix magnetic surface on the divertor plate (Fig. X.9-3)

Control of these geometrical factors is numerically studied in detail and the results are summarized as follows: The plasma center position

R_p* can be controlled by modifying a conventional method of a circular tokamak and only by a method such as the feedback control of vertical magnetic field B_V. The clearance δ_{30} is rather complex but can be essentially controlled by changing n index ($n = \frac{R}{B_V}\frac{\partial B_V}{\partial R}$) which is a strong function of quadrupole coil current. Since the throat clearance δ_t has a dependence of magnetic field pattern in the divertor chamber, the poloidal field direction at a suitable position (B_ρ/B_ω in Fig. X.9-3) gives a rather accurate value for δ_t under a wide range of discharge conditions (Fig. X.9-4). The position of the separatrix on the divertor plate X_p is a linear function of δ_t, i.e. $x_p = 4.2(\delta_t - 4) \pm 1$ cm. The separatrix magnetic surface, therefore, can be controlled by using B_ρ/B_ω in the divertor chamber. Dynamic analysis shows that the magnetic configuration with the divertor can be controlled by using magnetic sensors and by regulating various poloidal coil currents during current build-up phase, heating phase and also quenching phase. Even during a disruption, the divertor configuration can be maintanined by shell effect of the vacuum vessel when the plasma position and the reduction of $(\beta_p + \ell_i/2)$ are reasonable, e.g. $\Delta(\beta_p + \ell_i/2) \leqq 0.6$ and $R_p^* = 320$ cm, where β_p and ℓ_i are poloidal beta and internal inductance, respectively. In a high β_p plasma operation, $\Delta(\beta_p + \ell_i/2)$ becomes unity. Then the inward shift of a plasma column is so large that the configuration moves easily from a divertor configuration to a conventional one. In this case, the plasma position can be regulated to a correct position and the divertor configuration is recovered during 20 msec by controlling vertical field.

In order to reduce the time averaged heat flux density on the divertor plate or to change neutral particle conductance between the divertor and the main chamber, the separatrix magnetic surface can be moved from $\delta_t = 2$ cm to $\delta_t = 6$ cm or from $x_p = -9$ cm to $x_p = +8$ cm during 70 ms. If we take into account a finite width of the scrape-off layer, this scanning range has to be limited. For this reason, a direct measurement of heat flux profile onto the divertor plate will be done by using infrared cameras from the initial phase of experiment and the heat flux profile will be directly controlled in the heating experiment.

9.3 Plasma consideration

Ripple transport of confined banana particles in a very low collisionality regime.

Goldstone, White and Boozer have theoretically found a limit on field ripple for particles with large banana size[1], which is approximately given by

$$\delta_c = \frac{1}{(N_t \pi q/\varepsilon)^{3/2} \rho q'} , \tag{1}$$

where ρ is the gyroradius, ε the inverse aspect ratio, q the safety factor and $q' = dq/dr$. The particle whose banana tip is in the region

$$\delta > \delta_c \tag{2}$$

is predicted to be lost in a very short time because of collisionless stochastic orbits. The diffusion coefficient of banana particles in the region $\delta > \delta_c$ is given by the ripple-plateau diffusion, that is,

$$D^{RP} \sim \frac{(\Delta r_m)^2}{\tau_b} \tag{3}$$

where Δr_m is the radial displacement described by[1]

$$\Delta r_m = (N_t \pi / \sin\theta_b)^{1/2} (q/\varepsilon)^{3/2} \rho \delta , \tag{4}$$

with θ_b the poloidal angle of the banana tip.

In a large tokamak with low field ripple or with high plasma current, most of banana particles are in the region $\delta < \delta_c$ (non-ergodic). Therefore, the ripple transport of those confined banana particles becomes very important for the high energy (large banana size) particle confinement. Here, we show the diffusion coefficient D^{CB} for non-ergodic banana particles (confined banana particles) in Fig. X.9-5. The diffusion coefficient is defined as

$$D^{CB} = \frac{1}{2} \frac{d}{dt} \left[\sum_i (r_i - \langle r \rangle) \, w_i / \sum_i w_i \right] ,$$

where

$$\langle r \rangle = \sum_i r_i w_i / \sum_i w_i \ ,$$

r_i is the radial position of the i^{th} test particle and w_i the particle density weight. It is found that D^{CB} in this region is proportional to the ion collision frequency ν_i and is in the order of 10^{-1} m^2/s which is about 10 ∿ 100 times larger than the axisymmetric neoclassical transport coefficient D^{NC}, but much less than D^{RP}.

The pitch-angle change corresponding to the reduction of toroidal angle $\Delta_\phi = \pi/N_t$ of a banana tip can approximately be written as

$$\Delta\zeta_\phi \sim \frac{r\sin\theta_b}{R_t + r} \frac{\pi}{N_t q} \frac{1}{\sin 2\zeta} \tag{5}$$

and the effective collision frequency is given by

$$\nu_{eff} = [\pi/(2\Delta\zeta_\phi)]^2 \nu_i . \tag{6}$$

Then the diffusion coefficient for confined banana particles is roughly given by

$$D^{CB} \sim (2\Delta r_m)^2 \nu_{eff}$$

$$\sim \pi (N_t/\sin\theta_b)^3 (q/\varepsilon)^5 \sin^2 2\zeta (\rho\delta)^2 \nu_i \ . \tag{7}$$

The solid line in Fig. X.9-5 is the diffusion coefficient calculated by the above expression. The analytical diffusion coefficient agrees well with the numerical one. It should be noted that D^{CB} has a very strong dependence on (q/ε). The numerically derived diffusion coefficients are shown in Fig. X.9-6 as a function of the safety factor q_a. These values agree well with the analytical D^{CB} of eq. (7) (the soild line in Fig. X.9-6). This dependence of D^{CB} on q indicates that the plasma current is a very important parameter for the containment of charged fusion products.

Reference

1) R.J. Goldstone, R.B. White, A.H. Boozer: Phys. Rev. Lett. 47 (1981) 647.

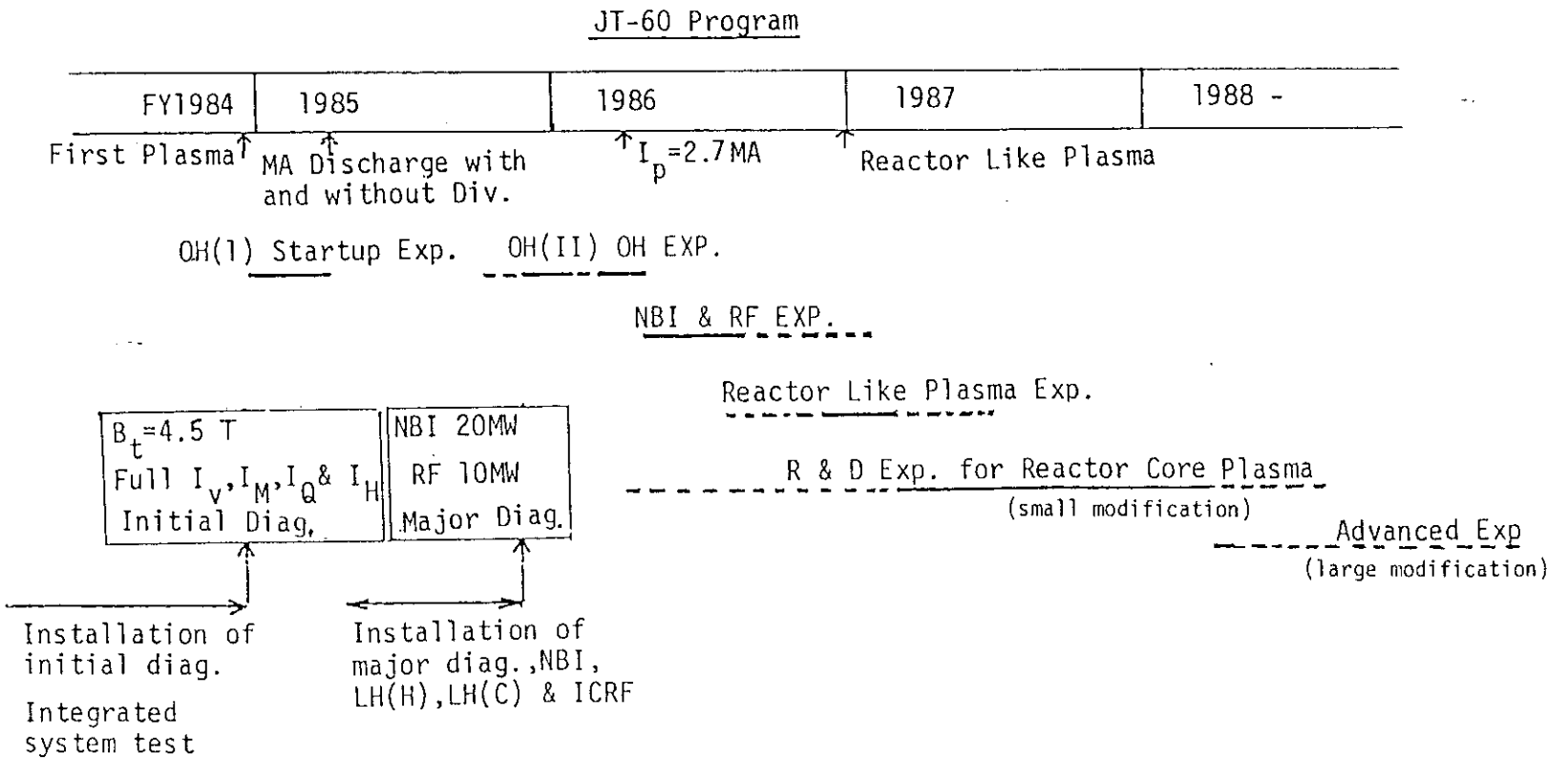

Fig. X.9-1 Experimental program and schedule of JT-60.

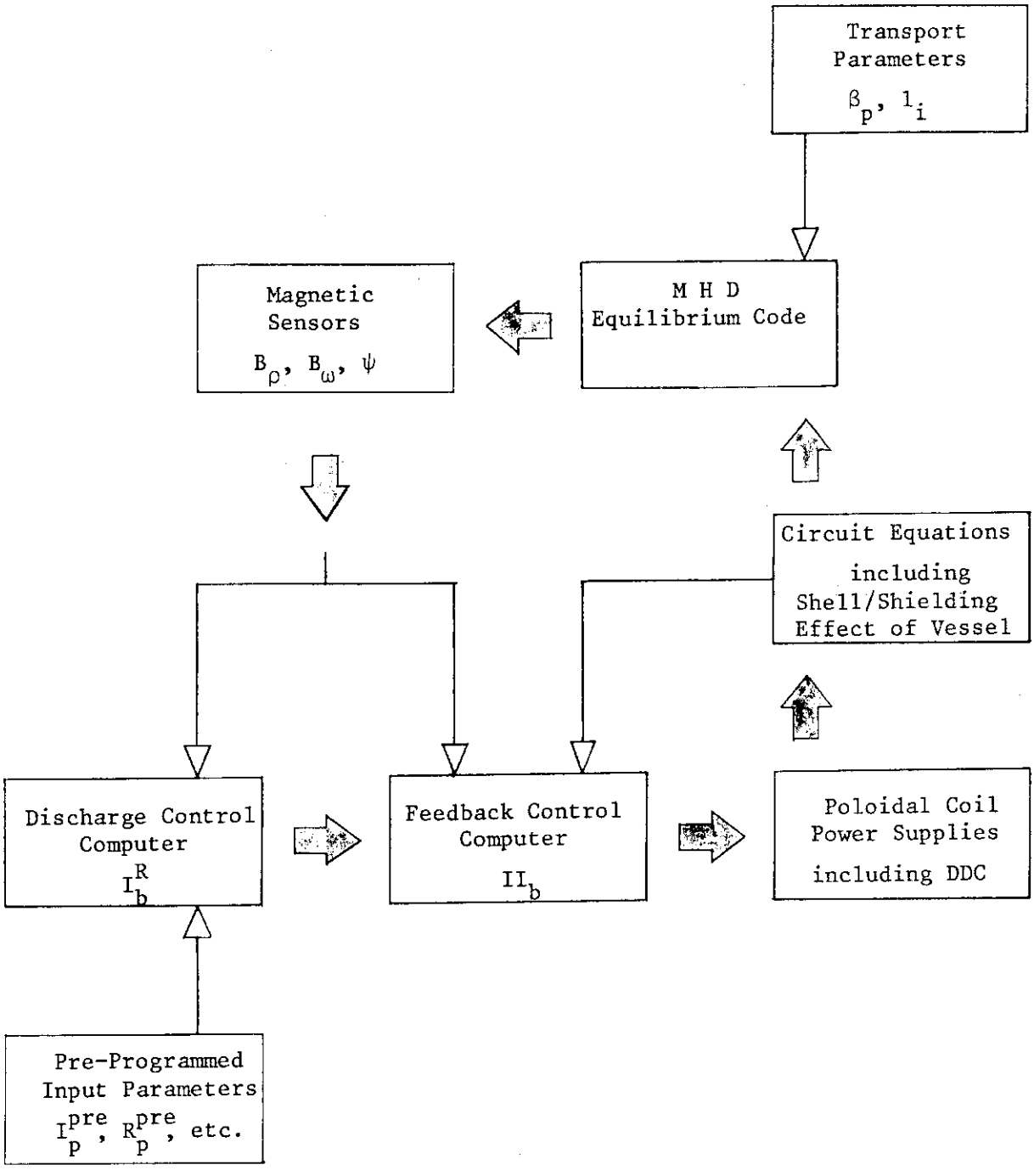

Fig. X.9-2 Main flow of dynamic simulation code.

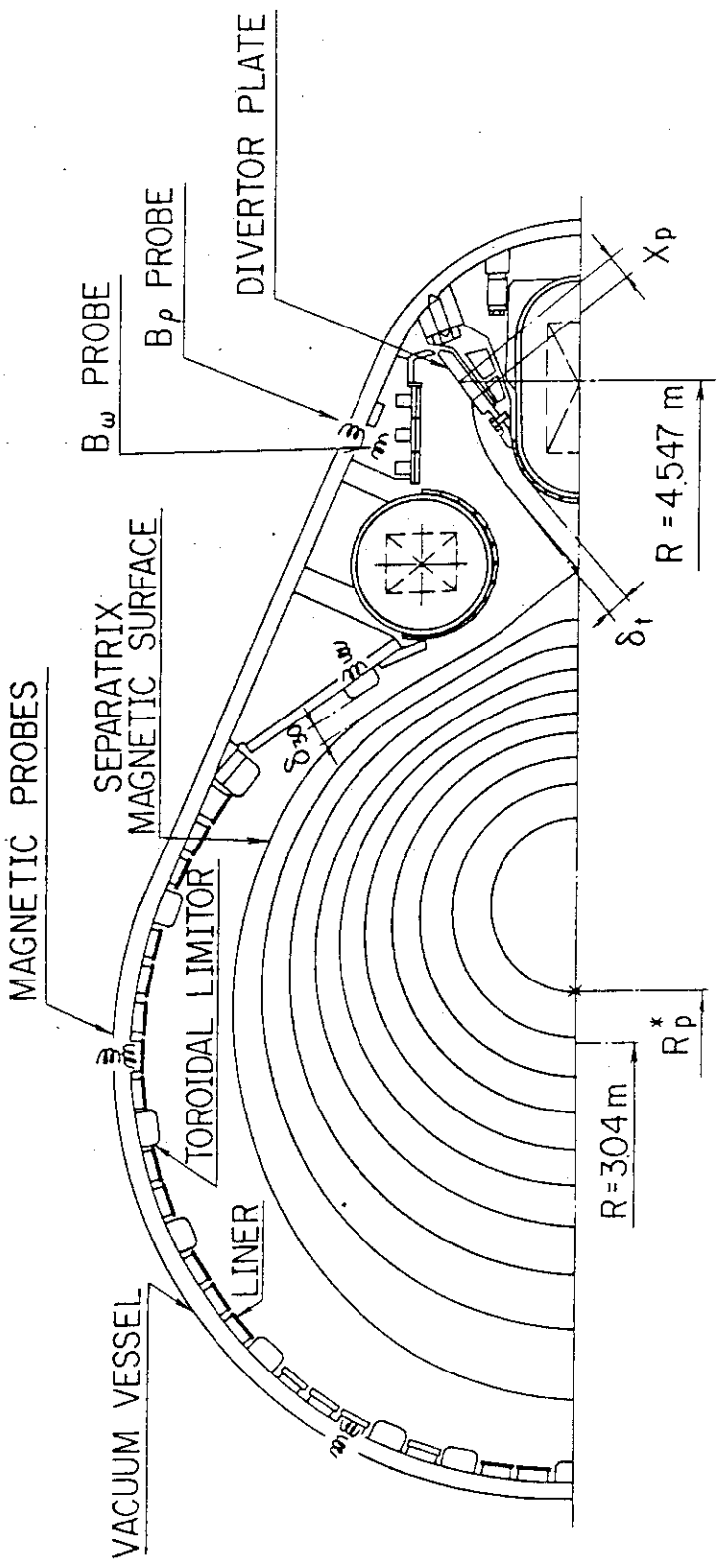

Fig. X.9-3 Cross sectional view of JT-60 vacuum vessel.
R_p^* : plasma center position
δ_{30} : the minimum clearance between separatrix magnetic surface and toroidal limiters
δ_t : clearance between separatrix magnetic surface and main divertor coil
x_p : position of separatrix magnetic surface on divertor plate

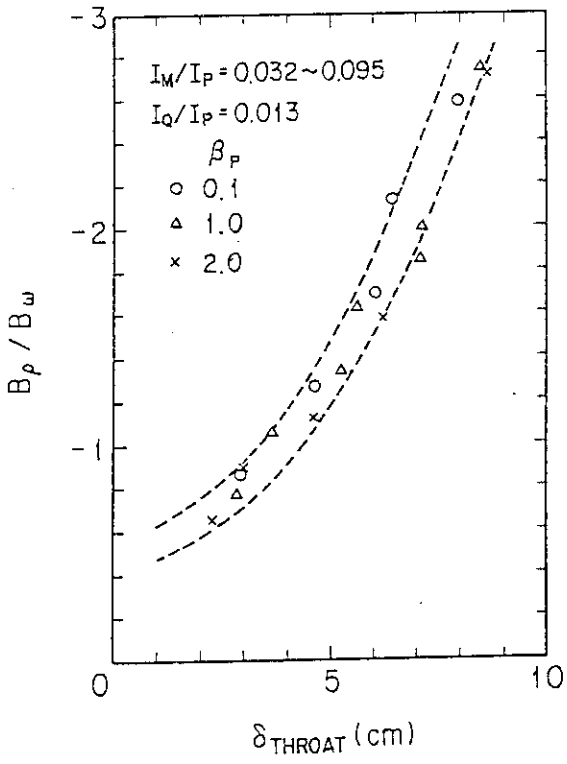

Fig. X.9-4
δ_t vs. B_ρ/B_ω in a wide range of discharge condition.
δ_t : clearance between separatrix magnetic surface and main divertor coil (see Fig. X.9-3)
B_ρ/B_ω : magnetic field direction in divertor chamber
I_p, I_M and I_Q : plasma current, main divertor coil current and quadrupole field coil current, respectively

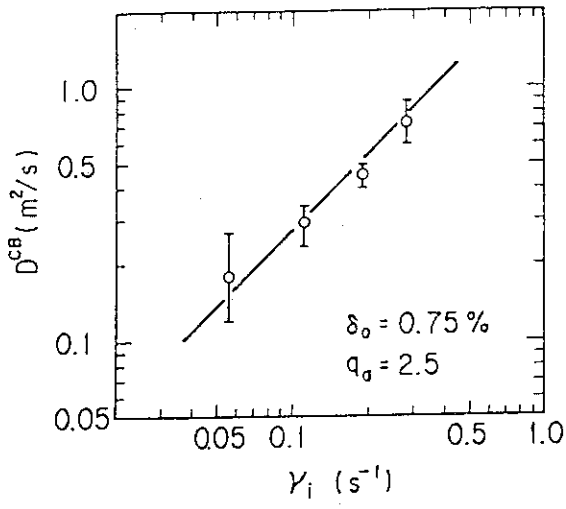

Fig. X.9-5
Diffusion coefficient D^{CB} versus collisionality for confined banana-trapped alpha particles with $E \sim 3.5 MeV$ at r/a=0.6. Field ripple δ_0=0.75%, safety factor q_a=2.5.

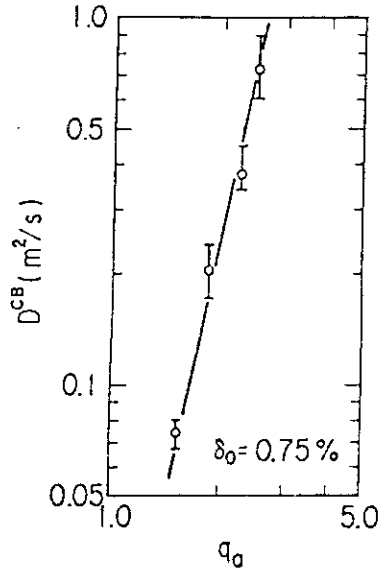

Fig. X.9-6
Diffusion coefficient D^{CB} versus safety factor q_a for confined banana-trapped alpha particles with $E \sim 3.5 MeV$ at r/a=0.6. The field ripple δ_0= 0.75%, collision frequency $\nu_i \sim 0.3\ s^{-1}$.

10. JT-60 Operation Program

The basic scheme of operation and maintenance was investigated succeeding to the efforts made in FY 1981. The standard cycle of JT-60 operation was set as a period of two weeks. A yearly plan of JT-60 operation is shown in Fig. X.10-1. Manpower and budget required for operation and maintenance were estimated based on this JT-60 yearly plan.

JT-60 is composed of a large number of equipments. They are operated selectively in accordance with experiment. A computer code was developed which can draw the operation schedule of selected equipments for one cycle operation of JT-60.

Preparation of JT-60 operation manuals was started in 1982 which would be used and revised in operation training during the performance test. These operation manuals will be completed in March 1985.

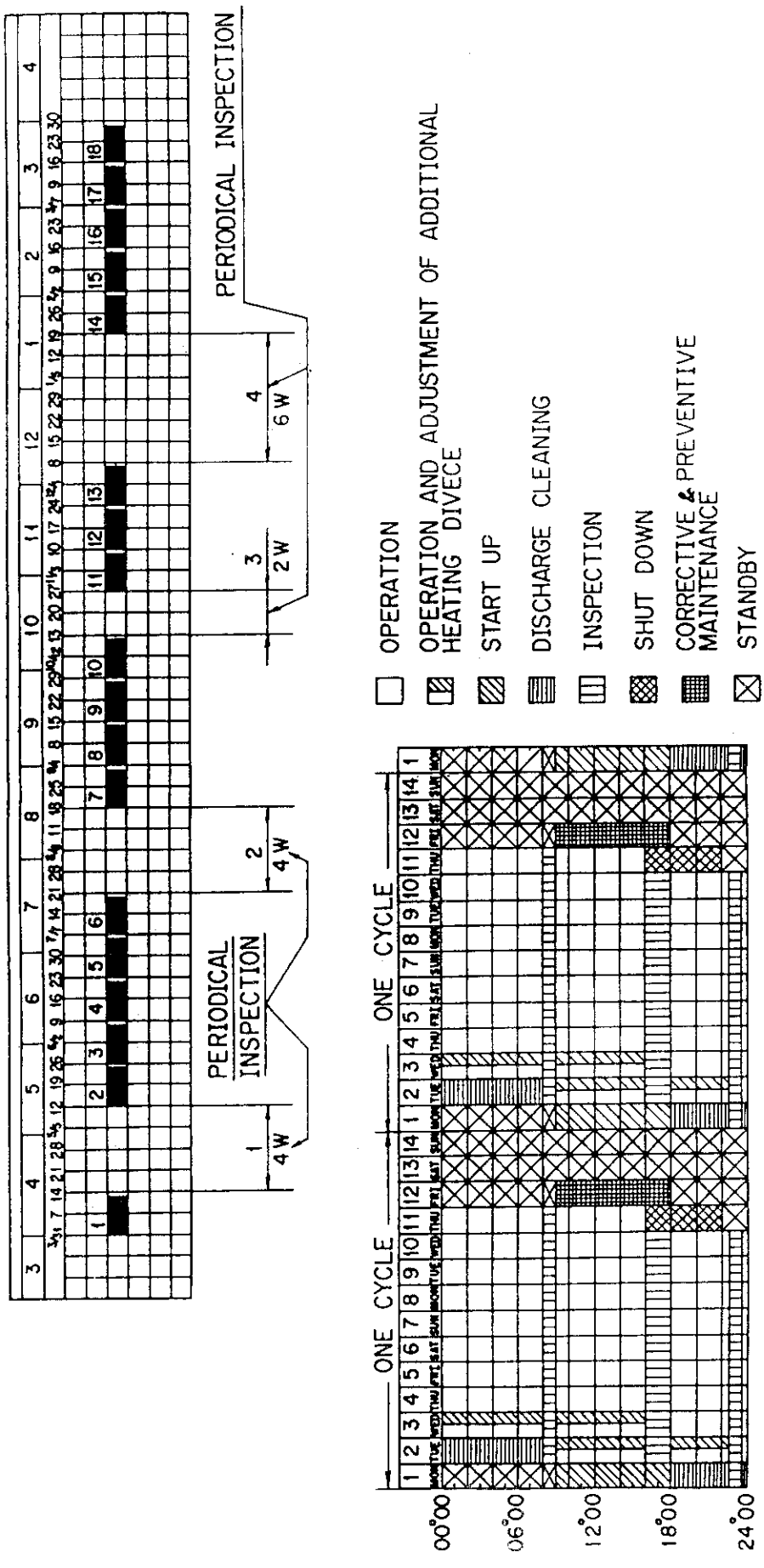

Fig. X.10-1 Yearly operation plan of JT-60.

XI. DESIGN STUDY OF THE NEXT GENERATION DEVICE

1. Fusion Experimental Reactor (FER)

1.1 Introduction

Conceptual design studies of the Fusion Experimental Reactor (FER)[1,2] have been performed at JAERI in line with a long-range plan for fusion reactor development laid out in the new long-term program of the Atomic Energy Commission issued in June 1982. The FER is an experimental tokamak reactor succeeding the large tokamak device JT-60 with a major mission of realizing ignited DT plasma and demonstrating engineering feasibility of fusion reactors including tritium breeding. The objectives and characteristics of the FER have been identified by the Review Subcommittee of Long-Term Strategy established under the Nuclear Rusion Council of the Atomic Energy Commission. The design of FER is conducted under the following guidelines: (1) to reach a DT ignition with a rather moderate neutron wall loading, (2) to obtain a breeding ratio of above unity and (3) to be designed with cost/benefit considrations.

The reference design of the FER is based on a D-shaped tokamak plasma with a double-null divertor. The major design parameters are listed in Table XI.1-1. The heating is provided by neutral beam injection (BNI) and radiofrequency (RF) heating. The superconducting coil system with the poloidal coils placed external to the toroidal coils is enclosed in a semipermanent common cryostat vacuum chamber (belljar type). Plasma parameters were determined by optimization studies with plausible plasma-physics and engineering restrictions such as confinement scaling, beta limit, divertor configuration and maximum magnetic fields on superconducting magnet. Priority is given to the divertor concept for impurity control and ash exhaust in view of its credible physics data base. A double-null divertor configuration is employed to reduce the major reactor radius and also to improve the coupling between OH coils and the plasma, since it will have a thinner scrape-off layer at the inboard plasma surface than a single-null divertor. Tritium breeding blanket, with Li_2O as breeding material, is installed all around the plasma and at the back side of divertor chambers to enhanced breeding ratio.

Three torus structure reference design options (A,B,C) are being developed to evaluate their configuration and design impacts when considering requirements of shield structure, space reduction, plasma vacuum boundary and assembly/disassembly. Figure XI.1-1 shows the vertical view of the FER for option A in which the outboard shield is separated into a TF coil shield and biological shield, and the plasma vacuum chamber and the superconducting coil system cryostat chamber form a common boundary in the inboard, top and bottom areas. For option B, the shield is divided into a semipermanent inboard shield and removable outboard sheild, the plasma vacuum boundary is installed at the permanent shield and the access door (based on the INTOR-J concept[3]). The shield of option C is integrated with the cryostat and the location of the plasma vacuum boundary is similar to that of option B.

In parallel with the reference design studies have been initiated to evaluate advanced reactor concepts such as pumped limiter and RF current drive, and comparative studies for single-null divertor/pumped limiter.

Table XI.1-1 Major Design Parameters.

Power	
Fusion power(MW)	440
Average neutron wall loading (MW/m^2)	1.0
Operation	
Burn time(s)	100
Duty factor(%)	50 ∿ 70
Availability(%)	25 ∿ 50
Neutron fluence ($MW \cdot y/m^2$)	3
Plasma	
Major radius(m)	5.5
Plasma radius(m)	1.1
Plasma elongation	1.5
Burn average beta(total)(%)	4
Plasma current(MA)	5.3
Safety facotr(q_ψ)	2.5
Average ion temperature(keV)	10
Average ion density(m^{-3})	1.4×10^{20}
Energy confinement time(s)	1.4
Toroidal field on plasma axis(T)	5.7
Divertor Plates	
Total energy(MW)	40
Particles(s^{-1})	1.4×10^{24}
Temperature near plate(eV)	30
Average energy of ions(eV)	135
Ratio of heat to outer to inner	4
Heating	
NBI/RF power(MW)	30/30
Plasma Disruption	
Disruption number	1000
Total Energy deposition(MJ)	180
Energy to first wall(MJ)	120
Energy to divertor(MJ)	60
Time constant for energy deposition to divertor/ first wall(ms)	5/15
Current decay constant(ms)	15
First wall/Blanket	
Surface heat flux(W/cm^2)	12
Nuclear heating rate(W/cc)	10
Structural material	316 SS
Maximum temperature(°C)	350
Breeding material	Li_2O
Breeding temperature(°C)	400 ∿ 1000
Tritium breeding ratio	1.05
Coolant	H_2O
Toroidal Field Coils(TFC)	
Number	14
Conductor	Nb_3Sn, NbTi
Maximum field(T)	12
Poloidal Field Coils(PFC)	
Location	external to TFC
Conductor	NbTi
Maximum field(T)	8

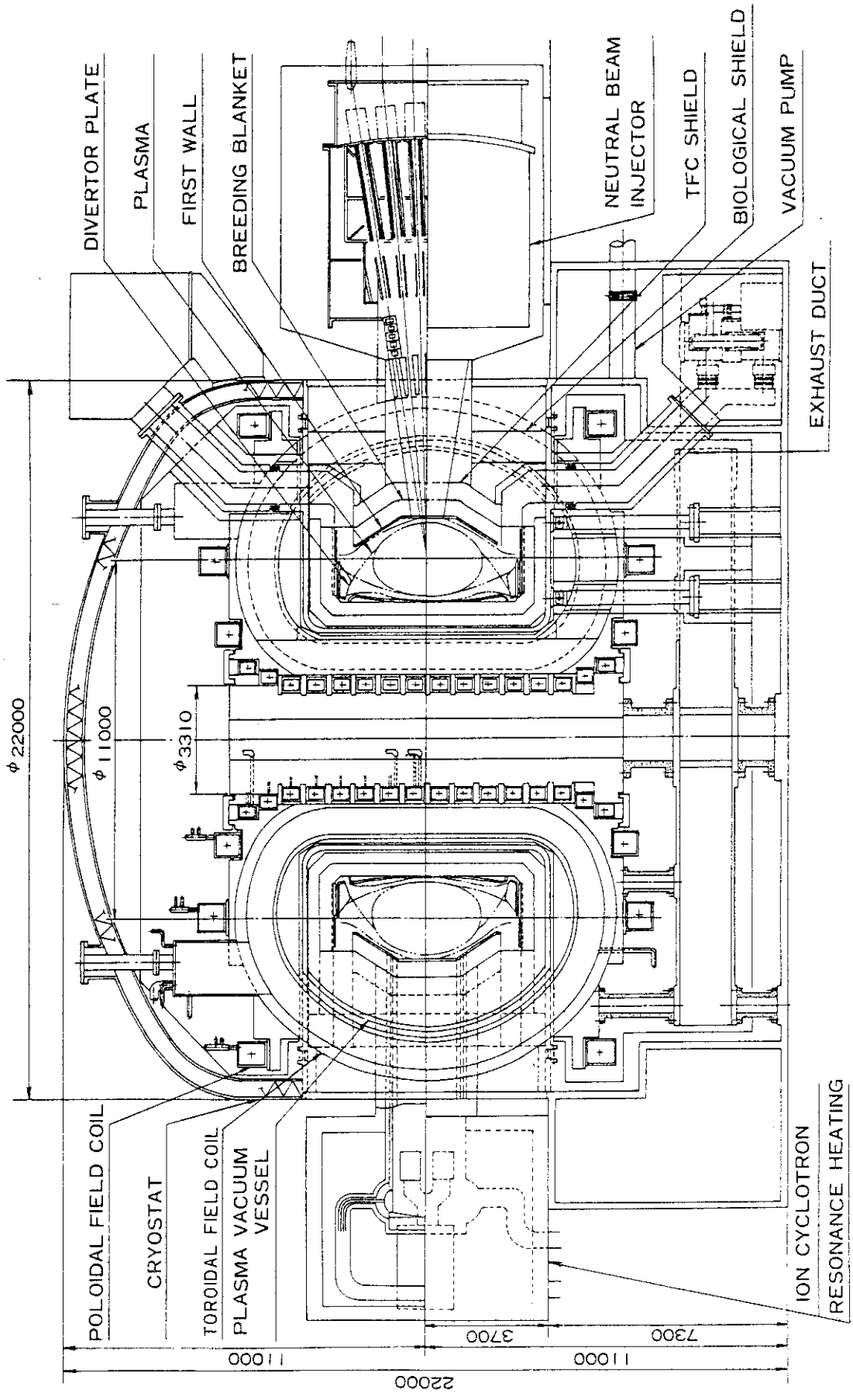

Fig. XI.1-1 Fusion Experimental Reactor (Double-Null Divertor).

1.2 Plasma design

The major plasma parameters shown in Table XI.1-1 are the same as the previous year, since no big changes in data base emerged in the reporting year. Some changes were observed in the plasma confinement performance, i.e. confinement time and beta value. The high beta results of 4.5 % obtained in Doublet III elongated plasmas consolidate the data base of tokamak plasma, and the so-called H-modes obtained diverted discharges improve the confinement time deteriorated by the NBI heating of MW level. Those changes, however, are not so remarkable to reconsider the FER plasma parameters, and they rather approach the expected one. Considerable improvements have been made in a noninductive current drive using radio frequency waves, particularly lower hybrid resonance range of frequency. The FER with the current drive concept was preliminarily designed as an advanced option.

Small changes in plasma specification are in a disruption scenario and divertor plasma parameters. New parameters of the divertor plasma reflect recent results of both divertor experiments and improved theoretical analyses, i.e., high-density and low-temperature plasmas in front of the divertor plates. The change in the disruption scenario also reflects the recent observations of disruptions. During the initial stage of the disruption before inward movement of the plasma column, around a half of the plasma kinetic energy is specified to flow into the divertor/limiter plates.

Major studies on the plasma design have been concentrated on impurity control, plasma vertical control, and plasma design adopting the RF current drive.

Both of the divertor and the pump limiter have been studied in parallel as plausible candidates for impurity control and helium ash exhaust in FER. The overall assessment on the limiter, including physics and engineering, has been performed, e.g. scrape-off plasma parameters realized in the limiter plasma, the necessary pumping speed, heat and particle fluxes onto the limiter plate, the desirable limiter shape, and the limiter life. The major results are as follows: (1) the electron temperature in the scrape-off layer decays rather rapidly with the typical decay length of about 2 cm, while the density distribution is fairly broad, (2) This long density decay length ease the pumping requirement and the pumping speed less than 1×10^5 ℓ/s could be enough to keep

the helium accumulation less than 5 % in the plasma, (3) The electron temperature at the separatrix is rather high, 400 - 500 eV, even with a gas-puffing fueling, and the high temperature operation regime (700 - 900 eV) could be realized by large pumping and ideal pellet injection, (4) limiter materials are limited to low-Z, and the life time of the limiter plate could become very short, e.g. half a year.

The divertor plasma analysis code has been developed. The scrape-off plasmas are described by the particle, momentum and energy balance equations along the magnetic field line. The neutral particle behavior is calculated by the Monte Carlo method. The self-consistent solution can be obtained by the iterative procedure between the scrape-off plasma and the neutral particles. The code is found to explain fairly well the experimental results such as Doublet III, i.e. high-density and low-temperature plasmas in front of the plate. The typical results of the FER divertor plasma are shown in Fig. XI.1-2. The fairly low temperature in front of the plate is expected to ease some difficulties on the impurity control issue.

Studies on control of plasma vertical position, which is inherent in the strongly elongated plasma, have been progressed. The position control needs both of the passive shell structure for fast motions and the active control coils for slow motions. The former passive shell structure must satisfy following various requirements: (1) multi-divided structure ensuring maintenance and assembly, (2) not to deteriorate the breeding efficiency, (3) to be consistent with the disruption scenario, (4) to provide sufficient shell effect. The potential candidate for the shell structure is illustrated in Fig. XI.1-3, and further detailed studies should be necessary.

A continuous or quasi-steady operation of FER is desirable, and so the possibility of steady FER was studied as an alternative. The most realistic method for FER with a non-inductive current drive will be using the lower hybrid range of frequency wave, which demonstrated experimentally the current sustain, ramp-up, although it has difficulties in high density plasmas as of now. The following two scenarios were studied in detail; (1) Scenario I, in which the burn phase is the same as the reference, i.e., inductively, and the start-up and the intermediate between two consecutive burn phases are operated by the RF current drive, (2) Scenario II, operated completely by the RF.

The plasma and RF parameters optimized for minimizing the recharge

time of OH coils in the intermediate phase of Scenario I and for maximizing the energy multiplication factor in the burn phase of Scenario II are shown in Table XI.1-2.

Table XI.1-2 Plasma and RF parameters for advanced alternative FER option with non-inductive current drive.

Plasma and RF parameter	Scenario I	Scenario II
Av. Plasma Temp. (keV)	6	22
Av. Plasma density ($1/m^3$)	3.4×10^{18}	5.2×10^{19}
RF current (MA)	28.5	5.3
RF power (MW)	14	38
RF frequency (GHz)	3.8	13.2
RF refractive index	1.04 - 3.1	1.56 - 1.6
Recharge time (s/volt.s)	3.3	—
Q value (s)	—	4
Burn time (s)	1800	∞
Dwell time	300	—

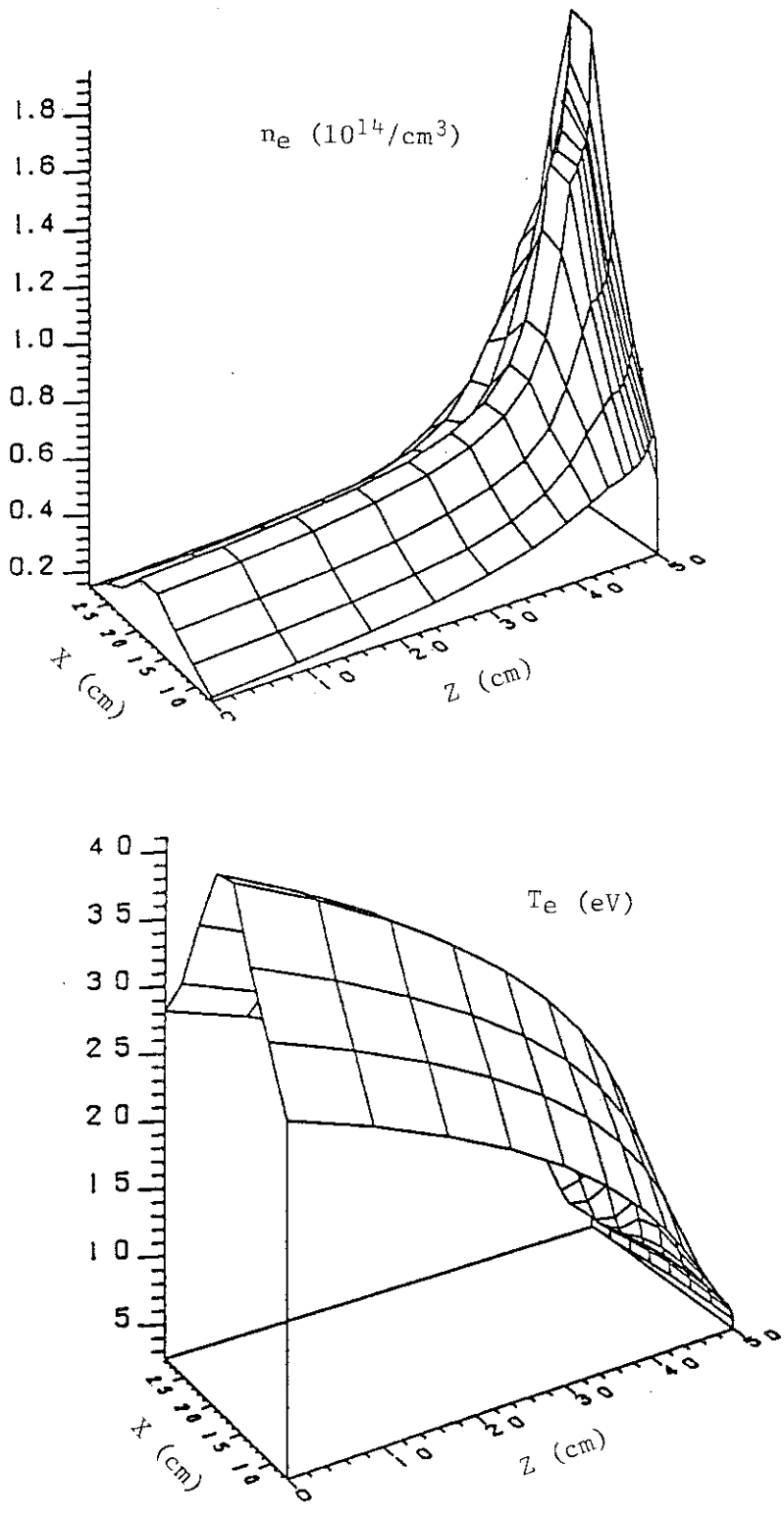

Fig. XI.1-2 Typical high density and low temperature divertor plasma for FER.

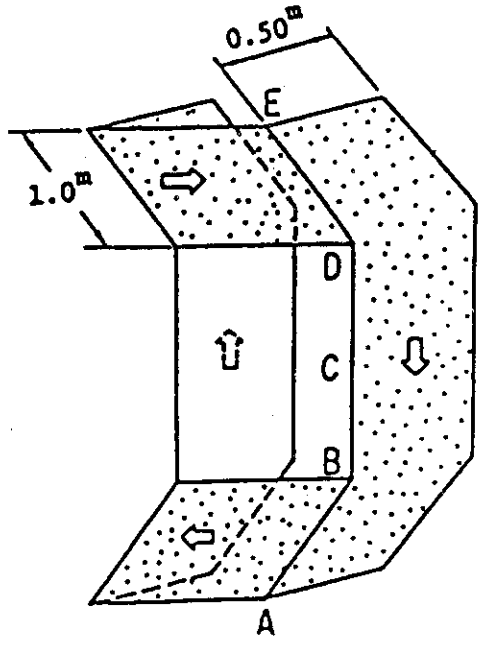

A (6.06m , － 1.77m) , B (6.60m , － 0.90m) ,

C (6.60m , 0.0m) , D (6.60m , 0.90m) ,

E (6.06m , 1.77m)

⇦ : Current Flow

Fig. XI.1-3 Structure of a new rectangular shell.

1.3 Engineering design

1.3.1 Torus structure

Design of the torus structure must provide for a sound support structure for all the reactor components, provide the proper vacuum topology, and allow a simple repair and maintenance scheme for the reactor modules. The torus structure of option A can be explained as follows with the help of Fig. XI.1-1.

The centering force of the TF coils is conveyed to a center column through support rings. Antitorque beams to support the overturning moment in the TF coils are placed at the upper and lower parts leaving all the openings between TF coils available for the maintenance procedure.

Both vacuum chambers for the plasma and the superconducting coil system (cryostat) have a common boundary except in the outer region where the access doors are located between TF coils. The major difference between the common vacuum boundary concept and the separate concept, in which the above chambers are installed independently, may appear in the bakeout capability, the tritium leakage from the plasma chamber into other regions (the cryostat and the reactor room) and most importantly the radial build of the torus.

The blanket-shield system consists of fourteen sectors which is the same number as the TF coils. Each sector is divided into three modules because of the limited space of the TF coils window. Construction of a sector is shown in Fig. XI.1-4. The three modules include a large central module of about 180 tons and two small side modules of about 60 tons each. They are connected to each other by key structures maintaining the necessary one-turn resistance by inserting ceramic coated metal multilayer sheets. For disassembly of the blanket-shield system, after cutting cooling tubes and lip welding for vacuum seal, the central module is extracted by single straight line motion and, the side module is initially rotated in the toroidal direction and then extracted by the same motion as the central module.

The upper and lower divertor systems are divided into 21 modules. Through a maintenance port located at the upper and lower regions on every other TF coil window (other windows are for pumping ducts), three modules (one central and two side) are extracted.

1.3.2 First wall and blanket

A configuration in which the first wall is integrated with the blanket is selected as a reference design. It leads to a simpler structure and higher tritium breeding ratio than the separated type. Figure XI.1-5 shows the cross sectional view of the first wall and blanket. The first wall is formed with a plate having rectangular shaped cooling channels in it. The thickness of the first wall should be determined so that the following requirements are satisfied.

1) The expected lifetime should be long enough to avoid scheduled replacement of the first wall and blanekt. The first wall will be eroded by about 6 - 9 mm during the reactor lifetime (depending on scrape-off plasma conditions) due to sputtering by neutrals. Evaporation caused by high heat flux accompanied with plasma disruption is not significant in our case.

2) Thermal stress due to temperature gradients in the first wall must be lower than the maximum allowable stress which is determined by thermal fatigue for $\sim 5 \times 10^5$ cycles. This problem can be eased if we employ grooved structure for the first wall. However, there is some concern about the first wall (blanket vessel) ridigity against the internal pressure (He purge gas pressure).

3) The thickness of the first wall should be thin enough to provide a tritium breeding ratio larger than unity.

After completing detailed two and three dimensional thermal stress analyses, an erosion rate evaluation and an extensive neutronics survey calculation for tritium breeding ratio were also performed. It is found to be rather difficult to satisfy all of the above requirements at the same time. We selected a reference design which satisfies only requirements 2 and 3. The first wall and blanket need to be replaced once during the FER lifetime.

The cooling system of the blanket is designed under the restriction that the temperature of the breeding material (Li_2O) be controlled within the range of 400 - 1000 °C. The minimum temperature can be kept high enough by the thermal resistance between cooling tubes and sleeves around them. Although the design is made assuming 0.5 of duty factor, sound temperature control is attainable even when the duty factor increases up

to 0.75. Table XI.1-3 shows the maximum and minimum temperatures of breeding material in four cases of reactor operating scenario.

Another requirement for the first wall and blanket is to provide a shell effect in order to control plasma position passively. A few structural concepts are now investigated. We show here one of the concepts in which the conducting shell consists of a lead layer in the front part and copper plates on the side wall of the outer blanket vessel. In this conducting shell, which provides about 20 msec of plasma vertical positional instability growth rate, large electromagnetic forces are caused by the plasma disruption. The maximum electromagnetic force is estimated to be 35 kg/cm^2 which appears on the side wall of the outer blanket. The stress in the first wall and blanket vessel caused by this force is evaluated using the NASTRAN code. The maximum stress appears on the inboard side first wall and is estimated to be 20 kg/mm^2 (membrane + bending). Since this value is marginal, further detailed analysis is required.

1.3.3 Neutronics

Net tritium breeding ratio greater than 1.05 has been obtained with the use of 5 cm Pb multiplier zone in front of the Li_2O blanket. The enrichment of ^6Li was 30 %. The impact of the blanket material heterogeneity effect on tritium breeding ratio was found to be small enough by two-dimensional calculations.

Bulk shielding design is conducted to protect the superconducting TF coils from radiation damage and nuclear heating. The dose rate distribution around a TF coil for the option C design one day after shutdown following 2 years of continuous operation is shown in Fig. XI.1-6. The neutron streaming effect through the insulator zone in TF coil prohibits personnel access to the reactor. Additional shield or some change in the design of the insulator zone is necessary.

References

1) Tomabechi, K., et al.: "Concept of the Next Tokamak", Proc. 3rd IAEA Technical Committee Meeting and Workshop on Fusion Reactor Design and Technology, Tokyo, Oct. 5 - 16, 1981, II-5 (in press).
2) Tone, T., et al.: "Conceptual Design of Fusion Experimental Reactor (FER)", Nuclear Technology/Fusion, Vol.4, No.2, Part 2, 573 (1983).

3) National (Japanese) Reports for INTOR Phase II-A, JAERI-M 82 - 170 ∿ 82 - 179 (1982).

Table XI.1-3 Maximum and minimum temperature of breeding material (Li_2O)

case	t(sec) -burn-	t(sec) -dwell-	duty factor	T(°C) max.	T(°C) min.
1	100	100	0.50	741	490
2	200	100	0.67	918	592
3	300	100	0.75	992	635
4	100	50	0.67	863	652

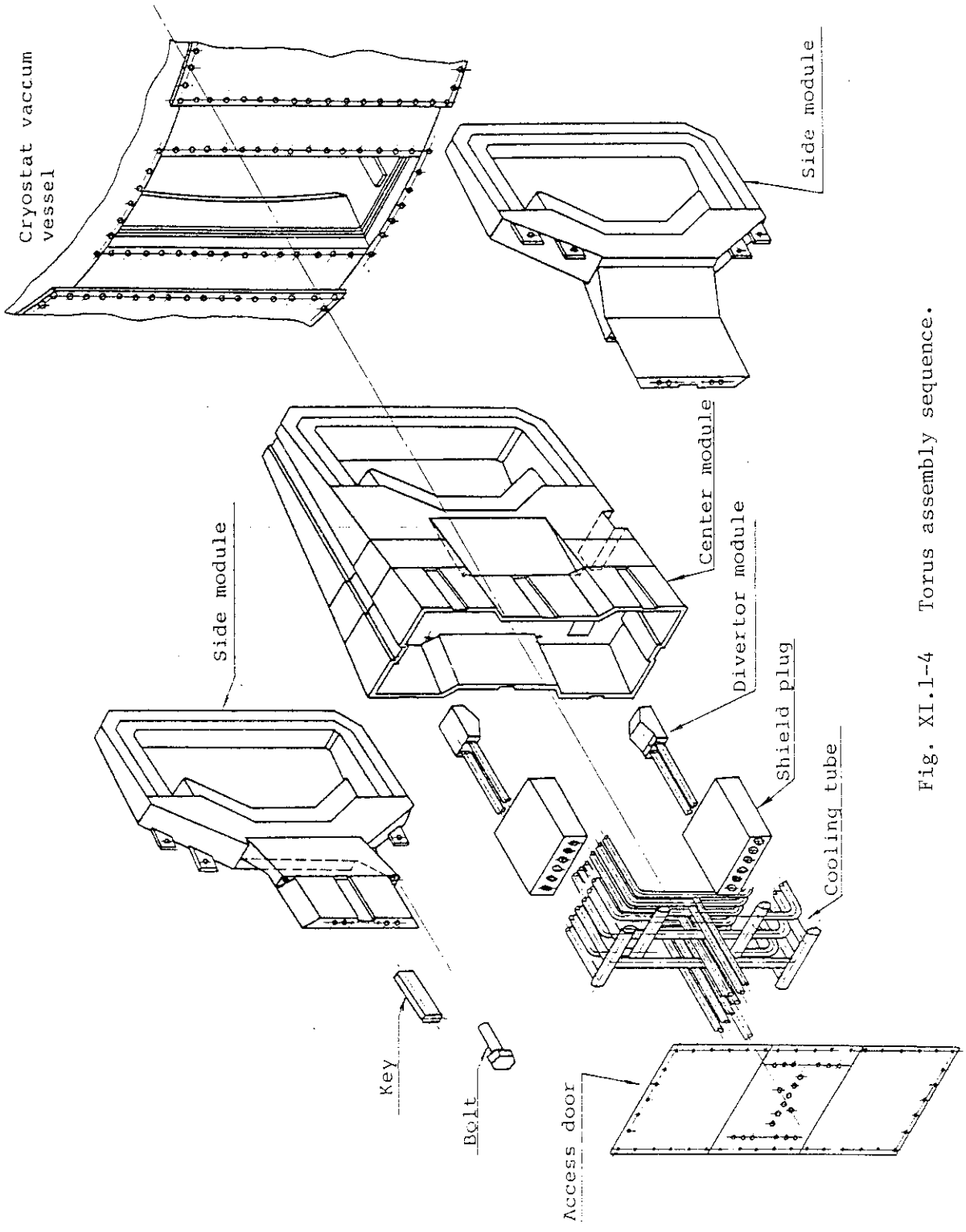

Fig. XI.1-4 Torus assembly sequence.

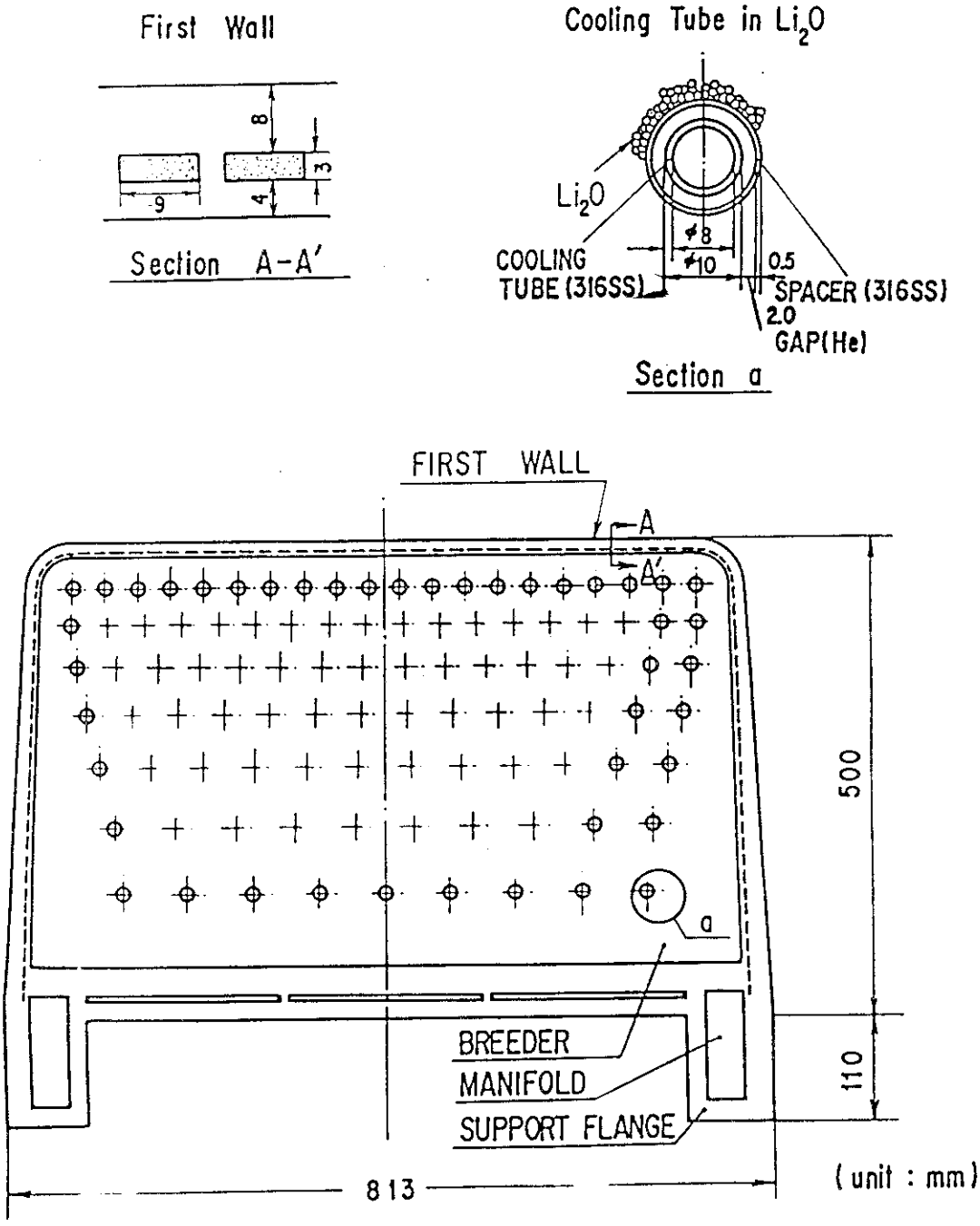

Fig. XI.1-5 First wall and tritium breeding blanket.

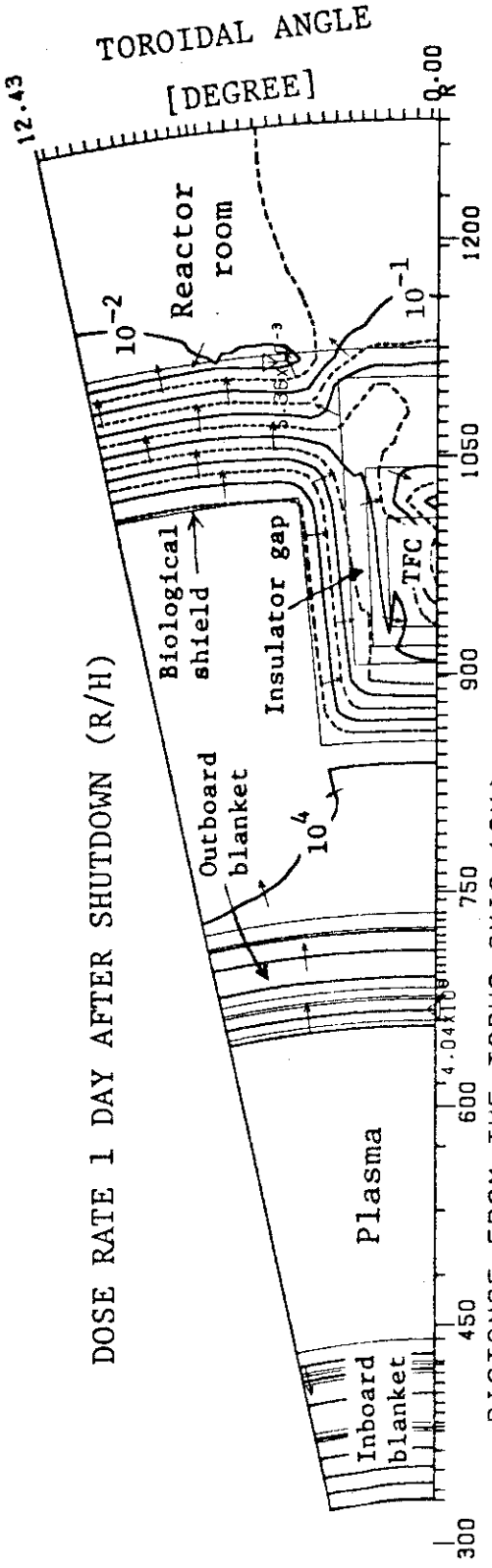

Fig. XI.1-6 Dose rate distribution around the reactor 1 day after shutdown (R/h).

2. INTOR

INTOR activity corresponding to INTOR Workshop of Phase 2A, Part 1 was continued. The major objective of this phase is that the major critical issues identified in the conceptual design during Phase 1 were concentratively assessed aiming size-minimization and high efficiency of the reactor. The studies on them have been almost finished, and the Japanese contributions to INTOR Phase 2A-1, which support the report of INTOR to be published from IAEA, were compiled. The major parameters are shown in Table XI.2-1 and its cross section is illustrated in Fig. XI.2-1. The major results of assessment are as follows.

(1) The RF (Ion Cycrotron Range of Frequency) heating is adopted as a reference instead of the NBI heating, which was chosen for the conceptual design of Phase 1. This choice needs the strong promotion for the RF heating research and development, and also expects a steady improvement on the NBI heating as a back-up option.

(2) The divertor concept is decided to be continued as a reference for impurity control, from concentrative comparative studies between the divertor and pump limiter. High density and low temperature divertor plasmas, which were demonstrated in the recent divertor experiments and are intensively analyzed theoretically, could ease engineering difficulties on the divertor plates. On the other hand, the limiter, which is a strong candidate in future tokamak reactors, has some difficulties in temperatures of scrape-off plasmas and limiter materials. The research and development on the limiter should be continued in parallel with the divertor.

(3) The breeding blankets employing lithium oxide were designed as a reference.

(4) The bore of the toroidal coils is reduced by 15 % in their area compared with the conceptual design of Phase 1. This induces the reduction of the power supply for the poloidal coil system. Those reductions result in major factors cutting down the capital cost. The reduction in size of the toroidal coils is realized by inceasing toroidal field ripple up to 1.2 %, which enhances the

loss of alpha-particle up to around 10 %.

(5) A universal design concept, which can accomodate the divertor or the limiter as shown in Fig. XI.2-1, is adopted for future critical issues studies in the INTOR workshop.

(6) The cost sensitivity analysis is performed changing major parameters such as toroidal field ripple, heating method (NBI → RF), impurity control (divertor → limiter), and so forth, from a reference of the conceptual design. It is found that the capital cost is reduced by 20 % by employing the reduced toroidal coils and the RF heating, and it seems that the major objective of the Phase 2A-1 has been accomplished.

The INTOR Workshop will be continued the same way as the Phase 2A-1, and the major critical issues, such as RF heating and current drive, impurity control, transient electromagnetic analysis, maintenance and so on, will be concentratively assessed aiming reasonable and efficient INTOR during the Phase 2A-2 in two years.

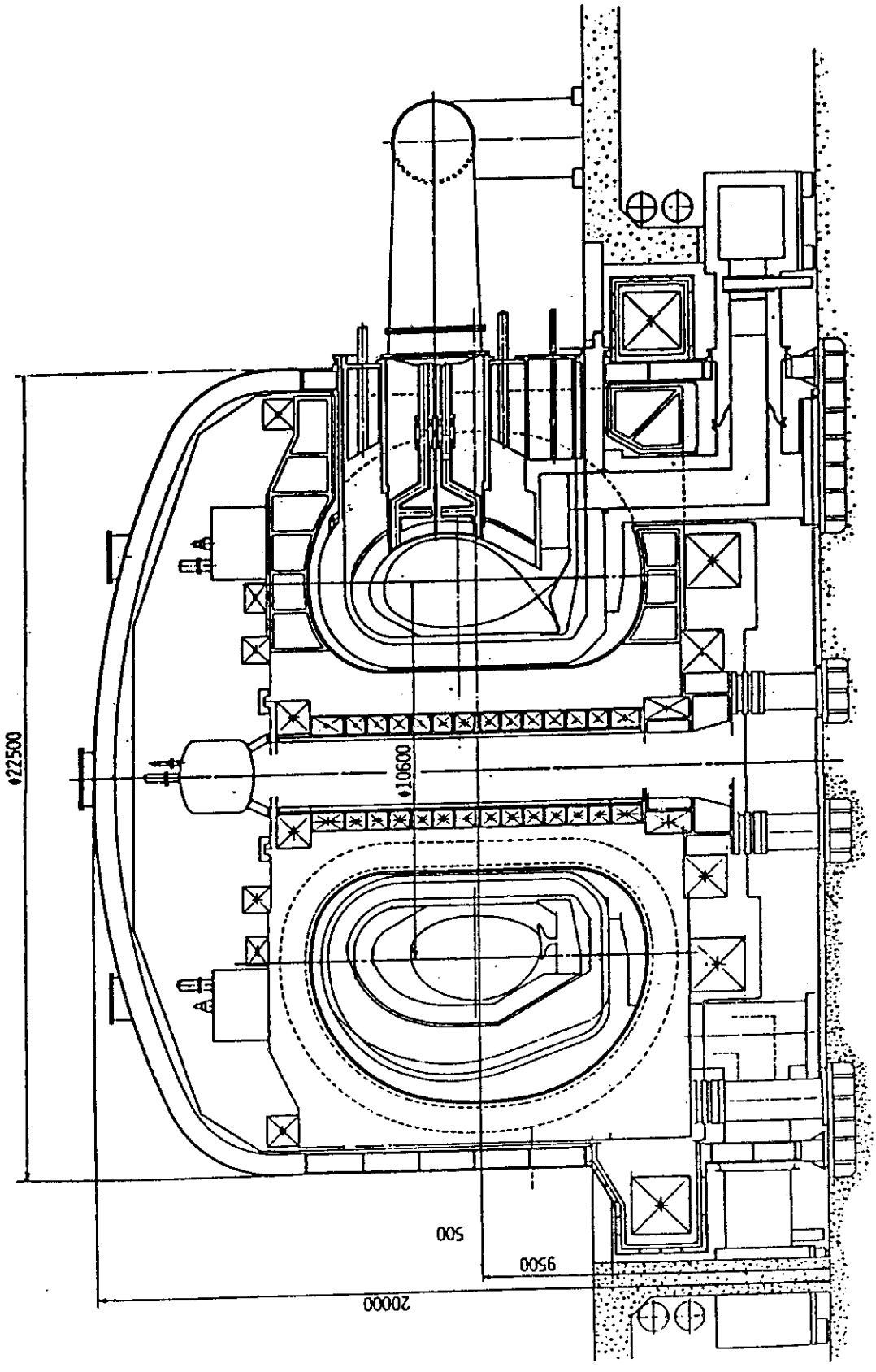

Fig. XI.2-1 INTOR universal configuration.

Table XI.2-1 Major deisgn parameters of INTOR

Plasma major radius (m)	5.3
Plasma minor radius (m)	1.2
Plasma elongation	1.6
Plasma volume (m^3)	240
Axial toroidal field (T)	5.5
Plasma current (MA)	6.4
Average ion temperature (keV)	10
Average ion density ($10^{20}/m^3$)	1.4
Energy confinement time (sec)	1.4
Average beta (%)	5.6
Q value	ignition
Peak fusion power (MW)	620
RF heating power (MW)	
ICRF (85 MHz)	60
ECRF (140 GHz)	10
Burn time (sec)	200
Duty cycle (%)/Availability (%)	80/50
Neutron wall load (MW/m^2)	1.3
Toroidal magnetic field coil	superconducting
Poloidal magnetic field coil	superconducting
Divertor	yes
Tritium consumption (kg/year)	7
Initial tritium inventory (kg)	~4
Tritium breeding ratio	0.65

APPENDIXES

A.1 Publication List

A.1.1 List of JAERI-M Reports

1) Tokuda S., Itoh K., Tuda T., Itoh S-I.[**1] : Matrix Method for Kinetic Ballooning Mode", JAERI-M 82-080.

2) Kurita G. : "MHD Stability Analyses of a Tokamak Plasma by Time-dependent Codes", JAERI-M 82-093.

3) Takeda T., Tsunematsu T., Kurita G. : "Preprocessor System EOS for a Variable-array-size Program", JAERI-M 82-097.

4) Tuda T., Azumi M., Kurita G., Takizuka T., Takeda T. : "Scaling of Critical Beta in a Tokamak", JAERI-M 82-104.

5) Tuda T., Itoh K., Itoh S-I.[**1] : "Destruction of Magnetic Surfaces by High-n Ballooning Mode", JAERI-M 82-113.

6) Kimura K., Matsumoto H., Odajima K., Konoshima S., Suzuki N., Yamamoto T., Hoshino K., Miura Y., Matsuda T., Takeuchi H. : "Experimental Results on ICRF Heating in JFT-2", JAERI-M 82-46 (May, 1982).

7) Nakamura N., Sengoku S., Maeno M., Yamamoto S., Seki M., Kazawa M. : "Development of TiC and TiN Coated Molybdenum Limiter System and Initial Results of the Thermal Testing in Neutral Beam Heated JFT-2 Tokamak", JAERI-M 82-065 (June, 1982).

8) Sone K., Maeno M., Yamamoto S., Ohtsuka H., Abe T. : "Surface Material Consideration for Fusion Reactors", JAERI-M 82-171 (November, 1982).

9) Miyamoto K.[**5], Sugihara M., Ueda K., Yamamoto S., Maeno M., Sengoku S., Suzuki N., Kasai S., Nagami M., Tsuda T., Tani K., Okamoto M., Fujisawa N. : "Japanese Contribution to IAEA INTOR Workshop, Phase IIA Chapter IV Plasma Confinement and Control JAERI-M 82-171 (November, 1982).

10) Miyamoto K.[**5], Sugihara M., Kimura H., Matsumoto H., Odajima K., Imai T., Fukuyama A.[**3], Okamoto M., Nagashima T., Yamamoto T., Ohno T.[*2], Kobayashi N.[*2], Uchida T.[*2], Ohmori T.[*2], Sawada T.[*2], Ebisawa K.[*2], Uchida K.[*2], Yamauchi M.[*2], Fujisawa N. : "Japanese Contribution to IAEA INTOR Workshop, Phase IIA, Chapter V: RF Heating and Current Drive", JAERI-M 82-172 (November, 1982).

11) Sengoku S., Shimada M., Miya N., Kasai M.[*3], Aikawa H., Azumi M., Hoshino K. : "Observation of Very Dense and Cold Divertor Plasma in

Beam Heated Doublet III Tokamak with Single-Null Poloidal Divertor", JAERI-M 83-008 (March, 1983).

12) Kasai S., Hirayama T., Yamauchi T., Sugie T., Yamamoto S., Maeno M., Sengoku S., Suzuki N., Miura Y., Kawashima H., Ogawa H. : "Time- and Spatial-behaviors of Metal Impurity during Neutral-Beam Injection on the JFT-2 Tokamak", JAERI-M 82-164 (November 1982).

13) Matsuzaki Y. : "Plasma Position Control by Iso-Flux Method in TEXTOR", JAERI-M 82-092 (July, 1982).

14) Ohtsuka M.[*4], Nagami M., and Matsuda T. : "BIRTH: A Beam Deposition Code for Non-circular Tokamak Plasmas", JAERI-M 82-129 (September, 1982).

15) Shimada M. : "Studies on Divertor Effects by Means of the Doublet Ⅲ High-Temperature Plasma Device", JAERI-M 82-195 (December, 1982).

16) Akiba M., Araki M., Horiike H., Itoh T., Kawai M., Kuriyama M., Kitamura S., Matsuda S., Matsuoka M., Mukaida H.[*2], Oguchi Y.[*6], Ohara Y., Ohga T., Ohtsuki H.[*4], Okumura Y., Shibanuma K., Shibata T., Shirakata H., and Tanaka S. : "Extraction of 10 Sec/75 keV/70 A Ion Beams at Prototype Neutral Beam Injector Unit for JT-60", JAERI-M 82-045 (May, 1982).

17) Ohara Y., and Kuriyama M. : "A Computer Code for Computing the Beam Profiles in the NBI Beam Line "BEMPROF" ", JAERI-M 82-066 (July, 1982) (in Japanese).

18) Matsuoka M. : "Control Characteristics on Accel Power Supply of Prototype Injector Unit for JT-60", JAERI-M 82-105 (August, 1982) (in Japanese).

19) Itoh T., Horiike H., Kuriyama M., Matsuda S., Matsuoka M., and Tanaka S. : "Design of Bending Magnet of Neutral Beam Injection for JT-60", JAERI-M 82-131 (September, 1982) (in Japanese).

20) Tanaka S., Horiike H., Itoh T., Kuriyama M., Matsuda S., Matsuoka M., Ohara Y., and Shirakata H. : "Magnetic Shields for JT-60 Neutral Beam Injector", JAERI-M 82-140 (October, 1982) (in Japanese).

21) Kawai M., and Akiba M. : "A Multi-Channel Optical Beam Monitor for the Prototype Neutral Beam Injector Unit for JT-60", JAERI-M 82-209 (December, 1982) (in Japanese).

22) Nakamura K. : "Thermal Shock Testing of Low-Z Coatings with Pulsed Hydrogen Beams", JAERI-M 82-026 (April, 1982) (in Japanese).

23) Gomay Y.[*2], Nakamura K., and Murakami Y. : "A Review on Development of Helium Pumping Systems for Tokamak Reactors", JAERI-M 82-037

(April, 1982) (in Japanese).

24) Sone K., Maeno M., Yamamoto S., Ohtsuka H., and Abe T. : "Surface Materials Considerations for Fusion Reactors", JAERI-M 82-156 (November, 1982).

25) Ohno H., Konishi S., Noda K., Takeshita H., Katsuta H., Yoshida H., Watanabe H. and Naruse Y. : "Lithium Movement and Tritium (Hydrogen) Behaviors in Li_2O, Li_2SiO_3 and $LiAlO_2$", JAERI-M 82-146 (in Japanese).

26) Yoshida H., Takeshita H., Konishi S., Ohno H., Kurasawa T., Watanabe H. and Naruse Y. : "A Feasibility Study of Catalytic Reduction Method for Tritium Recovery from Tritiated Water", JAERI-M 82-158 (in Japanese).

27) Konishi S., Ohno H., Yoshida H. and Naruse Y. : "Characteristics of Solid Oxide Electrolysis Cell for Decomposition of Tritiated Water", JAERI-M 82-186 (in Japanese).

28) Yoshida H., Konishi S., Takeshita H., Kurasawa T., Ohno H., Katsuta H., Watanabe H. and Naruse Y. : "Water Adsorption on Lithium Oxide Pellets in Helium Gas Stream", JAERI-M 82-194 (in Japanese).

29) Konishi S., Ohno H., Katsuta H., Takeshita H., Yoshida H., Watanabe H. and Naruse Y. : "Ionic Conductivity and Hydrogen Diffusion", JAERI-M 82-203 (in Japanese).

30) Kinoshita M. : "Mathematical Simulation Procedure for Single Cryogenic Distillation Column with Feedback Stream Processing Six Isotope Species of Molecular Hydrogen", JAERI-M 82-047.

31) Kinoshita M., Bartlit J.R. and Sherman R.H. : "Mathematical Simulation of Falling Liquid Film Condenser for Removal of Helium and Separation of Hydrogen Isotopes", JAERI-M 82-048.

32) Kinoshita M. : "Computor-Aided Simulation Model for Hydrogen Isotope Separating Column by Cryogenic Distillation", JAERI-M 82-108.

33) Kinoshita M., Bartlit J.R. and Sherman R.H. : "A New System for Complete Separation of ^3He and T_2 composed of a Falling Film Condenser and a Cryogenic Distillation Column with a Feedback Stream", JAERI-M 82-162.

34) Naruse Y., Tanaka K., Matsuda Y., Yoshida H., Okuno K., Konishi S., et al. : "Japanese Contributions to IAEA INTOR Workshop Phase IIA, Chapter VIII Tritium and Blanket", JAERI-M 82-175.

35) Kinoshita M. : "Derivation of Working Equations for a Dynamic Simulation of Cryogenic Distillation Column Incorporating Vapor Holdups on Stages within Column", JAERI-M 82-214.

36) Kinoshita M. : "Study on Computer-Aided Simulation Procedure for Multicomponent Separating Cascade", JAERI-M 82-185.

37) Tomabechi K., Hiraoka T., Fujisawa N., Nishio S., Sawada Y.[*2], and Kobayashi T.[*18] : "Japanese Contributions to IAEA INTOR Workshop, Phase II A; Chapter I, II, III: Summary and INTOR Concept", JAERI-M 82-170 (November 1982).

38) Fujisawa N., Sugihara M., Saito S.[*4], and Shimada M. : "Japanese Contributions to IAEA INTOR Workshop, Phase II A; Chapter VI: Impurity Control Physics", JAERI-M 82-173 (November 1982).

39) Hiraoka T., Fujisawa N., Nishio S., Nakamura H., Sone K., Maeno M., Yamamoto S., Ohtsuka H., Abe T., Fukai Y.[*2], Sawada Y.[*2], Miki N.[*5], Uchida T.[*2], Naganuma M.[*2], Hatayama A.[*2], Omori J.[*2], Tanaka Y.[*2], Ebisawa K.[*2], Terasawa M.[*2], Tachikawa N.[*2], Kawashima M.[*2], and Yamaoka M.[*2] : "Japanese Contributions to IAEA INTOR Workshop, Phase II A; Chapter VII: Impurity Control and First Wall-Engineering", JAERI-M 82-174 (November 1982).

40) Tone T., Shiraishi K., Watanabe H., Seki Y., Tomabechi K., Minato A.[*18], Tanaka Y.[*18], Kobayashi T.[*18], Suzuki T.[*18], Mori S.[*18], Kuroda T.[*18], Yamazaki S.[*18], Fukai T.[*2], Sawada Y.[*2], Honda T.[*2] : "Japanese Contributions to IAEA INTOR Workshop, Phase IIA, Chapter XII: Engineering Testing", JAERI-M 82-179 (1982).

41) Tone T., Seki Y., Minato A.[*18], Kobayashi T.[*18], Mori S.[*18], Kawasaki H.[*25], Sumita K.[**3] : "Japanese Contributions to the Japan-US Workshop on Blanket Design/Technology (Exchange B-39 in the Japan-US Fusion Cooperation Program, November 10-11, 1982)", JAERI-M 83-005 (1983).

42) Tone T., Seki Y., Minato A.[*18], Yamamoto T.[*6], Kitamura K.[*2] Nakae H.[*20] : "A Study of the Reactor Structure Concept of the Tokamak Power Reactor SPTR-P (Swimming Pool Type)", JAERI-M 83-031 (1983).

43) Seki Y., Iida H. and Kawasaki H.[*25] : "Graphical Representation of Transmutation and Decay Chain Data, Transmutation Cross Section and Delayed Gamma Ray Emission Data", JAERI-M 82-1280 (November 1982).

44) Seki Y., Iida H. and Kawasaki H.[*25] : "Comparison of Shielding Capabilities of Fusion Reactor Blanket and Shield Materials", JAERI-M 82-054 (June 1982).

45) Kawasaki H.[*25] and Seki Y. : "APPLE-2 An Improved Version of APPLE Code for Plotting Neutron and Gamma Ray Spectra and Reaction Rates", JAERI-M 82-091 (July 1982).

46) Saito S., Fujisawa N., Sugihara M., Ueda K. and Nakamura H. :

"Preparatory Evaluation on Heat and Particle Loads, Helium Pumping, and Limiter Material for INTOR Pumped Limiter", JAERI-M 83-017 (1983).

47) Nishio S., Shimada R., Shimamoto S., Ueda K., Fukai Y., Sawada Y., Yamaguchi M., Miki N., Hamajima T., Naganuma A., Fujiwara N., Tanabe Y., Miura A., Wachi Y., Sato Y., Honda T. : "Japanese Contributions to IAEA INTOR Workshop, Phase II A Chapter IX: Magnet", JAERI-M 82-176.

48) Nishio S., Ueda K., Miki N., Fujisawa N., Tanabe Y., Ohmori J., Naganuma M., Nakamura Y., Sawada Y. : "Japanese Contributions to IAEA INTOR Workshop, Phase II A Chapter X: Electromagnetics", JAERI-M 82-177.

49) Noshio S., Fujisawa N., Fukai Y., Yamaguchi M., Sawada Y., Uchida T., Miki N., Hamajima T., Naganuma M., Munakata T., Tachikawa N., Goto M., Ebisawa K., Honda T., Ashibe K. : "Japanese Contributions to IAEA INTOR Workshop, Phase II A Chapter XI: Mechanical Configuration", JAERI-M 82-178.

50) Ueda K., Nishio S., Fujisawa N., Sugihara M., Saito S., Miyamoto K. : "Vertical Position Control of The Elongated INTOR Plasma", JAERI-M 82-213.

51) Ueda K., Nishio S., Fujisawa N., Sugihara M., Saito S. : "Poloidal Field Distribution Studies in Tokamak Reactor", JAERI-M 82-217.

52) Yoshizu T., Sugihara M., Fujisawa N. : "Preliminary Investigation of Optimized Plasma Parameters for Steady Operation by RF Current Drive in Fusion Experimental Reactor", JAERI-M 82-165.

53) Hatayama A., Sugihara M., Hirayama T. : "Thermal Instability Analysis in a D-T Tokamak Reactor with Density Dynamics", JAERI-M 82-147.

54) Ogiwara N., Arai T., Kishida H.[*21] : "Secondary Electron Emission Rate under the Electron Bombardment (I) — Outline of the Experimental Apparatus and Some Experimental Data —", JAERI-M 82-123 (Aug. 1982) (in Japanese).

55) Hirayama T., Tani K., Azumi M., Nakanishi M., Orii S., Takizuka T., Yoshida H., Ninomiya H., Seki S., Shimomura Y. : "Library System for a One Dimensional Tokamak Transport Code (LIBJT60)", JAERI-M 82-204 (Dec. 1982) (in Japanese).

56) Takatsu H., Yamamoto M., Shimizu M., Suzuki K.[*4], Okabe T.[*4], Hayashi Y.[*27], Mizuno G.[*27] : "Mechanical Strength Evaluation of the Welded Bellows for the Ports of the JT-60 Vacuum Vessel", JAERI-M 82-205

(Dec. 1982) (in Japanese).

57) Suzuki K. : "Electric Breakdown Property of Halon Gas", JAERI-M 83-023 (Feb. 1983) (in Japanese).

58) Nakamura H., Hiraoka T., Hassanein A.M.[**17], Kulcinski G.L.[**18], Wolfer W.G.[**18] : "First Wall Erosion during a Plasma Disruption in Tokamak", JAERI-M 83-058 (March 1983).

A.1.2 List of GA-A Report

1) Mckelvey T.[*5], Taylor T.[*5], Trester P.[*5], Reis E.[*5], Gallix R.[*5], Gaklos P.[*5], Jhonson E.[*5], Puhn F.[*5], Doll D.[*5], Sevier L.[*5], Yokomizo H., Nishikawa M.[*3] and Kitsunezaki A. : " Graphite Limiter and Armor Damage in Doublet Ⅲ", GA-A 16748 (September, 1982) and reported at 12th Symposium on Fusion Technology (September 1982, Jülich).

A.1.3 List of Papers Published in Journals

1) Itoh K., Itoh S-I.[**1] : "On the RF Stabilization of MHD Instability", Jpn. J. Appl. Phys. 21 (1982) L203.

2) Nishikawa K-I., Itoh K., Tuda T., Terashima Y.[**2] : "Numerical Study on Drift and Alfvén Waves in a Current-carrying Plasma", J. Phys. Soc. Jpn. 51 (1982) 1606.

3) Itoh K., Itoh S-I.[**1] : "Stability of ∇T_e-driven Microscopic Tearing Mode", J. Phys. Soc. Jpn. 51 (1982) 1639.

4) Matsuura T.[*1], Tanaka T.[*1], Naraoka K.[*1], Takizuka T., Tsunematsu T., Tokuda S., Azumi M., Kurita G., Takeda T. : "Vector Processing Efficiency of Plasma MHD Codes by Use of the FACOM 230-75 APU", Comput. Phys. Commun. 26 (1982) 377.

5) Itoh K., Tuda T., Tokuda S., Itoh S-I.[**1] : "Universal Ballooning Instability", J. Phys. Soc. Jpn. 51, (1982) 2300.

6) Itoh K., Itoh S-I.[**1], Tokuda S., Tuda T. : "Kinetic Theory of Electromagnetic High-n Ballooning Instability", Nucl. Fusion 22 (1982) 1031.

7) Tuda T., Itoh K., Itoh S-I.[**1] : "Kinetic Theory of Ballooning Instabilities", Phys. Fluids 25 (1982) 1483.

8) Appert K.[**13], Balet B.[**13], Gruber R.[**13], Troyon F.[**13], Tsunematsu T., Vaclavik J.[**13] : "MHD Computations for Alfvén Wave Heating in Tokamaks", Nucl. Fusion 22 (1982) 903.

9) Itoh S-I.[**1], Itoh K., Nishikawa K. : "Kinetic Alfvén Wave Propagation in Cylindrical Tokamak", Plasma Phys. 24 (1982) 1027.

10) Gruber R.[**13], Troyon F.[**13], Tsunematsu T. : "Radial Structure of Internal Unstable Ideal MHD Modes in the Range of Intermediate Toroidal Wave Numbers", Plasma Phys. 25 (1983) 207.

11) Uesugi Y., Takamura S.[**2], Okuda T.[**2] : "Helical Slow Wave Antenna for Launching Lower Hybrid Waves in a Plasma", Plasma Phys. 24 (1982) 369.

12) Shimada M.[*2], Yoshida H., Brooks N.H.[*5], Hsieh C.L.[*5], Groebner R.[*5] : "Impurity Reduction and Remoto Radiative Cooling with Single-Null Poloidal Divertor in Doublet III", Nucl. Fusion 5 (1982) 643.

13) Matsumoto H., Kimura H., Sengoku S., Suzuki N., Ohasa K., Yamamoto S. : "Particle Confinement during High Power Neutral Beam Injection in JFT-2 Tokamak", Nucl. Fusion 22 (1982) 839.

14) Yokomizo H., Nagami M., Shimada M., Maeno M., Yoshida H., Shinya K.[*2], Ioki K.[*4], Izumi S.[*4], Rock P.[*5], Brooks N.H.[*5], Seraydarian R.[*5], Fujisawa N., Kitsunezaki A. : "Equilibrium and Axisymmentric Stability of Dee-Shaped Plasma in Doublet III", Nucl. Fusion 6 (1982) 797.

15) Ohtsuka H., Maeno M., Suzuki N., Konoshima S., Yamamoto S., Ogiwara N. : "Plasma Parameters Related to Arc Initiation on the Tokamak First Wall", Nucl. Fusion 6 (1982) 823.

16) Ninomiya H., Suzuki N. : "Estimation of Plasma Position and Bp+li/2 from Magnetic Measurement under High-β Condition in JFT-2", Jpn. J. Appl. Phys. 21 (1982) 1323.

17) Uesugi Y., Itoh T.[**2], Takamura S.[**2], Okuda T.[*1] : "Phase-Locked Heterodyne Reciever and its Application to Lower Hybrid Wave Detection by Microwave Scattering", Rev. Sci. Instrum. 53 (1982) 1730.

18) Maeno M., Sengoku S., Nakamura H., Yamamoto S., Seki M., Kawamura H. : "Thermal Load Test of a TiC Coated Mo limiter during Steady State and Major Current Disruption Phase in the JFT-2 Tokamak with Neutral Beam Injection", Jpn. J. Appl. Phys. 21 (1982) 45.

19) Shimada M., Nagami M., Ioki K.[*3], Izumi S.[*9], Maeno M., Yokomizo H., Shinya K.[*2], Yoshida H., Brooks N.H.[*5], Hsieh C.L.[*5], Groebner R.[*5], and Kitsunezaki A. : "Impurity Reduction and Remote Radiation Cooling with Single-Null Poloidal Divertor in Doublet Ⅲ", Nucl. Fusion 22 (1982) 643.

20) Yokomizo H., Nagami M., Shimada M., Maeno M., Yoshida H., Shinya K.[*2], Ioki K.[*3], Izumi S.[*4], Fujisawa N., and Kitsunezaki A. : "Equilibrium and Axisymmetric Stability of Dee-Shaped Plasmas in Doublet Ⅲ", Nucl. Fusion 22 (1982) 797.

21) Ioki K.[*3], Shimada M., Nagami M., Maeno M., Izumi S.[*4], Yokomizo H., Yoshida H., Shinya K.[*2], Brooks N.[*5], Seraydrian R.[*5], Taylor T.[*5], McMahon T.[*5], and Kitsunezaki A. : "Reduction of Heat Flux on Divertor Plates by Remote Radiative Cooling in Doublet Ⅲ", Nucl. Eng. Design 73 (1982) 45.

22) Tanaka S., Akiba M., Arakawa Y., Horiike H., and Sakuraba J.[*10] : "Reduction of Gas Flow into a Hollow Cathode Ion Source for a Neutral Beam Injector", Rev. Sci. Instrum. 53 (1982) 1038.

23) Horiike H., Kuriyama M., and Morita H.[*8] : "Burnout Experiment in Subcooled Forced-Convection Boiling of Water for Beam Dumps of a High Power Neutral Beam Injector", Nucl. Technology/Fusion 2 (1982) 637.

24) Akiba M., Araki M., Horiike H., Itoh T., Kawai M., Kuriyama M., Kitamura S., Matsuda S., Matsuoka M., Mukaida H.[*2], Oguchi Y.[*6], Ohara Y., Ohga T., Ohtsuki H.[*4], Okumura Y., Shibanuma K., Shibata T., Shirakata H., and Tanaka S. : "Production of 75-keV, 70-A, 10-S Ion Beams", Rev. Sci. Instrum. 53 (1982) 1864.

25) Uehara K., Yamamoto S., Kimura H., Suzuki N., Sugie T., Matsuda T., Takeuchi H., Yamauchi T., Yamamoto T., Hoshino K., Sengoku S., Maeno M., Imai T., Fujii T., and Nagashima T. : "Stabilization of Parametric Instabilities by Boundary Plasma Electron Heating in JFT-2", Nucl. Fusion 22 (1982) 428.

26) Uehara K., Yamamoto T., Fujii T., Suzuki N., Imai T., Iizuka S., Takeuchi H., Kasai S., Yoshida H., Fujisawa N., and Nagashima T. : "Role of Boundary Plasma in Lower-Hybrid-Frequency Heating of a Tokamak", J. Phys. Soc. Jpn. 51 (1982) 1959.

27) Fujii T., Imai T., Uehara K., and Nagashima T. : "Coupling Properties of Phased Waveguide in LHRF Heating Experiment in JFT-2 Tokamak", Jpn. J. Appl. Phys. 22 (1983) 319.

28) Ohtsuka H. : "A Relation between Light and Metal Impurities in a Tokamak Plasma", Nucl. Fusion 22 (1982) 827.

29) Yoshida H., Konishi S., Katsuta H., Shimizu T., and Naruse Y. : "Effects of Impurities on Hydrogen Permeability through Palladium-Silver Alloy Membrane", J. At. Energy Soc. Japan 24[6] (1982) 475 (in Japanese).

30) Konishi S., Yoshida H., and Naruse Y. : "Analysis and Design of Palladium Diffuser for Fusion Reactor Fuel Cleanup System", J. At. Energy Soc. 24[12] (1982) 973 (in Japanese).

31) Yoshida H., Okuno K., and Naruse Y. : "Gas Chromatographic Measurement of Hydrogen Isotopes Mixture by Using Catalytic Oxidation Type Detector", J. Nucl. Sci. Technol. 19[7] (1982) 578.

32) Yoshida H., Konishi S., and Naruse Y. : "Effects of Impurities on Hydrogen Permeability through Palladium Alloy Membranes at Comparatively High Pressure and Temperature", J. Less-Common Metals 88[3] (1983) 429.

33) Konishi S., Yoshida H., and Naruse Y. : "Design Study of Palladium Diffuser for D-T Fusion Reactor Fuel Cleanup System", J. Less-Common Metals 88[3] (1983) 457.

34) Konishi S., Ohno H., Yoshida H., and Naruse Y. : "Decomposition of Tritiated Water with Solid Oxide Electrolysis Cell", Nucl. Technol./Fusion 3 (1983) 193.

35) Kinoshita M., and Naruse Y. : "Separation Characteristics of Cryogenic Distillation Column with a Feedback Stream for Separation of Protium and Tritium", Nucl. Technol./Fusion 2 (1982) 410.

36) Kinoshita M., and Naruse Y. : "Improvement of the Mathematical Simulation Model for a Multicomponent Separating Cascade", Nucl. Sci. Eng. 82 (1982) 469.

37) Kinoshita M., and Naruse Y. : "A Mathematical Simulation Procedure for a Multistage-type Water / Hydrogen Exchange Column in Tritium System", Nucl. Technol./Fusion 3 (1983) 112.

38) Naruse Y. : "On the Handling Technology of a Large Amount of Tritium", Health Physics 17 (1982) 527.

39) Johns G.[*5], Ejima S.[*5], Groebner R.[*5], Brooks N.[*5], Fisher P.[*5], Hsieh C.[*5], Taylor T.[*5], Wesley J.[*5], Fujisawa N., and Sugawara T.[*2] : "Dynamic Behavior of Intrinsic Impurities in Doublet III Discharges", Nucl. Fusion 22 (1982) 1049.

40) Sako K., Tone T., Seki S., Iida H., Minato A.[*18], Sakamoto H.[*8], Yamamoto T., Kitamura K.[*2] : "Design Study of Swimming Pool Type Tokamak Reactor (SPTR)", J. Nucl. Sci. Technol. 19 (1982) 491-503.

41) Seki Y., Iida H., Santoro R.T.[**14], Kawasaki H.[*27], and Yamauchi M.[*18] : "Radiation Streaming Calculations for INTOR-J", Nucl. Technol./Fusion 2 (1982) 272-285.

42) Mori S.[*18], Seki Y., and Kawasaki H.[*25] : "Neutronics Design of Tritium Breeding Blanket for Fusion Experimental Reactor", J. Nucl. Sci. Technol. 20 (1983) 154-162.

43) Sugihara M., Fujisawa N., Ueda K., Saito S., Hatayama, Shimada R. : "Plasma Design Considerations of Near Term Tokamak Fusion Experimental Reactor", J. Nucl. Sci. Tech. 19 (1982) 628.

44) Arakawa K., Shimada R., Kishimoto H., Yabuno K.*9, Ishigaki Y.*9, Itoh S.*9 : "Study of Grounding System of Large Tokamak Device JT-60", Trans. IEE of Japan 102-B (1982) 379.

45) Tani K., Shimada R., Tamura S., Yabuno K.*9, Koseki S.*9, Ishigaki Y.*9 : "Ohmic Heating Coil Power Supply Using Thyristor Circuit Breaker in a Thermonuclear Fusion Device", Trans. IEE of Japan 102-B (1982) 453.

46) Yoshida H., Kishimoto H., Tamura S. : "Ergodic Behavior of Magnetic Field Lines in a Poloidal Divertor Tokamak", Jpn. J. Appl. Phys. 21 (1982) 1068.

47) Tani K., Kishimoto H. : "Localized Heat Deposition on Tokamak First Wall due to Ripple-Trapped Loss of Superthermal Ions Produced by NBI", Nucl. Fusion 22 (1982) 1107.

48) Miyazaki K.**7, Takatsu H., Fukuzawa Y.**12, Fujiie Y.**2 : "Boiling of Potassium in Vertical Tube under Transverse Magnetic Field", J. Nucl. Sci. Technol. 19 (1982) 729.

49) Shimada R. : "Controls of Tokamak Current and Equilibrium with Hybrid Poloidal Field Coils", Trans. IEE of Japan 102-A (1982) 483.

50) Takatsu H., Shimizu M., Ohta M., Imai Y.*31, Ono S.*31, Minami M. : "Dynamic Response of the JT-60 Vacuum Vessel under the Electromagnetic Force", J. Nucl. Energy Des. 71 (1982) 161.

A.1.4 List of Papers Published in Conference Proceedings

1) Tokuda S., Tsunematsu T., Azumi M., Takizuka T., Takeda T. : "2nd Stability Regions Against Ideal MHD Instabilities", 1982 International Conference on Plasm Physics (Göteborg, Sweden).
2) Itoh K., Itoh S-I.[**1] : "Radial Absorption Structure of Kinetic Alfvén Wave and Heating Efficiency", ibid.
3) Itoh S-I.[**1], Itoh K. : "Micro-instability, Entropy Production and Plasma Confinement", ibid.
4) Takeda T., Tsunematsu T., Tuda T., Azumi M., Takizuka T., Tokuda S., Kurita G., Itoh K., Naraoka K.[*1], Tanaka Y.[*1], Itoh S-I.[**1] : "Physics of Intensely Heated Tokamak Plasma", 9th International Conference on Plasma Physics and Controlled Nuclear Fusion Research (Baltimore, USA, 1982).
5) Tsunematsu T., Azumi M., Tokuda S., Kurita G., Takeda T., Tanaka Y.[*1] : "Numerical Study of Resistive Mode in Tokamak(I)", 10th Conference on Numerical Simulation of Plasma", (San Diego, USA, 1982).
6) Tanaka Y.[*1], Azumi M., Tsunematsu T., Tokuda S., Kurita G., Takeda T. : "Numerical Study of Resistive Mode in Tokamak(II)", ibid.
7) Itoh S-I.[**1], Itoh K., Fukuyama A.[**3] : "2D Kinetic and 3D MHD Analyses of ICRF Waves in Tokamaks", ibid.
8) Itoh K., Itoh S-I.[**1], Tokuda S., Tuda S. : "Matrix and Contor-map Method for Kinetic Ballooning Mode", ibid.
9) Itoh S-I.[**1], Itoh K., Fukuyama A.[**3] : "2D Kinetic Analysis of ICRF Waves in Tokamaks", Fifth Topical Conference on RF Plasma Heating", (Madison, USA, 1983).
10) Itoh K., Itoh S-I.[**1], Fukuyama A. : "3-D Collisional MHD Analysis of ICRF Waves in Tokamaks", ibid.
11) Tuda T. : "Kinetic Effects on MHD Stabilities in a Tokamak", US-Japan Workshop on Anomalous Transport and Critical Beta Value (Nagoya, Japan, 1983).
12) Tokuda S. : "High-β Effects on MHD Stabilities in Tokamaks", ibid.
13) Takizuka T. : "Motion of Electrons due to High Mode Number Ballooning Mode", ibid.
14) Takeda T. : "MHD Computations at JAERI", US-Japan Workshop on 3D MHD Computations", (Nagoya, Japan, 1983).
15) Azumi M. : "Numerical Study of Resistive Internal Kink Mode", ibid.
16) Tsunematsu T. : "Finite Beta Effect on Tearing Mode", ibid.
17) Shimada M., Nagami M., Nishikawa M.[*3], Ioki K.[*3], Yokomizo H.,

Izumi S.[*9], Maeno M., Shinya K.[*2], Yoshida H., Kitsunezaki A., Brooks N.H.[*5], Hsieh C.L.[*5], Degrossie J.S.[*5], Groebner R.[*5] : "High Density Single-Null Polidal Divertor Results in Doublet III", 10th Int. Nati. Conf. on Plasma Surface Interaction E.5.

18) Isler R.C.[**14], Murray L.E.[**14], Kasai S., Sheffield J.[**14] : "Impurity Transport in the ISX-B Tokamak", IAEA Technical Committee Meeting on Divertors and Impurity Control IV, C4.

19) Yamamoto S., Maeno M., Sengoku S., Suzuki N., Kasai S., Yamauchi T., Miura Y., Sugie T., Yamamoto T., Ogawa T., Kawashima H., Kawakami T., Hoshino K., Kimura H., Matsumoto H., Mori M., Odajima K., Shoji T., Matsuda T., Funahashi A., Tanaka Y., Ohtsuka H., Kunieda S., Suzuki K., Matsuzaki Y., Anno K., Tani T., Shibata T., Yokoyama K., Kikuchi K., Kazawa M., Tajima Y., Hasegawa K., Okano K., Honda A., Kashiwa Y., Shiina T., Ishibori I., Sunaoshi H., Kashimura T., Nakamura H., Hirayama T., Takeuchi H., Ohasa K., Tani K., Konoshima S., Matsuda T., Amano T.[**2], Okamoto M.[**2], Shimizu K.[**2], Katagiri M. : "Transport Studies in the JFT-2 Tokamak", 9th IAEA conference IAEA-CN-41/A-5 (Baltimore USA, 1982).

20) Kimura H., Matsumoto H., Odajima K., Konoshima S., Yamamoto T., Suzuki N., Hoshino K., Miura Y., Matsuda T., Takeuchi H., Sugie T., Kasai S., Yamauchi T., Kawashima H., Ogawa T., Kawakami T., Shoji T., Mori M., Ogawa H., Uesugi Y., Ohasa K., Yamamoto S., Maeno M., Sengoku S., Nakamura H., Ohtsuka H., Matoba T., Funahashi A., Tanaka Y. : "ICRF Heating Experiment in JFT-2", ibid, IAEA-CN-41/J-3.

21) Yokomizo H., Shimada M., Aikawa H., Hoshino K., Ioki K.[*3], Izumi S.[*4], Kasai M.[**3], Kitsunezaki A., Maeno M., Matsuda T., Miya N., Nagami M., Konoshima H., Nishizawa M.[*3], Ohtsuka M.[*4], Sengoku S., Shinya K.[*2], Yamauchi T., Yoshida H., GA Team : "Vertical Stability of Elongated Plasma and Divertor Experiment in Doublet III", ibid, IAEA-CN-41/R-1.

22) Aikawa H., Hoshino K., Kasai M.[*3], Kitsunezaki A., Kobayashi T.[*4], Konoshima S., Matoba T., Miya N., Nagami M., Minomiya H., Nishikawa M.[*4], Ohtsuka M.[*4], Sengoku S., Shimada M., Shinya K.[**2], Yamauchi T., Yokomizo H., Yoshida H., GA team : "High-β Injection Experiment with Shaped Plasma in Doublet III", ibid, IAEA-CN-41/A-2.

23) Sengoku S., Shimada M., Miya N., Kasai M.[*3], Aikawa H., Azumi M., Hoshino K., Kitsunezaki A., Konoshima S., Matsuda T., Nagami N., Ninomiya H., Nishikawa M.[*4], Tokutake T., Yamauchi T., Yokomizo H., Burrell K.H.[*5], Kahn C.L.[*5] : "Langmuir Probe Measurements in the

Single-Null Poloidal Divertor in Doublet III", APS 24th Annual Meeting (New Orleans USA, 1982).

24) Yamamoto T., Odajima K., Kimura H., Matsumoto H. : "Study on Non-loop Coupler for ICRF Heating", Japan-US Workshop on RF Heating Technology (Tokai Japan, 1982).

25) Yamamoto S., Maeno M., Sengoku S., JFT-2 Group : "JFT-2 Experiments with Additional Heating", Japan-US Workshop on Anomalous Transport and Beta Limit (Nagoya, Japan, 1982).

26) Odajima K. : "JFT-2M Program", Japan-US Workshop on RF Heating Technology (Tokai, Japan, 1982).

27) Kimura H. : "Ridged Waveguide Coupler for JT-60", ibid.

28) Shinya K.[*2] and Yokomizo H. : "On-line Prediction of Shaping Parameters for Doublet Ⅲ Plasmas from Magnetic Signals", 1982 IEEE International Conference on Plasma Science (May 1982, Ottawa).

29) Ohtsuka M.[*4], Nagami M., and Matsuda T. : "Development of Fast Tokamak Data Analysis Code for Studying Non-Linear Beam Heated High-β Plasmas", ibid.

30) Yokomizo H., Nishikawa M.[*3], Kitsunezaki A., Matsuda T., Nagami M., Ohtsuka M.[*4], Shimada M., Shinya K.[*2], McKelvey T.[*5], Taylor T.[*5], Doll D.[*5], Seiver L.[*5], Johnson E.[*5], Brooks N.[*5], Seraydarian R.[*5] : "Temperature Evolution and Damage to Limiter Surface Caused by Runaway Electrons", ibid.

31) Nagami M., Aikawa H., Kasai M.[*3], Kitsunezaki A., Kobayashi T.[*4], Konoshima S., Matsuda T., Miya N., Ninomiya H., Nishikawa M.[*9], Ohtsuka M.[*4], Sengoku S., Shimada M., Shinya K.[*2], Yamauchi T., Yokomizo H., Yoshida H., Angle T.[*5], Armentrout C.[*5], Blau F.[*5], Bramson G.[*5], Brooks N.[*5], Burrell K.[*5], Callis R.[*5], Chase R.[*5], Colleraine A.[*5], Fasolo J.[*5], Fisher R.[*5], Freeman R.[*5], Gilleland J.[*5], Groebner R.[*5], Harvey R.[*5], Hsieh C.[*5], Hong R.[*5], Johns G.[*5], Kamperschroer J.[*5], Kim J.[*5], Lieber A.[*5], Lohr J.[*5], Luxon J.[*5], Mahdavi M.[*5], Marcus F.[*5], McColl D.[*5], Petersen P.[*5], Petrie T.[*5], Pfeiffer W.[*5], Riviere A.[*5], Rottler L.[*5], Scoville J.[*5], Seraydarian R.[*5], Silagi R.[*5], Smith J.[*5], Snider R.[*5], Stambaugh R.[*5], Stav R.[*5], Taylor T.[*5], Tadd T.[*5], Tooker J.[*5], Wong S.[*5], Zawadski G.[*5] : "High-β Injection Experiments with Shaped Plasmas in Doublet-Ⅲ", 9th International Conference on Plasma Physics and Controlled Nuclear Fusion Research (September 1982, Baltimore) IAEA-CN-41/A-2.

32) Yokomizo H., Shimada M., Aikawa H., Hoshino K., Ioki K.[*3], Izumi S.[*4],

Kasai M.[*3], Kitsunezaki A., Kobayashi T.[*4], Konoshima S., Maeno M., Matsuda T., Miya N., Nagami M., Ninomiya H., Nishikawa M.[*4], Ohtsuka M.[*4], Sengoku S., Shinya K.[*2], Yamauchi T., Yoshida H., Angle T.[*5], Armentrout C.[*5], Baker D.[*5], Blau F.[*5], Bramson G.[*5], Brooks N.[*5], Brown B.[*5], Burrell K.[*5], Callis R.[*5], Chase R.[*5], Colleraine A.[*5], deGrassie J.[*5], Fairbanks E.[*5], Fasolo J.[*5], Fisher R.[*5], Groebner R.[*5], Hong R.[*5], Hsieh C.[*5], Jhans G.[*5], Kamperschroer J.[*5], Kim J.[*5], Lohr J.[*5], McColl D.[*5], McMahon T.[*5], Peterson P.[*5], Rottler L.[*5], Scoville J.[*5], Seraydarian R.[*5], Silagi R.[*5], Snider R.[*5], Stav R.[*5], Tooker J.[*5], Treglio J.[*5], Wesley J.[*5], Wojtowicz S.[*5] : "Vertical Stability of Elongated Plasmas and Divertor Experiments in Doublet III", ibid, IAEA-CN-41/R-1.

33) Nagami M., Matsuda T., Ohtsuka M.[*4], Aikawa H., Kasai M.[*3], Kitsunezaki A., Kobayashi T.[*4], Konoshima S., Miya N., Ninomiya H., Sengoku S., Shimada M., Yokomizo H., and GA Team[*5] : "High-β Studies in Beam Heated Doublet III Plasmas with D-Shaped and Circular Cross Sections", APS 24th Annual Meeting (November 1982, New Orleans).

34) Shimada M., Sengoku S., JAERI Team, Hseih C.[*5], Groebner R.[*5], Brooks N.[*5], Jhans G.[*5], GA Team[*5] : "Radiation Loss and Behavior of Impurities during NBI Heating in Doublet III", ibid.

35) Ninomiya H., Nagami M., JAERI Team, and GA Team : "Operational Characteristics of D-Shaped Circular Plasmas during the Neutral Beam Injection in Doublet III", ibid.

36) Matsuda T., Nagami M., JAERI Team, Armentrout C.[*5], Bramson G.[*5], GA Team[*5] : "Study of Charge Exchange Neutral Behaviors during Neutral Beam Injection in Doublet III", ibid.

37) Kitsunezaki A., Shimada M., Sengoku S., Nagami M., JAERI Team, and GA Team[*5] : "A Model for an Open Divertor", ibid.

38) Ohtsuka M.[*4], Nagami M., Matsuda T., and JAERI Term : "BIRTH: A Beam Deposition Code for Non-Circular Tokamak Plasmas", ibid.

39) Shinya K.[*2], Yokomizo H., Nagami M., and JAERI Team : "Fast and Simple Indication of $\beta p + \frac{1}{2} \ell i$ from Magnetic Measurement", ibid.

40) Yokomizo H., Kobayashi T.[*4], Shinya K.[*2], Kitsunezaki A., JAERI Team, and GA Team[*5] : "Plasma-Size Effects for Vertical Instability of Elongated Dee-Shaped Plasma in Doublet III", ibid.

41) Kasai M.[*3], Yokomizo H., JAERI Team, Taylor T.[*5], Doll D.[*5], Callis R.[*5], and GA Team : "Thermal Analysis of the Doublet III Primary Limiter", ibid.

42) Shimada M. and JAERI Team : "A Fast Numerical Simulation of the Dense and Cold Divertor Plasmas in the Single-Null Poloidal Divertor in Doublet III", 10th Conference on Numerical Simulation of Plasmas (February 1983, San Diego).

43) Shimada M. and JAERI Term : "High Density, Cold Divertor Experiments and its Numerical Simulation", Workshop on Computer Codes in High Power and Heated Tokamaks (March 1983, Princeton).

44) Shibata T., Akiba M., Horiike H., Kuriyama M., Matsuda S., Matsuoka M., Okumura Y., and Shibanuma K. : "Cryopumps and Cryogenic Systems of Prototype Injector Unit for JT-60", Proc. 9th Int. Cryogenic Engineering Conf., (Kobe, May 1982) p.612.

45) Matsuda S., Akiba M., Araki M., Horiike H., Itoh T., Kawai M., Kuriyama M., Kitamura S., Matsuoka M., Mukaida H.*2, Oguchi Y.*6, Ohara Y., Ohga T., Ohtsuki H.*4, Okumura Y., Shibanuma K., Shibata T., Shirakata H., and Tanaka S. : "Extraction of 75 keV, 70 A, 10 Sec Ion Beam at the Prototype Injector Unit for JT-60", Proc. 12th Sympo. Fusion Technology, (Jülich, Sept. 1982) p.199.

46) Matsuoka M., Higa O.*2, Kawai M., Oguchi Y.*6, Ohara Y., Ohga T., Ohtsuki H.*4, Matsuda S., Shibata T.*2, and Yoshida K.*2 : "100 kV, 80 A, 10 Sec Power Supply for Neutral Beam Injector", ibid, p.1361.

47) Imai T., Nagashima T., Uehara K., Fujii T., Sakamoto K., Honda M., Saigusa M., Ikeda Y., Nakamura T.*16, Kamakura A.*26, and Shirakata H. : "Design and R & D of RF Heating System for JT-60", 5th Topical Conf. on Radio Frequency Plasma Heating Madison, USA, (1983) Paper C-L-1.

48) Nagashima T. : "Status of JT-60 RF Heating Programm", US-Japan Workshop on RF Heating Technology (Tokai, Japan, 1982).

49) Uehara K. : "High Power Klystron Development for JT-60", ibid.

50) Yamada R. : "Chemical Sputtering of Graphite and TiC using Quadrupole Mass Spectrometer", Proc. Symp. on Effective Utilization of Surface Analysis Techniques in Plasma Surface Interactions (Sapporo, Oct. 1982).

51) McCracken G.M.**15, Fielding S.J.**15 and Ohtsuka H. : "Global Estimates of Impurity Levels and Wall Erosion in INTOR", J. Nucl. Mater. 111&112 (1982) 396, i.e. Report at International Conference on Plasma Surface Interactions in Controlled Fusion Devices (May 1982, Gatlinburg).

52) Sone K. and McCracken G.M.**15 : "The Effect of Radiation Damage on

Deuteron Reemission and Trapping in Carbon", ibid, 606.

53) Yamada R., Nakamura K. and Saidoh M. : "Chemical Sputtering Yield of Titanium Carbides", ibid, 744.

54) Saidoh M., Nakamura K. and Yamada R. : "Surface Erosion and Reemission Behaviour of TiC Coatings under Hydrogen and Helium Ion Bombardments", ibid, 848.

55) Nakamura K., Yamada R., Saidoh M. and Murakami Y. : "Thermal Shock Testing of Low-Z Coatings for JT-60", ibid, 852.

56) Yamada R., Nakamura K., Saidoh M. and Murakami Y. : "Thermal Fatigue Testing of Low-Z Coatings on Molybdenum and Inconel 625", ibid, 856.

57) Yoshida K., Koizumi K., Nakajima H., Shimada M.[*14], Sanada Y.[*2], Takahashi Y., Tada E., Tsuji H., and Shimamoto S. : "Development of Cryogenic Structural Materials for Tokamak Reactors", International Cryogenic Materials Conference (Kobe, May 1982).

58) Shimamoto S., Ando T., Hiyama T., Tsuji H., Takahashi Y., Yoshida K., Tada E., Nishi M., Okuno K., Koizumi K., Kato T., Nakajima H., Dresner L.[**14], Iida F.[*4], Shimada M.[*14], Sanada Y.[*2], Takahashi O.[*15], Ogasawara T.[**6], Kuroda K.[*4], Hattori Y.[*11], Fujioka T.[*2], and Yasukochi K. : "Advances in High-current Poloidal Conductors at JAERI", The 9th International Cryogenic Engineering Conference (Kobe, May 1982).

59) Shimamoto S., Ando T., Hiyama T., Tsuji H., Takahashi Y., Yoshida K., Nishi M., Tada E., Okuno K., Koizumi K., Nakajima H., Kato T., Takahashi O.[*15], Dresner L.[**14], Iida F.[*4], Shimada M.[*14], Sanada Y.[*2], and Yasukochi K. : "Construction and Cool-down Test of the Japanese LCT Coil", ibid.

60) Ando T., Shimamoto S., Hiyama T., Tsuji H., Takahashi Y., Nishi M., Yoshida K., Tada E., Okuno K., Koizumi K., Kato T., Nakajima H., Dresner L.[**14], Iida F.[*4], Sanada Y.[*2], Shimada M.[*14], Takahashi O.[*15], and Yasukochi K. : "TMC-I, 10T-60CM Bore Nb_3Sn Test Module Coil for the Cluster Test Program", ibid.

61) Tada E., Hiyama T., Kato T., Takahashi O.[*15], and Shimamoto S. : "350-l/h, 1,200-W Helium Cryogenic System for the Development of Fusion Technology", ibid.

62) Takahashi Y., Yoshida K., Shimada M.[*14], Tada E., Miura R.[*12], and Shimamoto S. : "Nitrogen Strengthned Stainless Steels at 4K", Advanceds in Cryogenics Engineering, Vol.28, 1982.

63) Shimamoto S., Ando T., Hiyama T., Tsuji H., Takahashi Y., Tada E., Nishi M., Yoshida K., Okuno K., Koizumi K., Kato T., Nakajima H.,

Takahashi O.[*15], Shimada M.[*14], Iida F.[*4], and Yasukochi K. : "Domestic Test Result of the Japanese LCT Coil", Applied Superconductivity Conference (Knoxville, Nov. 1982).

64) Shimamoto S., Ando T., Hiyama T., Tsuji H., Tada E., Takahashi Y., Yoshida K., Koizumi K., Kato T., Nakajima H., Takahashi O.[*15], and Sanada Y.[*2] : "Cryogenic System for Superconducting Tokamak", ibid.

65) Ando T., Shimamoto S., Hiyama T., Tsuji H., Takahashi Y., Nishi M., Yoshida K., Tada E., Okuno K., Koizumi K., Kato T., Nakajima H., Dresner L.[**14], Sanada Y.[*2], Shimada M.[*14], Iida F.[*4], Takahashi O.[*15], and Yasukochi K. : "Experiment of 10-T, 60-CM-Bore Nb_3Sn Test Module Coil (TMC-I) for the Cluster Test Program", ibid.

66) Nishi M., Ando T., Hiyama T., Kato T., and Shimamoto S. : "Boiling Helium Heat Transfer Characteristics in Narrow Cooling Channel", ibid.

67) Takahashi Y., Dresner L.[**14], Tsuji H., Tada E., Okuno K., Kato T., Nishi M., Sanada Y.[*2], Iida F.[*4], Ando T., Shimamoto S., and Yasukochi K. : "Development of a 30-KA cable-in-conduit Conductor for Pulsed Poloidal Coils", ibid.

68) Ando T., Takahashi Y., Nishi M., Tsuji H., Shimamoto S., Yasukochi K., Hamajima T.[*2], Miura A.[*2], Fujiwara N.[*2], Osaki O.[*2], Sasaki K.[*2], and Fuzioka T.[*2] : "Development of Large Bore-high Current Nb_3Sn Coil", The 12th Symposium on Fusion Technology (Jülich Sep. 1982).

69) Kinoshita M., Bartlit J.R. and Sherman R.H. : "Design Study of a Falling Liquid Film Condenser under Flow Conditions of the Tritium Systems Test Assembly", 9th IEEE Conf. on Fusion Technol. (Chicago, Oct. 1981).

70) Hirata S., Naruse Y., Tanaka K., Matsuda Y., et al. : "Tritium Safety Issues in Fusion Reactor-Tritium Containation in Reactor Room", Japan-US Workshop on Fusion Safety (Naka-machi, Ibaraki-ken, Japan, January 1983).

71) Obata Y. : "Present Status of Tritium Activity Related to Fusion Research in JAERI", Japan-US Workshop on Fusion Fuel Handling, (Los Alamos, N.M. US, March 1983).

72) Yoshida H., Konishi S. and Naruse Y. : "Use of Palladium Alloy Membrane for a Fusion Fuel Cleanup System", ibid.

73) Yoshida H., Takeshita H., Konishi S., Naruse Y. : "Decomposition of Water Vapor by Catalytic Reduction Method", ibid.

74) Konishi K., Ohno H., Yoshida H. and Naruse Y. : "Decomposition of

Water by Ceramic Electrolysis Cell", ibid.

75) Okuno K. : "Tritium Behavior of Neutron Irradiated Lithium Compounds", ibid.

76) Naruse Y., Tanaka K. and Matsuda Y. : "Present Status of Tritium Process Laboratory", ibid.

77) Fujisawa N., Nishio S., Hiraoka T., Fukai Y.[*2], Sawada Y.[*2], Uchida T.[*2], Miki N.[*2], Honda T.[*2] and Hamajima T.[*2] : "Design Consideration and Remote Maintenance of INTOR J-ⅡA", 12th Symposium on Fusion Technology (September 1982, Jülich).

78) Tomabechi K., Fujisawa N., Hiraoka T., Iida H., Naruse Y., Nishio S., Sako K., Seki Y., Shimada R., Shimamoto S., Sugihara M., Tone T., and Yoshikawa M. : "Fusion Experimental Reactor Development at JAERI", 9th International Conference on Plasma Physics and Controlled Nuclear Fusion Research (September 1982, Baltimore) IAEA-CN-41/E-4.

79) Shimada M., Nagami M., Ioki K.[*3], Izumi S.[*4], Maeno M., Matsuda T., Nishikawa M.[*3], Ohtsuka M.[*9], Shinya K.[*2], Yokomizo H., Yoshida H., Kitsunezaki A., Brooks N.H.[*5], deGrassie J.S.[*5], Groebner R.J.[*5], Hsieh C.L.[*5] : "High Density, Single-Null Poloidal Divertor Results in Doublet Ⅲ", J. Nucl. Mat. 111 & 112 (1982) 362, i.e. reported at International Conference on Plasma Surface Interactions in Controlled Fusion Device (May 1982, Gatlinburg).

80) Murakami Y., Abe T., Nakamura H. : "Development of Low-Z Surface Coatings for JT-60 First Wall", 5th International Conference on Plasma Surface Interaction (Gatlinburg May, 1982).

81) Obara K., Abe T., Murakami Y. : "Preliminary Experiment of Leak Location of Large Vacuum Vessels", Proceedings of 4th Meeting on Ultra-High Vacuum Technology (Tsukuba June, 1982), (in Japanese).

82) Masuda M., Miyauchi Y.[*18], Shimizu M., Shimizu T. : "A Transient Finite Element Analysis of Natural Convection Based upon Stream Function and Vorticity", 4th International Symposium on Finite Element Method in Flow Problems (Tokyo July, 1982).

83) Miyauchi Y.[*18], Masuda M., Shimizu M., Fujita K.[*18] : "Finite Element Analysis of Natural Convection with Penalty Function Method", ibid.

84) Wagner F.[**20], Becker C.[**20], Behringer K.[**20], Campbell D.[**20], Eberhagen A.[**20], Engelhardt W.[**20], Fußmann G.[**20], Gehre O.[**20], Gernhardt J.[**20], Gierke G.V.[**20], Glock E.[**20], Haas G.[**20], Huang M.[**25], Karger F.[**20], Keilhacker M.[**20], Klüber O.[**20], Kornherr M.[**20],

Lackner K.[**20], Lisitano G.[**20], Lister G.G.[**20], Mayer H.M.[**20], Meisel D.[**20], Müller E.R.[**20], Murmann H.[**20], Niedermeyer H.[**20], Poschenrieder W.[**20], Rapp H.[**20], Röhr H.[**20], Schneider F.[**20], Shimomura Y., Siller G.[**20], Smeulders P.[**20], Söldner F.[**20], Speth E.[**20], Stäbler A.[**20], Steuer K.H.[**20], Szymanski Z.[**26], Venus G.[**20], Vollmer O.[**20], Yü Z.[**25], Steinmetz K.[**24], Hübner K.[**24] : "Confinement and β_p-Studies in Neutral Beam Heated ASDEX Plasmas", 9th Conference on Plasma Physics and Controlled Nuclear Fusion Research (Baltimore, September 1982).

85) Keilhacker M.[**20], Becker G.[**20], Behringer K.[**20], Campbell D.[**20], Eberhagen A.[**20], Engelhardt W.[**20], Fußmann W.[**20], Gehre O.[**20], Gernhardt J.[**20], Gierke G.V.[**20], Glock E.[**20], Haas G.[**20], Huang M.[**25], Karger F.[**20], Klüber O.[**20], Kornherr M.[**20], Lackner K.[**20], Lisitano G.[**20], Lister G.G.[**20], Mayer H.M.[**20], Meisel D.[**20], Müller E.R.[**20], Murmann H.[**20], Niedermeyer H.[**20], Poschenrieder W.[**20], Rapp H.[**20], Röhr H.[**20], Schneider F.[**20], Shimomura Y., Siller G.[**20], Smeulders P.[**20], Söldner F.[**20], Speth E.[**20], Stäbler A.[**20], Steuer K.H.[**20], Szymanski Z.[**26], Venus G.[**20], Vollmer O.[**20], Wagner F.[**20], Yü Z.[**25] : "Divertor Operation at Large Power Flows in Neutral Beam Heated ASDEXS Discharges", 9th IAEA Conference on Plasma Physics and Controlled Nuclear Fusion Research (Baltimore, September 1982).

86) Yoshida Z.[**5], Nakanishi M., Inoue N.[**5], Uchida T.[**5], et al. : "Suppression of Disruptive Instability in Low-q Regime by External Ergodization of (2, 1) Island", ibid.

87) Johnson D.[**19], Bell M.[**19], Bitter M.[**19], Bol K.[**19], Brau K.[**19], Buchenauer D.[**19], Budny R.[**19], Growley T.[**19], Davis S.[**19], Dylla F.[**19], Eubank H.[**19], Fishman H.[**19], Fonck R.[**19], Goldston R.[**19], Grek B.[**19], Grimm R.[**19], Hawryluk R.[**19], Hsuan H.[**19], Kaita R.[**19], Kaye S.[**19], Kugel H.[**19], Manos D.[**19], Marty D.[**21], Manickam J.[**19], Mansfield D.[**19], Mazzucato E.[**19], McCann R.[**19], McCune D.[**19], McGuire K.[**19], Motley R.[**19], Mueller D.[**19], Oasa K., Olivain J.[**21], Okabayashi M.[**19], Owens K.[**19], Ramette J.[**21], Reverdin C.[**21], Reusch M.[**19], Sauthoff N.[**19], Schilling G.[**19], Schmidt G.[**19], Sesnic S.[**20], Slusher R.[**22], Surko C.[**22], Strachan J.[**19], Suckewer S.[**19], Takahashi H.[**19], Tenney F.[**19], Thomas P.[**23], Towner H.[**19], Valley J.[**22] : "High Beta Experiments with Neutral Beam Injection on PDX", ibid.

88) Kajiura S.[*4], Ohwada K.[*4], Sato H.[*4], Furuyama M.[*4], Shimizu M.,

Shimizu T. : "Tests of a Cooling and Heating System Model for JT-60 Vacuum Vessel", 12th Symposium on Fusion Technology (Jülich Sep. 1982).

89) Ohkubo M. : "The Design Bending Stress Criterion for JT-60 Coil", ibid.

90) Nakamura K., Ozeki T. : "Eddy Current Analysis in JT-60", ibid.

91) Takatsu H., Shimizu M., Ohta M., Nakamura Y.[*28], Sakai K.[*28], Uchino K.[*28] : "Evaluation of Fatigue Strength of the JT-60 Vacuum Vessel", ibid.

92) Watanabe T.[*28], Kamiya H.[*28], Aki F.[*28], Nagai M.[*28], Kadotani K.[*28], Ohkubo M., Ando T., Masuda M. : "Electrical Insulation System Fit for Cyclic High Strain", ibid.

93) Abe T., Inagawa K.[*21], Obara K., Murakami Y. : "In-Situ Coating of Titanium Carbide", ibid.

94) Tani K., Shimada R., Tamura S., Ishigaki Y.[*28], Koseki S.[*28], Yabuno K.[*28] : "Study of Ohmic Heating (OH) Power Supply System Using DC Thyristor Circuit Breaker", ibid.

95) Shimada R., Miya N., Ishigaki Y.[*28], Yabuno K.[*28], Kuroda K.[*28] : "A Preliminary Study on Feeding Power and Energy to the Poloidal Field Power Supply for a Tokamak Reactor", ibid.

96) Kondo I., Kimura T., Hosogane N., Yoshino R., Kurihara K., Suzuki Y. : "System Design of ZENKEI, the Central Control System of JT-60", ibid.

97) Kimura T., Hosogane S., Kurihara K., Yonekawa I., Yoshino R., Kondo I. : "Safety Design of the JT-60 Control System", ibid.

98) Yoshino R., Kimura T., Hosogane N., Kurihara K., Yonekawa I., Kondo I., Suzuki Y. : "Design and Development of the Real Time Control System for JT-60 Plasma Discharge", ibid.

99) Toyokawa R.[*26], Ogata A.[**11], Shiho M., Maeda H., Kambe T.[*1], Tahira S.[*1], Kawahara T., Tanamura K.[*1], Fujioka A.[*1] : "PCM Recorder for New Diagnostic Data Storage", ibid.

100) Kambe T.[*1], Ogata A.[**11], Toyokawa R.[*26], Tahira S.[*1], Nishitani T., Maeda H. : "Soft Ware Tool for Design and Maintenance of a Large CAMAC System", ibid.

101) Abe T., Inagawa K.[*21], Obara K., Hiroki S., Murakami Y. : "Studies of In-Situ Coating Techniques for JT-60 (I)", 23th Vacuum Symposium (Kobe Nov. 1982).

102) Inagawa K.[*21], Abe T., Obara K., Hiroki S., Murakami Y. : "Studies of In-Situ Coating Techniques for JT-60 (II)", ibid.

103) Obara K., Hiroki S., Abe T., Murakami Y. : "Preliminary Experiment on Leak Location of Large Vacuum Vessels", ibid.

104) Obara K., Abe T., Murakami Y., Yamamoto M., Shimizu M., Chiba K.[*29], Itoh K.[*29] : "Development of All Metal Gate Valve for JT-60 Diagnostic Ports (I) & (II)", ibid.

105) Nakamura H. : "Design and Development for JT-60 Limiter", Workshop on Advanced Limiter Concepts for Large Tokamak (Culham Feb. 1983).

106) Shimada R., Aoyagi T., Ieda Y.[*2], Arai J.[*2] : "Computer Simulation of Power Supply Systems of JT-60", International Power Electronics Conference (Tokyo March 1983).

107) Matsukawa T., et al. : "The Power Supply System of JT-60", ibid.

A.1.5 List of Other Reports

1) Itoh K., Itoh S-I.[**1] : "Energy Deposition Profile of Efficient Heating by Shear Alfvén Wave", HIFT-64 (Hiroshima Univ., July 1982).

2) Fukuyama A.[**3], Nishiyama S.[**3], Itoh K., Itoh S-I.[**1] : "Kinetic Analysis of Propagation and Absorption Structure of ICRF Wave", HIFT-68 (Hiroshima Univ., Oct. 1982).

3) Itoh S-I.[**1], Itoh K., Fukuyama A.[**2] : "Kinetic Theory of RF Waves in a Plasma in an Inhomogeneous Magnetic Field", IFSR-74 (Univ. of Texas at Austin, Nov. 1982).

4) Itoh K., Itoh S-I.[**1], Tuda T., Tokuda S. : "Kinetic Theory of Global n=1 Instabilities in Toroidal Plasmas", IFSR-75 (Univ. of Texas at Austin, Jan. 1983).

5) Itoh K., Itoh S-I.[**1], Fukuyama A.[**2] : "Three Dimensional Structure of ICRF Waves in Tokamak Plasmas", IFSR-86 (Univ. of Texas at Austin, March 1983).

6) Takahashi H.[**19], Bol K.[**19], Maeda M., Okabayashi N.[**19], Rausch M.[**19] : "Experimental Determination of the Vertical Instability Strength in PDX Tokamak", PPPL-1911 (June 1982).

7) Shimomura Y., Keilhacker M.[**20], Lackner K.[**20], Murmann H.[**20], Siller G.[**20] : "Characteristics of Divertor Plasma in Neutral Beam Heated ASDEX Discharge", IPP Report III/180 (Dec. 1982).

A.2 Personnel of the Center

A.2.1 Number of the Staff of the Divisions

	FY 1980	FY 1981	FY 1982
Regular staff*1	171	185	220
Staff on loan*2	20	32	30
Guest scientist	3	5	3*3
Scholarship fellow	5	1	1

*1 Including scientists, technicians and secretaries.

*2 From industry

*3 One from Nihon University
Two from University of Tokyo

A.2.2 List of Scientific Staffs and Officers during FY 1982

Fusion Research Center

ISO Yasuhiko (Center Director)

(A) Division of Thermonuclear Fusion Research

OBATA Yukio (Head)
TANAKA Masatoshi (Deputy Head)
HAYASHI Takashi (Administrative Manager)

Plasma Theory Laboratory

AZUMI Masafumi (Senior Scientist)
HARAFUJI Kenji**4 (Scholarship Fellow)
ITOH Kimitaka
KUMAGAI Michikazu*2
KURITA Gen-Ichi
TAKEDA Tatsuoki (Chief)
TAKIZUKA Tomonori
TOKUDA Shinji
TSUNEMATSU Toshihide
TUDA Takashi

Experimental Plasma Physics Laboratory

TANAKA Yuji (Chief)
FUNAHASHI Akimasa (Principal Scientist)

* JFT-2 and JFT-2M

HOSHINO Katsumichi
KAWASHIMA Hisato
KIMURA Haruyuki
MATSUMOTO Hiroshi
MORI Masahiro
ODAJIMA Kazuo
SHOJI Teruaki
SUZUKI Norio

* NBI

MAENO Masaki (Senior Scientist)
SENGOKU Seio
YAMAMOTO Shin
YAMAMOTO Takumi

* Diagnostics of JFT-2M

KASAI Satoshi
KAWAKAMI Tomohide
MATOBA Tohru (Senior Scientist)
MIURA Yukitoshi
OGAWA Hiroshi
OGAWA Toshihide
UESUGI Yoshihiko
YAMAUCHI Toshihiko

Facility Operation and Engineering Section

HASEGAWA Kouichi
KASHIMURA Takanori
KAZAWA Minoru
KIKUCHI Kazuo
KUNIEDA Shunsuke (Chief)
MATSUZAKI Yoshimi
OKANO Fuminori
ISHIBORI Ikuo

KASHIWA Yoshitoshi
HONDA Atsushi
SHIBATA Takatoshi
SHIINA Tomio
SUZUKI Kihachiro (Deputy Chief)
TANI Takashi
TAJIMA Yoshihiro
YOKOYAMA Kenji
YOKOKURA Kenji

Plasma Heating Laboratory I

AKIBA Masato
DAIRAKU Masayoshi
HORIIKE Hiroshi
ITOH Takao
KITAMURA Shigeru
MATSUDA Shinzaburo (Senior Scientist)
MATSUOKA Mamoru
MIZUHASHI Kiyoshi
OHARA Yoshihiro
OKUMURA Yoshikazu
SHIBANUMA Kiyoshi
SHIBATA Takemasa
TANAKA Masatoshi (Chief)
TANAKA Shigeru
WATANABE Kazuhiro

Plasma Heating Laboratory II

FUJII Tuneyuki
HARA Mitsuru*16
IIDA Kazuhiro*9
IMAI Tsuyoshi
NAGASHIMA Takashi (Chief)
NAKAMURA Tetsurou*2
SAIGUSA Mikio
SAKAMOTO Keishi
SAWAHATA Masayuki

Plasma Engineering Laboratory

MURAKAMI Yoshio (Chief)
NAKAMURA Kazuyuki
OHTSUKA Hidewo
SAIDOH Masahiro
SONE Kazuho
YAMADA Rayji

Superconducting Magnet Laboratory

ANDO Toshinari
IIDA Fumio*4
DORESNER Lawrence*13
HIYAMA Tadao
KATO Takashi
KOIZUMI Koichi
NAKAZIMA Hideo
NISHI Masataka
OKUNO Kiyoshi
OSHIKIRI Masayuki*13
SANADA Yoshinao*2
SHIMADA Masao*14
SHIMAMOTO Susumu (Chief)
TADA Eisaku
TAKAHASHI Osamu*15
TAKAHASHI Yoshikazu
TSUJI Hiroshi
YOSHIDA Kiyoshi

Tritium Engineering Laboratory

YAMADA Masayuki
YAMANISHI Toshihiko
KONISHI Satoshi
KINOSHITA Masahiro
OKUNO Kenji
YOSHIDA Hiroshi (Senoir Scientist)
MATSUDA Yuji
TACHIKAWA Katsuhiro

TANAKA Kichizo (Senior Scientist)
NARUSE Yuji (Chief)

(B) Division of Large Tokamak Development

TOMABECHI Ken (Head)
YOSHIKAWA Masaji (Deputy Head)

Large Tokamak Administration Section

NARUI Masao (Chief)
KAWAGUCHI Masahiro (Deputy Chief)

JT-60 Program Office

HIRAOKA Toru (Chief)
KISHIMOTO Hiroshi (Deputy Chief)

* Planning and Coordinating Group

OIKAWA Akira
SUZUKI Kunihiro
TOKUTAKE Toshikuni

* Experimental Planning Group

HIRAYAMA Toshio
SEKI Shogo
SHIMOMURA Yasuo (Senior Scientist)
TANI Keiji
YOSHIDA Hidetoshi
NAKANISHI Masahiro

* Doublet-III Experiment Group

AIKAWA Hiroshi
KASAI Masao*3
KITSUNEZAKI Akio (Senior Scientist)
KOBAYASHI Tomofumi*4
KONOSHIMA Shigeru
MATSUDA Toshiaki
NAGAMI Masayuki
NINOMIYA Hiromasa
OHTSUKA Michio*4
SHIMADA Michiya

SHINYA Kichiro*2

YOKOMIZO Hideaki

* Operation Planning Group

KODAMA Kozo

SUNAOSHI Hidenori

TOTSUKA Toshiyuki

JT-60 Project Office I

IIJIMA Tsutomu (Chief)

OHTA Mitsuru (Deputy Chief)

* Machine Group

AKINO Noboru

ANDO Toshiro

ARAI Takashi

HIRATSUKA Hajime

HORIE Tomoyoshi

INOUE Hiromi

ISAKA Masayoshi

KASUGA Takemitsu

KAWAMOTO Nobunari

KAWASAKI Kozo

KISHIDA Haruo*21

KOIKE Tsuneyuki

MASUDA Michio

NAKAMURA Hiroo

NAKAMURA Yukiharu

NAKAO Keizo

NISHIO Satoshi

NISHIYAMA Takeji*4

OGIWARA Norio

OHKUBO Minoru

OZEKI Takahisa

SATO Osamu

SEIMIYA Munetaka

SERIZAWA Yasunori

SHIMIZU Masatsugu (Senior Scientist)

SHIMIZU Tohru

TAKATSU Hideyuki
TANAKA Takejiro
TOYOSHIMA Noboru
YAMAMOTO Masahiro
YANAI Munetoshi
YASUDA Masaharu

* Vacuum Technology Group
ABE Tetsuya
HIROKI Seiji
OBARA Kenjiro
INAGAWA Konosuke*21

JT-60 Project Office II

TAMURA Sanae (Chief)

* Power Supplies Group
AOYAGI Tetsuo
ARAKAWA Kiyotsugu
IMAHASHI Koichi
MATSUKAWA Makoto
MATSUKAWA Tatsuya
MIYA Naoyuki
MIZUNO Makoto
NAGAYA Susumu
SATO Hiroshi
SEKIGUCHI Shuichi
SHIINA Minoru
SHIMADA Ryuichi
TAKAHASHI Shunji
TERAKADO Tsunehisa
TOMIYAMA Yoshimi
TSUNEOKA Masaki

* Auxiliary Facilities Group
AKAO Yohichiro
HIRUTA Kazuharu
HOSODA Ryujiro
MURANAGA Hiromi*6
OHMORI Kenichiro

JT-60 Project Office III

SUZUKI Yasuo (Chief)
KONDO Ikuo (Deputy Chief)

* Control Group

ANNO Katsuto
HOSOGANE Nobuyuki
MIMURA Toyoaki
KURIHARA Kenichi
OHASA Kazumi
SATO Masayasu
SUGIE Tatsuo
TAHIRA Shigeo
TAKAHASHI Minoru
YAMASHITA Osamu
YONEKAWA Izuru
YOSHINO Ryuji

* Diagnostics Group

KANBE Toshihiko*1
KITAHARA Katsumi
MAEDA Hikosuke (Senior Scientist)
NAGASHIMA Akira
NEYATANI Yuzuru
NISHITANI Takeo
OIKAWA Hisashi*23
OHSATO Yukio*24
SHIHO Makoto
TAKEUCHI Hiroshi
TOYOKAWA Ryoji
URAMOTO Yasuyuki

JT-60 Project Office IV

* NBI Group

ARAKI Masanori
KAWAI Mikito
KURUYAMA Masaaki
OGUCHI Yoshiaki*19

OHGA Tokumichi
SHIGEMATSU Hirotsugu*8
SHIRAKATA Hirofumi (Chief)
SUGAWARA Tadayoshi*4

* RF Group

HONDA Masao
IKEDA Yoshitaka
KAMAKURA Akira*16
SUZUKI Norio
UEHARA Kazuya

Fusion Reactor System Laboratory

FUJISAWA Noboru (Senior Scientist)
IIDA Hiromasa (Senior Scientist)
MINATO Akio*18
NISHIO Satoshi
SAITO Seiji*4
SEKI Yasushi (Senior Scientist)
SUGIHARA Masayoshi
TONE Tatsuzo (Principal Scientist)
TACHIKAWA Katsuhiro
TACHIKAWA Nobuo*2
YAMAMOTO Takashi*6
UEDA Koju*11
YOSHIKAWA Masaji (Chief)

Guest Scientist

MIYAMOTO Goro**5
YAMAMURA Sakae**5
YASUKOCHI Ko**6

*1 Fujitsu Ltd.
*2 Tokyo Shibaura Electric Co., Ltd.
*3 Mitsubishi Atomic Power Industry Co.
*4 Hitachi Ltd.
*5 GA Technologies Inc.
*6 Fuji Electric Co., Ltd.
*7 Kaihatsu Denki Co., Ltd.
*8 Mitsubishi Heavy Indu., Ltd.
*9 Nuclear Engineering Co., Ltd.
*10 Sumitomo Heavy Ind., Ltd.
*11 Mitsubishi Electric Co., Ltd.
*12 Japan Steel Works Ltd.
*13 Nippon Atomic Industry Group
*14 Kobe Steel Ltd.
*15 Saginomiya Johnson Controls Co., Ltd.
*16 Nippon Electric Co., Ltd.
*17 Hitachi Cable Co.
*18 Kawasaki Heavy Ind., Ltd.
*19 Nissin Electric Co., Ltd.
*20 Touyo Information System Co., Ltd.
*21 ULVAC Co.
*22 Nippon Kogaku Co., Ltd.
*23 Osaka Vacuum Ltd.
*24 Nissei Sangyo Co., Ltd.
*25 Century Research Center Co.
*26 Yokokawa Electric Works Ltd.
*27 Irie Koken Co., Ltd.
*28 Ishikawajima-Harima Heavy Ind. Co., Ltd.
*29 Kishikawa Special Valve Co., Ltd.
*30 Mitsui Engineering & Shipbuilding Co.

**1 Hiroshima University
**2 Nagoya University
**3 Okayama University
**4 Tohoku University
**5 The University of Tokyo
**6 Nihon University
**7 Osaka University

**8	Tokyo Institute of Technology
**9	Kyoto University
**10	National Research Institute for Metals
**11	National Laboratory for High Energy Physics
**12	Power Reactor and Nuclear Fuel Development
**13	Confédération Suisse, Ecole Polytechnique Fédérale de Lausanne
**14	Oak Ridge National Laboratory
**15	Culham Laboratory
**16	FB-National Magnetic Laboratory
**17	Argonne National Laboratory
**18	University of Wisconsin
**19	Princeton Plasma Physics Laboratory
**20	Max-Planck Institute für Plasmaphysik
**21	Centre d'Etude Nucléaires, Fontenay-aux-Rose
**22	Bell Laboratories
**23	JET Joint Undertaking
**24	Institute für Angewandte Physik II , Universitäte Heidelberg
**25	Academia Sinica, Peking, The Peoples Republic of China
**26	The Institute of Fundamental Technological Research, Warsaw/Poland

A.3 Budget of the Center

(unit: Million ¥)

	FY 1980*1	FY 1981*1	FY 1982*1
JT-60 Construction*2	19,969	23,943	28,936
Research & Development*3	2,716	3,619	3,117
Japan-US Cooperation	3,677	3,875	3,042
Site Construction	2,520	4,100	5,633

*1 From April to March

*2 Including cashing of the financial obligation in each FY

*3 Excluding fusion-related R&D in other divisions than the Center